CHALMERS
UNIVERSITY OF TECHNOLOGY

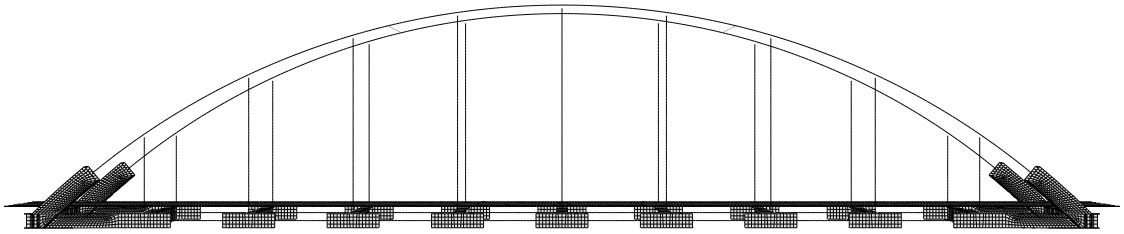

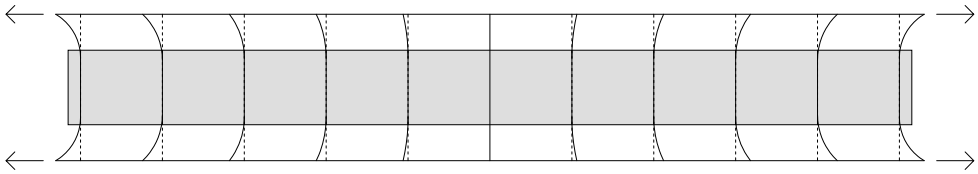

FE-modelling of a tied arch bridge with regard to restraining forces

A comparison of modelling techniques

Master's thesis in the Master's Programme Structural Engineering and Building Technology

FRIDA GUSTAVSSON
SOFIA JORHOLM

Department of Civil and Environmental Engineering
Division of Structural Engineering
Concrete Structures
CHALMERS UNIVERSITY OF TECHNOLOGY
Master's thesis BOMX02-17-12
Gothenburg, Sweden 2017

MASTER'S THESIS BOMX02-17-12

FE-modelling of a tied arch bridge with regard to restraining forces

A comparison of modelling techniques

Master's thesis in the Master's Programme Structural Engineering and Building Technology

FRIDA GUSTAVSSON
SOFIA JORHOLM

Department of Civil and Environmental Engineering

Division of Structural Engineering

Concrete Structures

CHALMERS UNIVERSITY OF TECHNOLOGY

Gothenburg, Sweden 2017

FE-modelling of a tied arch bridge with regard to restraining forces
A comparison of modelling techniques
FRIDA GUSTAVSSON
SOFIA JORHOLM

Master's thesis BOMX02-17-12
ISSN 1652-8557
Department of Civil and Environmental Engineering
Division of Structural Engineering
Concrete Structures
Chalmers University of Technology
SE-412 96 Gothenburg
Sweden
Telephone: +46 (0)31-772 1000

Cover:
The tied arch bride studied in this master thesis modelled in the most complex level (top figure) and elongation of the lower chord resulting in secondary bending in the transversal beams (bottom figure).

Chalmers Reproservice
Gothenburg, Sweden 2017

FE-modelling of a tied arch bridge with regard to restraining forces
A comparison of modelling techniques
Master's thesis in the Master's Programme Structural Engineering and Building Technology
FRIDA GUSTAVSSON
SOFIA JORHOLM
Department of Civil and Environmental Engineering
Division of Structural Engineering
Concrete Structures
Chalmers University of Technology

ABSTRACT

Before finite element methods were used, structural calculations were conducted in two dimensions, which resulted in three dimensional effects being overseen or missed. With today's finite element modelling techniques a more detailed analysis can be made to obtain a more accurate description of the structural behaviour. Developing a finite element model can be time consuming and demands high computer capacity. The complexity of the analysis depends on the choices made concerning the element type and the number of degrees of freedom used.

In the tied arch bridge studied in this master thesis, restraining forces may arise in the transversal beams as a consequence of movements of adjacent structural parts. The magnitude of these forces depends on the stiffness in the weak direction of the transversal beams, which may lead to difficulties in design. The deformation of the deck in relation to the transversal beams is also a parameter that affects the restraining forces, hence the elements used in a finite element model may affect the result.

In this master thesis the impact of modelling techniques on the restraining forces is investigated. The bridge was modelled with three different levels of complexity. In the simplest approach beam elements were used for all structural parts, including the deck as a beam grillage. In the second level the deck was changed to shell elements meanwhile in the most complex approach shell elements were used for the majority of the model.

The secondary bending moment in the transversal beams together with the normal force in the longitudinal beams and deck presented the largest difference between the modelling approaches. That might indicate that important three dimensional effects occurs in the structure and needs to be considered in design. The results shows that the beam grillage model is conservative, meanwhile no major differences are observed between the intermediate and the most complex model.

Keywords: Restraining forces, tied arch bridge, beam grillage, beam elements, shell elements, Brigade/PLUS, FE-modelling, bridge design

FE-modellering av en dragen bågbro med avseende på tvångskrafter
En jämförelse av modelleringstekniker
Examensarbete i Structural Engineering and Building Technology
FRIDA GUSTAVSSON
SOFIA JORHOLM
Institutionen för bygg- och miljöteknik
Avdelningen för Konstruktionsteknik
Betongbyggnad
Chalmers tekniska högskola

SAMMANFATTNING

Före användandet av finita elementmetoder gjordes konstruktionsberäkningar i två dimensioner, vilket kunde resultera i att tredimensionella effekter förbisågs. Med dagens modelleringstekniker kan en mer detaljerad analys göras för att erhålla en mer korrekt beskrivning av konstruktionens beteende. Att modellera en finit elementmodell kan vara tidskrävande och den kräver hög datorkapacitet. Komplexiteten av analysen beror på beslut tagna om vilken elementtyp och antal frihetsgrader som används.

I den specifika bågbro studerad i detta mastersarbete kan tvångskrafter uppstå i de transversella balkarna som en konsekvens av skillnader i rörelse mellan närliggande konstruktionsdelar. Storleken av dessa krafter beror på styvheten i den veka riktningen av de transversella balkarna, vilket kan leda till svårigheter i design. Deformation av plattan i relation till de transversella balkarna är också en parameter som påverkar, vilket betyder att elementtypen som används i den finita elementmodellen kan ha en inverkan på resultatet.

I detta mastersarbete undersöks hur olika modelleringstekniker påverkar dessa tvångskrafter. Bron modellerades i tre olika nivåer av komplexitet. I den enklaste metoden användes balkelement för alla bärande delar vilket inkluderar plattan modellerad som en balkrost. I den andra nivån ändrades plattan till skalelement och i den mest komplexa metoden användes skalelement för majoriteten av de bärande delarna.

Det sekundära böjmomentet i de transversella balkarna tillsammans med normalkraften i de longitudinella balkarna samt plattan visade störst skillnad mellan de olika modelleringsteknikerna. Detta kan indikera att viktiga tredimensionella effekter uppstår i konstruktioner och bör beaktas i design. Resultaten visar att balkrostmodellen är konservativ medans det inte går att se några större skillnader mellan de två mer komplexa modellerna.

Nyckelord: Tvångskrafter, bågbro, balkrost, balkelement, skalelement, Brigade/PLUS, FE-modellering, brodesign

Contents

PREFACE

In this master thesis a comparison between finite element modelling techniques has been performed. A tied arch bridge has been evaluated with regard to restraining forces in the transversal beams. The master thesis has been carried out at Norconsult AB between January 2017 and June 2017 in cooperation with the Department of Civil and Environmental Engineering at Chalmers University of Technology.

A special thank is addressed to our supervisor Emanuel Trolin, Norconsult AB, for his highly appreciated guidance and valuable inputs throughout the project and for always sharing his knowledge with us. We also like to express our gratitude to our examiner Senior Lecturer Ignasi Fernandez at the Department of Civil and Environmental Engineering for his critical review and feedback on the project.

Finally we would like to thank our opponents, Joel Eriksson and Adam Jonsson for their comments and feedback during the project and for all interesting discussions.

Göteborg, June 2017
Frida Gustavsson and Sofia Jorholm

NOMENCLATURE

Roman upper case letters

A	Area
E	Young's modulus
D	Constitutive matrix
I	Moment of inertia
L	Length
M	Bending moment
M_{ii}	Bending moment per unit length
N	Normal force
Q_{ik}	Characteristic concentrated load
R_i	Reaction force
ΔT	Temperature change
V	Shear force
V_{ii}	Shear force per unit length

Roman lower case letters

b	Center to center distance in composite section
b_{eff}	Effective flange width
b_w	Thickness of web
f_{yd}	Yield strength
h	Height
h_{de}	Height of deck
h_w	Height of web
l_0	Distance between zero moment points
q	Distributed load per meter
q_{ik}	Characteristic distributed load
r_{ha}	Radius of hanger
t	Thickness
t_f	Thickness of flange
t_w	Thickness of web

u_0 Displacement in x-direction

w Displacement in z-direction

w_c Carriageway width

w_{c1} Width of lane

w_{de} Width of deck

w_f Width of flange

x x-coordinate

y y-coordinate

z z-coordinate

Greek lower case letters

α_{cT} Thermal expansion coefficient for concrete

α_q Adjustment factor traffic load

α_Q Adjustment factor traffic load

γ_{ij} Shear strain in ii direction

κ Curvature matrix

ν Poisson's ratio

ϵ_{cT} Concrete strain due to temperature change

ϵ_{ii} Normal strain in ii direction

ρ Density

σ_{ii} Normal stress in ii direction

τ_{ii} Shear stress in ii direction

1 Introduction

1.1 Background

In the recent years, finite element (FE) methods has been developed to increase the level of accuracy in structural analysis. The FE-method is a numerical approximation that should represent the response of a structure. Establishing an FE-model can be time consuming and it demands high computational capacity. It also results in a large amount of data that sometimes can be difficult to sort and interpret. The complexity of the model depends on the choices made concerning the extent of the model, material response and the element types used. It is therefore important to think about which results are of interest before starting the process of the FE-model development and to adjust the level of detail to the needed accuracy in the results.

Assumptions and simplifications are generally made to make the model less complex. There are several element types with various properties that can represent different structural behaviours. It is hard to establish a unique suitable model that represents the response of a structure in a good way and it is therefore important to have a good understanding of structural behaviours so that no relevant parameters are missed.

Before FE-analyses were used, structural calculations were conducted in two dimensions where the structure is divided into longitudinal and transversal load carrying parts. The behaviour is then analysed separately and the reaction forces and stresses are calculated independently. This simplification may result in three dimensional effects being overseen or missed. With today's FE-modelling techniques and higher computational capacity a more detailed analysis can be made and the structural response can be studied more accurately. One of the effects that can be missed when using the two dimensional way of designing is the effect from restraining forces, which arises when a structure is prevented to deform freely.

The type of bridge studied in this master thesis is a tied arch bridge, consisting of a lower chord made of steel with transversal steel beams in between supporting a concrete deck. In such a structure restraining forces may occur in the transversal beams, and depending on how the structure is loaded, different phenomena can give rise to restraining forces; due to elongation of the lower chord while the transversal beams are prevented to move by the concrete deck, the change of temperature and local effects from a traffic load. The magnitude of such forces is dependent on the stiffness in the weak direction of the transversal beams. These restraining forces may not be decisive in the ultimate limit state and may not cause failure of the structure, however, the serviceability limit state and primarily fatigue strength of the structure are highly affected.

When designing a tied arch bridge, with respect to fatigue, it is important that the restraining forces are as accurate as possible to get an optimized cross section. In this master thesis it will be investigate if the magnitude of the stresses in the transversal beams, as a consequence of the restraining forces, are affected by the modelling technique used.

1.2 Aim

The general aim of this master thesis is to study how the restraining forces in the transversal beams in a tied arch bridge are affected by FE-modelling techniques. Different levels of complexity will be studied and it is of interest to find a suitable model to describe the effect of restraining forces while in the same time being as simple and time efficient as possible. A parametric study will be conducted to investigate how the stiffness of the transversal beams and different loading conditions affects the restraining forces.

1.3 Scope and limitations

In this master thesis the focus will be on how the restraining forces in the transversal beams and the area around them will be affected by three different modelling techniques, limited to beam and shell elements. Other failure modes will not be examined in this master thesis. The study will be made on one tied arch bridge with predefined geometry and dimensions.

When designing a bridge there are several load cases that needs to be considered. In this master thesis the load cases are limited to three types of loads; uniformly distributed vertical load, temperature load and traffic load. The temperature load will be limited to a uniform temperature decrease in the concrete deck. Only load model 1 according to Eurocode will be included in the traffic load.

1.4 Methodology

A tied arch bridge will be modelled in full scale using three different modelling techniques. In the first technique beam elements will be used for the whole geometry, including the deck as a beam grillage. The approach in the second technique is similar to the first one, with the difference that the slab will be modelled using shell elements. In the third and last technique the deck as well as the transversal beams and the areas connected to them will be modelled in more detail using shell elements.

The effect of restraining forces will be investigated by comparing the secondary bending moment in the transversal beams and the normal force in the longitudinal beams and deck for all models. To study the impact of the stiffness of the transversal beams, a parametric study will be conducted by changing the width of the flanges. The effect of uniformly distributed load, temperature load and traffic load will be examined.

The FE-software used in this master thesis is Brigade/PLUS 6.1-11. Brigade/PLUS is a further development of the general FE-software Abaqus, and is developed for the design and analysis of bridges with regard to moving loads and load combinations.

1.5 Outline

Chapter 2 presents a theoretical background to the subjects treated in this thesis. It includes different mathematical theories for beams and plates, the difference between beam and plate elements and how the elements works. Further, special features in Brigade/PLUS, such as the interaction between

different parts in an FE-model as well as stress integration is discussed. The theory behind all loads applied is also presented.

In Chapter 3 the geometry of the analysed bridge is decribed. The different effects from the loads applied; elongation of the lower chord, deformation due to temperature change and local effects from a concentrated load, are also presented.

Chapter 4 describes how the three models were established and what choices and simplifications has been made for each developed modelling level.

In Chapter 5, results for the three different models are presented, investigating how and why the secondary bending moment in the transversal beams and the normal force in the longitudinal beam differs between models. A parametric study is also included for the three different models, where the influence of the width of the flanges of the transversal beams has been studied.

Finally, Chapter 6 and 7 presents the discussion and conclusions of the master thesis and some suggestions for further investigations.

2 Theoretical background

In order to understand the different modelling techniques and the results of the analysis, a theoretical background is presented in this chapter. The FE-application and the post-processing of the results in Brigade/PLUS are also presented in this chapter.

2.1 Mathematical models

An FE-model is an approximation of the real behaviour of a structure. However, modelling a full scale three dimensional structure with solid elements is highly computational time consuming hence simplifications are generally made when choosing elements used in the model. In order to simplify the mathematical formulation of a structure, assumptions about the kinematic and constitutive relations can be made. The element types used in this master thesis are beam and shell elements, which are based on beam and plate theories. Those mathematical formulations will be presented in the following sections.

2.1.1 Beam theory

A beam is a structure that can be loaded in both the axial and transversal direction. Its geometry is mainly extended in the longitudinal direction and therefore it is possible to simplify the three dimensional geometry to a simpler one dimensional mathematical problem (Ottosen and Peterson 1992). Beam elements are based on beam theories, the most commonly used are the Euler-Bernoulli and the Timoshenko beam theories.

A beam, symmetric and loaded with a uniform load in the xz-plane, will only deflect in the z-direction. A section normal to the x-axis will have three stress components, one normal to the section, σ_{xx}, and two in the directions of the section, τ_{xy} and τ_{xz}, see Figure 2.1.

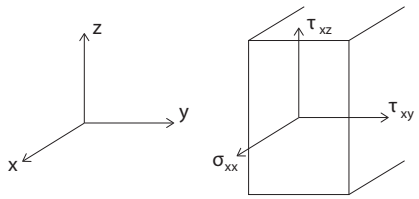

Figure 2.1 Stress components in a beam element in a cross section normal to the x-axis.

Since the loading only occurs in the xz-plane, the stress component τ_{xy} is zero. The bending moment, M and the shear force, V can be defined, using these stress components, as

$$M = \int_A z\sigma_{xx} dA, \qquad V = \int_A \tau_{xz} dA \tag{2.1}$$

where A is the area of the cross section and z is the lever arm in z-direction.

The vertical equilibrium and the moment equilibrium around the left end of a very small part of the beam, see Figure 2.2, assuming that the distributed load, $q\,dx$, and the change of shear force, dV, are very small, will result in the equilibrium equations

$$q\,dx + (V + dV) - V = 0 \qquad \Rightarrow \qquad \frac{dV}{dx} = -q \tag{2.2}$$

$$M + (V + dV)dx + q\frac{dx^2}{2} - (M + dM) = 0 \qquad \Rightarrow \qquad \frac{dM}{dx} = V \tag{2.3}$$

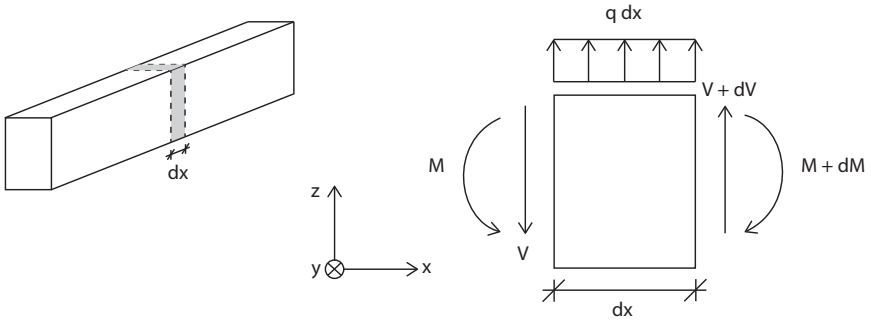

Figure 2.2 Vertical forces and moments acting on each side of a small part of the beam.

The Euler-Bernoulli beam theory is based on the assumptions that a section normal to the longitudinal direction of the beam remains plane and normal to the longitudinal direction during deformation and that the section does not deform in its own plane, see Figure 2.3. Hence, the shear deformation is neglected in the Euler-Bernoulli beam theory, and the only strain component, ϵ, that is not zero is in the x-direction, ϵ_{xx} (Ottosen and Peterson 1992).

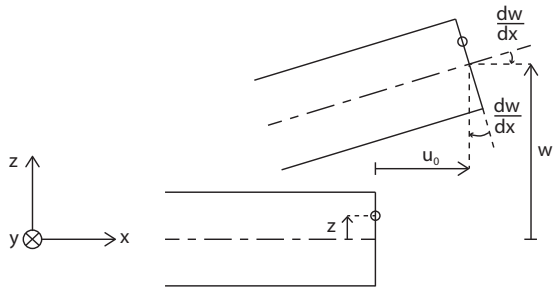

Figure 2.3 Deformation of a beam according to Euler-Bernoulli beam theory. A section normal to the longitudinal direction of the beam remains plane and normal to the longitudinal direction during deformation.

To be able to express the normal stress, σ_{xx}, according to the Euler-Bernoulli beam theory, some more assumptions must be made. The assumptions that the deformations are small and the constitutive relation is linear elastic result in the expression

$$\sigma_{xx} = E\epsilon_{xx} = E\left(\frac{du_0}{dx} - z\frac{d^2w}{dx^2}\right) \tag{2.4}$$

where E is Young's modulus and u_0 and w are the displacements in x- and z-direction respectively. The bending moment in Equation (2.1) can be expressed in terms of Young's modulus and the displacements, using the expression above in Equation (2.4), as

$$M = \int_A Ez\frac{du_0}{dx}dA - \int_A Ez^2\frac{d^2w}{dx^2}dA \tag{2.5}$$

By assuming that the x-axis is located in the center of mass of the cross section and that Young's modulus is constant in the cross section, the bending moment can be expressed as

$$M = -EI\frac{d^2w}{dx^2} \tag{2.6}$$

where $\quad I = \int_A z^2 dA$

The equilibrium conditions in Equation (2.2) and Equation (2.3) combined with Equation (2.6) gives the differential equation for Euler-Bernoulli beams as

$$\frac{d^2M}{dx^2} + q = 0$$

$$\frac{d^2}{dx^2}\left(EI\frac{d^2w}{dx^2}\right) - q = 0 \tag{2.7}$$

The assumptions and simplifications made for the Euler-Bernoulli beam theory makes it impossible to represent shear. All beams work both in bending and in shear but for slender beams the bending is more pronounced and the shear can be neglected. The Euler-Bernoulli beam theory is therefore accurate for beams where the length of the beam is much greater than the height of the beam. For beams with the ratio $L/h < 5 - 10$, where L is the length of the beam and h is the height of the beam, the Timoshenko beam theory gives a more accurate results (Ottosen and Peterson 1992).

The Timoshenko beam theory resemble the Euler-Bernoulli beam theory in the assumption that a section normal to the longitudinal direction of the beam does not distorts in its plane, however the Timoshenko beam theory does not assume that a section normal to the longitudinal direction of the beam remains plane and normal to the beam axis during deformation, see Figure 2.4. Hence, shear deformations are regarded in this theory (Carrera, Giunta, and Petrolo 2011).

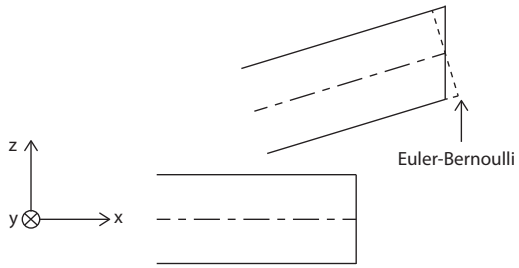

Figure 2.4 Deformation of a beam according to Timoshenko beam theory. The section normal to the longitudinal direction is not assumed to be normal to the beam axis during deformation.

2.1.2 Plate theory

A plate is a structure that only can be loaded in the normal to its plane. It is mainly extended in the plane of the plate and therefore it is possible to simplify the three dimensional problem to a two dimensional problem, similar to beam elements. The definition of a plate is an element that has a thickness which is much smaller than the other dimensions of the element (Ottosen and Peterson 1992). Plate elements are based on plate theories, the most commonly used are Kirchoff plate theory and Mindlin-Reissner plate theory.

A plate, with the xy-plane in the center of the thickness, loaded in the normal to the xy-plane will deflect in the z-direction. Sections perpendicular to the x-direction and the y-direction will have the stress components σ_{xx}, τ_{xy}, τ_{xz}, σ_{yy} and τ_{yz}, see Figure 2.5. Just as for beam elements, the bending moment, M, the shear force, V, and the normal force, N, can be defined using these stress components.

$$M_{xx} = \int_{-t/2}^{t/2} z\sigma_{xx} dz, \qquad M_{yy} = \int_{-t/2}^{t/2} z\sigma_{yy} dz, \qquad M_{xy} = \int_{-t/2}^{t/2} z\tau_{xy} dz \tag{2.8}$$

$$V_{xz} = \int_{-t/2}^{t/2} \tau_{xz} dz, \qquad V_{yz} = \int_{-t/2}^{t/2} \tau_{yz} dz \tag{2.9}$$

$$N_{xx} = \int_{-t/2}^{t/2} \sigma_{xx} dz, \qquad N_{yy} = \int_{-t/2}^{t/2} \sigma_{yy} dz, \qquad N_{xy} = \int_{-t/2}^{t/2} \tau_{xy} dz \tag{2.10}$$

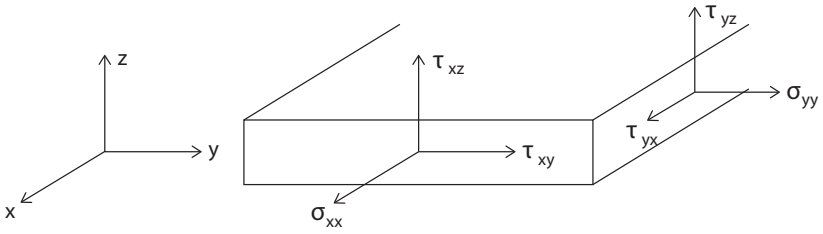

Figure 2.5 Stress components in a plate in sections normal to the x- and y-axis.

The moments, the shear forces and the normal force can be written in matrix form as

$$M = \begin{bmatrix} M_{xx} \\ M_{yy} \\ M_{xy} \end{bmatrix}, \qquad V = \begin{bmatrix} V_{xz} \\ V_{yz} \end{bmatrix}, \qquad N = \begin{bmatrix} N_{xx} \\ N_{yy} \\ N_{xy} \end{bmatrix} \tag{2.11}$$

The vertical equilibrium and the moment equilibrium around the x-axis on the left side of a very small part of the plate, see Figure 2.6, can be derived in the same way as for beams, and will result in the equilibrium equations

$$\frac{\partial V_{xz}}{\partial x} + \frac{\partial V_{yz}}{\partial y} + q = 0 \tag{2.12}$$

$$\frac{\partial M_{xy}}{\partial x} + \frac{\partial M_{yy}}{\partial y} = V_{yz} \tag{2.13}$$

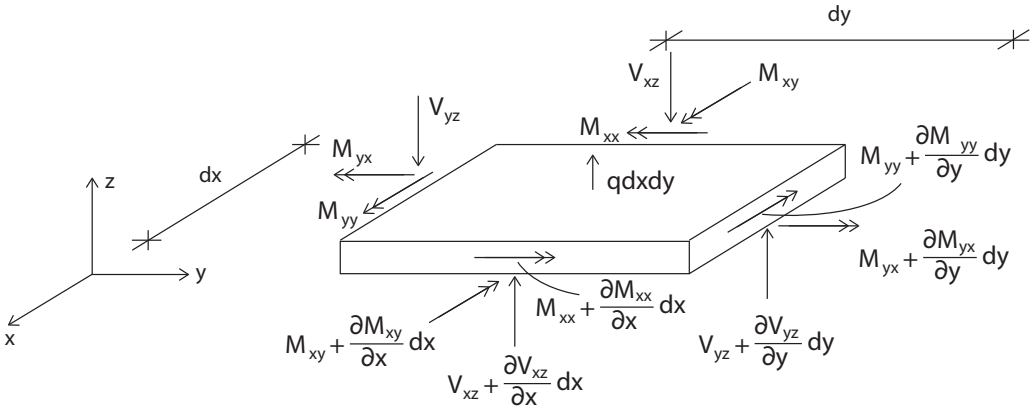

Figure 2.6 Vertical forces and moments acting on the sides of a small part of the plate.

The moment equilibrium around the y-axis of a very small part of the plate can be derived in the same way as for Equation (2.13) and will result in

$$\frac{\partial M_{xx}}{\partial x} + \frac{\partial M_{xy}}{\partial y} = V_{xz} \tag{2.14}$$

The assumption made for the Euler-Bernoulli beam theory that plane sections remains plane is assumed for the Kirchhoff plate theory as well. Hence, the shear deformation is neglected and consequently the shear strains γ_{xz} and γ_{yz} are zero (Ottosen and Peterson 1992).

The strains ϵ_{xx}, ϵ_{yy} and γ_{xy}, can be expressed in terms of displacements, u_0, v_0 and w, and can be written in matrix form as

$$\epsilon = \epsilon_0 - z\kappa \tag{2.15}$$

$$\text{where} \quad \epsilon_0 = \begin{bmatrix} \dfrac{\partial u_0}{\partial x} \\ \dfrac{\partial v_0}{\partial y} \\ \dfrac{\partial u_0}{\partial y} + \dfrac{\partial v_0}{\partial x} \end{bmatrix} \qquad \kappa = \begin{bmatrix} \dfrac{\partial^2 w}{\partial x^2} \\ \dfrac{\partial^2 w}{\partial y^2} \\ 2\dfrac{\partial^2 w}{\partial x \partial y} \end{bmatrix}$$

The constitutive relation in the Kirchhoff plate theory is assumed to be linear, just as for the Euler-Bernoulli beam theory, which leads to the relation

$$\sigma = D\epsilon \tag{2.16}$$

where σ and ϵ are vectors consisting of σ_{xx}, σ_{yy} and τ_{xy} and ϵ_{xx}, ϵ_{yy} and γ_{xy} respectively. D is the constitutive matrix, and for isotropic elasticity it is given by

$$D = \frac{E}{1-\nu^2} \begin{bmatrix} 1 & \nu & 0 \\ \nu & 1 & 0 \\ 0 & 0 & \frac{1}{2}(1-\nu) \end{bmatrix} \tag{2.17}$$

The bending moment and the normal force can be expressed in terms of the constitutive matrix and the strains, using Equation (2.11), Equation (2.15) and Equation (2.16), as

$$M = D\epsilon_0 \int_{-t/2}^{t/2} z dz - D\kappa \int_{-t/2}^{t/2} z^2 dz \tag{2.18}$$

$$N = D\epsilon_0 t \tag{2.19}$$

Since the plate is loaded only in the z-direction there will be no normal force acting on the plate, and it can be concluded that ϵ_0 is zero and the bending moment can be written as

$$M = -D\kappa \frac{t^3}{12} \tag{2.20}$$

The equilibrium conditions in Equation (2.12), Equation (2.13) and Equation (2.14), combined with Equation (2.15) and Equation (2.20) gives the differential equation for the plate theory as

$$\frac{\partial^4 w}{\partial x^4} + 2\frac{\partial^4 w}{\partial x^2 \partial y^2} + \frac{\partial^4 w}{\partial y^4} = q\frac{12(1-\nu^2)}{Et^3} \tag{2.21}$$

The Kirchhoff plate theory is accurate for plates where the assumption that the shear strains are zero or close to zero is true, in other words for thin plates. For plates with a greater thickness, the shear strains are non-zero and the Mindlin-Reissner plate theory gives a more accurate result (Ottosen and Peterson 1992).

2.2 Elements

In FE-modelling, the structure is divided into different elements to approximate the behaviour of the real structure. Common types of elements used in structural analysis are solid, shell, beam and truss elements, which are based on different assumptions and theories. They can in different ways reflect how the FE-model behaves. Hence, it is important to have good knowledge about finite elements as well as structural mechanics and how a real structure behave to be able to establish a realistic model.

The choices concerning element type and properties affect the computational capacity. It is therefore important to think about the purpose of the model, the degree of detail level needed and which results that are desirable when choosing element types for an FE-model. For example, if a concrete beam is to be analysed and the results of interest are sectional forces, a simple beam element can be used; but if the desired results are crack propagation, an element type that can represent such a behavior needs to be used, for example a shell element.

The element types are characterized by four aspects, degrees of freedom, number of nodes, mathematical theories and integration (Simulia 2009b).

The fundamental parameters that are calculated during analysis are called degrees of freedom. For structural analyses the degrees of freedom are the possible movements of an element at each node, translation and rotation. If the element has nodes only in its corners, linear interpolation is used and the element is often called linear- or first-order element. It is possible to have extra nodes in between the corner nodes, then quadratic interpolation is used and the element is often called quadratic- or second-order element. In Figure 2.7 a first-order shell element and a second-order shell element is shown.

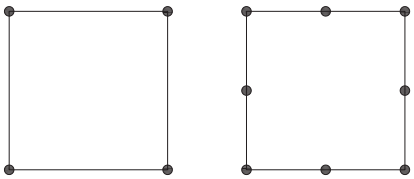

(a) *(b)*

Figure 2.7 a) A first-order shell element with four nodes and b) a second-order shell element with eight nodes.

Each element has a number of integration points within its boundary, see Figure 2.8, more points gives a more accurate result. It is in these points the stiffness matrix is evaluated and where the material response, including the sectional forces, are calculated. For very simple models, analytical solutions can be made however for most models it is not a good solution and numerical integration is used instead. There are different mathematical methods that can be used, the most common is Gauss integration. In Brigade/PLUS it is also possible for some elements to use reduced integration, where there is only one integration point located at the centre of the element. The choice of full or reduced integration can have a large effect on the accuracy of the result and the computational cost (Simulia 2009b).

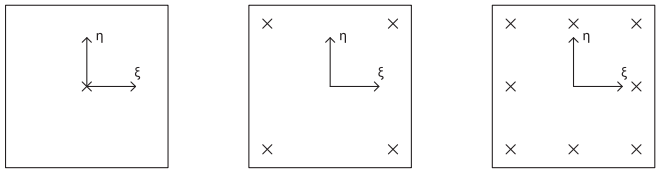

(a) *(b)* *(c)*

Figure 2.8 Locations for integration points with Gauss integration with a) one, b) four and c) nine integration points, adopted from (Ottosen and Peterson 1992).

2.2.1 Beam elements

A beam element is a one dimensional approximation of a three dimensional problem and can be used in both two and three dimensional models. The simplification to one dimension is only possible to make with the assumption of a slender element where the height of the cross section is relative small compared to the length of the element. A first-order beam element has one node at each end and has, if placed in a three dimensional space, three translational and three rotational degrees of freedom in every node, see Figure 2.9. The advantages of a beam element is the simplicity in the geometry, which results in short computational time.

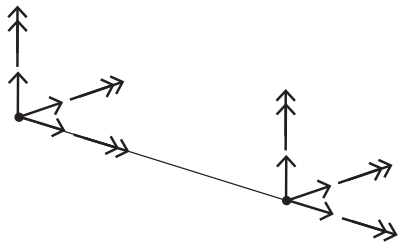

Figure 2.9 Degrees of freedom in a beam element; three translational and three rotational in each node.

In Brigade/PLUS there are several beam elements, using different assumptions and calculation methods. The beam elements based on the Euler-Bernoulli beam theory, with small strains and large rotations, use cubic interpolation. Beam elements with large strains and large rotations uses linear or quadratic interpolation and are based on the Timoshenko beam theory. The latter elements are according to the Timoshenko beam theory only valid for beams with a small length to height ratio, but in Brigade/PLUS the elements are designed to work for slender beams as well (Simulia 2009b).

According to the definition of the differential equation, see Section 2.1.1, the stresses and deformations in a model using beam elements are calculated in the integration points and interpolated to the nodes of an element. Hence, the sectional forces at these points can be calculated without any post-processing after finishing the analysis. In Brigade/PLUS there are three translational forces and three rotational moments that can be extracted from all nodes, see Figure 2.10 (Simulia 2009b).

The three translational forces are:

- SF1 - Axial force
- SF2 - Transverse shear force in local 2-direction
- SF3 - Transverse shear force in local 1-direction

The three rotational moments are:

- SM1 - Bending moment around the local 1-axis
- SM2 - Bending moment around the local 2-axis
- SM3 - Twisting moment around the beam axis

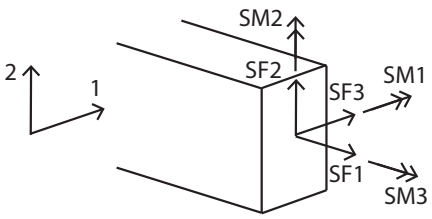

Figure 2.10 Definition of the local coordinate system of a beam element in Brigade/PLUS and the possible sectional forces and moments to be extracted after analysis.

2.2.2 Shell elements

There are three common types of elements used to model structures where the third dimension, the thickness, is relatively small compared to the extent in the other directions; plate, membrane and shell elements. They are represented as a surface and the thickness is taken into account in the element properties. Plate elements are based on plate theory and can only carry load in the direction perpendicular to its plane. Hence, no normal force acts in the plate, the only forces available are normal force perpendicular to the plane and bending of the plate, as described in Section 2.1.2, see Figure 2.11a. If the structure is loaded in another direction there will be a membrane action, such elements are called membrane elements. A membrane element has only normal forces acting in the two directions of the plane, see Figure 2.11b, and can be used when plane stress elasticity is applicable (Ottosen and Peterson 1992).

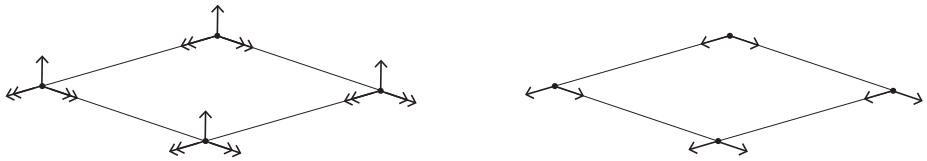

Figure 2.11 a) Degrees of freedom for a plate element and b) degrees of freedom for a membrane element.

A shell element is a combination of a plate element and a membrane element and can be loaded both in plane and out of plane directions. The bending of the plate and the membrane action will be treated separately, using the plate theory and the plane stress elasticity (Ottosen and Peterson 1992). A shell element usually has four nodes with five degrees of freedom, three translational and two rotational, in each node. Due to possible problems with convergence some shell elements have a sixth degree of freedom, the rotation around the axis normal the the plane, see Figure 2.12. However, this degree of freedom is not associated with stiffness.

In Brigade/PLUS it is also possible to use reduced integration hence, there will be only one centered integration point in an element. This reduces the computational time and the consequence is that the sectional forces are only calculated in one point and is therefore constant over the element (Simulia 2009b).

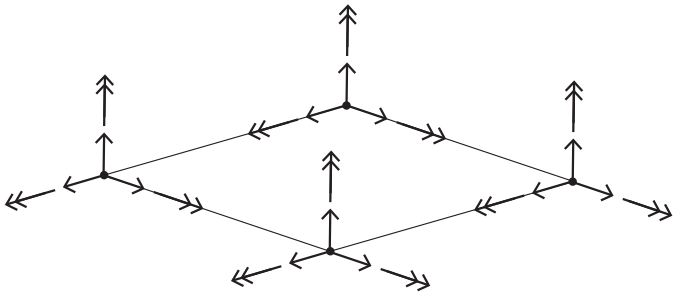

Figure 2.12 Degrees of freedom in a shell element; three translational and three rotational in each node.

In Brigade/PLUS the shell elements are divided in general-purpose shell elements, thin shell elements and thick shell elements. The thin shell elements and the thick shell elements are based on the Kirchhoff plate theory and the Mindlin-Reissner plate theory respectively. The choice of element type should be made considering if shear stresses are important or negligible. The general-purpose shell elements are a combination of the other two and can describe shear. If the element is thick, Mindlin-Reissner plate theory is used and Kirchhoff plate theory is used when the thickness decrease (Simulia 2009b).

As for beam elements, the displacement and stresses are obtained in the integration points and interpolated to the nodes of the elements. In Brigade/PLUS there are five translational forces and three rotational moments that can be extracted from all nodes (Simulia 2009b), see Figure 2.10. It is important to notice that the third bending moment is not the twisting moment of a node but rather the twisting of the element.

The five translational forces are:

- SF1 - Direct membrane force per unit width in local 2-direction
- SF2 - Shear membrane force per unit width in local 1–2 plane
- SF3 - Shear membrane force per unit width in local 1–2 plane
- SF4 - Transverse shear force per unit width in local 1-direction
- SF5 - Transverse shear force per unit width in local 2-direction

The three rotational moments are:

- SM1 - Bending moment around the local 2-axis
- SM2 - Bending moment around the local 1-axis
- SM3 - Twisting moment force per unit width in local 1–2 plane

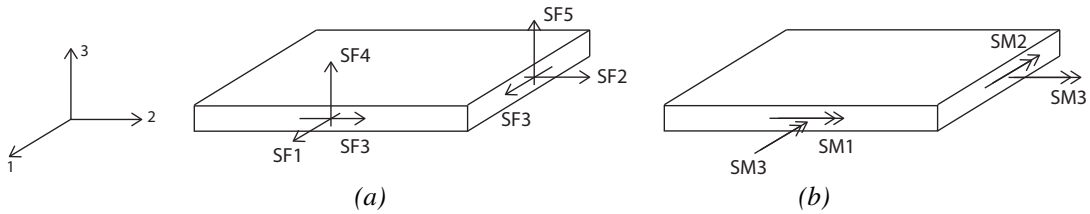

Figure 2.13 Definition of the local coordinate system of a shell element in Brigade/PLUS and the possible a) sectional forces and b) moments to be extracted after analysis.

2.3 Interaction between elements

When different element types are used in an FE-model, interactions between the elements are required to create a global structure. In Brigade/PLUS there are a lot of possible interactions, in this master thesis kinematic coupling constraint, connector elements and surface-based tie constraint are used.

The kinematic coupling constraint is used to connect two nodes by defining one node as the reference node and the other as the coupling node. The degrees of freedom that shall be constrained are then specified. The reference node has all the translational and rotational degrees of freedom while the coupling node will have the specified constrained degrees of freedom eliminated. By this elimination, the computational time of the FE-model is reduced, however the output is limited in the point of connection. If all the translational and rotational degrees of freedom are eliminated, the coupling node follows the reference node completely and the nodes will move as a rigid body (Simulia 2009a).

The connector element can be used to connect two elements that are not geometrically connected to each other. The constrained translational and rotational degrees of freedom shall be specified, and in contrast to the kinematic coupling constraint, the connector element constraints the degrees of freedom but does not eliminate the them (Simulia 2009a). This constraint is more computational demanding compared to the kinematic coupling constraint, however it is possible to extract forces and moments in all degrees of freedom.

The surface-based tie constraint is constraining all the translational and rotational degrees of freedom of the nodes in one surface, called the slave surface, to the closest nodes in another surface or three-dimensional beam, called the master surface. The translation and rotation of the nodes on the slave surface are rigid to the nodes in the master surface and no relative movement between the surfaces will occur (Simulia 2009a).

The chosen master surfaces can either be an element-based or a node-based surface, see Figure 2.14 and Figure 2.15. For an element-based master surface, the node on the slave surface is constrained to the closest node on the master surface within the position tolerance. The default position tolerance in Brigade/PLUS ensures that the nodes on the master and slave surfaces are close to each other. The position tolerance can also be specified by the user or a node set from the slave surface can be specified to be constrained regardless of the distance to the nodes on the master surface. For a node-based master surface the nodes on the slave surface are constrained to all the nodes on the master surface within the position tolerance (Simulia 2009a).

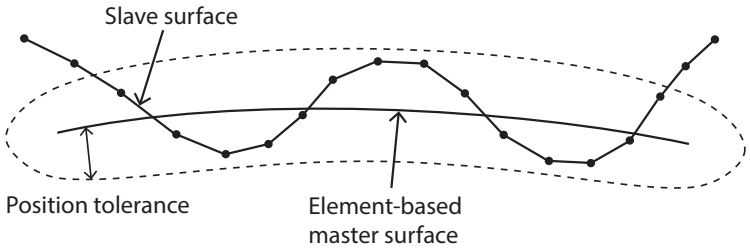

Figure 2.14 Slave surface constrained to an element-based master surface within the position tolerance, adapted from (Simulia 2009a).

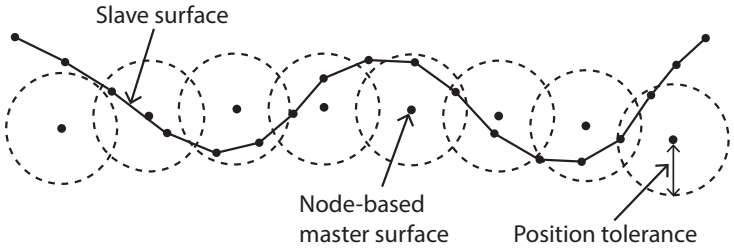

Figure 2.15 Slave surface constrained to a node-based master surface within the position tolerance, adapted from (Simulia 2009a).

2.4 Stress integration

When extracting results from a model in brigade/PLUS there are several methods to use, one of them is *Free body cut*. Normally, deformations and stresses are calculated individually in the nodes of an element. If the model is created using shell or solid elements is it possible, with *Free body cut*, to calculate sectional forces such as normal and shear forces and bending moment for a specific predefined section (Scanscot Technology AB 2015).

A *Free body cut* is dependent on the mesh and is therefore created after the mesh has been generated. The first step is to decide the extension of the section of interest and then to select the edges related to that section, see Figure 2.16a. The next step is to assign a direction for a normal vector, which will be created in the same direction for all edges. If the sectional forces are of interest in several cuts along a line a sweep option can be used. The desired number of cuts can be defined together with a number of intermediate elements to be skipped between two sweep definitions and the program will generate several *Free body cuts* in a row, see Figure 2.16b.

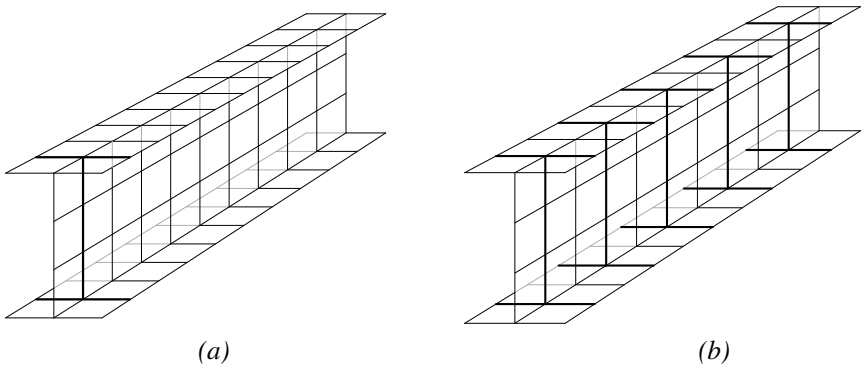

Figure 2.16 a) The selected edges of the section of interest of the Free body cut are defined. b) Several Free body cuts are generated by the sweep definition.

After defining the section for the *Free body cut* the program will calculate its centre of gravity and the average normal vector. If a normal vector of a single edge deviate from the chosen normal vector more than 60 degrees, this edge will not be included. Hence, the *Free body cut* is dependent on the shape of the mesh and it is important to have a structured mesh. Finally, the sectional forces and sectional moments are calculated by integration of the internal nodal forces from the adjacent elements in the negative normal direction, see Figure 2.17. These values are then summarised and presented in the centre of gravity of the section.

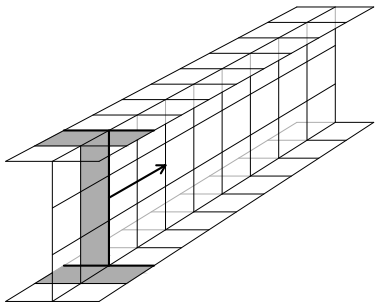

Figure 2.17 The internal nodal forces from the adjacent elements in the negative direction of the normal, used to calculate the sectional forces.

It is important to remember that the *Free body cut* is mesh dependent. The choice of critical section must therefore be made before running the analysis, consequently it is not possible to look at the deformed shape and stress distribution before defining the critical section. The mesh dependency also means that the *Free body cut* needs to be repeated if the mesh is changed (Scanscot Technology AB 2015). It is therefore convenient to create a suitable mesh before defining the *Free body cut* to avoid additional work.

2.5 Material properties

Since the FE-model should describe the behaviour of a real structure, the material behaviour is an important part of the modelling procedure. The bridge analysed in this master thesis consists of steel and concrete, which behaviours are described in the following sections.

2.5.1 Concrete

A concrete structure behaves differently in compression and in tension, see Figure 2.18. In either case, micro cracks will form evenly distributed in the material. When subjected to compressive stresses the micro cracks will remain uniformly spread throughout the whole loading process until failure in crushing. It is then safe to assume that the concrete can be modelled as a homogeneous and isotropic material and to use plasticity models with stress-strain as a constitutive relation. The stress-stain relationship for linear models can be determined from load-displacement curves measured in laboratory tests. The strain is defined as the elongation of the specimen divided by the initial length (Plos 1996).

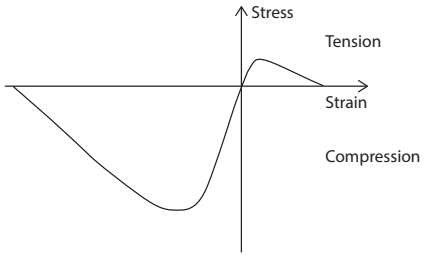

Figure 2.18 Typical stress-strain relation for concrete.

When the concrete is loaded in tension, in contrast to when loaded in compression, the micro cracks will concentrate in a small area and form larger cracks. Before cracking a linear elastic model can be used, however, when the concrete structure has cracked, it is no longer possible to assume a homogeneous and isotropic material and a new material model based on fracture mechanism that takes non linear behavior into account is needed (Plos 1996).

2.5.2 Steel

Steel is characterised as a linear elastic material up until it reaches yielding, see Figure 2.19. The strength of steel is defined as the strength where the material behavior is no longer linear, i.e. at its yield strength f_{yd}. If the material is loaded and unloaded before the yield point the deformation will go back to its original value. When the material reaches yielding it experience plastic deformations that will remain after unloading. After yielding it is possible to increase the strength even more due to hardening of the material but this extra capacity is rarely taken into consideration in design and elasto-plastic models with perfect plasticity are used.

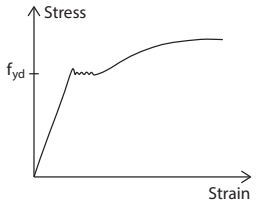

Figure 2.19 Typical stress-strain relation for steel.

Steel structures can be exposed to serious damages that cause failure even for stresses well below to yield strength. This is because of fatigue which occurs when a structure is subjected to repeated or varying load below stresses that otherwise would not cause any damage. Fatigue damage is permanent and takes many repetitions of loading to develop. It localizes in a few points where the stresses are concentrated or at local defects in the material.

Bridges are always subjected to varying load from traffic and it is therefore very important to consider fatigue when designing steel bridges. It is important to carefully design the details in a manner that lower the stress concentrations and increases the fatigue life. Fatigue life is defined as the number of loading cycles that is needed to cause failure. It is affected by many factors, some load related, for example amplitude of loading and number of repetitions, and some related to the structure, for example which types of connections to use and how they are shaped.

2.6 Loads

When designing a bridge there are several load cases that needs to be considered. The load cases studied in this master thesis are uniformly distributed load, temperature load and traffic load and the theory behind them are presented in the following section.

2.6.1 Distributed load

A distributed load can be the self weight of the bridge or for example paving on the bridge deck. The bridge is constructed in steps, where the concrete deck is cast over the erected steel structure. The interaction between the deck and the steel beams starts to work first after hardening of the concrete. Hence, the self weight is applied on the structure before the interaction is complete and will thereby not cause any restraining forces. On the other hand, other distributed loads are applied when the bridge is completed, consequently restraining forces may occur, which will be discussed in Section 3.2.1.

2.6.2 Temperature load

Deformations in a structure that occur independent on the present stresses results in non-mechanical strains, which does not produce stresses. In concrete structures there are especially two sources for non-mechanical strains; shrinkage and temperature changes. If the structure is free to move there will be no stresses due to deformations caused by non-mechanical strains, but if it is prevented to move restraining stresses may occur.

When a structure is subjected to a positive or negative temperature change it wants to elongate or shorten. The resulting thermal concrete strain, ϵ_{cT}, is mainly dependent on two factors; the magnitude of the temperature change, ΔT, and the coefficient of thermal expansion, α_{cT}, see Equation (2.22) (Engström 2014). The coefficient of thermal expansion is different depending on which aggregate the concrete contains, but according to Eurocode 1992-1-1, (CEN 2005a) a value of $\alpha_{cT} = 1 \cdot 10^{-5}$ can be used for all types of concrete.

$$\epsilon_{cT} = \alpha_{cT} \cdot \Delta T \tag{2.22}$$

The concrete thermal strain can be uniform across the cross section but it can also vary linearly or non-linearly, see Figure 2.20. An uniform temperature distribution is rarely found in reality but is convenient to assume for approximate calculations. If the temperature distribution is non-linear but has the same temperature on both the top and the bottom side and the thickness of the cross section is reasonable, a uniform distribution is a good approximation, on the other hand if the temperature is different at both sides non-uniform linear distribution is better (Engström 2014).

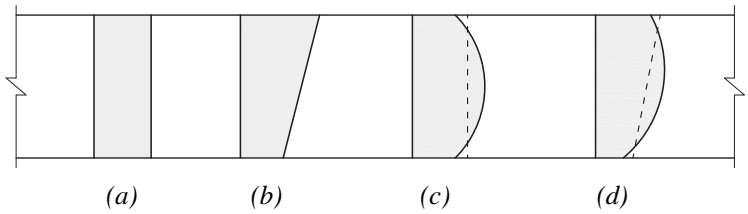

Figure 2.20 a) Uniform temperature distribution, b) linear temperature distribution, c) non-linear distribution that often can be simplified to uniform distribution and d) non-linear distribution that often can be simplified to linear distribution.

2.6.3 Traffic load

One of the most important load to consider when designing bridges is the traffic load. The rules and guidelines on how to do this is regulated in Eurocode 1991-2 (CEN 2007). There are different load models depending on the type of load on the bridge, and for road bridges there are four load models, LM1-LM4. The load models do not describe real loads, but the loads represent the same effects as for real traffic load (CEN 2007). Generally when designing bridges, LM1 and LM2 needs to be checked, but for simplicity only load model LM1 will be included in this analysis.

The first step, independent of load model, is to divide the carriageway width, w_c, into a number of lanes, with a width w_{c1} and a remaining area, according to table Table 2.1. They are placed and numbered according to Figure 2.21. The lane that provides the most unfavorable effect should be named 1 and the second most unfavorable lane should be named 2 and so on.

Table 2.1 Number of lanes and their width (CEN 2007).

Carriageway width, w_c	Number of lanes	Width of a lane, w_{c1}	Width remaining area
$w_c < 5.4\,\text{m}$	$n_1 = 1$	$3\,\text{m}$	$w_c - 3\,\text{m}$
$5.4\,\text{m} \leq w_c > 6\,\text{m}$	$n_1 = 2$	$w_c/2$	0
$6\,\text{m} \leq w_c$	$n_1 = int(w_c/3)$	$3\,\text{m}$	$w_c - 3 \cdot n_1$

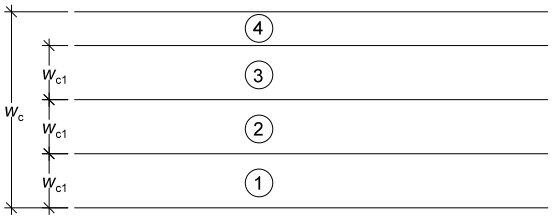

Figure 2.21 The carriageway width is divided into a number of lanes. Adapted from (CEN 2007).

LM1 contains concentrated as well as uniformly distributed forces and covers the main effects of traffic coming from cars, trucks and pedestrians. It should be used in global and local calculations. The load model is divided into two subsystems. The first one is a load group with two boogie axles each with a load of $\alpha_Q Q_k$, and the second one is uniformly distributed with a load of $\alpha_q q_k$. The load should be placed on every lane and on the remaining area in a manner described in Figure 2.22 and Table 2.2. α_Q and α_q are national adjustment factors that are used if the expected magnitude of traffic is different than the proposed one in Eurocode.

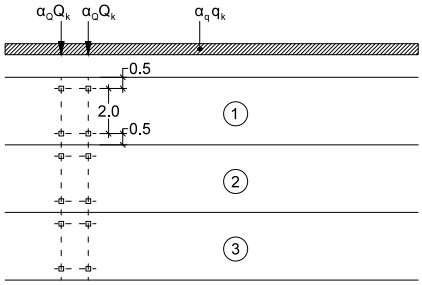

Figure 2.22 Positions of axle load and uniform load according to LM1. Adapted from (CEN 2007).

Table 2.2 Characteristic values for loads according to LM1.

	Boogie system Axle load Q_{ik} [kN]	Uniform load q_{ik} [kN/m^2]
Lane number 1	300	9
Lane number 2	200	2.5
Lane number 3	100	2.5
Other lanes	0	2.5
Remaining area	0	2.5

3 Preconditions

The bridge studied in this master thesis is based on the geometry of an existing tied arch bridge. The main structure is made of steel and consists of one arch on each side, longitudinal and transversal beams and bracings. The deck is made of concrete and is connected to the transversal beams by dowels. The geometry will be discussed further in Section 3.1

Due to the type of bridge and its geometry, restraining forces that are specific for the tied arch bridge may arise. How these restraining forces are affected by loading condition is discussed further in Section 3.2.

3.1 Geometry

The bridge studied in this master thesis is a tied arch bridge. It is a one lane road bridge, 33 m long and 6 m wide. The arch is shaped as an arc of an circle with an inner radius of 23 m. The bridge is supported on four points with roller supports. The bridge seen from the side is shown in Figure 3.1.

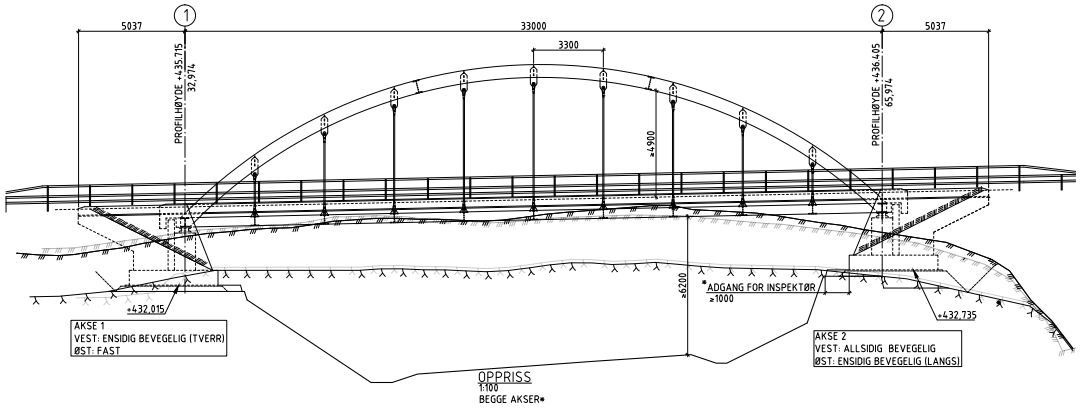

Figure 3.1 The bridge studied in this master thesis seen from the side.

On each side of the bridge there are nine hangers that are vertically straight and connected to the longitudinal beams. The longitudinal beams are connected to transversal beams that carries a concrete deck, see Figure 3.2 and Figure 3.3. Two transversal bracings are connecting the two arches, stabilizing the bridge in the horizontal direction.

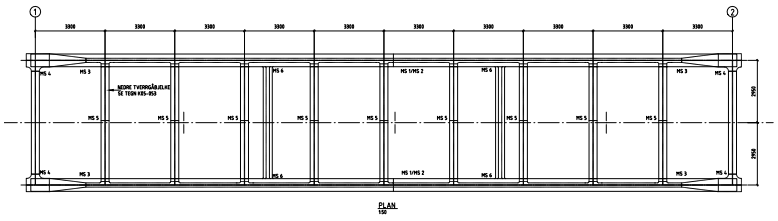

Figure 3.2 The transversal and longitudinal beams of the bridge studied in this master thesis seen from above.

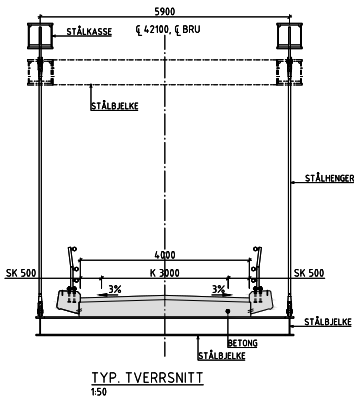

Figure 3.3 A section through the bridge studied in this master thesis.

The longitudinal beams, the transversal beams and the bracing have an I-shaped cross section. The arches have a box cross section and the hangers have a circular section. All the dimensions of the cross sections are shown in Table 3.1. For more dimensions and details, see drawings in Appendix A.

Table 3.1 Dimensions of the cross section of all main structural parts of the bridge.

Part	Dimensions	Cross section
Arch	$w_f = 600\,\text{mm}$ $t_f = 40\,\text{mm}$ $h_w = 530\,\text{mm}$ $t_w = 20\,\text{mm}$	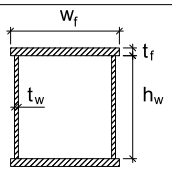
Longitudinal beam	$w_f = 200\,\text{mm}$ $t_f = 30\,\text{mm}$ $h_w = 382\,\text{mm}$ $t_w = 16\,\text{mm}$	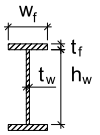
Transversal beam	$w_f = 38\,\text{mm}$ $t_f = 36\,\text{mm}$ $h_w = 370\,\text{mm}$ $t_w = 16\,\text{mm}$	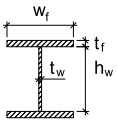
Bracing	$w_f = 300\,\text{mm}$ $t_f = 40\,\text{mm}$ $h_w = 530\,\text{mm}$ $t_w = 20\,\text{mm}$	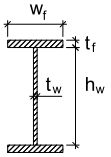
Hanger	$r_{ha} = 24\,\text{mm}$	
Deck	$h_{de} = 380\,\text{mm}$ $w_{de} = 4\,\text{m}$	

3.2 Problem description

Depending on how the bridge is loaded, different phenomena can give rise to restraining forces. The effects that will be studied in this master thesis are the elongation of the lower chord due to vertical loads, the deformation of the concrete deck due to a temperature change and the local deformation due to concentrated loads. In the following sections the theory behind the effects will be explained.

The magnitude of the restraining forces is dependent on the stiffness in the weak direction of the transversal beams. When designing a bridge, this phenomena can cause problems since increasing the stiffness of the beam attracts more load. Due to the stiffness dependency, increasing the cross section may be an insufficient solution. The restraining forces may not be decisive in the ultimate limit state and may not cause failure of the structure, however, the fatigue strength of the structure is highly affected.

The transferring of load through the structure is a crucial part to understand how the phenomena causing restraining forces work. A vertical load is transferred through the structure as following and according to Figure 3.4.

1. The main load acts on the deck that distribute the load in the longitudinal direction to the transversal beams.
2. The transversal beams divide the load in the transversal direction to the longitudinal beams.
3. The load is transferred vertically through the hangers to the arches.
4. The arches transfer the load to the ends of the arches.
5. The load will either be carried by heavy foundation or by tension in the lower cord.

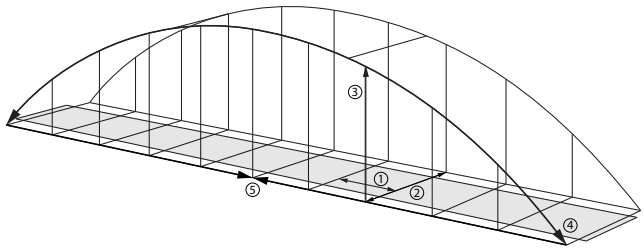

Figure 3.4 The steps that the load is transferred through the structure in a tied arch bridge.

Due to the inclined compression force from the arches the resulting forces at the support will be inclined as well. The horizontal component of the reaction forces can either be carried by heavy foundations, transferring the force to the ground, see Figure 3.5a or by a lower cord working in tension and connected to both ends of the arch, see Figure 3.5b. The latter one is called a tied arch bridge, which is the bridge of study in this master thesis. The lower chord must be suitable to work in

tension and can either be made with a large amount of reinforcement in the concrete deck or by steel beams as is the case for the bridge studied in this master thesis. If the lower chord is made of steel beams, restraining forces may develop as a consequence of movements of adjacent structural parts.

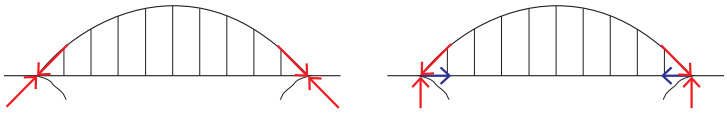

Figure 3.5 Force pattern in a) an arch bridge and b) a tied arch bridge.

3.2.1 Elongation of lower chord

The bridge studied in this master thesis has a lower cord consisting of longitudinal steel beams. As described in Section 3.2 the beams are supposed to compensate the inclined compression forces from the arch by working in tension. These tensional forces will result in elongation of the longitudinal beams. The transversal beams, connected to the longitudinal beam, wants to follow this elongation. Since the transversal beams are connected to the concrete deck, the transversal beams are prevented to move freely. This prevention of movement may result in restraining forces. The restraining forces can cause secondary bending in the weak axis of the transversal beam, see Figure 3.6. The secondary bending of the transversal beams will be larger near the ends of the bridge, since the elongation of the longitudinal beams are larger the further away from the middle, and therefore the transversal beams located at the ends will be the most exposed ones.

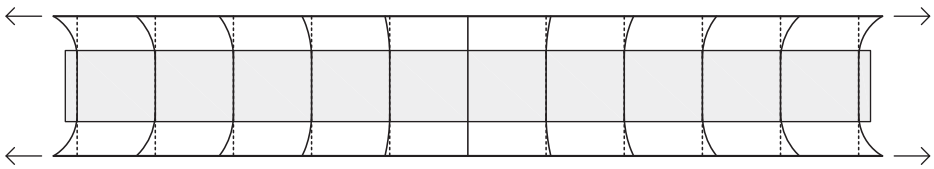

Figure 3.6 Elongation of the longitudinal beams may cause movement in the transversal beams which are prevented to move by the concrete deck.

3.2.2 Temperature

For the bridge studied in this master thesis only a uniform negative change of temperature will be considered since the behaviour of interest is when the concrete deck shortens and the steel structure prevents the movement. The temperature change will be added to the concrete deck only, resulting in a temperature difference between the concrete and steel elements. The concrete deck will shrink due to the negative temperature change and the transversal beams wants to follow the movement. Since the transversal beams are prevented to move by the longitudinal beams, restraining forces can arise and the transversal beams may be subjected to secondary bending, see Figure 3.7.

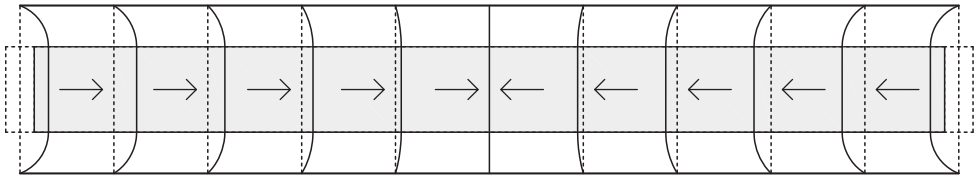

Figure 3.7 Shrinkage in the concrete deck may cause movement of the traversal beams that are prevented to move by the longitudinal beams, which may result in secondary bending in the transversal beams.

3.2.3 Local effects from a concentrated load

A bridge is rarely subjected to only uniformly distributed load, but rather to a traffic load that consists of a combination of distributed and concentrated loads. A concentrated load acting on the bridge deck can cause local effects that needs to be considered. If the bridge studied in this master thesis is subjected to a concentrated load placed in between two transversal beams, the deck will deflect locally at the point where the load is placed. With the deflection, a small horizontal movement of the deck may occur and and the transversal beams follow this movement, see Figure 3.8. Since the transversal beams are connected to the longitudinal beams, that do not want to move, the movement is prevented and restraining forces can arise. These restraining forces may cause secondary bending in the transversal beams.

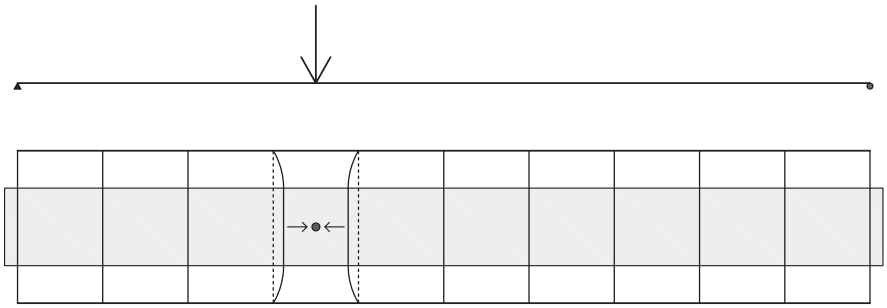

Figure 3.8 A concentrated load between two transversal beams may cause deflection and horizontal movement of the deck. The transversal beam wants to follow the deck but are prevented to move by the longitudinal beams, which may result in secondary bending in the transversal beams.

3.3 Influence on the secondary bending moment

The magnitude of the restraining forces is dependent on the stiffness in the weak direction of the transversal beams. If the beam is stiff it will attract more load and thereby more restraining forces and higher secondary bending moment. If the beam, on the other hand, is weak it will be subjected to less restraining forces but it will also have less capacity. This phenomena causes problem when designing bridges of this type.

How much secondary bending the transversal beam is subjected to and the shape of the secondary bending moment curve depends partly on the stiffness of the connection between the transversal beam and the longitudinal beam and the connection between the transversal beam and the concrete deck, see Figure 3.9. If the connection is fully stiff the moment will be high, as for the moment in the connection for a fixed beam, see Figure 3.10a. If the connection has no stiffness the moment in that point will be zero, as for a simply supported beam, see Figure 3.10b. A connection can never be fully stiff or without stiffness but rather somewhere in between. The secondary bending moment in the transversal beams will therefore be related to the level of stiffness in the connection.

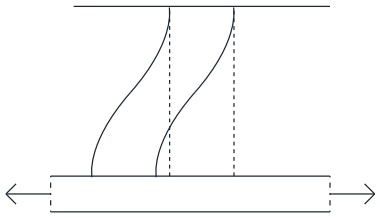

Figure 3.9 Elongation of the longitudinal beams can cause secondary bending in the transversal beam and dependent of the stiffness of the connection the amplitude of the secondary bending moment may differ.

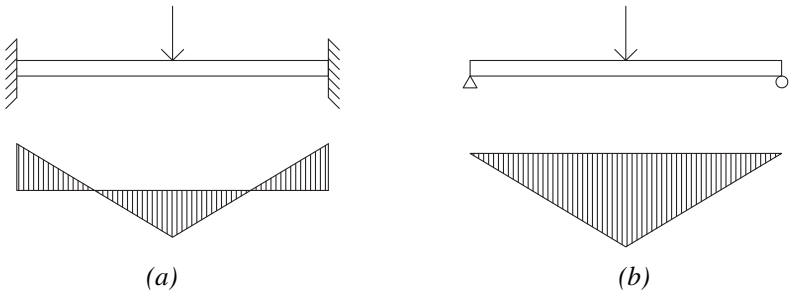

Figure 3.10 Moment distribution of a) a fixed and b) a simply supported beam. The rate of stiffness in the connection affects the moment distribution.

4 Model description

The bridge was modelled with three different modelling techniques, with different level of complexity. The first and the simplest model, which demands the least computational and development time, consisted of only beam elements which for the deck conform a beam grillage. It is hereafter refereed to as level 1 and the model can be seen in Figure 4.1. In the second model, a higher level of complexity, the bridge deck was modelled using shell elements and the remaining part of the bridge was modelled using beam elements. This model is hereafter refereed to as level 2 and can be seen in Figure 4.2. The third and most complex model was modelled in more detail to capture the real behavior in the areas of interests and to be able to evaluate the accuracy of the results from level 1 and 2. This model demands the highest computational capacity. It is hereafter refereed to as level 3 and can be seen in Figure 4.3. In the following chapter the modelling process and the simplifications and assumptions that were made are presented.

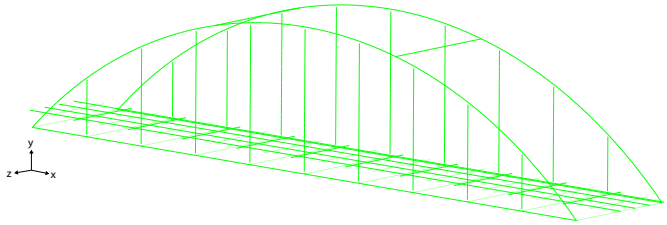

Figure 4.1 The bridge modelled in level 1. The deck modelled as beam grillage.

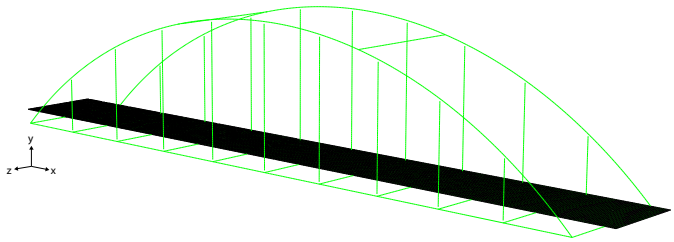

Figure 4.2 The bridge modelled in level 2. The deck modelled using shell elements.

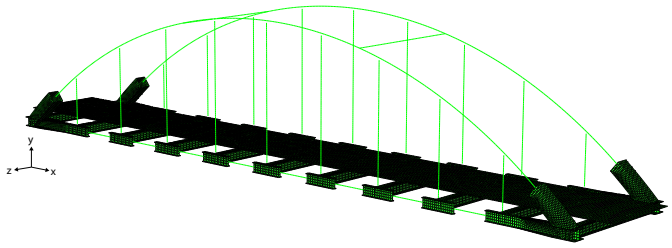

Figure 4.3 The bridge modelled in level 3. The deck and beams modelled using shell elements.

4.1 Geometry

When modelling the bridge, some simplifications were made with regard to the geometry. The simplifications were made to make the modelling simpler and it will insignificantly affect the global behaviour of the bridge and the desired sectional forces. The inclination of the bridge in the longitudinal direction was disregarded in the models and the bridge was modelled horizontally. The bridge deck has a varying cross section height in the transversal direction, this was neglected in the models and the height of the bridge deck was modelled as an average height. The reinforcement in the bridge deck was disregarded. The changes in the longitudinal beam geometry in the supports zone where it meet the arch are neither considered in level 1 and 2.

4.2 Element type

4.2.1 Level 1

In level 1 the bridge deck was modelled as a beam grillage with longitudinal and transversal beams. In the longitudinal direction, the deck was divided in four equal sized beams, each with a width of 1 m. In the transversal direction, the beams were placed right above the transversal steel beams. When the steel beam and concrete deck is connected they will work as a composite section and according to Eurocode 1992-1-1 (CEN 2005a), only a part of the concrete deck can be assumed to contribute to the composite action. The effective flange width, b_{eff}, is calculated according to Eurocode 1992-1-1 (CEN 2005a) using the thickness of the web of the transversal beam, b_w, the center to center distance of the mid parts between the transversal beams, b, and the distance between the zero moment points, l_0, see Equation (4.1).

$$b_{eff} = \sum b_{eff,i} + b_w \leq b \tag{4.1}$$

$$\text{where} \quad \begin{aligned} b_{eff,i} &= 0,2b_i + 0,1l_0 \leq 0,2l_0 \\ b_{eff,i} &\leq b_i \end{aligned}$$

The calculated effective width was smaller than the distance between the transversal steel beams, so therefore an additional transversal beam was added in the beam grillage, with a width that is equal to the centre to centre distance between the transversal steel beams minus the effective width of the transversal beams in the beam grillage, see Figure 4.4, Figure 4.5 and Appendix D.

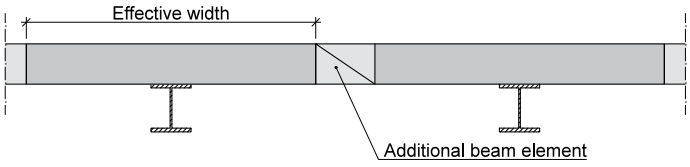

Figure 4.4 Cross section of the deck and steel beams in the transversal direction showing the effective width of the composite section and the additional transversal beam element.

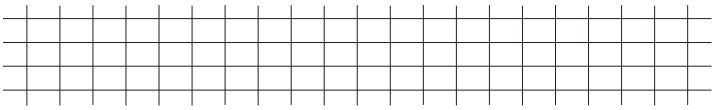

Figure 4.5 The arrangement of longitudinal and transversal beam in the beam grillage for level 1.

All elements in the model was modelled with the same beam elements, B31, which are based on the Timoshenko beam theory, described in Section 2.1.1. It has one node in each end of the element and therefore uses linear interpolation. They are suitable if the element are subjected to large axial strains, as described in Section 2.2.1 which is the case for some of the elements in this bridge, especially for the longitudinal beam. The different cross sections was defined according to the dimensions in Section 3.1.

4.2.2 Level 2

The same element type, beam elements B31, as in level 1 was used for the arches, the longitudinal and transversal beams and the bracings in level 2. The deck was modelled with a three dimensional shell element with four nodes and reduced integration, S4R, described in Section 2.2.2.

4.2.3 Level 3

In level 3, the more detailed modelled parts were modelled using shell elements. The cross section of the beams were built up by modelling the flanges and web as shell elements. Since the connection between the transversal beam and longitudinal beam has a large impact on the secondary bending of the transversal beams, a part of the longitudinal beam was also modelled using shell elements. In order to reduce the computational time needed, only a part of the longitudinal beam was modelled using shell, the remaining part in between were left as beam elements, see Figure 4.6. The length of the longitudinal beam modelled in shell elements was determined so that no stress concentration occurred in the connection of the shell element and the beam element. The length on each side of the transversal beam is equal to the height of the transversal beam. In order to get a realistic connection at the end of the bridge, where the arch is connected to the longitudinal beam, a small part of the arch was modelled using shell elements, see Figure 4.6. The type of shell element used for all detailed parts and the deck was S4R, the same element used for the deck in level 2. The beam element used was B31, the same as in level 1 and 2.

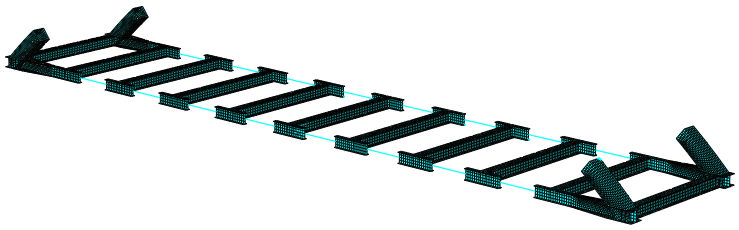

Figure 4.6 A part of the longitudinal beam was modelled with shell elements and a part was modelled with beam elements. A part of the arch was also modelled with shell elements.

4.3 Material properties

Two different materials were used in the models, concrete and steel. The material were modelled as elastic materials, and Young's modulus, E, poisson's ratio, ν, and the density, ρ, was defined. For concrete, the expansion coefficient, α_{cT}, was defined as well. The concrete used was C45/55, and the parameters for concrete were chosen according to Eurocode 1992-1-1 (CEN 2005a). The material parameters for steel was chosen according to Eurocode 1993-1-1 (CEN 2005b). The values for the different parameters is presented in Table 4.1.

Table 4.1 Material parameters for the materials used in the models.

Material	E [GPa]	ν	ρ [kg/m^3]	α_{cT}
Concrete (C45/55)	36	0.2	2500	$1 \cdot 10^{-5}$
Steel	210	0.3	7850	-

4.4 Interaction

The interaction between the different elements of the structure was taken into account in the model development. In level 1 and 2, the center lines for the arch and the longitudinal beam and the center lines for the arch and the bracing was modelled connected to each other. Their degrees of freedom should follow each other, so therefore the interaction between these parts could be modelled using the kinematic coupling constraint, as described in Section 2.3.

The hangers were modelled 0.1 m shorter at the top and the bottom and connector elements, described in Section 2.3, connects them to the arch and the longitudinal beams. The connector elements between the hangers and the longitudinal beams were modelled as a hinged connection, free to rotate around all axis and fixed translation in all directions. The connector elements between the hangers and the arches were modelled as a hinged connections as well, but fixed in the rotation around the y-axis. This was to prevent the hanger to rotate freely around the y-axis.

The transversal beams and concrete deck are in reality connected by dowels, that makes the two parts work as a composite section. There are several types of interaction that can be used to represent this interaction and an investigation was made, presented in Appendix B, to assess what kind of interaction was more suitable. The investigation showed that the interaction method surface-based tie constraint, described in Section 2.3, gave good results and was therefore used. In level 1 and 2, where the transversal beams were modelled using beam elements, one line on the deck was constraint to the beam element. In level 3, in order to represent the reality more accurately, where two rows of dowels with a distance of 250 mm are fixed on the transversal beam, two lines on the deck were constrained to two lines on the upper flange of the transversal beam.

4.5 Boundary conditions

The bridge is resting on four supports, one at each point where the arch is connected to the longitudinal beam. Due to deflection and temperature changes the bridge will have small movements in the horizontal x-, and z-direction. To avoid the extra stresses that develop from this movement the bridge should be able to expand freely in the x-, and z-direction. Normally, the boundary condition would be

modelled as shown in Figure 4.7a, with one support fixed in translation in all directions, one fixed in x-, and y-direction, one fixed in y-, and z-direction and one fixed in only the y-direction and with all supports free to rotate in all directions. However, the boundary condition used in this master thesis were modified. When using the common boundary condition in Brigade/PLUS, it results in reaction forces at the supports in the x-, and z-direction to prevent the rotation. These reaction forces is not present in reality, so to avoid these extra forces there has been some modifications in the boundary condition, see Figure 4.7b. All supports was modelled fixed in translation in the y-direction. One support was modelled fixed in translation in x-, and z-direction as well, and to prevent the rotational movement of the bridge, the support was also modelled fixed in rotation around the y-axis.

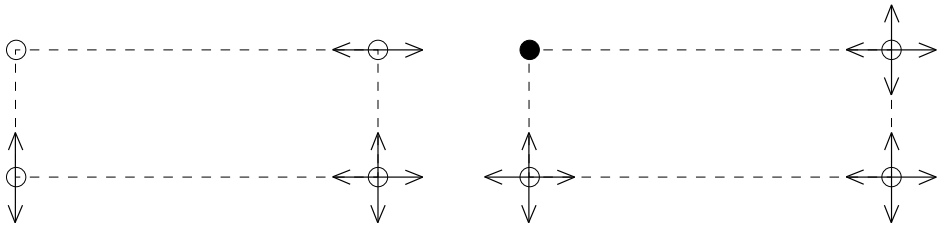

Figure 4.7 The arrows represent the possible movement at each support and the filled circle represent the rotation fixed in the y-direction. a) The boundary condition representing the reality best. b) The boundary condition used in this master thesis.

In level 1 and 2, the boundary condition were applied in the nodes connecting the longitudinal beams to the arches, see Figure 4.8a. The boundary condition were applied in only one node at each support in level 3 as well, see Figure 4.8b. When applying boundary condition to one node in a shell element it can result in stress concentrations. Since these stresses does not influence the global response and the areas affected are not of interest in this master thesis, the simplification of boundary condition in only one node is possible.

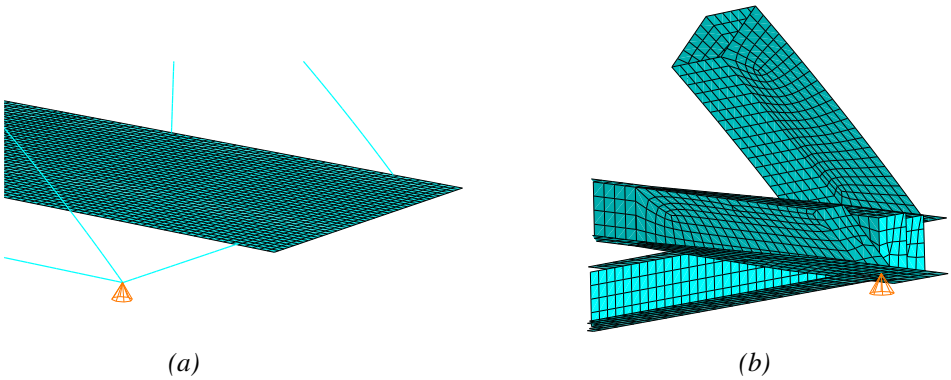

Figure 4.8 The boundary condition applied to a) level 1 and 2 and b) level 3.

4.6 Loads

In level 1, the uniformly distributed load, with a magnitude of 20 kN, was recalculated to a line load to be able to apply the load on the beam grillage. The distributed load was multiplied with the center to center distance of the transversal beam and the line load was applied on the beam grillage, with half of the magnitude on the transversal beams and half of the magnitude on the longitudinal beams, see Figure 4.9a. In level 2 and 3, the uniformly distributed load was applied as a pressure load on the whole deck surface, see Figure 4.9b.

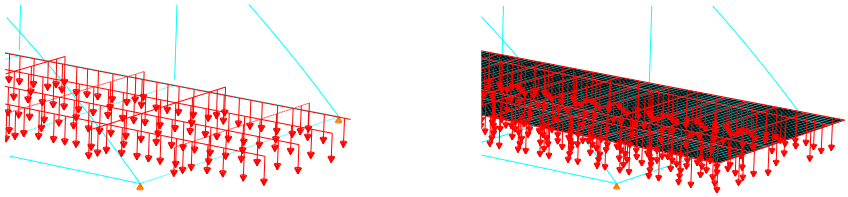

(a) *(b)*

Figure 4.9 *The uniformly distributed load applied on the deck as a) a line loads in level 1 and b) a pressure load in level 2 and 3.*

The aim with the temperature load is to study the response of the bridge when the concrete deck shortens while the steel structure prevents the movement, as described in Section 3.2.2. In order to represent this behavior the temperature load was applied only on the deck, with a temperature decrees of 10°.

There are predefined traffic loads in Brigade/PLUS that can represent LM1, described in Section 2.6.3, but the models become very time consuming. Hence, it was decided to model the traffic load manual, still according to Eurocode, with several concentrated and distributed loads. The concentrated loads represents the boggie axle loads and were place in the spans between the transversal beams and directly over the transversal beams. In Figure 4.10, an example of how the loads was placed over one transversal beam and in one span is shown. The distributed loads was placed in all spans between the transversal beams. The locations for the load was chosen to make sure that the worst case was covered. Since the concrete deck is four meters wide and one traffic lane is only three meters wide, the worst placement of the load is shifted to one side. Hence, in level 1 the line loads representing the distributed load was placed on three of the longitudinal beams and in level 2 and 3 the distributed load was placed according to Figure 4.10.

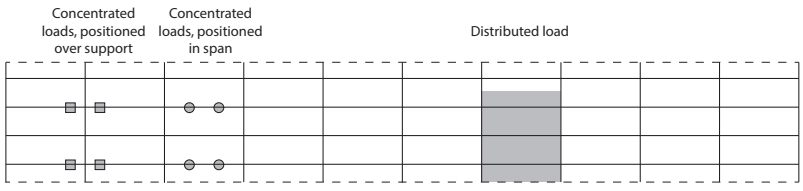

Figure 4.10 *An example of how the concentrated loads was placed over one transversal beam, in one span between the transversal beams and how the distributed load was placed.*

After defining the loads, the load combination tool from Brigade/PLUS was used to envelope the different concentrated loads to find the worst case for each element in the structure. The distributed loads in each span between the transversal beams were combined in such a way that the contribution of each load was only added if it was unfavorable.

4.7 Verification

A convergence study was made for all three models to decide a suitable mesh size. Different mesh sizes, from 0.5 m to 0.05 m, where tested and values for secondary bending moment in the most exposed transversal beam, bending moment in transversal direction in the deck and the deflection in mid span of the bridge were compared, see Appendix C.

Hand calculations were made to verify the models and the applied loads. By comparing the reaction forces for the self weight it was concluded that the models had the right geometry and that all elements had the right sections assigned. The values from the verification of the self weight can be seen in Table 4.2. The reason that the self weight differ in level 3 compared to level 1 and 2 is because the fact that level 3 was modelled more accurate, with a more detailed end part of the bridge including, among other, wider flanges and stiffeners.

For the uniformly distributed load case, the reaction forces and the bending moment in transversal direction in the middle of the bridge were compared. The reaction forces can easily be calculated by hand by dividing the load by four, assuming that the forces are equal in all four supports. When calculating the moment it is assumed that one transversal beam carry a distributed load which is equal to the load times the center to center distance. The assumption of a simply supported beam was made, with a load distribution according to Figure 4.11.

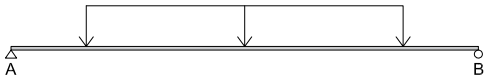

Figure 4.11 Calculation model for the transversal beam subjected to uniformly distributed load.

For the temperature load the reaction forces was verified. Due to the possibility of movement at the supports described in Section 4.5 the reaction force due to temperature change should be zero.

For the traffic load, the concentrated load and the distributed load, was verified separately, controlling reaction forces for both loads and bending moment in transversal direction in the middle of the bridge for the distributed load case. The concentrated load placed closest to the supports was verified and for the hand calculations it was assumed that the whole load was carried by the supports on one side. These two supports will not have the same reaction force due to the unsymmetrical placement of the load, and the reaction forces were calculated according to Figure 4.12.

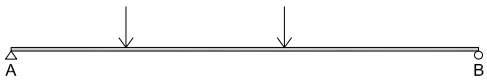

Figure 4.12 Calculation model for the transversal beam subjected to concentrated traffic load.

For the distributed traffic load it is assumed that the worst case for the reaction forces appear when the load are applied in all spans. All four supports will not have the same reaction force due to the unsymmetrical placement of the load, but it is assumed that half of the load is transferred in the longitudinal direction to each end of the bridge. The bending moment was calculated in the same way as for the uniformly distributed load case but for an unsymmetrical load. The assumption of a simply supported beam was made, with a load distribution according to Figure 4.13.

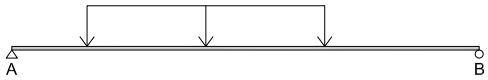

Figure 4.13 Calculation model for the transversal beam subjected to distributed traffic load.

The hand calculations were compared with values from the models in Brigade/PLUS. The reaction forces for each load case could easily be extracted from Brigade/PLUS and the comparison for the uniformly distributed load and the temperature load can be seen in Table 4.2 and for the traffic load in Table 4.3

Table 4.2 Verification of reaction force for uniform load and temperature load.

	Hand calculation [kN]	Brigade/PLUS [kN]	Difference [%]
Level 1			
Self weight	506.2	506.3	0.0
Uniform load	714.8	714.8	0.0
Temperature	0.0	0.0	0.0
Level 2			
Self weight	506.2	506.3	0.0
Uniform load	714.8	714.8	0.0
Temperature	0.0	0.0	0.0
Level 3			
Self weight	512.8	511.2	0.31
Uniform load	714.8	714.8	0.0
Temperature	0.0	0.0	0.0

Table 4.3 Verification of reaction force for traffic load.

	Hand calculation [kN]	Brigade/PLUS [kN]	Difference [%]
Level 1			
Distributed load R_A	282.1	281.5	0.21
Distributed load R_B	200.4	201.8	0.70
Concentrated load R_A	350.9	351.0	0.03
Concentrated load R_B	249.2	249.0	0.0
Level 2			
Distributed load R_A	282.1	281.3	0.28
Distributed load R_B	200.4	202.0	0.80
Concentrated load R_A	350.9	351.1	0.05
Concentrated load R_B	249.2	248.9	0.12
Level 3			
Distributed load R_A	282.1	282.6	0.17
Distributed load R_B	200.4	200.7	0.14
Concentrated load R_A	350.9	350.9	0.0
Concentrated load R_B	249.2	249.1	0.0

The transversal beam and the deck can be treated as a composite section working together in bending. The total sectional bending moment for such section is the bending moment for the transversal beam and the deck element together with the normal force multiplied with the eccentricity from the combined centre of gravity to the centre of gravity for each element, see Figure 4.14. The comparison for the uniformly distributed load and the traffic load can be seen in Table 4.4

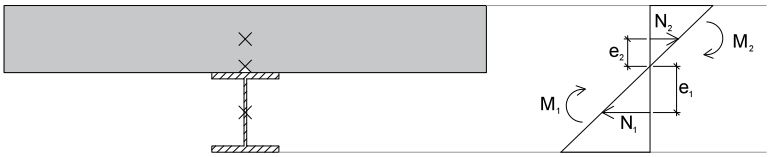

Figure 4.14 Stress distribution for composite cross section.

Table 4.4 Verification of the bending moment in the transversal beam

	Hand calculation [kN]	Brigade/PLUS [kN]	Difference [%]
Level 1			
Uniform load	257.4	248.6	3.42
Distributed traffic load	94.3	92.4	2.01
Level 2			
Uniform load	257.4	248.6	3.42
Distributed traffic load	94.3	92.0	2.44
Level 3			
Uniform load	257.4	248.5	3.46
Distributed traffic load	94.3	91.1	3.35

5 Results

The results from the analyses are presented in the following chapter and in Appendix E. The effect of the different modelling techniques on restraining forces are presented separately for the three load cases; uniformly distributed load, temperature load and traffic load. The results from a parametric study are presented and the effect of the stiffness in the weak direction of the transversal beams for the three modelling techniques is shown.

5.1 Post-processing

The FE-models in this master thesis are complex and produces large amount of data, hence the focus was put in the relevant results concerning the scope of the master thesis. The models are, for the uniformly distributed load case and the temperature load case, symmetrical in the transversal direction, hence the arches, the longitudinal beams and the hangers will show the same results on both sides of the bridge and thereby are only the results from one side of the bridge presented. The traffic load is not applied symmetrically, however the only difference between the two sides is the magnitude. Since the overall behavior of the structure is the same only the values from one side of the bridge are presented. The models are also symmetric in the longitudinal direction for all load cases, hence the transversal beams on each side of the mid span will have the same results and it is only necessary to discuss the results from one side.

The relevant forces and moments are presented in the arch, the longitudinal beam, the longitudinal direction of the deck and the transversal beams. The elements from where the results were extracted are highlighted in red and presented in Figure 5.1. The transversal beam are numbered from one to eleven, see Figure 5.2, and will hereafter be referred using the numbers.

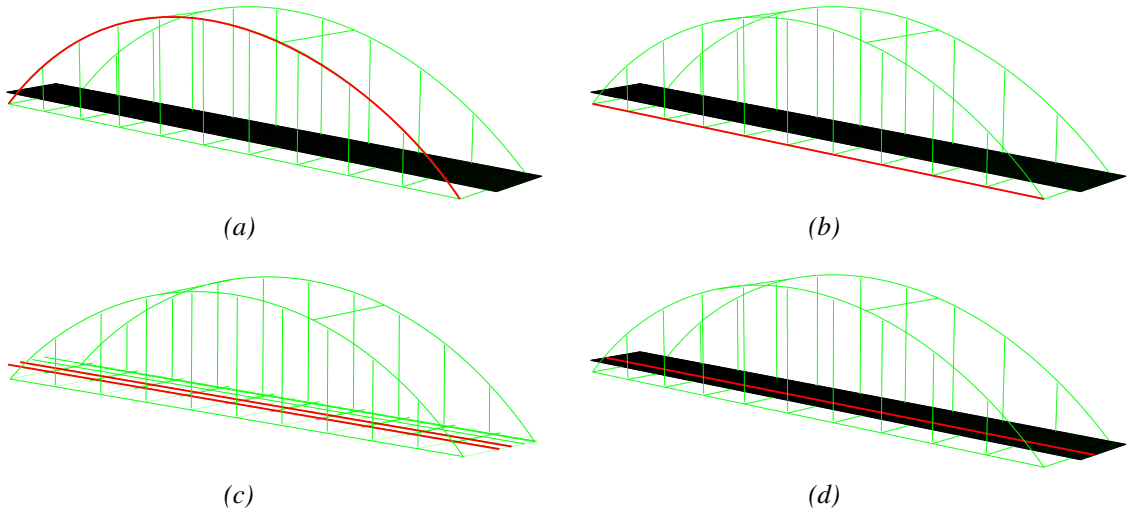

Figure 5.1 *The paths where the results are extracted from in, a) the arch, b) the longitudinal beam, c) the longitudinal direction of the beam grillage in level 1 and d) the longitudinal direction of the deck in level 2 and 3.*

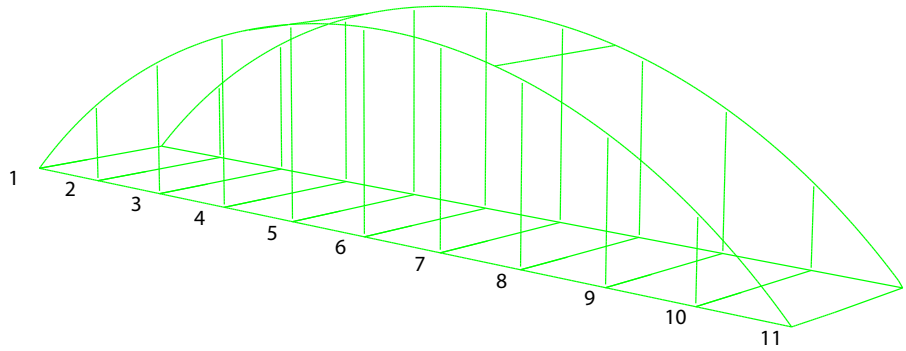

Figure 5.2 The transversal beams are numbered from 1 to 11.

Results extracted from parts modelled using beam elements are generated using the built in tool *Path* in Brigade/PLUS. For the parts modelled using shell elements the results are extracted using *Free body cut*, described in Section 2.4. The sections of the *Free body cut* are for the transversal and longitudinal beams defined as the whole cross section, with cuts at every element along the length of the beams, see Figure 5.3a. When using *Free body cut* the sectional forces and moments are calculated by integration of the internal nodal forces from the adjacent elements in the negative normal direction of the *Free body cut*, as described in Section 2.4. At an abrupt changed geometry the calculation method can give inaccurate results. In this master thesis difficulties occur at the immediate point where the transversal beam and the deck are connected. If the *Free body cut* is defined in one direction along the transversal beam the values at the immediate connection on both sides of the deck differ. At one side of the deck, the sectional forces and moments are integrated from the elements before the connection starts, in other words where the deck and transversal beam are not connected. However, at the other side of the deck the forces and moments will be integrated from the elements right before the deck ends, in other words where the deck and transversal beam are connected. To avoid this problem, the *Free body cut* is defined from the outside to the middle of the beam. The *Free body cut* in the longitudinal direction of the deck is defined in half the width of the deck, with cuts at every element along the length of the deck, see Figure 5.3b.

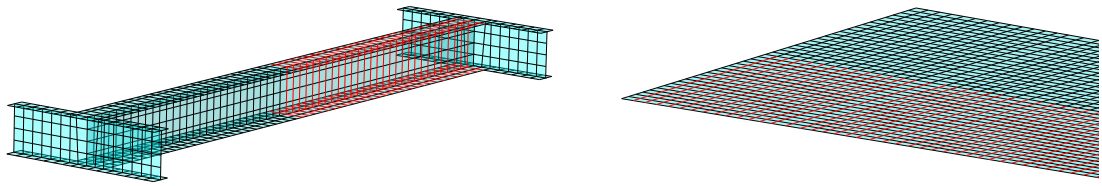

(a) *(b)*

Figure 5.3 The Free body cut defined in a) half the length of the transversal beam and b) the longitudinal direction of the deck.

Since level 3 is modelled in more detail using shell elements it require more attention to the mesh both in the modelling process and in the post-processing. When using *Free body cut* it is important

to have a structured mesh as discussed in Section 2.4. One of the areas modelled in detail is the connection between the arch and longitudinal beam. Since there are several parts with different sizes and shapes connected to each other the mesh is constructed using both triangular and quadrilateral shapes, see Figure 5.4. Hence, the mesh is not as structured as needed and it is hard to define a suitable *Free body cut*. As a result, the paths for the arch and the longitudinal beam does not include results from the first and last approximately 2 m for level 3.

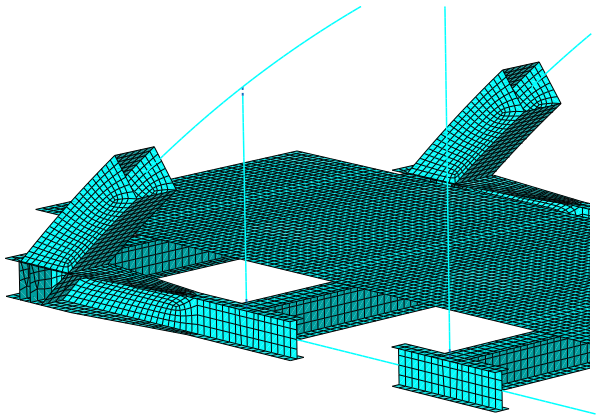

Figure 5.4 The area where the arch is connected to the longitudinal beam is modelled in more detail in level 3, resulting in an irregular mesh and difficulties to define a Free body cut.

Another difficulty in level 3 arises since the deck is constrained to the transversal beams in two lines using the surface-based tie constraint, as described in Section 4.4. When constraining two lines in the deck close to each other, the elements in between the lines are restrained from two directions, resulting in unrealistically high forces in those elements. These high forces have no significant influence in the overall results hence, they are removed from the results of the normal force in the longitudinal direction of the deck.

5.2 Effect of restraining forces

To investigate the main effects of the restraining forces, the secondary bending moment in the transversal beams is examined. The secondary bending moment is analysed in all transversal beams however the outermost transversal beams are the most exposed, as discussed in Section 3.2, and the focus will therefore be on the results from the first transversal beam. The majority of the results are presented in graphs where the values from all three levels are compared in the same graphs. All extracted results for all load cases are presented in Appendix E.

As discussed in Section 3.2, there are different effects that give rise to restraining forces; elongation of the lower chord, temperature change and local effects from a concentrated load. To distinguish and analyse these effects in a good way, results from the three load cases has been studied separately and are presented in the following three sections.

5.2.1 Uniformly distributed load

The global deformation of the bridge subjected to uniformly distributed load is presented in Figure 5.5. The contour plot shows the displacement in the direction vertical to the bridge. The overall behaviour is as expected, with a double symmetric deflection with its maximum at the middle. The deformation of the bridge seen from above is presented in Figure 5.6. The contour plot shows the displacement in the direction longitudinal to the bridge. The deformation of the transversal beams are as expected, when the longitudinal beams elongate, the deck prevents the transversal beams to deform freely and the transversal beams bend in the weak direction.

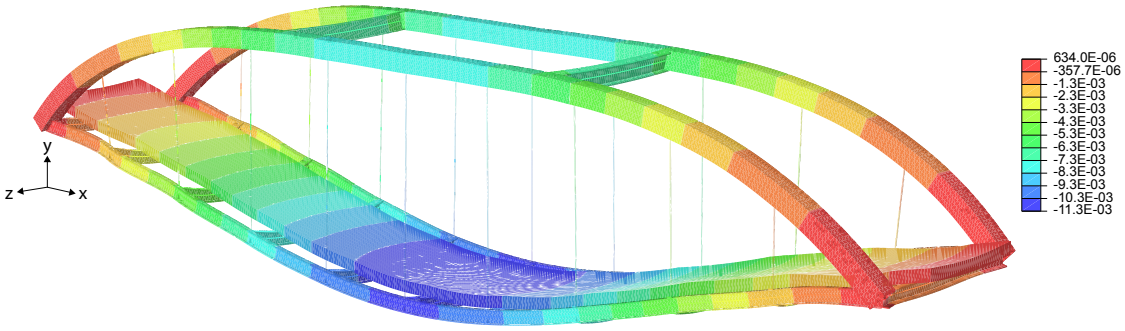

Figure 5.5 *Deformation of the bridge subjected to uniformly distributed load. The contour display the deformation in y-direction [m]. The displayed model is level 2, however all levels show the same global behaviour.*

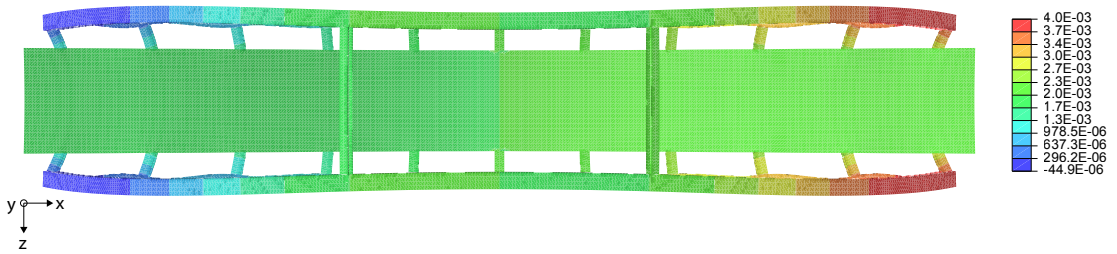

Figure 5.6 *Deformation of the bridge subjected to uniformly distributed load, seen from above. The contour display the deformation in x-direction [m]. The displayed model is level 2, however all levels show the same global behaviour.*

The bending moment and the normal force in the arch is presented in Figure 5.7 and Figure 5.8 respectively. They are similar in all three levels, which indicates that the same amount of force is transferred from the deck, through the hangers, to the arches, hence the global behaviour of the models are the same.

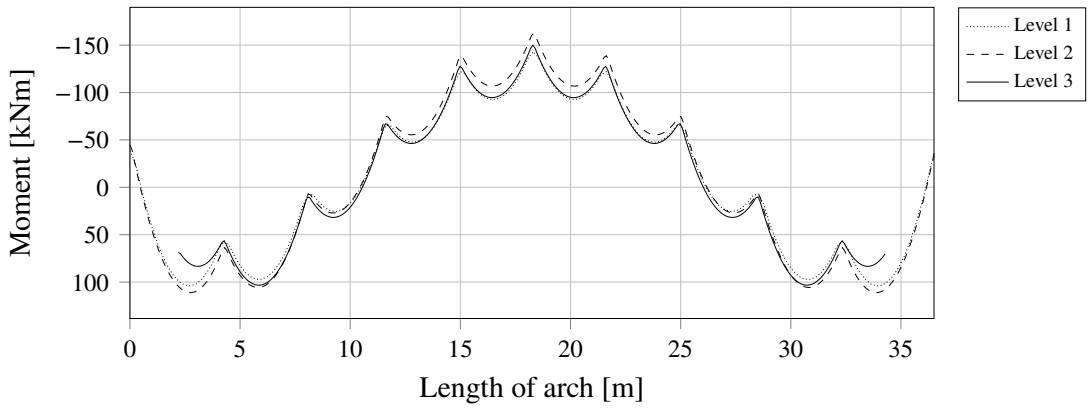

Figure 5.7 Bending moment in the arch for level 1, 2 and 3, subjected to uniformly distributed load.

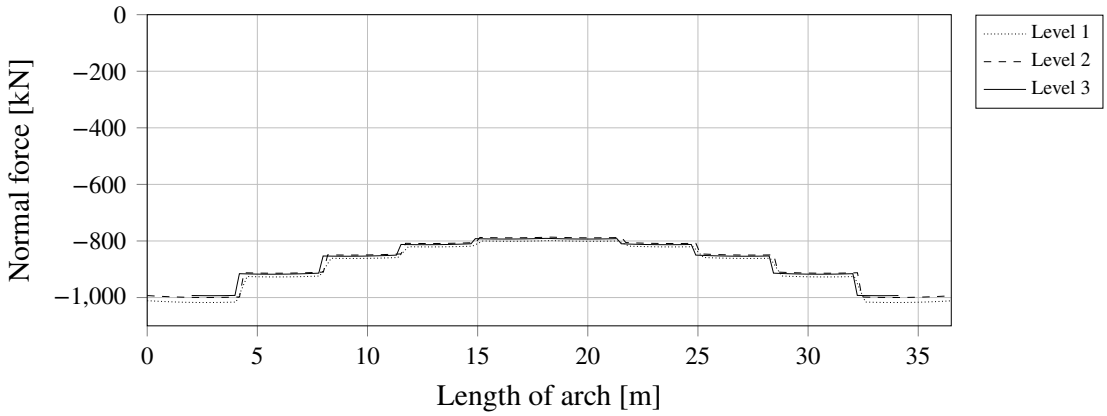

Figure 5.8 Normal force in the arch for level 1, 2 and 3, subjected to uniformly distributed load.

The normal force in the longitudinal beam is presented in Figure 5.9. In all three levels the normal force is positive, in other words, the beams are subjected to tension. The normal force is constant between the connection to the hangers and transversal beams and is decreasing towards the middle in all three levels. It is larger close to the supports since the elongation of the beams is larger there. The normal force is in direct proportion to the elongation as long as the area of the cross section is uniform, which is the case for all three levels.

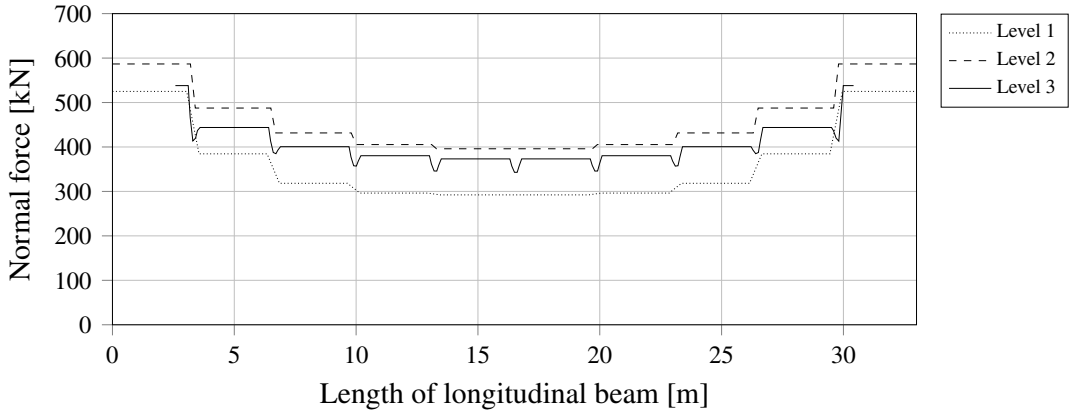

Figure 5.9 *Normal force in the longitudinal beam for level 1, 2 and 3, subjected to uniformly distributed load.*

In level 3 the normal force shows drops where it is connected to the transversal beams. In Figure 5.10, the contour plot of the normal force in the longitudinal direction of the bridge is presented, showing that some of the normal force is transferred into the transversal beam. The *Free body cut* section is only defined in the longitudinal beam and will therefore only include the normal force transferred in the longitudinal beam, resulting in a lower normal force at these locations.

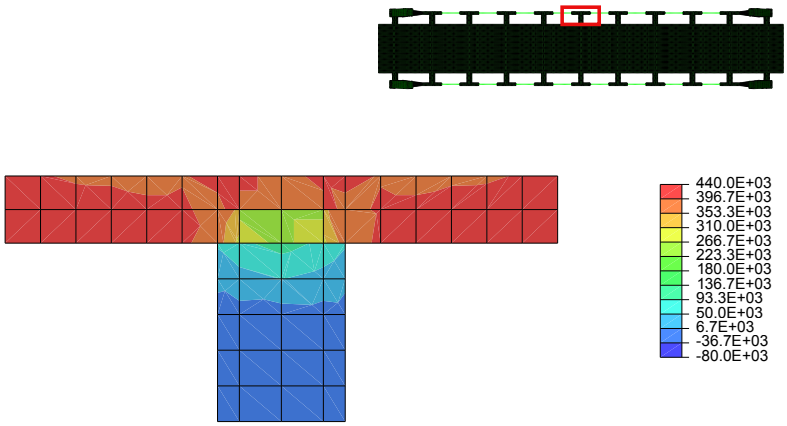

Figure 5.10 *Contour plot of the normal force [N] in the longitudinal direction of the bridge in the connection between the longitudinal and transversal beam in level 3, showing how the normal force is spread into the transversal beam.*

The integrated normal force over half of the width of the deck, in the longitudinal direction, is presented in Figure 5.11. In contrast to the normal force in the longitudinal beam, the normal force in the deck increases towards the middle of the bridge. A summation of the normal force in half of the deck and the normal force in one longitudinal beam results in a constant total normal force along the length of the bridge.

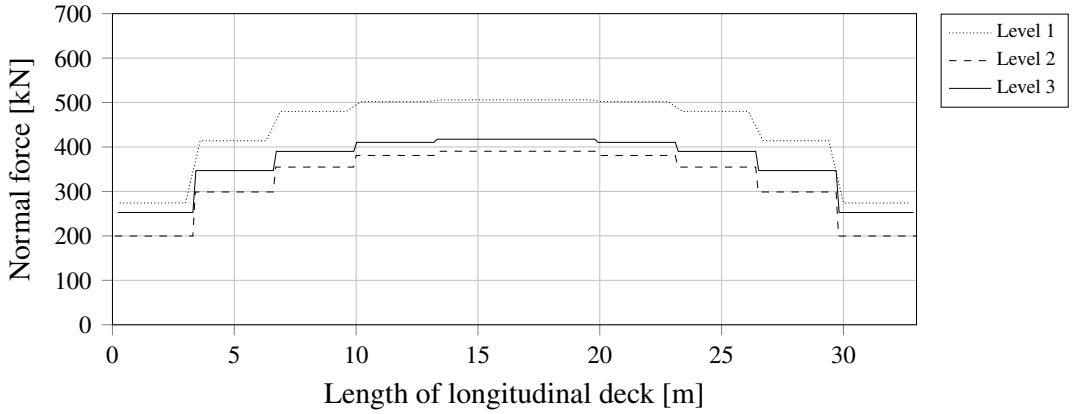

Figure 5.11 The integrated normal force over half the width of the deck in the longitudinal direction for level 1, 2 and 3, subjected to uniformly distributed load.

In Figure 5.12, the normal force distribution in the longitudinal direction along the width of the deck in the span between the first and second transversal beam is shown. In level 1, the normal force distribution is divided in four equally sized steps, since the beam grillage is consisting of four beams in the longitudinal direction. Level 2 and 3 has a smoother normal force distribution and is peaking at the ends of the deck, where level 3 has the largest normal force.

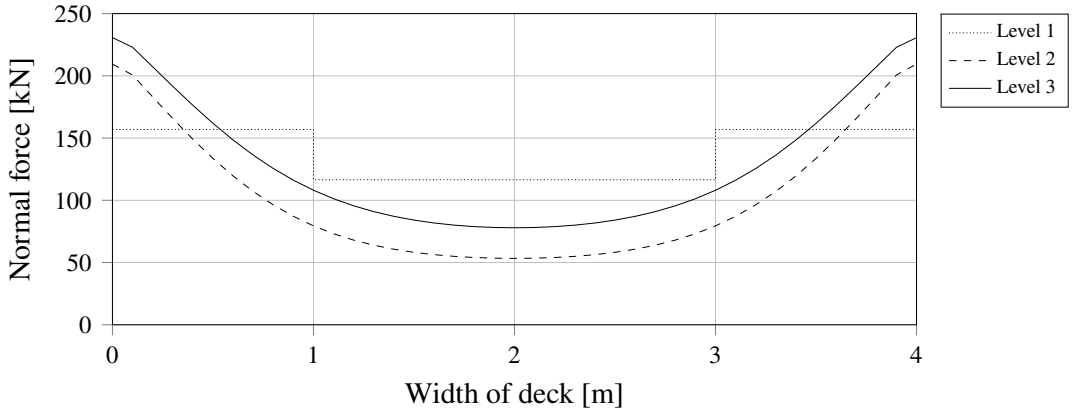

Figure 5.12 Normal force distribution in the longitudinal direction along the width of the deck in the span between the first and second transversal beam for level 1, 2 and 3, subjected to the uniformly distributed load.

The secondary bending moment in the first transversal beam is presented in Figure 5.13. It increases linear in all three levels to the immediate point where the transversal beam and the deck are connected, see cut (1) in Figure 5.14. In level 1 the secondary bending moment decreases rapidly down to zero after its peak. However, in level 2 and 3 the secondary bending moment decreases in a smooth curve but it only reaches zero in level 2.

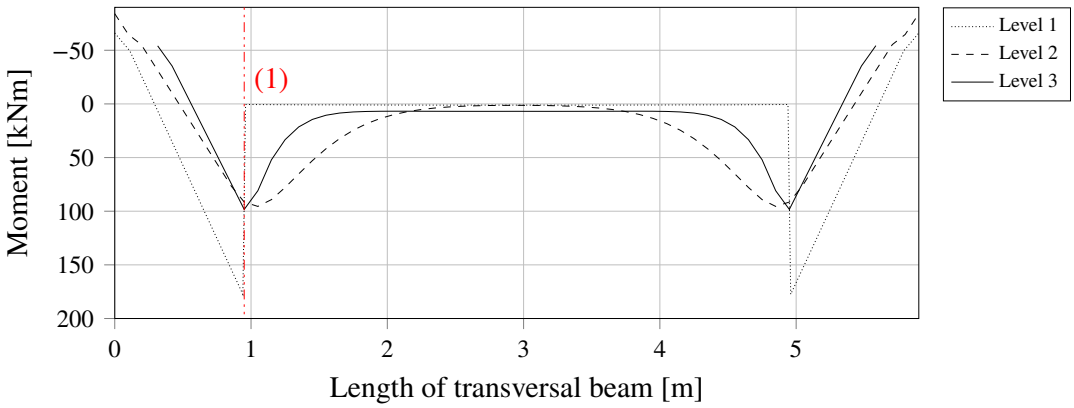

Figure 5.13 *Secondary bending moment in the first transversal beam for level 1, 2 and 3, subjected to uniformly distributed load.*

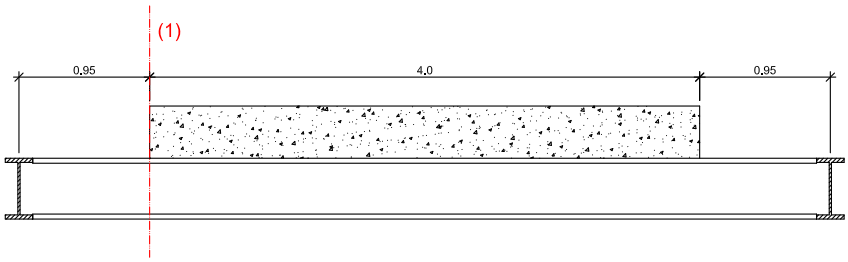

Figure 5.14 *A transversal cut trough the bridge, showing the the cross section of the longitudinal beams, the transversal beam and the deck.*

In contrast to level 1 and 2, the secondary bending moment in level 3 does not reach zero in the middle of the beam due to the different element used for the transversal beam. In level 1 and 2, the beam is modelled using beam elements and thereby the entire cross section of the beam is constrained to the deck and no secondary bending in any part of the cross section will occur. In level 3 only the upper flange of the cross section is constrained to deck and therefore the other parts of the cross section are free to bend, see Figure 5.15. The secondary bending moment in level 3 represent an average value of the cross section, calculated using stress integration, as described in Section 2.4.

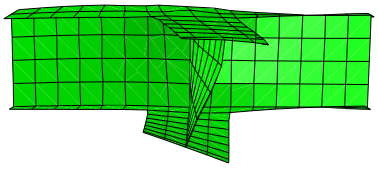

Figure 5.15 *A section through the middle of one transversal beam, showing the deformation of the cross section for level 3.*

The variation of maximum horizontal shear force in the transversal beams along the bridge is presented in Figure 5.16. Since the magnitude of the secondary bending moment in the transversal beam is similar in level 2 and 3 the difference in normal force in the longitudinal beam may be explained by the shear force. The horizontal shear force in level 2 and 3 is equal in all transversal beams except in the first and eleventh beam. This implies a reduction of the normal force in the longitudinal beam in level 3 compared to level 2.

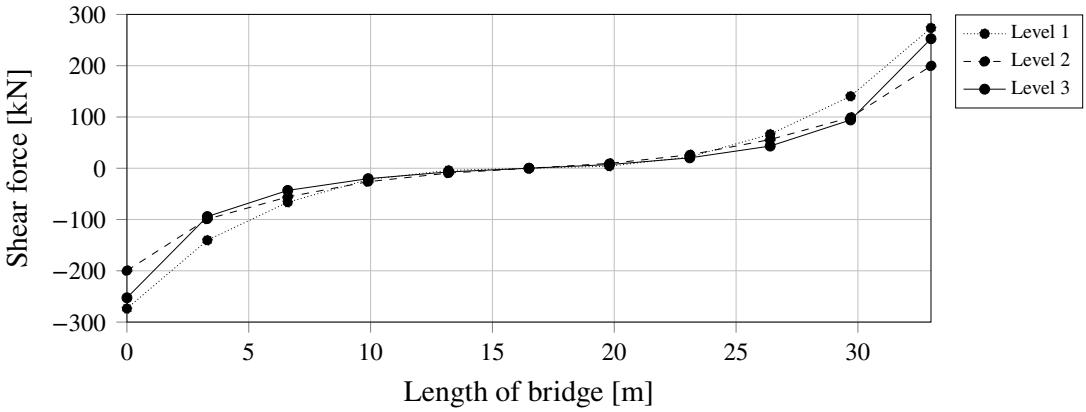

Figure 5.16 Variation of maximum horizontal shear force in the transversal beam along the bridge for level 1, 2 and 3, subjected to uniformly distributed load.

The difference between the secondary bending moments for the three levels depends on how the deck is modelled, with beam grillage or with shell elements. A section, consisting of the transversal beam and the deck, work as a composite section and the level of composite action along the transversal beam is different in the three levels.

In level 1, the transversal beam in the beam grillage is constrained to the main transversal beam. Both beams are modelled using beam elements, where the cross section by definition is fixed to its centre line. Hence, full composite action apply at all points where the beams are connected. When there is full composite action the whole effective width of the composite cross section can be utilized. Since the transversal beam in the beam grillage has a width of 2.37 m it is too stiff to bend in the horizontal direction. Hence the secondary bending moment will be carried by the transversal beam in the beam grillage. The sudden decrease of secondary bending moment in level 1 may thereby be explained by the full composite action of the cross section.

In level 2 and 3, the deck is constrained to the transversal beam as described in Section 4.4. In level 2 one line in the shell element is constrained to the transversal beam and in level 3 two lines are constrained to the transversal beam. The stresses in the transversal beam are transferred to the deck where the transversal beam and deck are connected. From that point the stresses are spread out across the deck. This effect can be seen in Figure 5.17 where the normal force in the transversal direction is plotted for level 2 and 3. Where the force field is evenly thick the whole effective width of the cross section is utilized and full composite action is reached. As the composite action increases the influence of the deck increases and the secondary bending moment in the transversal beam is thereby decreasing gradually.

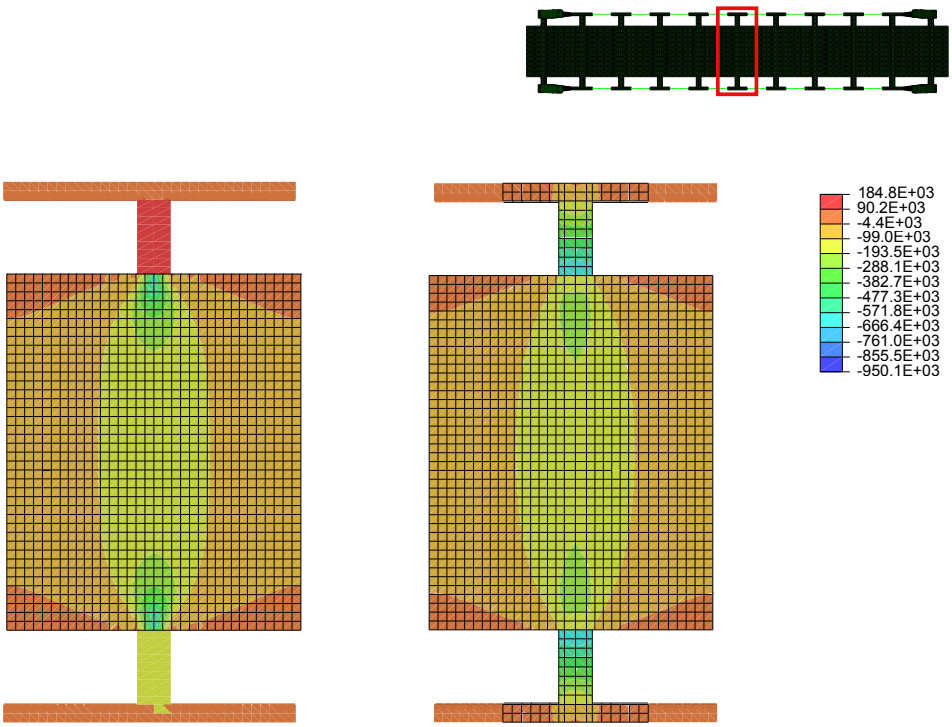

Figure 5.17 Normal force [N] in the transversal direction of the deck in a) level 2 and b) level 3.

The deformation in the connection between the transversal beam and deck is presented in Figure 5.18 for level 1 and 2. In level 1, the deformation of the transversal beam starts at the point where the deck starts, see cut (1) in Figure 5.19. However in level 2 the deformation of the transversal beam starts a small distance into the deck. The moment, according to the differential equation for beams, see Equation (2.6), is proportional to the second derivative of the deformation and since the deformation of the transversal beam in level 1 changes faster the secondary bending moment should be higher.

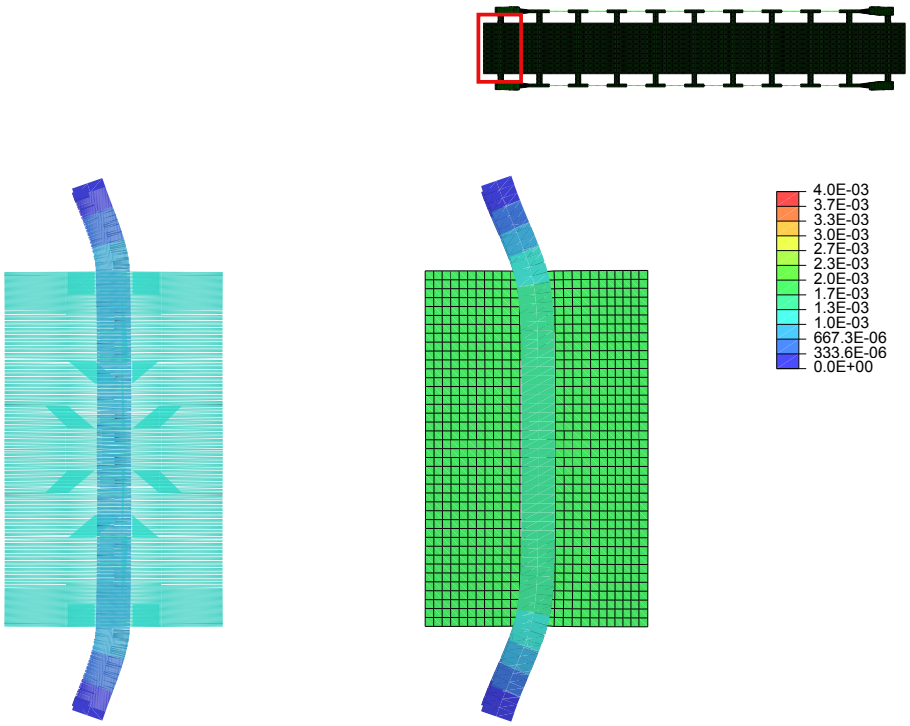

Figure 5.18 *Deformation [m] of the connection between the first transversal beam and the deck in a) level 1 and b) level 2.*

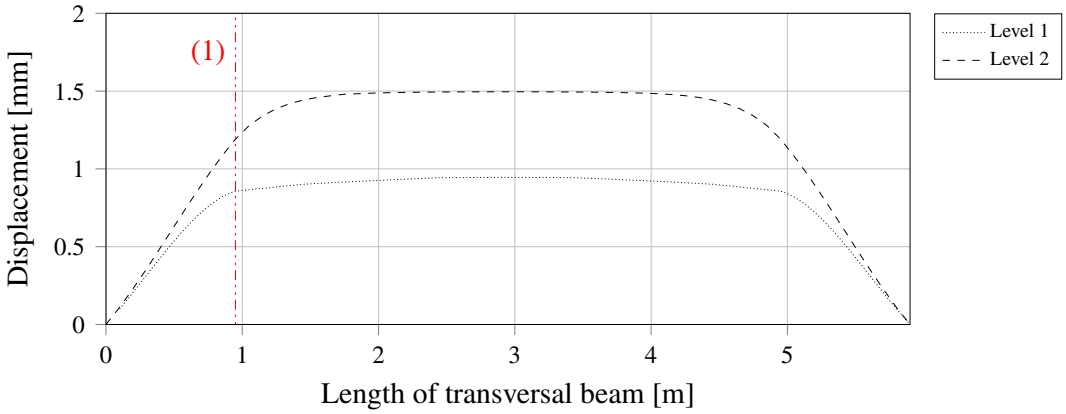

Figure 5.19 *The deformation in the weak direction of the first transversal beam for level 1 and 2.*

Results from a beam element are represented with three translational forces and three rotational moments in each node, as described in Section 2.2.1. A shell element on the other hand has five

translational forces and three rotational forces in each node, with the notation that the third rotational moment is the twisting moment of the element and not the rotation normal to the plane, as described in Section 2.2.2. Hence in level 1, the rotational moment in y-direction in the transversal beam can be taken up by the corresponding rotational moment in the beam element in the beam grillage. It is thereby full interaction between the transversal beam and the beam grillage along the width of the deck.

In level 2 and 3, the rotational moment in y-direction can not be taken by a rotational moment in the shell element, but rather by a translational force couples in the plane of the shell element. If the translational forces should be able to counteract the moment there must be a distance between the forces, hence full interaction between the transversal beam and deck is reached after some distance into the deck.

This difference in the behaviour of the elements affect the stiffness of the connection between the transversal beam and deck. Level 1 has the stiffest connection while level 2 and 3 has a lower stiffness and are similar to each other. This may explain the different magnitude of the secondary bending moment and the different change of deformation in the transversal beams in level 1 compared to level 2 and 3. As discussed in Section 3.3, stiffer connections results in higher moment and as shown in Figure 5.13, level 1 has the highest secondary bending moment.

The secondary bending moment for the third and fifth beam is presented in Figure 5.20 and Figure 5.21 respectively. The results from all transversal beams are shown in Appendix E. The same behaviour of the secondary bending moment can be seen for all transversal beams, however the magnitude of the secondary bending moment differs. The variation of the maximum secondary bending moment along the bridge is presented in Figure 5.22. The magnitude decreases further towards the middle and the most exposed transversal beams are the two beams at the ends.

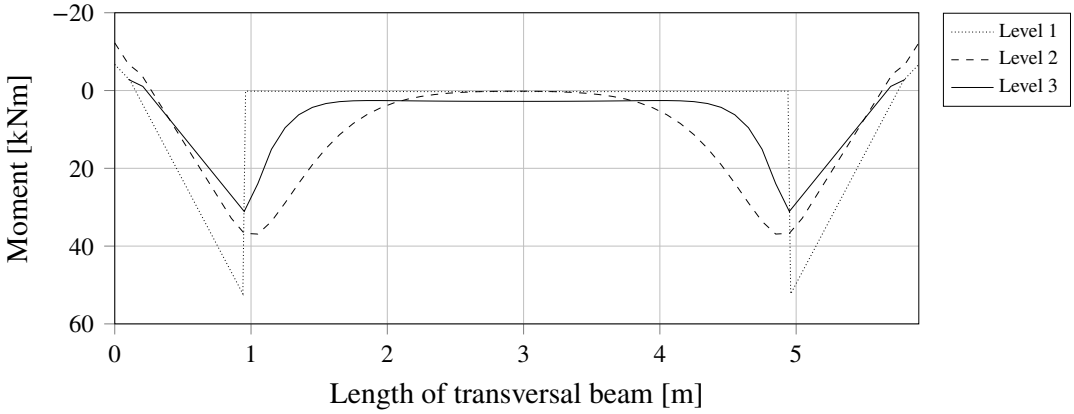

Figure 5.20 Secondary bending moment in the third transversal beam for level 1, 2 and 3, subjected to uniformly distributed load.

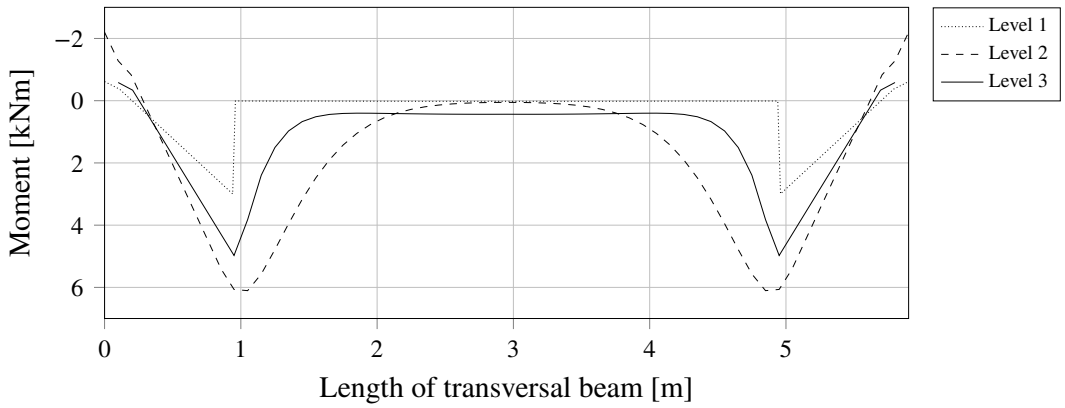

Figure 5.21 Secondary bending moment in the fifth transversal beam for level 1, 2 and 3, subjected to uniformly distributed load.

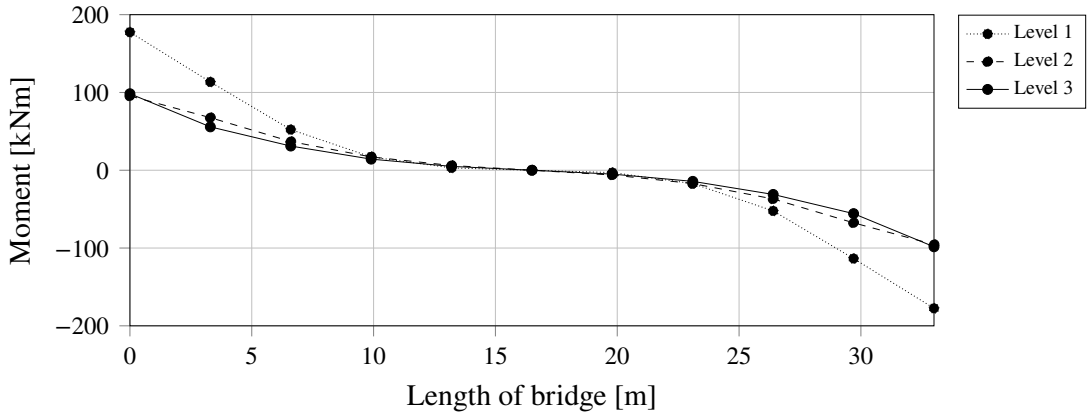

Figure 5.22 Variation of maximum secondary bending moment in the transversal beams along the bridge for level 1, 2 and 3, subjected to uniformly distributed load.

Figure 5.22 shows that the bridge is symmetric but the sign of the secondary bending moment in the transversal beam shifts in the middle due to bending of the transversal beams in the other direction. In the sixth transversal beam the secondary bending moment is zero since there is no relative displacement between the longitudinal beams and deck in the middle of the bridge.

5.2.2 Temperature load

The global deformation of the bridge subjected to temperature load is presented in Figure 5.23. The contour plot shows the displacement in the direction vertical to the bridge. The overall behaviour is as expected, with a double symmetric negative deflection with its maximum at the middle. The deformation seen from above is presented in Figure 5.24. The contour plot shows the displacement in the direction longitudinal to the bridge. When the deck shorten the transversal beams are prevented to move freely by the longitudinal beams and bends in the weak direction as expected.

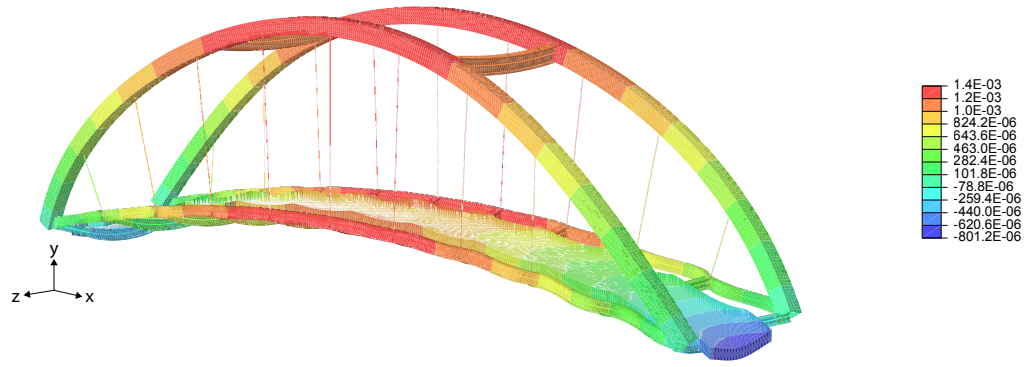

Figure 5.23 *Deformation of the bridge subjected to temperature load. The contour display the deformation in y-direction [m]. The displayed model is level 2, however all levels show the same global behaviour.*

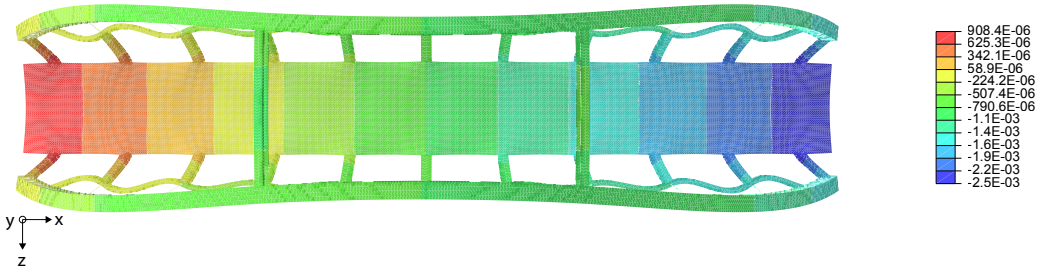

Figure 5.24 *Deformation of the bridge subjected to temperature load, seen from above. The contour display the deformation in x-direction [m]. The displayed model is level 2, however all levels show the same global behaviour.*

The bending moment and the normal force in the arch is presented in Figure 5.25 and Figure 5.26 respectively. In contrast to the uniformly distributed load case, the bending moment and the normal force differ between modelling techniques for the temperature load. When the temperature changes, the bridge is not subjected to any vertical load but only internal forces, hence all elements in the structure are affected by the restraining forces.

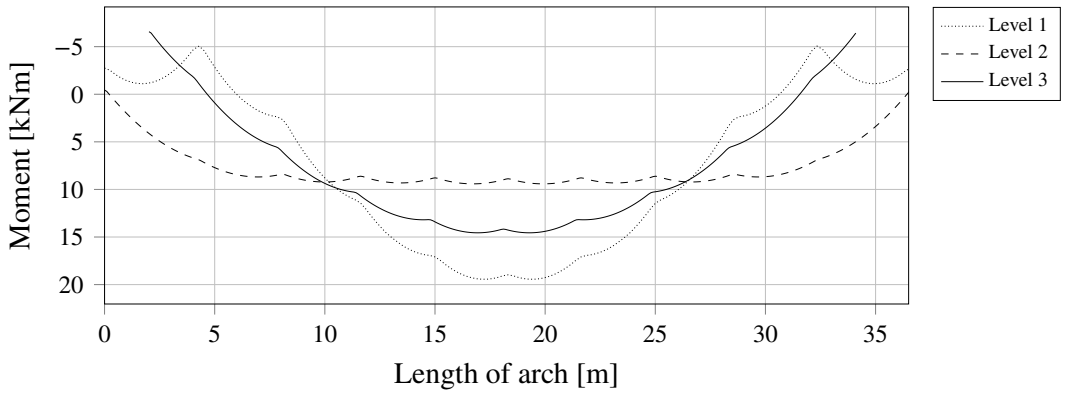

Figure 5.25 Bending moment in the arch for level 1, 2 and 3, subjected to temperature load.

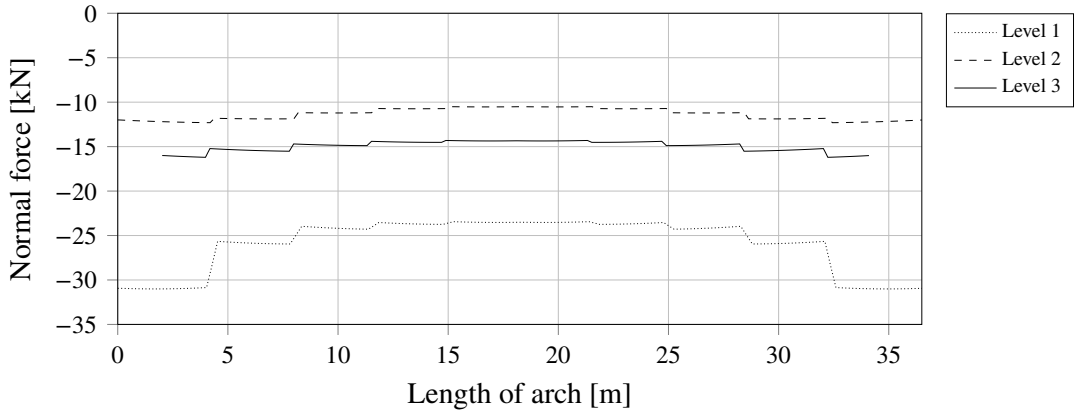

Figure 5.26 Normal force in the arch for level 1, 2 and 3, subjected to temperature load.

The normal force in the longitudinal beam is presented in Figure 5.27. In contrast to the uniformly distributed load case, the longitudinal beams have a negative normal force; they are subjected to compression. The normal force is constant between the connection to the hangers and the transversal beams and has a drop of force at every connection to the transversal beams, just as for the uniformly distributed load case, see Section 5.2.1. The compression in the longitudinal beam is increasing towards the middle of the bridge in all three levels.

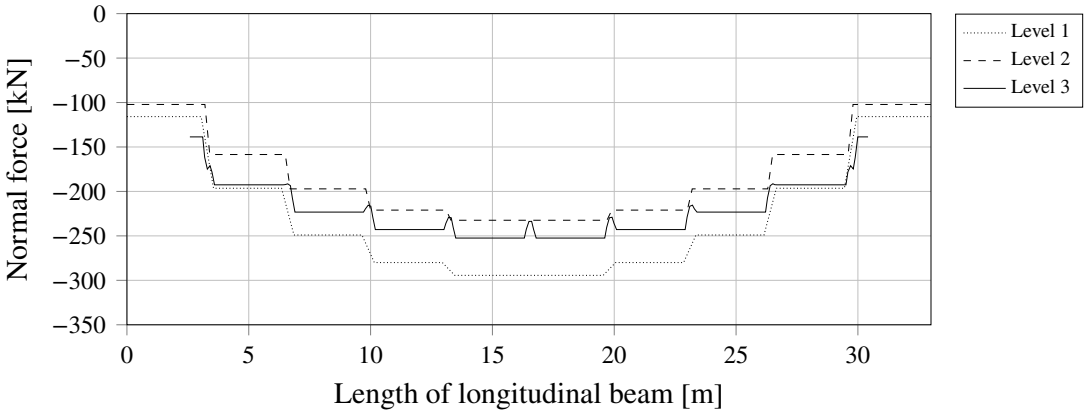

Figure 5.27 Normal force in the longitudinal beam for level 1, 2 and 3, subjected to temperature load.

The integrated normal force over half of the width of the deck in the longitudinal direction is presented in Figure 5.28. As for the uniformly distributed load case, the summation of the normal forces in half of the deck and in one longitudinal beam results in a constant normal force along the length of the bridge. Since there is no vertical or horizontal load applied on the structure the additional summation of the horizontal component of the normal force in the arch results in zero normal force.

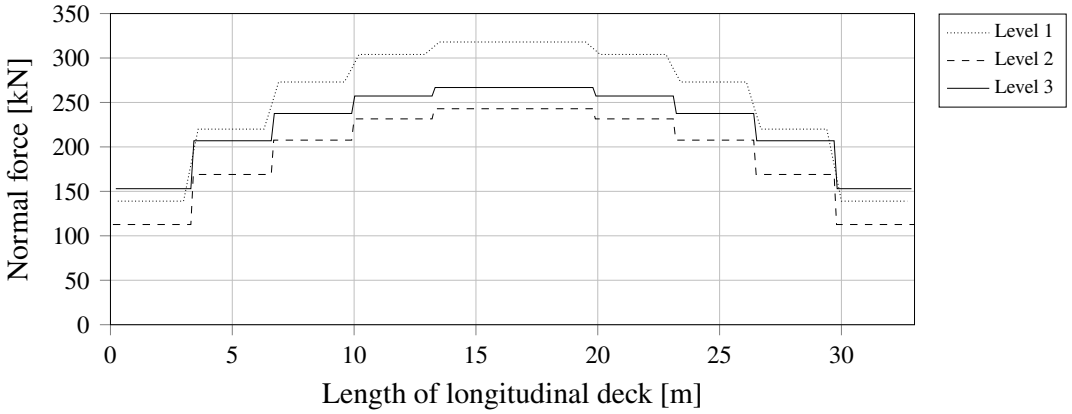

Figure 5.28 The integrated normal force over half the width of the deck in the longitudinal direction for level 1, 2 and 3, subjected to temperature load.

The secondary bending moment in the first transversal beam is presented in Figure 5.29. The secondary bending moment due to the temperature load resembles the observed for the uniformly distributed load case presented in Figure 5.13 for all three levels. The same explanation regarding the differences in the secondary bending moment discussed in Section 5.2.1 also applies for the temperature load case since the differences in secondary bending moment is the element type used rather then the applied load. However, the global structural response due to restraining forces is different for the different load cases.

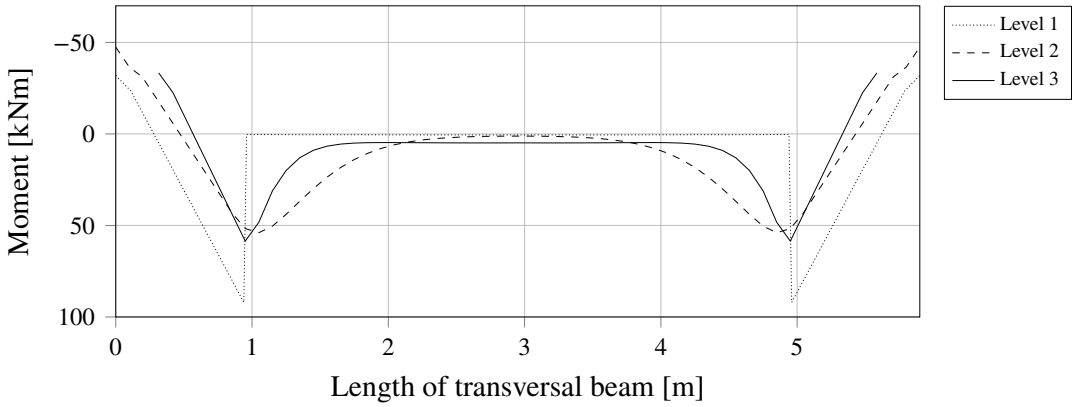

Figure 5.29 Secondary bending moment in the first transversal beam for level 1, 2 and 3, subjected to the temperature load.

The variation of maximum horizontal shear force in the transversal beams along the bridge is presented in Figure 5.30. As for the uniformly distributed load case the difference in normal force in the longitudinal beam between level 2 and 3 may be explained by the difference in shear force in the first and eleventh transversal beam.

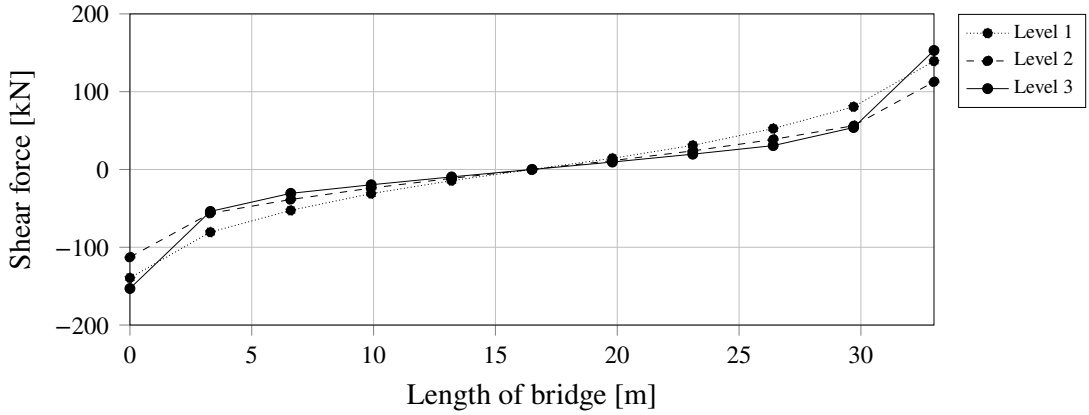

Figure 5.30 Variation of maximum horizontal shear force in the transversal beam along the bridge for level 1, 2 and 3, subjected to temperature load.

The variation of maximum secondary bending moment along the bridge is presented in Figure 5.31. The magnitude decreases further towards the middle and the most exposed transversal beams are the two beams at the ends. The secondary bending moment has the same behaviour in all transversal beams and are presented in Appendix E.

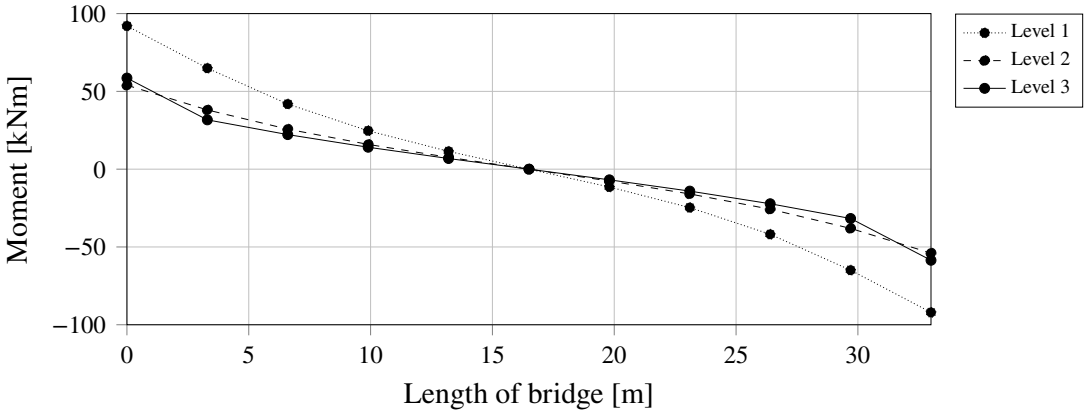

Figure 5.31 Variation of maximum secondary bending moment in the transversal beams along the bridge for level 1, 2 and 3, subjected to temperature load.

5.2.3 Traffic load

The traffic load consists of concentrated traffic loads and distributed traffic load, as described in Section 4.6, and the load cases are analysed separately. In order to find the most critical load case, the concentrated loads were enveloped and the distributed loads were combined to the most unfavourable load case, as described in Section 4.6. The results from Brigade/PLUS are divided in maximum and minimum values. For the concentrated traffic load these values are from the most unfavourable positioning of the load for each element. For the distributed traffic load these values are from the most unfavourable combination of the distributed loads for each element.

The global deformation of the bridge subjected to one concentrated traffic load placed between the seventh and eight transversal beam is presented in Figure 5.32. The larges deflection is observed at the loading point. The contour plot shows the displacement in the direction vertical to the bridge. The contour plot in Figure 5.33 shows the deformation produced by the same load case but in the direction longitudinal to the bridge instead.

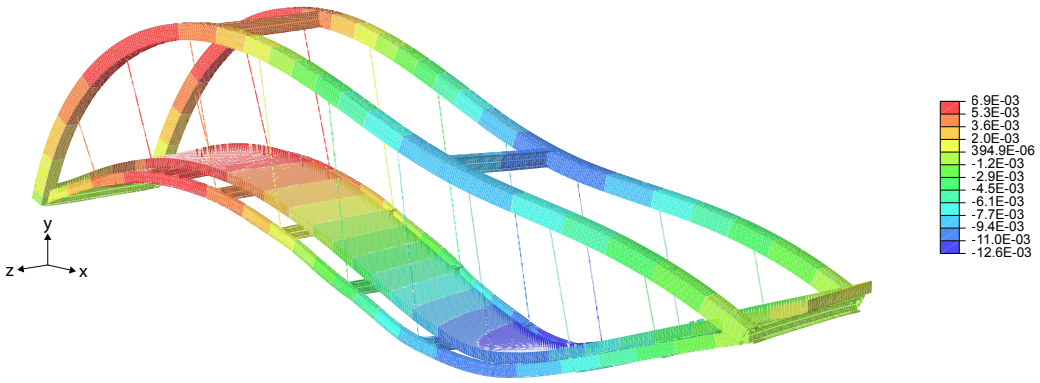

Figure 5.32 *Deformation of the bridge subjected to one concentrated traffic load placed between the seventh and eight transversal beam. The contour display the deformation in y-direction [m]. The displayed model is level 2, however all levels show the same global behaviour.*

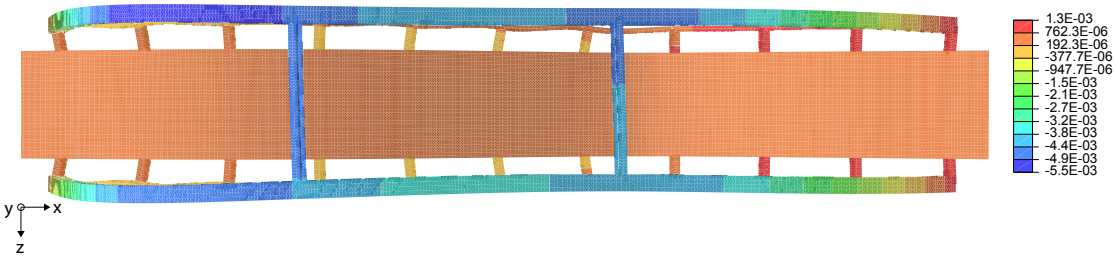

Figure 5.33 *Deformation of the bridge subjected to one concentrated traffic load placed between the seventh and eight transversal beam, seen from above. The contour display the deformation in x-direction [m]. The displayed model is level 2, however all levels show the same global behaviour.*

The maximum and minimum bending moment and normal force in the arch, subjected to the concentrated traffic load, is presented in Figure 5.34 and Figure 5.35 respectively. In Figure 5.36 and Figure 5.37, the maximum and minimum bending moment and normal force in the arch, subjected to the distributed traffic load are presented. Likewise for the uniformly distributed load case, the bending moment and the normal force are similar for the concentrated traffic load and the distributed traffic load, both for the minimum and the maximum values in all three levels. That implies that similar behaviour is described in all levels.

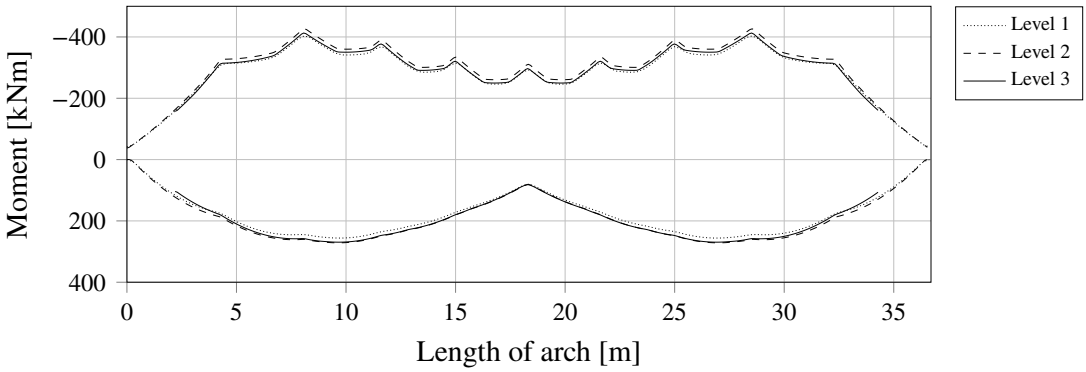

Figure 5.34 Maximum and minimum bending moment in the arch for level 1, 2 and 3, subjected to the concentrated traffic load.

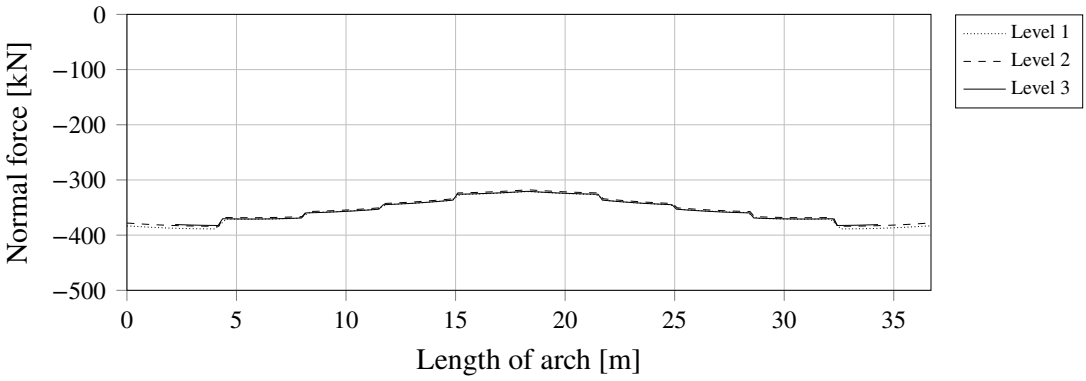

Figure 5.35 Maximum and minimum normal force in the arch for level 1, 2 and 3, subjected to the concentrated traffic load.

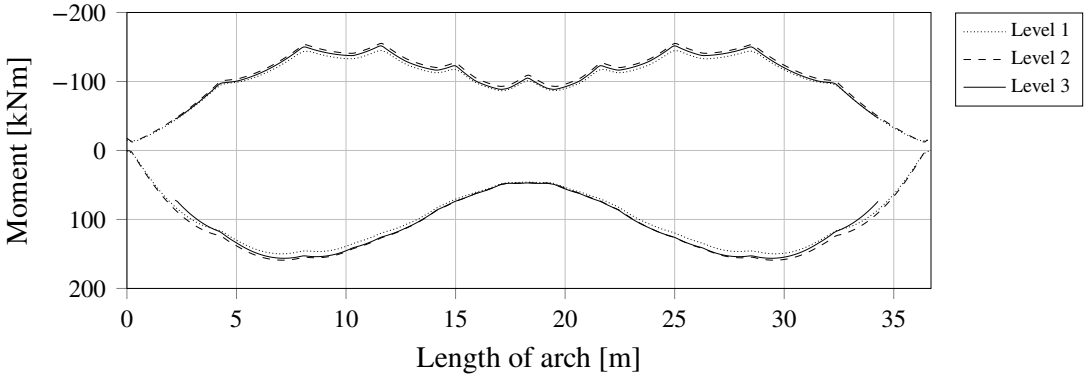

Figure 5.36 Maximum and minimum bending moment in the arch for level 1, 2 and 3, subjected to the distributed traffic load.

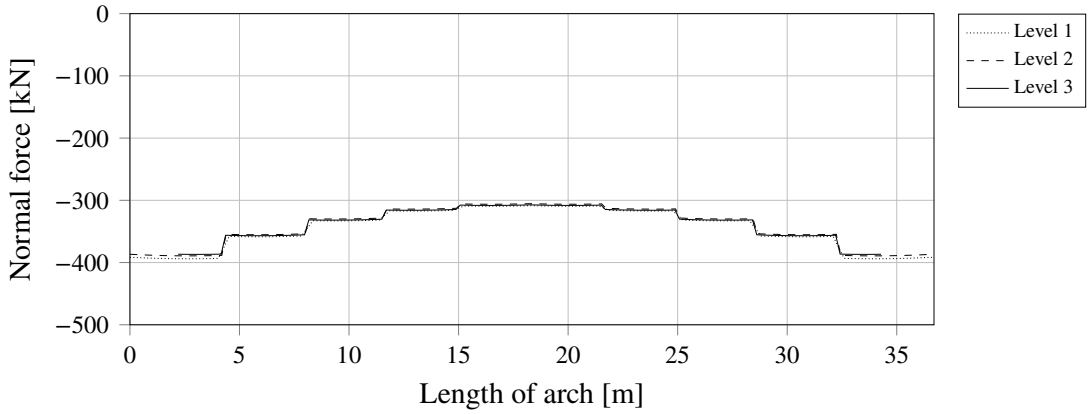

Figure 5.37 Maximum and minimum normal force in the arch for level 1, 2 and 3, subjected to the distributed traffic load.

The maximum and minimum normal force in the longitudinal beam, subjected to the concentrated traffic load, is presented in Figure 5.38. In Figure 5.39 the maximum and minimum normal force in the longitudinal beam, subjected to the distributed traffic load, is presented. In level 2 and 3, the minimum normal force is close to zero and no compression occurs in the longitudinal beam. In level 1 however, the normal force is negative at some points, in other words, the longitudinal beams are subjected to compression for some load positions. The most unfavourable load case for the distributed traffic load is when all the load is applied, and thereby large similarities to the uniformly distributed load case can be seen in the maximum normal force. The maximum normal force for the concentrated traffic load is between the third and forth transversal beam which implies that the placement of the load has an influence. Hence, local effects from a concentrate load, as described in Section 3.2.3 occur.

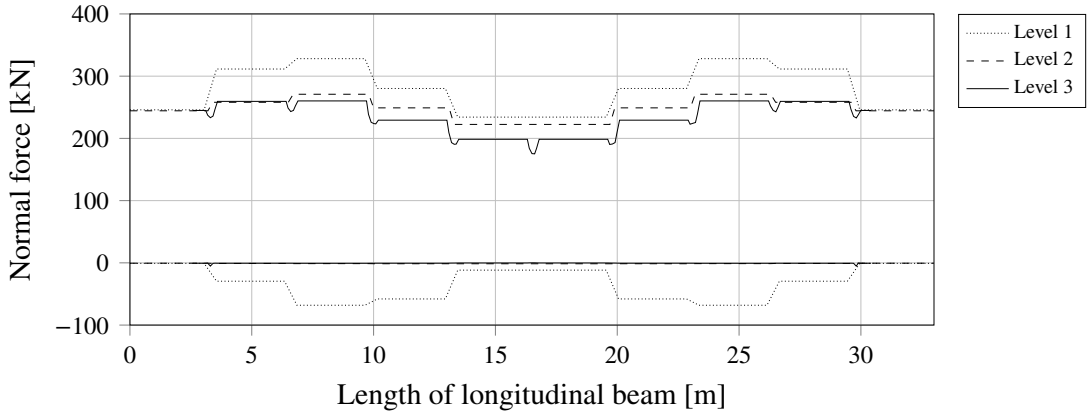

Figure 5.38 Maximum and minimum normal force in the longitudinal beam for level 1, 2 and 3, subjected to the concentrated traffic load.

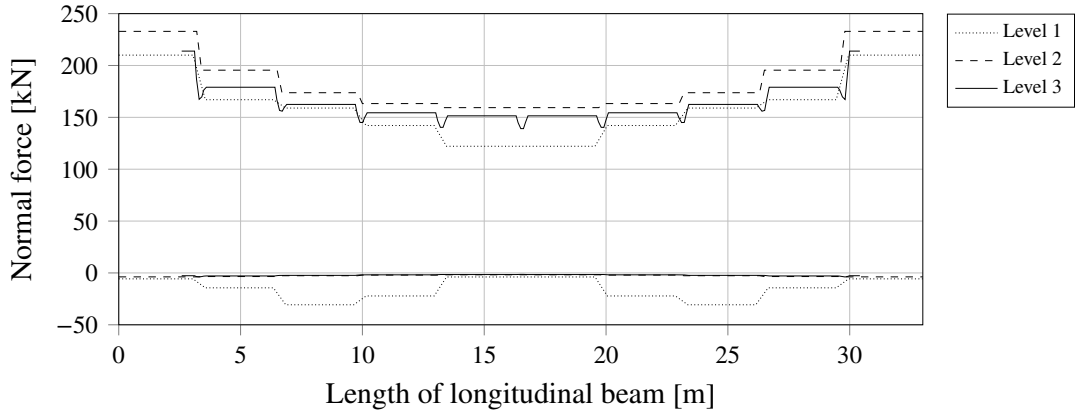

Figure 5.39 Maximum and minimum normal force in the longitudinal beam for level 1, 2 and 3, subjected to the distributed traffic load.

The integrated maximum and minimum normal force over half the width of the deck in the longitudinal direction subjected to concentrated traffic load and distributed traffic load is presented in Figure 5.40 and Figure 5.41 respectively. Since the results are from the most unfavourable load placement for each element, the summation of normal force in the longitudinal beam and deck will not be constant.

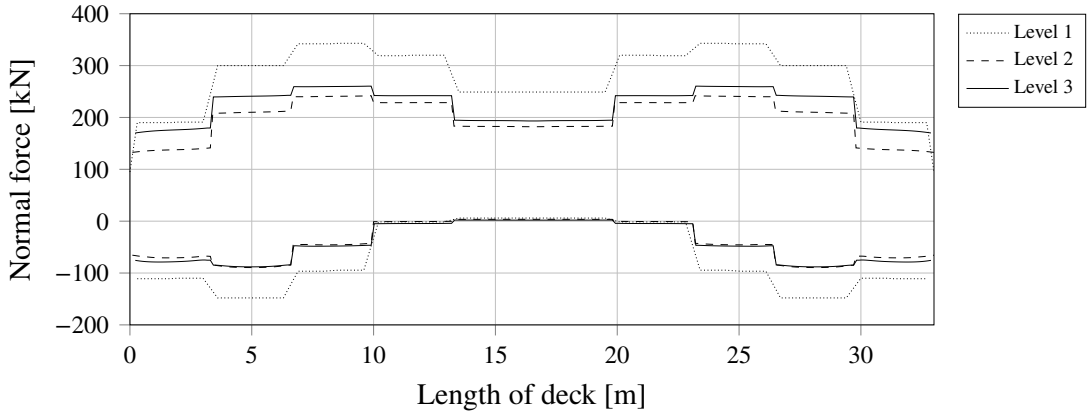

Figure 5.40 The integrated maximum and minimum normal force over half of the width of the deck in the longitudinal direction for level 1, 2 and 3, subjected to the concentrated traffic load.

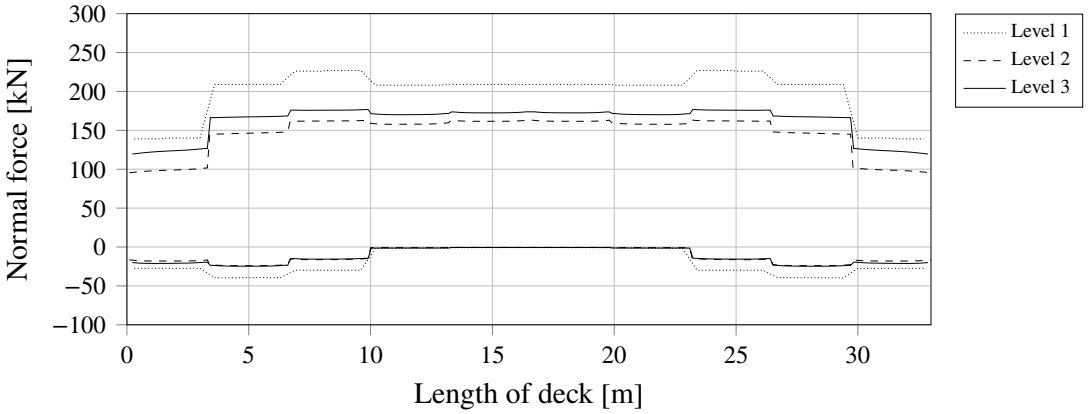

Figure 5.41 The integrated maximum and minimum normal force over half of the width of the deck in the longitudinal direction for level 1, 2 and 3, subjected to the distributed traffic load.

The maximum and minimum secondary bending moment distribution in the first transversal beam, subjected to the concentrated traffic load, is presented in Figure 5.42. In Figure 5.43, the maximum and minimum secondary bending moment distribution in the first transversal beam, subjected to the distributed traffic load is presented. The secondary bending moment for both load cases are very similar to the uniformly distributed load case. The moment in level 1 is the largest for all cases and the moment suddenly decreases. The moment in level 2 and 3 has smoother distribution and are more equal to each other. The maximum and minimum secondary bending moment distribution for all the transversal beams can be seen in Appendix E

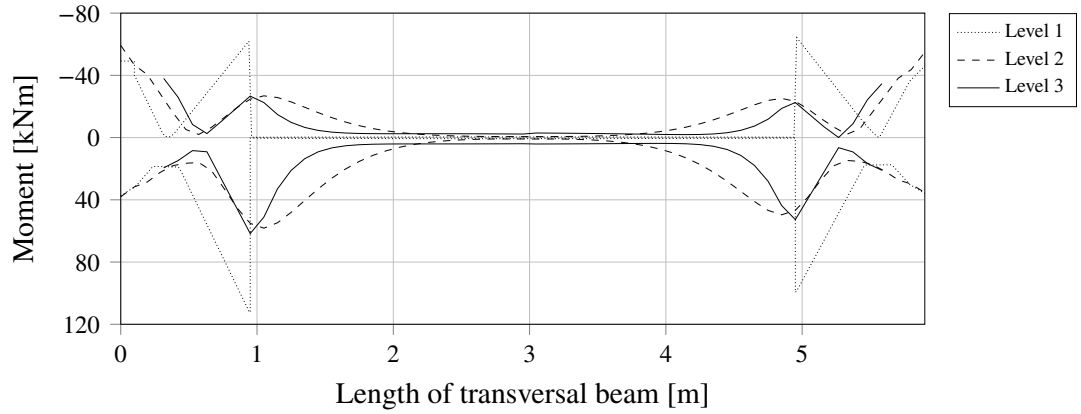

Figure 5.42 Maximum and minimum secondary bending moment distribution in the first transversal beam for level 1, 2 and 3, subjected to the concentrated traffic load.

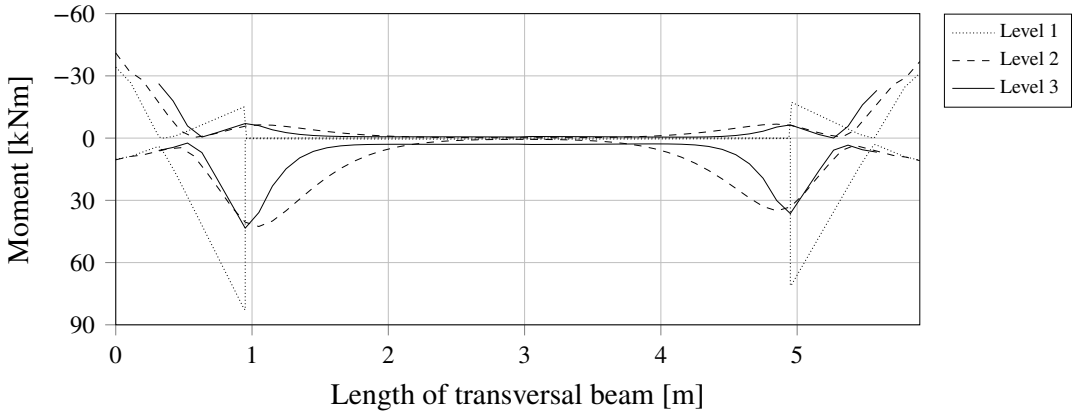

Figure 5.43 Maximum and minimum secondary bending moment distribution in the first transversal beam for level 1, 2 and 3, subjected to the distributed traffic load.

The variation of the maximum and minimum secondary bending moment along the bridge, subjected to concentrated traffic load and distributed traffic load is presented in Figure 5.44 and Figure 5.45 respectively. In contrast to the uniformly distributed and the temperature load case the variation of the secondary bending moment in the transversal beam does not decrease towards the middle of the bridge. Instead, the secondary bending moment is more equal in all beams. The large difference between the maximum and minimum secondary bending moment implies that fatigue may cause problem in several transversal beams.

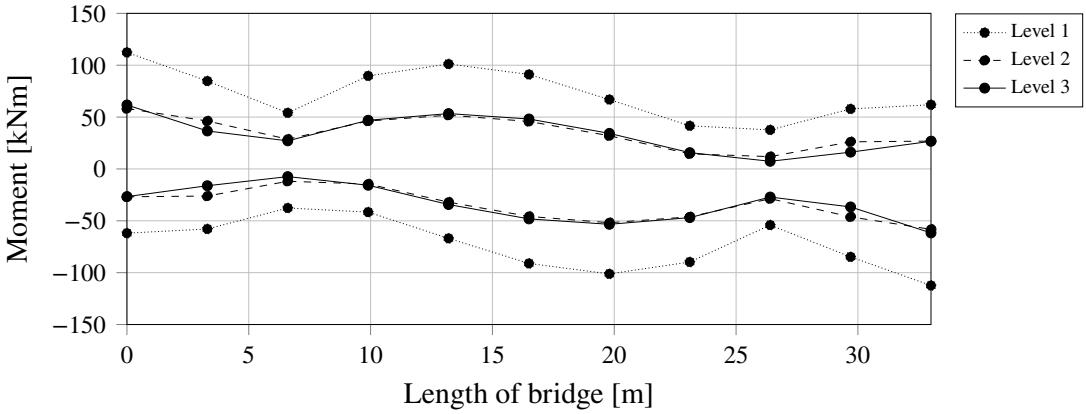

Figure 5.44 Variation of maximum and minimum secondary bending moment in the transversal beams along the bridge for level 1, 2 and 3, subjected to the concentrated traffic load.

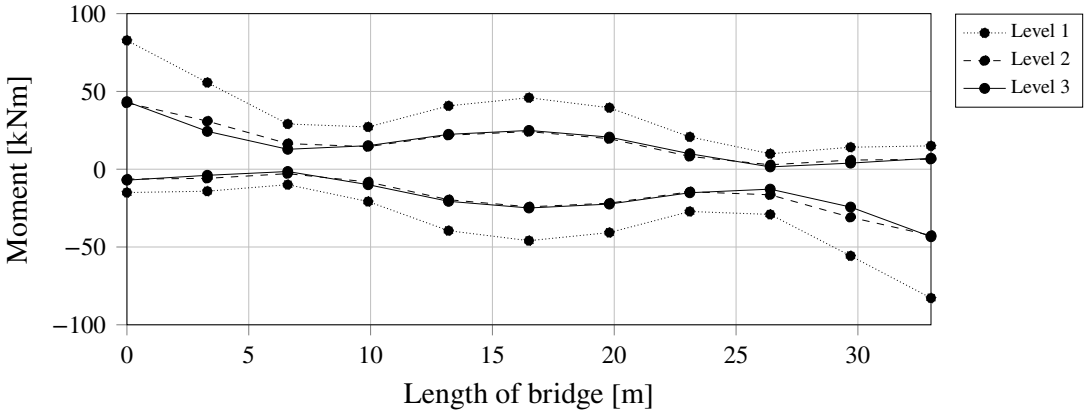

Figure 5.45 Variation of maximum and minimum secondary bending moment in the transversal beams along the bridge for level 1, 2 and 3, subjected to the distributed traffic load.

In order to analyse the local effect from the concentrated load, described in Section 3.2.3, the influence of the placement of the concentrated traffic load has been studied. The normal force in the longitudinal beam and the secondary bending moment in the transversal beam for the different positions of the concentrated traffic load is presented. The most exposed transversal beams are the first and the sixth and the results has therefore been evaluated in these places. The maximum normal force in the longitudinal beam at the the first and the sixth transversal beam is presented in Figure 5.46 and Figure 5.48. In Figure 5.47 and Figure 5.49 the maximum secondary bending moment in the first and the sixth transversal beam is presented.

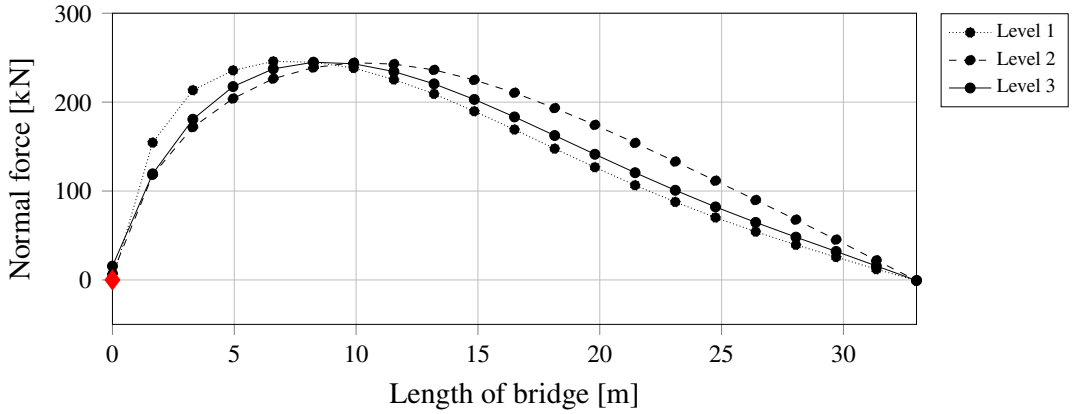

Figure 5.46 The maximum normal force in the longitudinal beam at the first transversal beam for the different positions of the concentrated traffic load along the length of the deck.

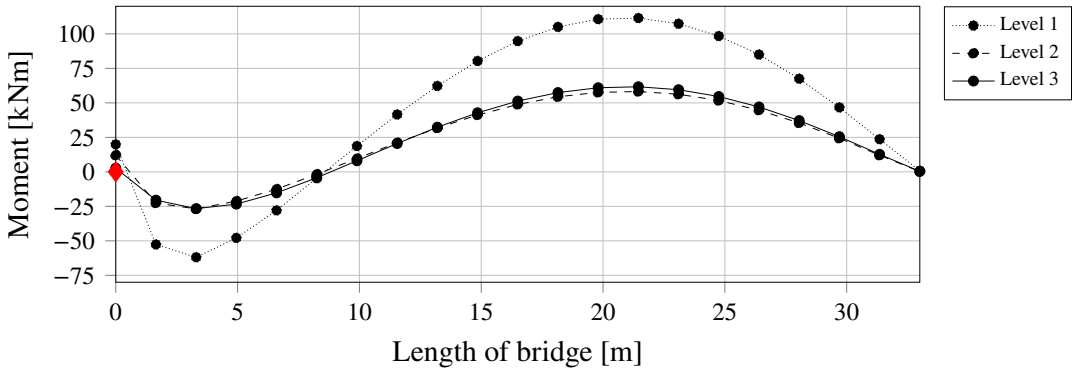

Figure 5.47 *The maximum secondary bending moment in the first transversal beam for the different positions of the concentrated traffic load along the length of the deck.*

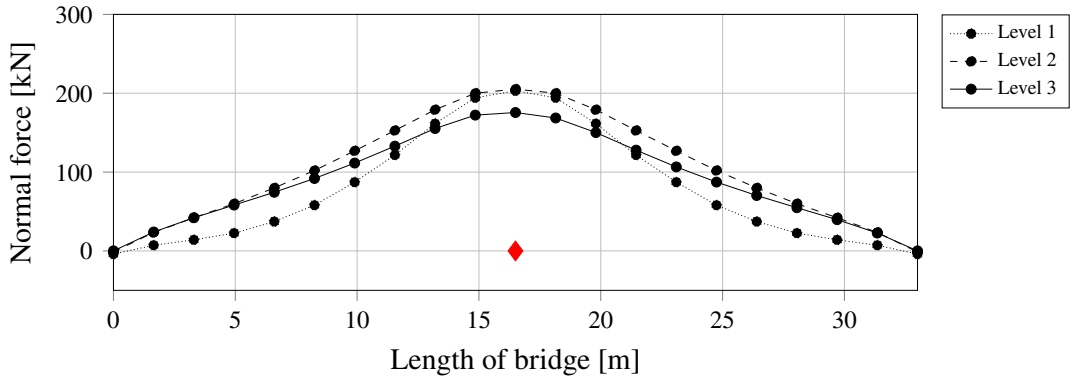

Figure 5.48 *The maximum normal force in the longitudinal beam at the sixth transversal beam for the different positions of the concentrated traffic load along the length of the deck.*

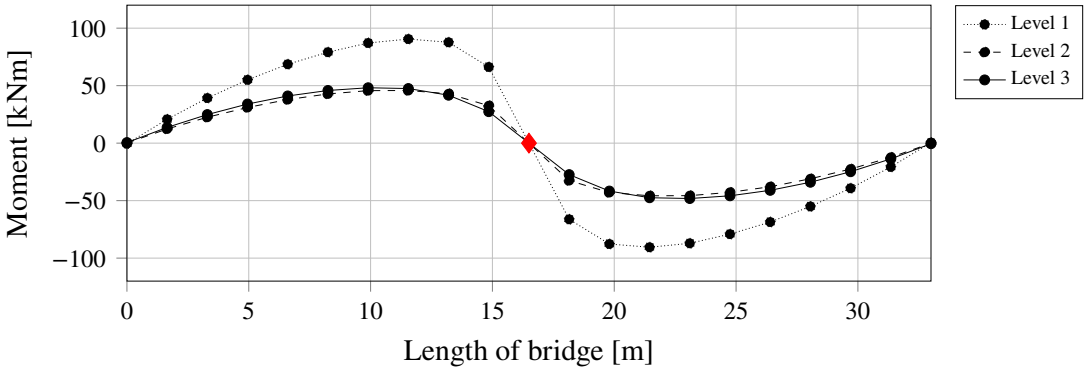

Figure 5.49 *The maximum secondary bending moment in the sixth transversal beam for the different positions of the concentrated traffic load along the length of the deck.*

5.3 Parametrization

The aim of the parametric study is to investigate how the stiffness of the transversal beams affects the secondary bending moment for the three different levels. To change the stiffness of the transversal beams in the weak direction, the width of the flanges was changed. Eleven different widths were studied, from 0.23 to 0.48 m. The elastic and plastic moment capacity in the weak direction is shown in Figure 5.50 for the different widths of the flanges. The elastic moment capacity in the weak direction for the cross section is, as expected, increasing when the width of the flanges is increasing. The plastic moment capacity in the weak direction increases even faster when the width of the flanges increases. Same behaviour is described in all three levels and for all load cases studied since it only depends on the cross section of the beam. The elastic moment capacity in the weak direction is of interest when designing in the serviceability limit state (SLS) and the fatigue limit state (FLS) meanwhile the plastic moment capacity in the weak direction is of interest when designing in the ultimate limit state (ULS).

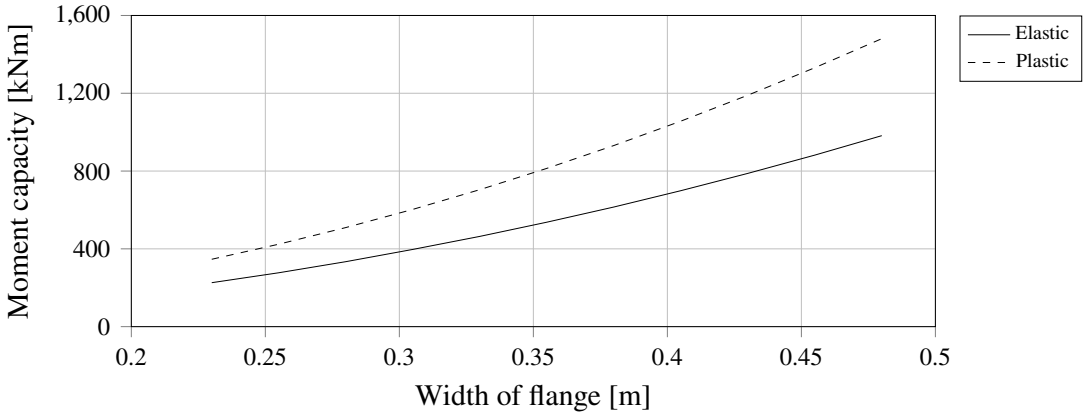

Figure 5.50 Variation of the elastic and plastic moment capacity in the weak direction for the transversal beams for different widths of the flanges. The values are independent on the type of load case, type of modelling technique and position of the transversal beam.

In Figure 5.51, the variation of maximum secondary bending moment in the first transversal beam is shown for the different flange widths for the uniformly distributed load case. The variation of secondary bending moment show the same behavior for all load cases and are presented in Appendix E. Level 1 has the highest secondary bending moment for all widths of the flanges. For all three levels the maximum secondary bending moment increases when the width of the flanges increases. The maximum secondary bending moment increases faster in level 1 than in level 2 and 3.

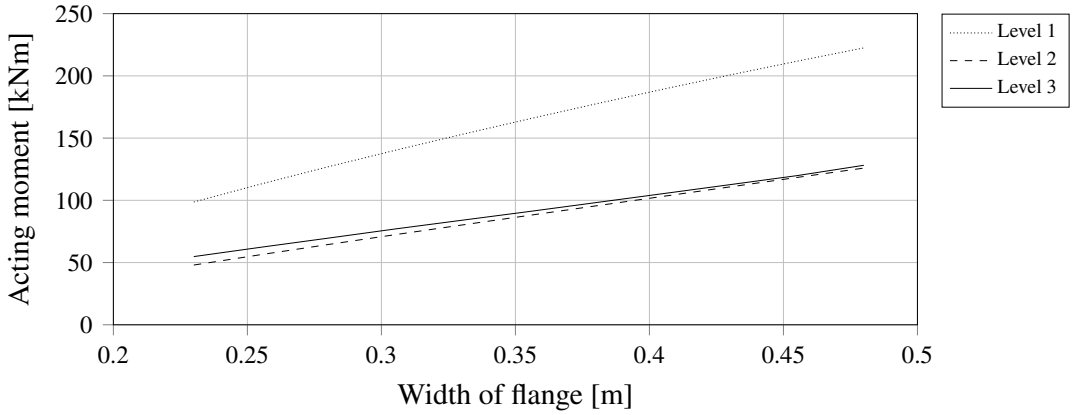

Figure 5.51 Variation of maximum acting secondary bending moment in the first transversal beam for different widths of the flanges, for the uniformly distributed load case.

When designing in SLS, the utilization ratio regarding the elastic moment capacity in the weak direction is of interest. The utilization ratio, regarding SLS, of the first transversal beam for the uniformly distributed load case for different widths of the flanges is presented in Figure 5.52.

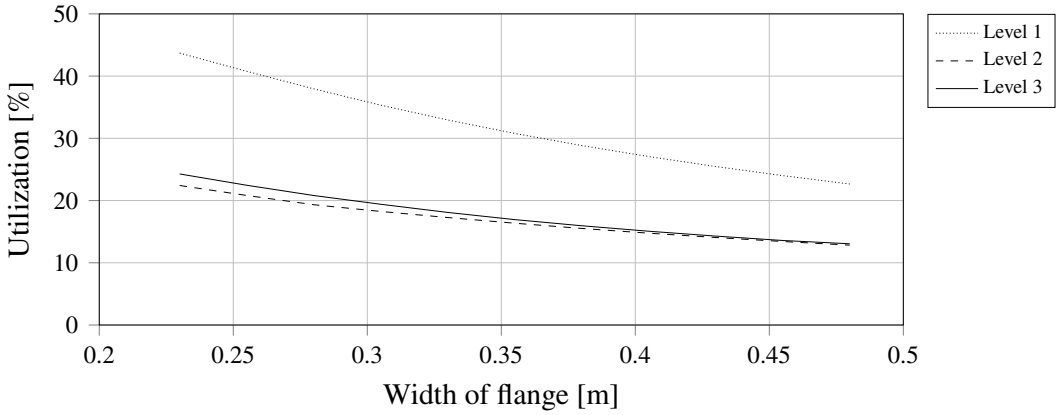

Figure 5.52 The utilization ratio, regarding SLS, of the first transversal beam for different widths of the flanges, for the uniformly distributed load case.

The utilization ratio, regarding SLS, of the first transversal beam for the temperature load case for different widths of the flanges is presented in Figure 5.53. The utilization ratio, regarding SLS, of the first transversal beam for the concentrated and the distributed traffic load case are presented in Figure 5.54 and Figure 5.55 respectively. The same behaviour is observed for the uniformly distributed load case when compared to the other load cases.

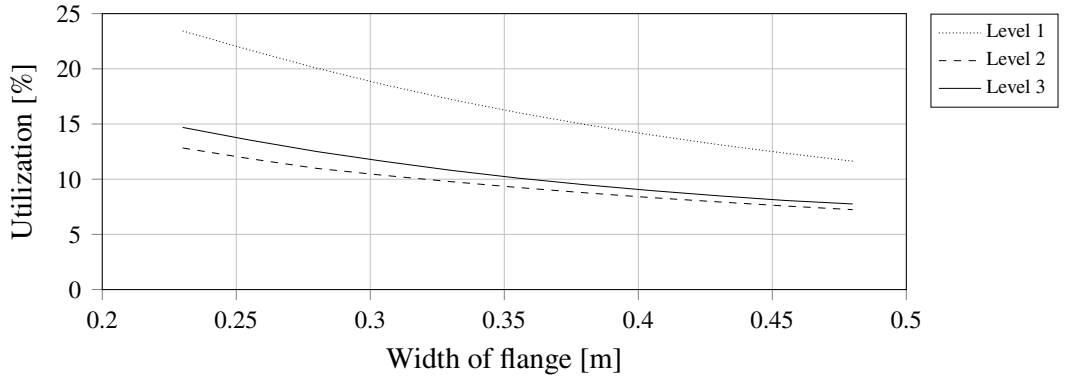

Figure 5.53 The utilization ratio, regarding SLS, of the first transversal beam for different widths of the flanges for the temperature load case.

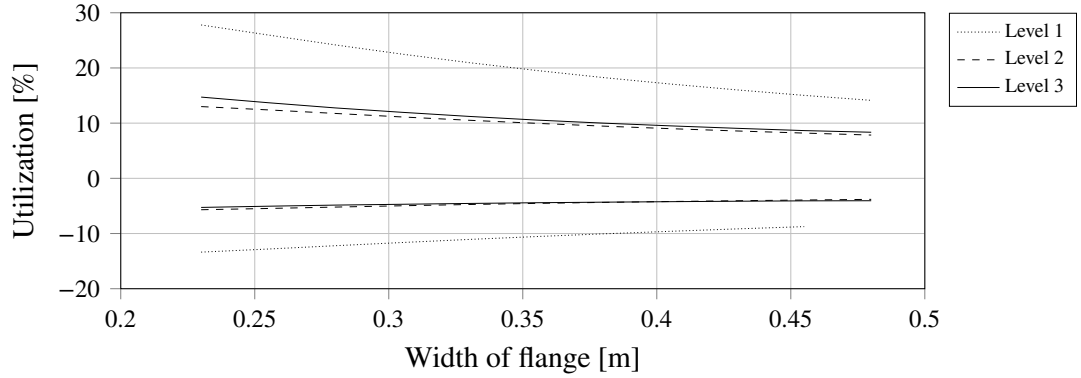

Figure 5.54 The utilization ratio, regarding SLS, of the first transversal beam for different widths of the flanges for the concentrated traffic load case.

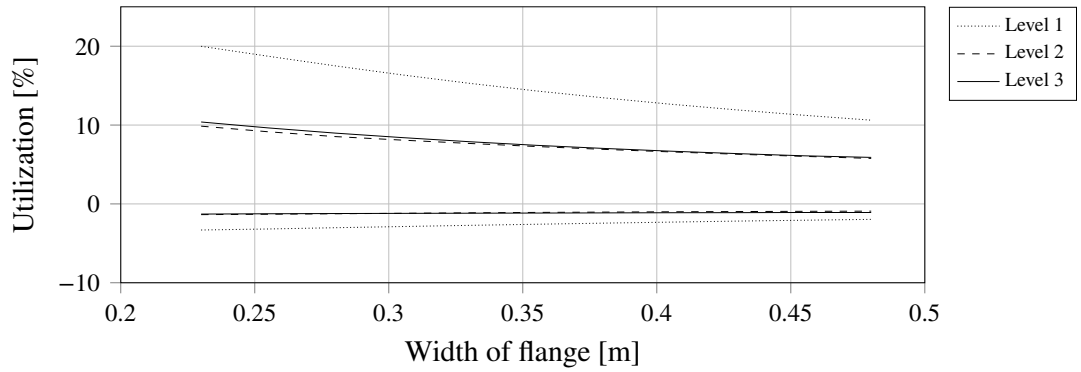

Figure 5.55 The utilization ratio, regarding SLS, of the first transversal beam for different widths of the flanges for the distributed traffic load case.

In SLS, the moment capacity in the weak direction, for all three levels, increases faster than the acting secondary bending moment for the first transversal beam for all load cases. For all load cases, the utilization ratio of the transversal beam is the highest in level 1. For level 2 and 3, the utilization ratio is similar.

The fatigue life depends on the largest difference of maximum and minimum stresses. The largest range of the secondary bending moment is in the sixth transversal beam. The difference between the maximum and minimum secondary bending moment in the sixth transversal beam is presented in Figure 5.56 and Figure 5.57 for different widths of the flanges, for the concentrated and distributed traffic load case respectively. The difference between the maximum and minimum secondary bending moment increases with increasing width of the flange. The secondary bending moment increases faster in level 1 than in level 2 and 3.

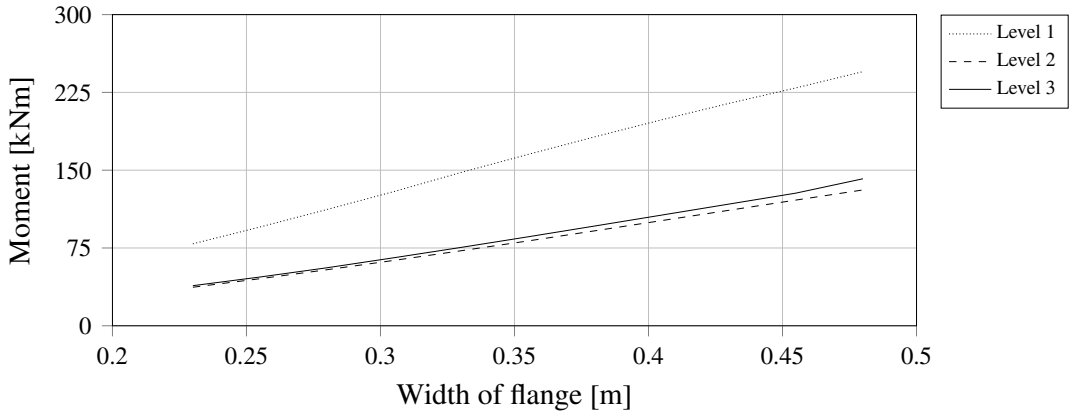

Figure 5.56 The difference in maximum and minimum secondary bending moment in the sixth transversal beam for different widths of the flanges for the concentrated traffic load case.

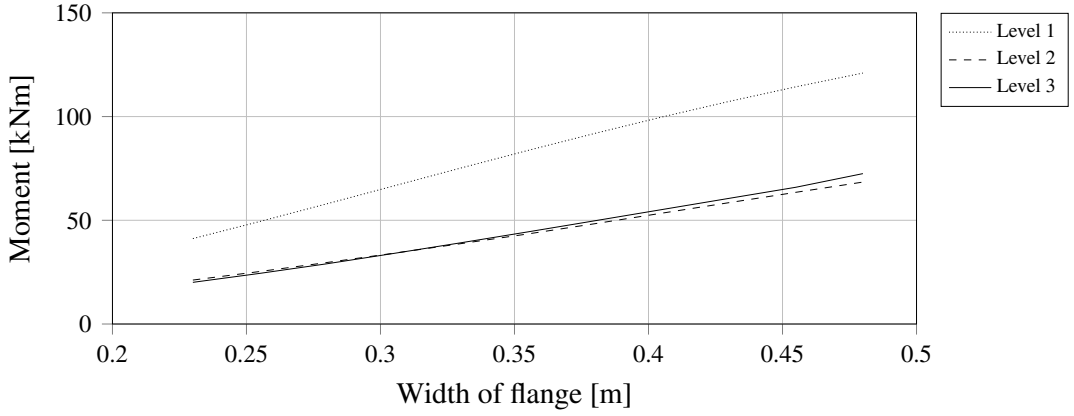

Figure 5.57 The difference in maximum and minimum secondary bending moment in the sixth transversal beam for different widths of the flanges for the distributed traffic load case.

When designing in ULS, the utilization ratio regarding the plastic moment capacity in the weak direction is of interest. The utilization ratio, regarding ULS, of the first transversal beam for all load cases for different widths of the flanges are presented in Figure 5.58, Figure 5.59, Figure 5.60 and Figure 5.61.

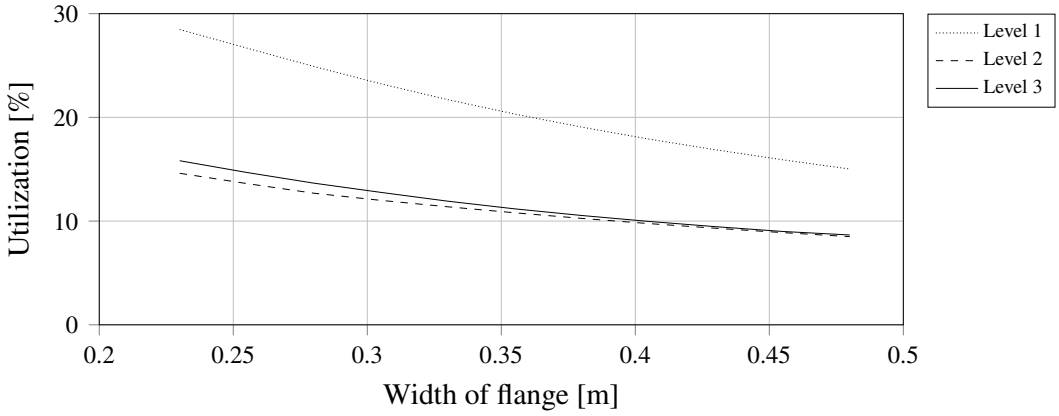

Figure 5.58 The utilization ratio, regarding ULS, of the first transversal beam for different widths of the flanges, for the uniformly distributed load case.

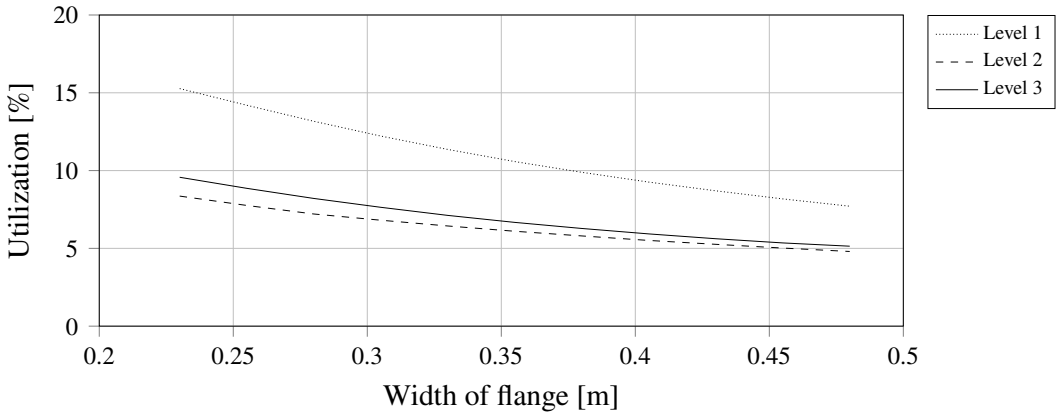

Figure 5.59 The utilization ratio, regarding ULS, of the first transversal beam for different widths of the flanges for the temperature load case.

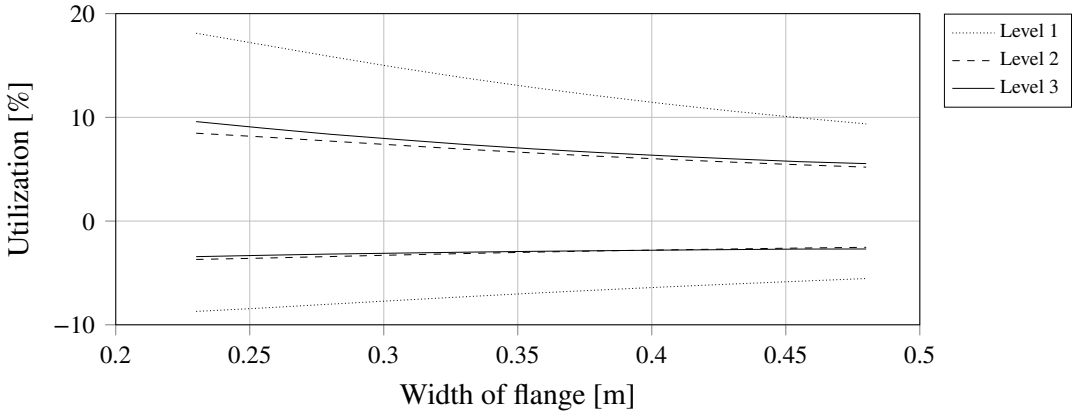

Figure 5.60 The utilization ratio, regarding ULS, of the first transversal beam for different widths of the flanges for the concentrated traffic load case.

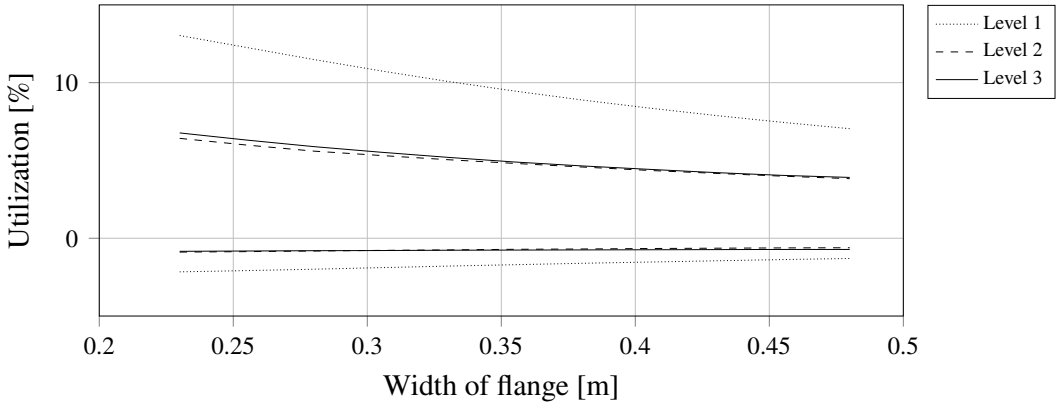

Figure 5.61 The utilization ratio, regarding ULS, of the first transversal beam for different widths of the flanges for the distributed traffic load case.

In ULS, the behaviour of the moment capacity in the weak direction is similar to SLS, for all three levels. For all load cases, the utilization ratio of the transversal beam is the highest in level 1. For level 2 and 3, the utilization ratio is similar.

6 Discussion

The aim of this master thesis is to investigate the effect of using different modelling techniques when designing a tied arch bridge with focus on how the restraining forces in the transversal beams are affected. The bridge was modelled with three different levels of complexity. In the simplest approach all structural parts were modelled using beam elements with the deck as a beam grillage. In the second level the deck was instead modelled using shell elements meanwhile in the most complex level the majority of the bridge was modelled using shell elements. The load cases studied were uniformly distributed load, temperature load and traffic load.

The results from the analyses are discussed and compared in the following chapter. Further, the difference between the three modelling techniques are pointed out. All discussions are only valid for the results extracted from the analysis made on the bridge in this master thesis.

6.1 Evaluation of results

Before FE-modelling was used, tied arch bridges were designed using two dimensional calculation methods, hence possible three dimensional effects could easily be missed. The results from the FE-analysis made in this master thesis shows that there are important three dimensional effects that are important to be included in design. It can also be seen that the choices concerning modelling technique and especially element type have a large impact on the result with regard to the restraining forces for the bridge studied in this master thesis.

The most apparent difference between the modelling techniques are the results of the secondary bending moment in the transversal beams, primarily in the outermost beams. The maximum secondary bending moment, i.e. the design moment, is approximate 50% larger in level 1, the beam grillage model, compared to in level 2 and 3, the models using shell elements for the deck. The distribution of the secondary bending moment in the transversal beam differ between level 2 and 3, however the maximum values are about the same. The same effect of the modelling technique can be noticed for all load cases studied.

In this master thesis, level 3, due to its higher complexity, gives a . Consequently, it can be considered as reference in the comparison between modelling techniques. The consequence of the high secondary bending moment in level 1 is that the design of the cross section becomes highly conservative, resulting in unnecessary use of material and higher self-weight than needed.

From the parametric study it can be seen that the magnitude of the restraining forces is dependent on the stiffness in the weak direction of the transversal beams. In all levels, the acting secondary bending moment increases with increased width of the flanges, both in SLS and in ULS. The comparison between the acting moment to the moment capacity of the cross section in the week direction shows that the beams capacity increases faster. Hence, the utilization ratio decreases when the width of the flanges increases. This effect of increasing the width of the flanges can be seen for all load cases studied in this master thesis. Level 1 is conservative regarding the secondary bending moment in the transversal beams for all widths of the flanges.

If a beam grillage model is used in design and the utilization ratio of the secondary bending moment

in the transversal beams needs to be decreased, one option is to increase the width of the flanges. However, this solution results in unnecessary use of material therefore a better solution would be to increase the complexity of the modelling level. The extra time required to create a more complex model is worth the effort since the design of the bridge would be more efficient. The difference in modelling technique can be displayed by comparing the needed flange width for a specific utilization ratio. If considering the utilization ratio in SLS for the uniformly distributed load case, the approximately needed flange widths to reach a utilization ratio of 20% for the different levels are presented in Figure 6.1.

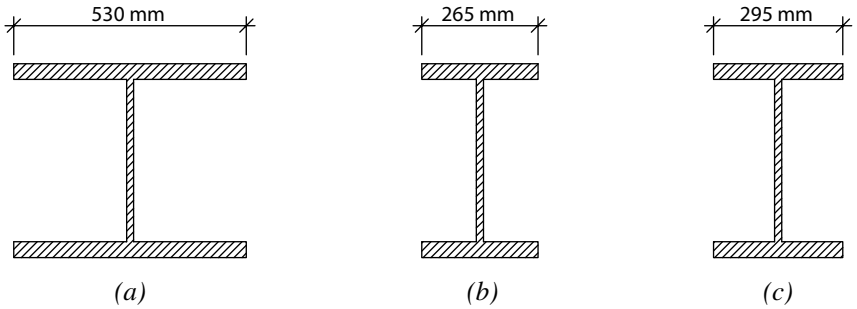

Figure 6.1 The needed cross section for the first transversal beam to reach the utilization ratio of 20%, regarding the secondary bending moment in SLS, for the uniformly distributed load case for a) level 1, b) level 2 and c) level 3.

The most reasonable explanation to justify the observed differences in the described behavior according to the different modelling levels might depend on how the deck is modelled, with beam grillage or with shell elements. The transversal beams and the deck work as composite sections. When the whole effective width is utilized, the secondary bending is mainly carried by the stiff transversal beam in the beam grillage: the effective width of the composite section could be utilized over the whole width of the deck. In a model with the deck modelled using shell elements, the whole effective width could not be utilized until a distance into the deck was reached, i.e. the stresses in the deck are transferred progressively from the transverse beam to the deck. However the composite action decreases towards the edges of the deck.

Another modelling choice that influence the secondary bending moment may be the interaction between the transversal beams and the deck. As described in Appendix B, it is clear that the modelling of the interaction affects the results. The magnitude of the secondary bending moment in the transversal beams increases with a stiffer interaction. The interaction between the deck and the transversal beams were, in level 3, modelled using the surface-based tie constraint in two lines. Interaction in two lines is a stiffer connection than interaction in one line and better describes the actual connection made by dowels. Since the transversal beams in level 1 and 2 were modelled using beam elements, it was impossible to constrain two lines on the beam element to the deck, therefore only one line was used. The fact that the surface-based tie constraint in one or two lines differ from each other indicated that using one line in level 1 and 2 affects the results.

In additional to the secondary bending moment in the transversal beams, differences in the normal

force in the longitudinal beams and the longitudinal direction of the deck can be seen. The summation of the normal forces is constant and equal for all modelling techniques, however the distribution between the deck and the longitudinal beam differs. If level 1 and 2 are conservative or not concerning the normal force depends on the load case studied. However, the difference in magnitude compared to level 3 is always larger for level 1 than for level 2. Compared to an overestimation leading to unnecessary use of material, the consequence of an underestimation can have negative effects. The design of the cross section can become too weak and the bridge could fail. Another effect to consider regarding the normal force in the deck is the distribution of the normal force over the width of the deck. The normal force distribution should be lowest in the middle and increase gradually towards the edges of the deck. This can be captured in level 2 and 3, however level 1 is not able to of capture the peak at the edges. If using a beam grillage model, this effect must be kept in mind when designing the reinforcement in the deck, a larger amount of reinforcement at the edges is needed than what the results indicated. The dowels are also influenced by the normal force distribution and needs to be designed according to the highest normal force.

The temperature load differ from the other load cases concerning the bending moment and the normal force in the arch. For the other load cases, these sectional forces and moments are similar for all three levels but for the temperature load they differ substantially. The bending moment and the normal force in the arch in level 1 is highly overestimated but in level 2 they are underestimated. These effects most be considered when choosing modelling technique.

Local effects from the traffic load can be seen in the secondary bending moment in the transversal beams. All transversal beams are exposed to similar magnitude of secondary bending moment and the most unfavourable placement of the concentrated load is, for each transversal beam, a few meters away from the beam considered. The local effect of a concentrated load can also be seen in the normal force in the longitudinal beams. In contrast to the other load cases, where the most critical section is at the ends, the most critical section for the concentrated traffic load is between the third and forth transversal beam.

The traffic load is important to consider in bridge design since problems with fatigue may occur. When the load is moving, the transversal beams are exposed to repeated varying load and the difference between the maximum and minimum secondary bending moment in each transversal beam is large. The most exposed beams are the ones in the middle and are thereby the most critical when designing with regard to fatigue.

6.2 Evaluation of the different modelling techniques

The most important differences between the three modelling techniques are, besides the overall accuracy of the results, the complexity of the modelling process and the computational time needed. Creating a model using only beam elements, including the deck as a beam grillage demands short computational time but the results are strongly dependent on the modelling choices concerning geometry. For example, the amount of beams in the longitudinal and transversal direction of the deck has to be decided as well as the positioning of the beams relative to the outer boundary of the deck. A beam grillage also requires a recalculation of a distributed load to line loads and how the line loads should be applied also needs to be considered. A model consisting of beam elements with the deck modelled using shell elements feel more intuitive since the deck is a structure resembling

the definition of a shell. The geometry of the deck is more straight forward than for a beam grillage and the load could be applied in a more realistic way. This type of model demands somewhat more computational time than a beam grillage model but considerable less than the more complex approach using shell elements for all structural parts. The modelling development of the complex model is also more demanding since less simplifications can be made and more attention to details is required.

The computational time and the complexity of the model development must be weighted against the accuracy of the results. For the bridge studied in this master thesis, a model combining beam and shell element gave relative accurate results compared with a model using mainly shell elements, while a beam grillage model gave highly conservative results concerning the secondary bending moment in the transversal beams. If the secondary bending moment is of interest, a beam grillage model is easy to use but gives conservative results, a model combining beam and shell element demands more computational time but gives more accurate results and a model using mainly shell elements is complex to establish and heavy to compute.

An additional subjects that need to be considered when choosing modelling technique is the level of post-processing. The level of post-processing is insignificant for the beam grillage model and small for the model combining beam and shell elements, hence it is easy to extract and interpret the results. The model using mainly shell elements however needs considerable more post-processing as well.

The needed adjustment of the mesh could also be a factor to consider. In the beam grillage model the mesh is easy to create and only a small risk of local defects in the mesh exists. When using shell elements, local irregularities in the geometry of the structure can give rise to distortion of the mesh, hence such model is more time consuming to develop.

7 Final remarks

The conclusions made in this master thesis regarding how the restraining forces are affected by the modelling techniques used are presented in this chapter followed by suggestions for further investigations.

7.1 Conclusion

In this master thesis the impact of the modelling techniques on restraining forces in a tied arch bridge was investigated. The bridge was modelled with three different levels of complexity. From the analyses made on the bridge studied in this master thesis the following conlclusions can be made:

- For the secondary bending moment in the outermost transversal beams, the beam grillage model is highly conservative and is therefore not a suitable model regarding the restraining forces. The model established with the deck as shell element and the remaining parts as beam elements gave a good approximation of the secondary bending moment in the transversal beams. This holds for all load cases studied.
- The normal force in the longitudinal beams and in the longitudinal direction of the deck are affected by the different modelling techniques. The beam grillage model gives inaccurate results and is again not a suitable model regarding the restraining forces. The model with combined beam and shell elements also gives inaccurate results, however the variation of horizontal shear force in the transversal beams indicates that if the area where the arches are connected to the longitudinal beams are modelled more in detail, the results may be improved.
- If a beam grillage model is used the high normal force in the longitudinal direction at the edges of the deck is not captured. Hence, the model is not suitable when designing the reinforcement in the deck and the dowels connecting the deck and the transversal beams.
- The parametric study shows that the restraining forces depends on the stiffness in the weak direction of the transversal beams. For all modelling techniques the utilization ratio of the transversal beams regarding the secondary bending moment decreases with increased stiffness in the weak direction of the beam, hence increased stiffness is a solution when the utilization ratio is to high.
- The restraining forces affects the fatigue strength of the structure. The secondary bending moment vary depending on where the load is applied and the most critical transversal beams are the ones in the middle. The difference between the maximum and minimum secondary bending moment in the transversal beams is highly overestimated for the beam grillage model and the model is thereby not suitable when designing with regard to fatigue life.

The recommended suitable detail level of the model, in view of the bridge studied in this master thesis, is to model the deck using shell elements and the remaining structural parts using beam elements. The area where the arches are connected to the longitudinal beams should be modelled in more detail, otherwise the possible underestimation of the normal force in the longitudinal beams and in the deck must be kept in mind.

7.2 Suggestions for further investigations

Since the subject of this master thesis is complex and there are many factors that affects the structure with regard to restraining forces further investigations are of interest. Some examples of interesting aspects are:

- The conclusions made in this master thesis is only valid for the specific bridge studied. In order to draw conclusions that holds for all tied arch bridges, more bridges with different geometry has to be investigated. All load cases and load combinations in design of bridges according to Eurocode needs to be included.
- The beam grillage model is convenient to use and for some finite element software the only possible way to model a deck. It would therefore be of interest to investigate if it is possible to modify the beam grillage to get more accurate results. For example by changing the amount of beams, the stiffness of the deck or the interaction between the beam grillage and the transversal beams.
- A more detailed study of the influence of the stiffness of the transversal beams should be addressed, i.e. the impact on the structural behavior when different cross sections are utilized for the outermost transversal beams or changing the detail of its connection to the longitudinal beams.
- It was observed that the temperature affected the structure in a large extend when compared to other load cases, hence it should be investigated in more detail with focus on the whole structure.

A Drawings bridge

The dimensions of the bridge studied in this master thesis are based on an existing tied arch bridge. The drawings of the bridge are made by Reinertsen Sweden AB, and the drawings relevant to creating the FE-model in this master thesis are shown in this appendix.

PROFILNUMMER	30	40	50	60	70
PROFILHØYDE	435.653	435.862	436.071	436.280	436.489
TERRENGHØYDE	434.101	435.238	435.167	434.977	433.259
VERTIKALKURVE	-2,090%				
HORISONTALKURVE	R= ∞				

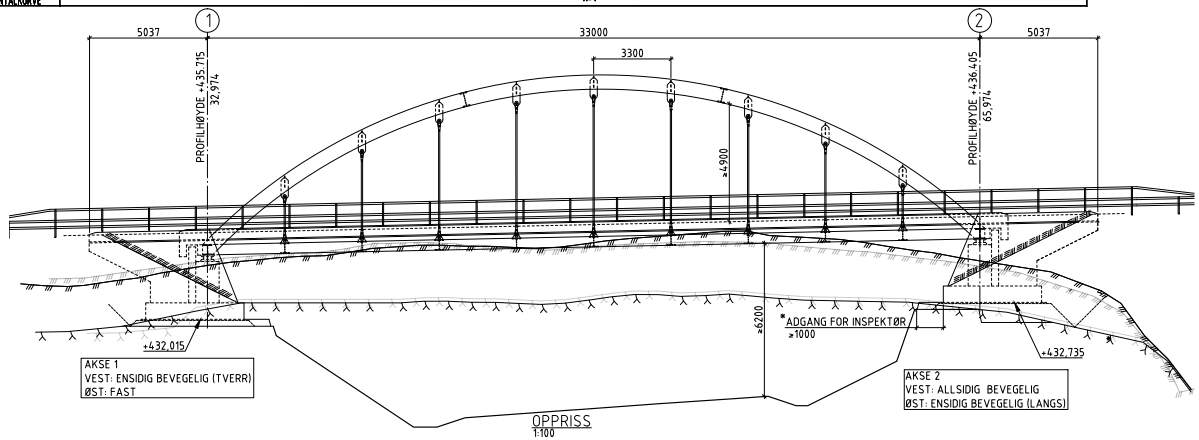

OPPRISS
1:100
BEGGE AKSER*

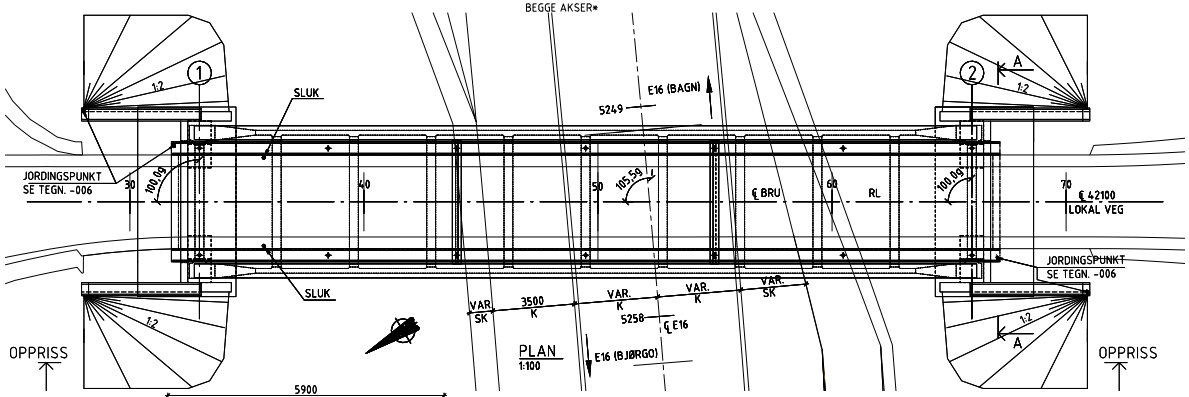

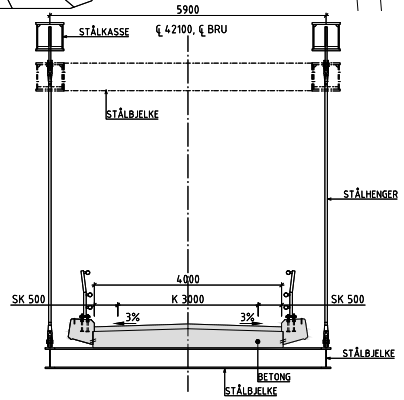

TYP. TVERRSNITT
1:50

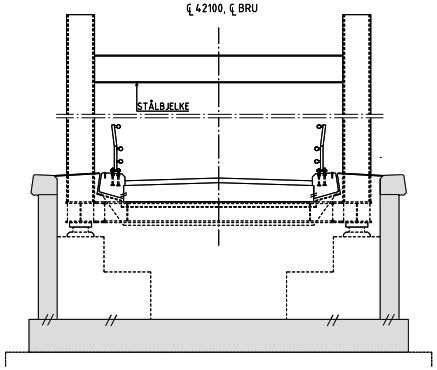

A-A
1:50

MERKNADER

E16: VEGTYPE S2(H2 IHT HB N100), ÅDT=3200, FARTSGRENSE 80km/t
LOKALVEG A1, ÅDT=1500, FARTSGRENSE 30km/t
FERDIGSTILLELSE/OVERTAKELSE: 2018

DIMENSJONERINGSGRUNNLAG:
- STATENS VEGVESEN HÅNDBOK N400, BRUPROSJEKTERING, EUROKODEUTGAVE (2011)
- KOORDINATSYSTEM: NTM SONE 9
- HØYDEREF: NN 1954

KONSTRUKSJONSTYPE:
- BUEBRU I SYREFAST STÅL OG BETONG.

BETONG/ARMERING

BETONGKVALITET:	B45 SV-40
BESTANDIGHETSKLASSE:	MF40
ARMERING:	B500NC
KONTROLLKLASSE:	UTFØRELSESKLASSE 3

STÅL
PLATER: KVALITET 1.4462 f_y =460MPa IHT NS EN 10088-2
LEVERINGSTILSTAND 1D
TILLEGGSKRAV 40Joule VED -40°C
HENGER: STREKKSTAGSYSTEM FOR HENGER SKAL HA ETA-GODKJENNING (EUROPÉEN TECHNICAL APPROVAL) TENSION ROD SYSTEM S460 M48 KVALITET 1.4462 IHT NS EN 10088-3, ELLER TILSVARENDE. ALLE DELER SKAL VÆRE RUSTFRIE/SYREFASTE.

DYBLER: KVALITET 1.4401 f_y =200MPa IHT NS EN 10088-3

FUNDAMENTERING:
LANDKAR AKSE 1 OG 2 DIREKTEFUNDAMENTERES PÅ AVRETTINGSBETONG PÅ SPRENGT BERG. AVRETTINGSBETONG B45.

BELEGNING:
DIMENSJONERENDE BELEGNING MED TYNGDE 3 kN/m²
BELEGNINGSKLASSE A3, IHT HB R762
TOTAL BELEGNINGSTYKKELSE PÅ BRUPLATE LIK 95 mm
12±3 mm TOPEKA S4
80 mm Ab 11 PmB

REKKVERK:
STYRKEKLASSE H2. BRØYTETETT OG KLATRESIKKERT. OVERGANG MELLOM BRU- OG VEGREKKVERK SAMT AVSLUTNING AV BRUREKKVERK SKAL UTFORMES IHT. HB N101 REKKVERK OG VEGENS SIDEOMRÅDER SAMT HB V160 VEGREKKVERK.

LAGRE :
LAGRE I BEGGE AKSER.

FORKLARINGER:

SK	SKULDER		
K	KJØRBANE		MARK
RL	RETT LINJE		BERG

Revisjon	Revisjonen gjelder	Utarb	Kontr	Godkjent	Rev. dato
		-	-	-	-

E16 Hp: 11
Bagn - Bjørgo
05-1931 KLOSBØLE BRU
K05, OVERSIKTSTEGNING
KONKURRANSEGRUNNLAG

Tegningsdato	13.05.2016
Bestiller	Statens Vegvesen
Produsert for	Region øst
Produsert av	REINERTSEN AS
PROF-nummer	104164
Arkivnummer	201303719B
Byggenr/anummer	05-1931
Målestokk A1	1:100

Utarbeidet av	Kontrollert av	Godkjent av	Konsulentaktiv	Tegningsnummer / revisjonsbokstav
AD	BG	EN	2700025	K05-001

NORMALER OG RETNINGSLINJER:

-DIMENSJONERENDE VEKT AV MEMBRAN OG SLITELAG:3,0kN/m²
-HÅNDBOK N400: BRUPROSJEKTERING
-HÅNDBOK R411: FORVALTNING, DRIFT OG VEDLIKEHOLD AV BRUER
-HÅNDBOK V441: INSPEKSJONSHÅNDBOK FOR BRUER
-HÅNDBOK R610: STANDARD FOR DRIFT OG VEDLIKEHOLD
-HÅNDBOK V440: BRUREGISTRERING
-HÅNDBOK R762: PROSESSEKODE 2

INSPEKSJON, DRIFT OG VEDLIKEHOLD:

SOM HOVEDREGEL UTFØRES INSPEKSJON, DRIFT OG VEDLIKEHOLD I HENHOLD TIL STANDARD RUTINER I STATENS VEGVESEN ETTER HÅNDBOK R610, V441 OG R411.

DET VISES OGSÅ TIL HÅNDBOK V440 BRUREGISTRERING OG BRUTUS.

KJØREBESKRIVELSE TIL BRUA:
FØLG E16 NORDOVER FRA BAGN, CA. 200 METER ETTER BAGNSKLEIVETUNNELEN.

SPESIELLE FORHOLD VED KLOSBØLE BRU:

- INSPEKSJON AV ALLE SLUK/AVLØPSRØR ÅRLIG OG EVENTUELL RENGJØRING VED BEHOV. PLASSERING AV SLUK ER VIST PÅ TEGNING K05-21.

- DET LIGGER TREKKERØR OG TREKKEKUMMER PÅ NORDRE SIDE AV BRUA, VED AKSE 1. EVENTUELLE GRAVEJOBBER, UTSKIFTING AV REKKVERK ETC. MÅ TA HENSYN TIL DETTE.

- OPPFØLGING AV KORROSJONSBESKYTTELSE PÅ BRU-LAGRE I ALLE AKSER FØR UTGANGEN AV GARANTIPERIODEN (INNEN XXXX)
DET MÅ SJEKKES OM PULVERLAKKEN BLÆRER ELLER FLASSER.

- OPPFØLGING AV REKKVERK OG INNFESTING AV DETTE FØR UTGANGEN AV GARANTIPERIODEN, OG DERETTER HVERT 5. ÅR. SPESIELT MED HENSYN TIL KORROSJONSBESKYTTELSE AV STÅL, OG EVENTUELT SKADE PÅ INNFESTING, SKJEVHETER ETC.

-PÅ SYNLIGE BETONGFLATER REGISTRERES TILFELLER AV STØRRE RISS, FORVITRING, AVSKALLING OG TEGN TIL ARMERINGSKORROSJON.

- ÅRLIG OPPFØLGING AV ASFALT INN MOT BRUENDE MED HENSYN PÅ EVENTUELL OPPSPREKKING OG SETNINGER.

- BELEGNINGSTYKKELSE FÅR IKKE ØKES. VED FRAMTIDIG ASFALTERING SKAL EKSISTERENDE SLITELAG FJERNES FØR NYTT LEGGES.
DET MÅ IKKE FRESES I MEMBRANEN SOM LIGGER UNDER BINDELAGET.

- SPESIELL OPPFØLGING AV SYREFAST KONSTRUKSJONSSTÅL I PUNKTER DER ANGREP KAN SKJE.

-BRUA ER IKKE PÅFØRT EKSTERN KORROSJONSBESKYTTELSE.

-HENSYN BØR TAS TIL OMRÅDER SOM KAN VÆRE UTSATT FOR MANGLENDE RENGJØRING AV SVEISER, KLORIDER (VEGSALT), ANSAMLING AV SKITT OG STØV UTSATT FOR FUKT.

FØLGENDE DETALJER INSPISERES SPESIELT VED HOVEDINSPEKSJON:
-OVERSIDE AV FLENSER TIL LANGSGÅENDE BJELKER OG NEDRE TVERRBJELKER.
-NEDRE INNFESTING AV HENGERE.
ÅRLIG RENGJØRING AV FØLGENDE DETALJER:
-OVERSIDE AV FLENSER TIL LANGSGÅENDE BJELKER OG NEDRE TVERRBJELKER.
-NEDRE INNFESTING AV HENGERE.

PROSEDYRER VED EVENTUELL UTSKIFTING/REPARASJON AV LAGRE:

OVERSIKT OVER VALGTE LAGERTYPER OG DIMENSJONERENDE LAGERLASTER ER OPPGITT PÅ TEGNING K05-004. FOR SELVE LAGRENES OPPBYGGING OG VIRKEMÅTE HENVISES DET TIL PRODUSENT.

VED OPPJEKKING SKAL DET FORTLØPENDE KONTROLLERES AT BRUA IKKE ER FASTHOLDT I REKKVERK, OPPLAGRING ELLER FUGESPALTER.

SKAL LAGERET SKIFTES UT MÅ MAN PÅREGNE Å JEKKE OPP BEGGE OPPLEGGSPUNKTER I AKSEN SAMTIDIG, MED TOTALT 2 JEKKER. DET MÅ ALLTID TILSEES AT MAKS LØFT FORBLIR UNDER 10mm. STENGNING AV BRU BØR VURDERES MENS OVERBYGNINGEN ER HEVET, PGA. UHELDIGE SLAG OG VARIABLE BELASTNINGER PÅ JEKKER.

PROSEDYRE FOR HENGESTENGER:

HENGESTENGER I FØLGE TEGNING K05-054.
DRIFTSPROSEDYRER UTARBEIDES I SAMRÅD MED LEVERANDØR.

INSPEKSJONSTYPER:

DE FØRSTE INSPEKSJONER:
- FERDIGBEFARING VED OVERTAGELSE
- REKLAMASJONSBEFARING ETTER 2 ÅR

RUTINEMESSIGE INSPEKSJONER:
- ENKEL INSPEKSJON, ANBEFALES ÅRLIG
- HOVEDINSPEKSJON, ANBEFALES HVERT 5 ÅR
- SPESIALINSPEKSJON, VED BEHOV

INNMÅLINGER AV NIVELLERINGSBOLTER

INNMÅLT DATO						
NIVELLERINGSBOLT NR.	X	Y	HØYDE	HØYDE	HØYDE	HØYDE
101						
102						
103						
104						
105						
106						
107						
108						
109						
110						
111						
112						
113						
114						

DET SKAL FORETAS INNMÅLING AV NIVELLERINGSBOLTER VED FERDIGSTILLELSE AV KONSTRUKSJON (X,Y OG HØYDE). DETTE SKAL UTFØRES FØR OVERTAGELSE AV BRU, ETTER ASFALT OG REKKVERK ER MONTERT. VERDIENE SENDES OPPDRAGSGIVER FOR INNTEGNING I DENNE TABELLEN. PLASSERING AV NIVELLERINGSBOLTER ER VIST PÅ TEGNING K05-021 OG K05-006. DET MÅ ENTYDIG OPPLYSES OM HVILKE FASTPUNKTER SOM ER BENYTTET, OG SØRGES FOR AT DET KUN BRUKES FASTPUNKTER SOM OGSÅ VIL VÆRE TILGJENGELIGE VED EVENTUELL FREMTIDIGE INNMÅLINGER. KRAV TIL MÅLENØYAKTIGHET ER I UTGANGSPUNKTET +/- 2mm. UTFØRT MÅLENØYAKTIGHET FØRES I TABELLENS NEDERSTE RAD. KOORDINATSYSTEM ER EUREF NTM SONE 9. VIDERE SKAL DET GJØRES EN KONTROLLMÅLING I GOD TID FØR GARANTITIDEN UTLØPER (KUN HØYDE). BEHOVET FOR VIDERE FREMTIDIGE INNMÅLINGER AVKLARES PÅ BAKGRUNN AV DENNE.

MERKNADER:

E16: VEGTYPE S2(H2 IHT HB N100), ÅDT= 3200, FARTSGRENSE 80 km/t.
LOKALVEG: VEGTYPE A1, ÅDT= 1500, FARTSGRENSE 30 km/t.

KOORDINATSYSTEM: NTM SONE 9
HØYDEREF: NN1954

IDV-GRUNNLAG:

- STATENS VEGVESEN HÅNDBOK R610 STANDARD FOR DRIFT OG VEDLIKEHOLD
- STATENS VEGVESEN HÅNDBOK V440 BRUREGISTRERING
- STATENS VEGVESEN HÅNDBOK V441 INSPEKSJONSBOK FOR BRUER
- STATENS VEGVESEN HÅNDBOK V411 FORVALTNING, DRIFT OG VEDLIKEHOLD AV BRUER.
- STATENS VEGVESEN HÅNDBOK R762 PROSESSKODE 2

DIMENSJONERINGSGRUNNLAG:

- STATENS VEGVESEN HÅNDBOK N400 BRUPROSJEKTERING EUROKODEUTGAVE (2011)

KONSTRUKSJONSTYPE:

- BUEBRU I SYREFAST STÅL OG BETONG.

BETONG/ARMERING:

BETONGKVALITET:	B45 SV-40
BESTANDIGHETSKLASSE:	MF40
ARMERING:	B500NC
UTFØRELSESKLASSE:	3

KONSTRUKSJONSSTÅL:

1.4462 f_y=460MPa IHT NS EN 10088-2 PLATER
1.4462 f_y=460MPa IHT NS EN 10088-3 HENGER
1.4401 f_y=200MPa IHT NS EN 10088-3 DYBLER

KVALITET BELEGNING:

FUKTISOLERINGSTYPE A3-4, 12±3mm TOPEKA 4S, SLITELAG 40mm (Ab), OG BINDELAG 40mm (Agb11 PmB) MED DIMENSJONERENDE VEKT PÅ 3,0kN/m²

FUNDAMENTERING:

LANDKAR AKSE 1 OG 2 DIREKTEFUNDAMENTERES PÅ AVRETTINGSBETONG PÅ SPRENGT BERG.

REKKVERK:

STYRKEKLASSE H2.

LAGRE:

LAGRE I BEGGE AKSER.

HENVISNINGER:

- OVERSIKTSTEGNING	K05-001
- GRAVE-/FYLLINGSPLAN	K05-002
- BRULAGER	K05-004
- BELEGNING OG UTSTYR	K05-005
- REKKVERK	K05-006
- AKSE 1 OG 2, MÅL	K05-011
- OVERBYGNING BETONG, MÅL	K05-021
- OVERBYGNING BETONG, TYP ARM.	K05-030
- STÅL, OVERSIKT	K05-051

Revisjon	Revisjonen gjelder	Utarb	Kontr	Godkjent	Rev. dato
		.			.

Statens vegvesen

E16 Hp: 11
Bagn - Bjørgo

05-1931 KLOSBØLE BRU

K05, INSPEKSJONS-, DRIFTS- OG VEDLIKEHOLDSPLAN

KONKURRANSEGRUNNLAG

Tegningsdato	30.11.2015
Bestiller	Statens Vegvesen
Produsert for	Region øst
Produsert av	REINERTSEN AS
PROF-nummer	104164
Arkivnummer	201303719B
Byggenrlenummer	05-1931
Målestokk A1	1:100
Tegningsnummer / revisjonsbokstav	K05-003

Utarbeidet av	Kontrollert av	Godkjent av	Konsulentarkiv
VV	BG	EN	2700025

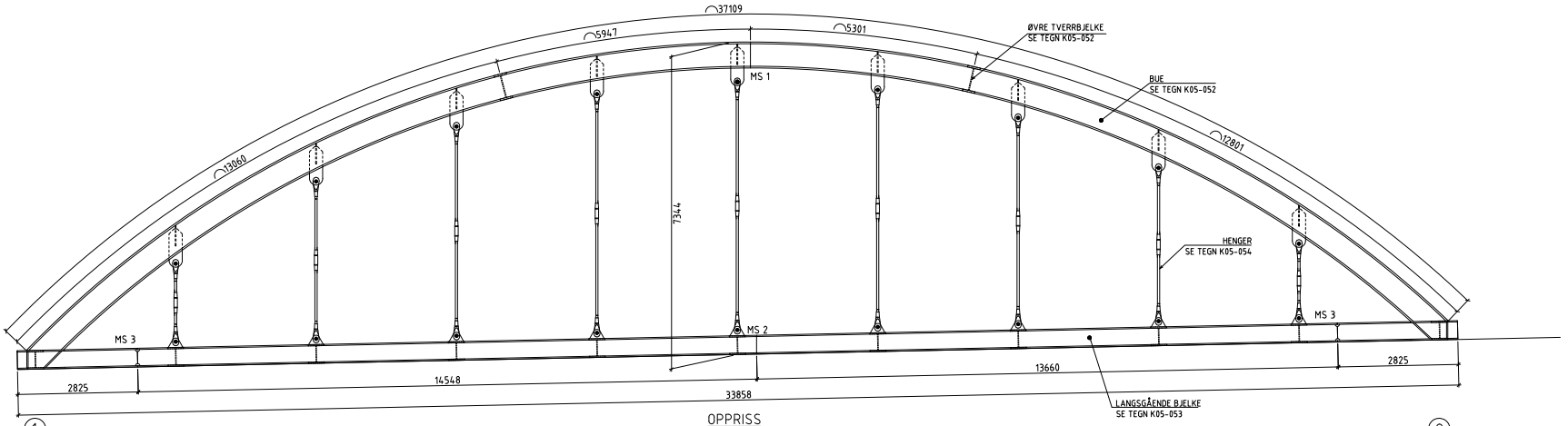

OPPRISS
1:50

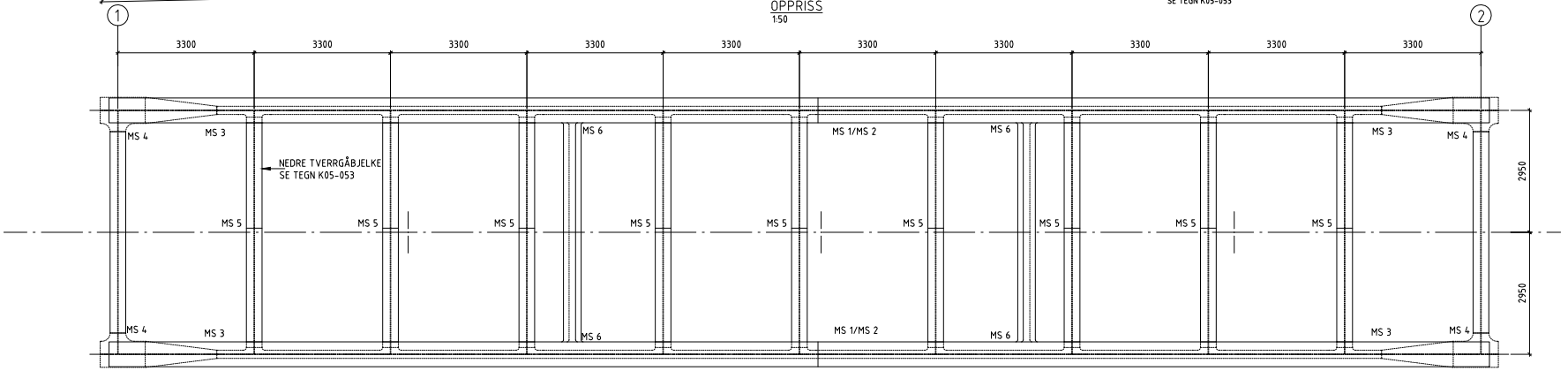

PLAN
1:50

MERKNADER

STÅL:
PLATER: KVALITET 1.4462 f_y =460MPa IHT NS EN 10088-2 LEVERINGSTILSTAND 1D
TILLEGGSKRAV 40Joule VED -40°C
HENGER: STREKKSTAGSYSTEM FOR HENGER SKAL HA ETA-GODKJENNING (EUROPÉEN TECHNICAL APPROVAL) TENSION ROD SYSTEM S460 M48 KVALITET 1.4462 IHT NS EN 10088-3, ELLER TILSVARENDE. ALLE DELER SKAL VÆRE RUSTFRIE/SYREFASTE.
DYBLER: KVALITET 1.4401 f_y =200MPa IHT NS EN 10088-3
VED SVEISING SKAL ELEKTRODER/TILSETTINGSMATERIALET VÆRE TILPASSET GRUNNMATERIALET.

UTFØRELSE OG KONTROLL IHT. HB R762 PROSESSKODE 2.
KONTROLLKLASSE IHT. HB R762 TAB. 85-1. KONTROLLKLASSE 3 FOR HENGESTANGSFESTET.

MÅLENE PÅ STÅLET ER ANGITT FOR EN TEMPERATUR LIK +10°C.

PLASSERING AV BUTTSKJØTER SKAL FORELEGGES BYGGHERREN OG GODKJENNES AV DEN PROSJEKTERENDE.

LANGSGÅENDE BJELKE (UNDERGURTEN) PRODUSERES MED EN OVERHØYDE, SE OVERHØYDEDIAGRAM TEGNING K05-053.

MONTASJESKJØTER:

MS-MONTASJESKJØT
SE TEGNING K05-054

MS 1	SE DETALJ 1
MS 2	SE DETALJ 2
MS 3	SE DETALJ 3
MS 4	SE DETALJ 4
MS 5	SE DETALJ 5
MS 6	SE DETALJ 6

HENVISNINGER

- STÅL, BUE OG ØVRE TVERRBJELKER	K05-052
- STÅL, LANGSGÅENDE BJELKER OG NEDRE TVERRBJELKER, OVERHØYDEDIAGRAM	K05-053
- STÅL, HENGER OG MONTASJEDETALJER	K05-054

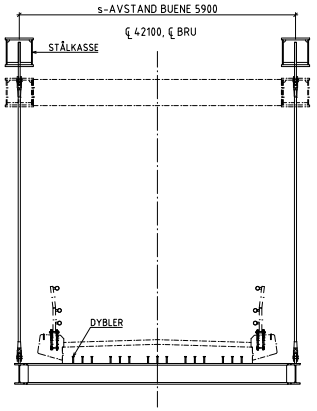

TYP. TVERRSNITT
1:50

Revisjon	Revisjonen gjelder	Utarb	Kontr	Godkjent	Rev. dato
		-			-

Tegningsdato	13.05.2016
Bestiller	Statens Vegvesen
Produsert for	Region øst
Produsert av	REINERTSEN AS

E16 Hp: 11
Bagn - Bjørgo
05-1931 KLOSBØLE BRU
K05, STÅL OVERSIKT
KONKURRANSEGRUNNLAG

PROF-nummer	104164
Arkivnummer	201303719 8
Byggenr/arnummer	05-1931
Målestokk A1	1:50

Utarbeidet av	Kontrollert av	Godkjent av	Konsulentaktiv
AD	BG	EN	2700025

Tegningsnummer / revisjonsbokstav: K05-051

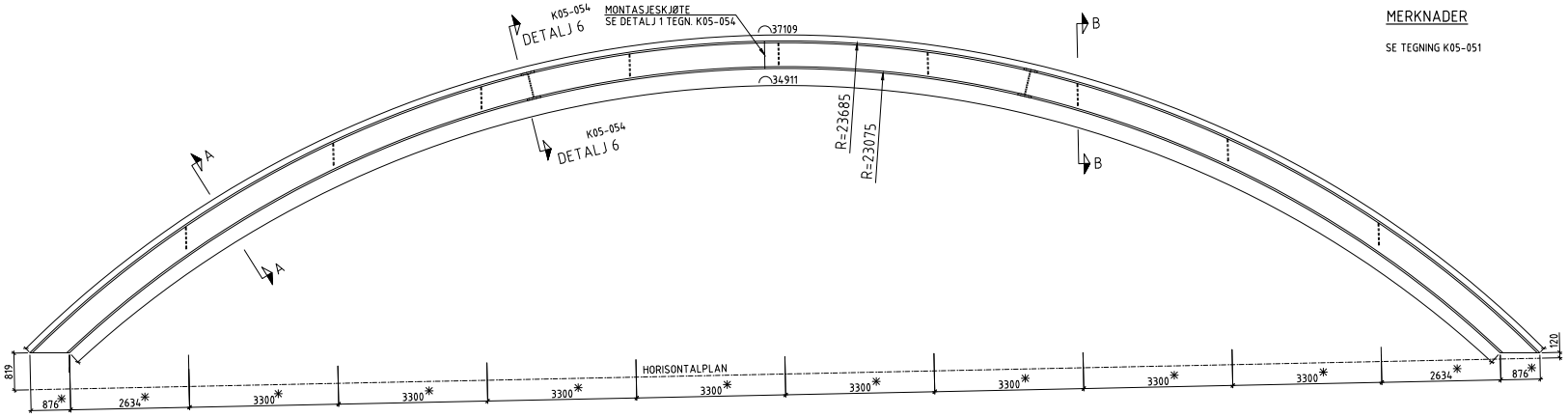

BUE
1:50

✱ MÅL ANGITT I HORISONTALRETNING

MERKNADER

SE TEGNING K05-051

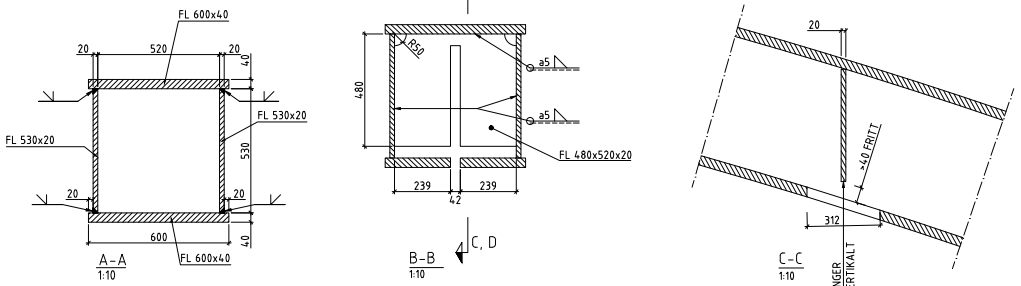

A-A
1:10

B-B
1:10

C-C
1:10

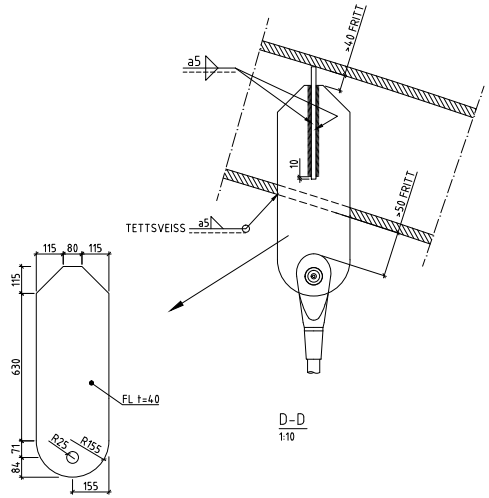

D-D
1:10

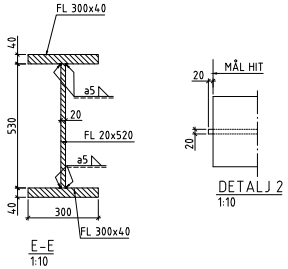

E-E
1:10

DETALJ 2
1:10

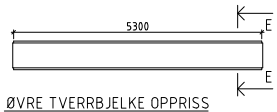

ØVRE TVERRBJELKE OPPRISS
1:50

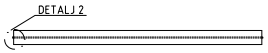

ØVRE TVERRBJELKE PLAN
1:50

Revisjon	Revisjonen gjelder	Utarb	Kontr	Godkjent	Rev. dato
		-			-

Tegningsdato	30.11.2015
Bestiller	Statens Vegvesen
Produsert for	Region øst
Produsert av	REINERTSEN AS

E16 Hp: 11
Bagn - Bjørgo

05-1931 KLOSBØLE BRU

K05, STÅL, BUE OG ØVRE TVERRGÅENDE BJELKE

KONKURRANSEGRUNNLAG

PROF-nummer	104164
Arkivnummer	201303719 8
Byggenr/anummer	05-1931
Målestokk A1	1:50, 1:10

Utarbeidet av	Kontrollert av	Godkjent av	Konsulentaktiv
AD	BG	EN	2700025

Tegningsnummer / revisjonsbokstav: **K05-052**

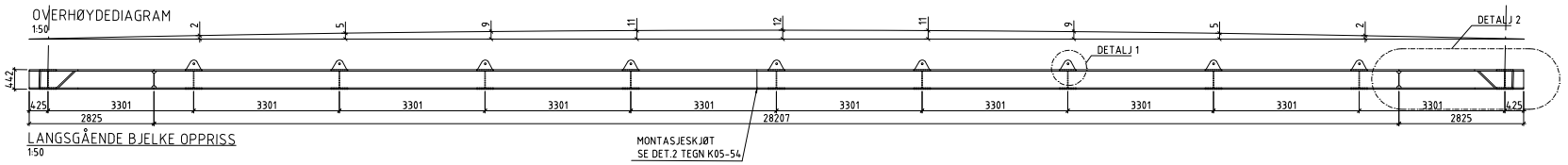

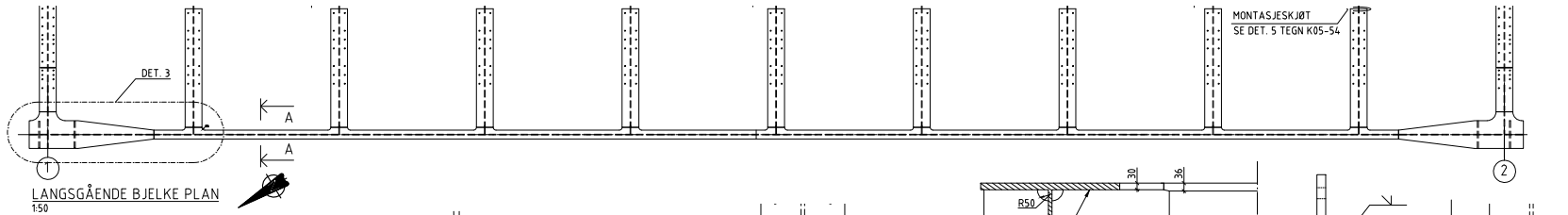

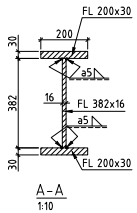

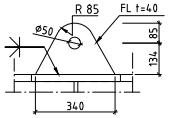

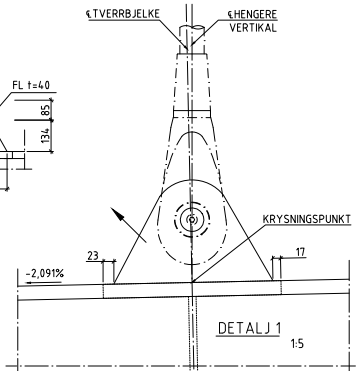

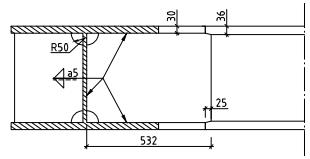

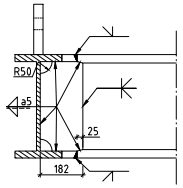

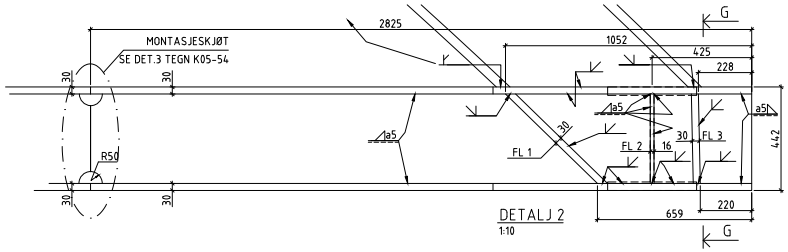

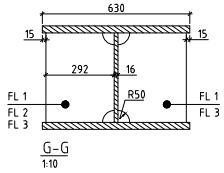

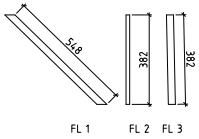

MERKNADER

SE TEGNING K05-051.

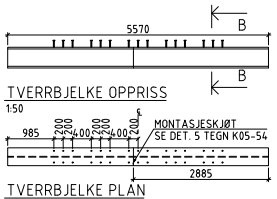

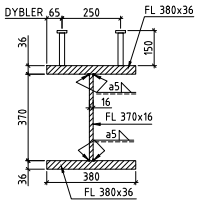

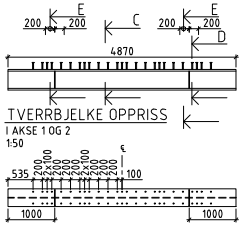

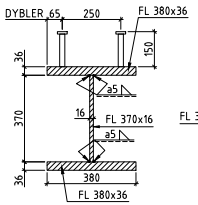

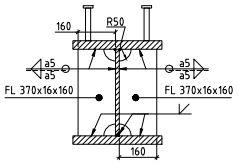

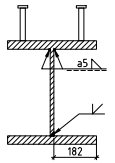

Revisjon	Revisjonen gjelder	Utarb	Kontr	Godkjent	Rev. dato
		-			

Tegningsdato	13.05.2016
Bestiller	Statens Vegvesen
Produsert for	Region øst
Produsert av	REINERTSEN AS
PROF-nummer	104164
Arkivnummer	201303719B
Byggherrenummer	05-1931
Målestokk A1	1:50, 1:10, 1:5
Tegningsnummer / revisjonsbokstav	K05-053

E16 Hp: 11
Bagn - Bjørgo

05-1931 KLOSBØLE BRU

K05, STÅL, LANGSGÅENDE BJELKE OG NEDRE TVERRBJELKER

KONKURRANSEGRUNNLAG

Utarbeidet av	Kontrollert av	Godkjent av	Konsulentaktiv
AD	BG	EN	2700025

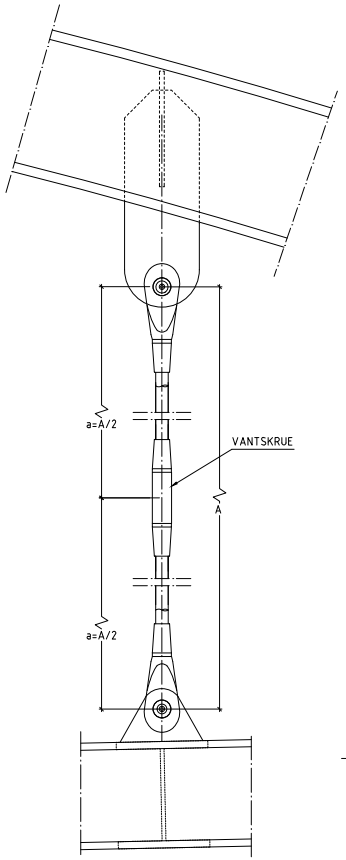

DETALJ 1
1:10

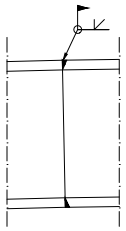

DETALJ 1
MONTASJESKJØT BUE
1:10
K05-051

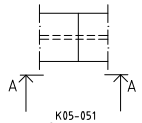

DETALJ 2
MONTASJESKJØT LANGSGÅENDE BJELKE
1:10
K05-051

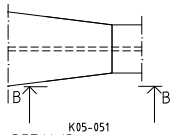

DETALJ3
MONTASJESKJØT LANGSGÅENDE BJELKE
1:10
K05-051

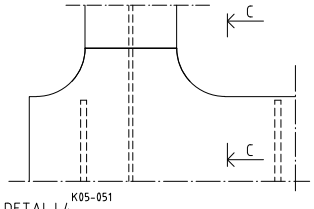

DETALJ 4
MONTASJESKJØT LANGSGÅENDE BJELKE/NEDRE TVERRBJELKE
1:10
K05-051

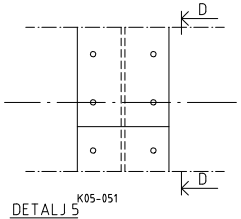

DETALJ 5
MONTASJESKJØT NEDRE TVERRBJELKE
1:10
K05-051

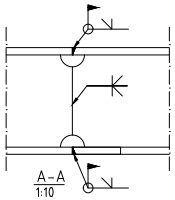

A-A
1:10

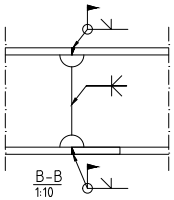

B-B
1:10

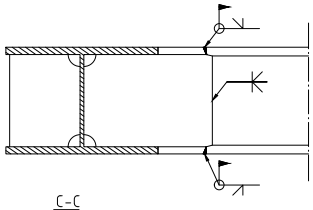

C-C
1:10

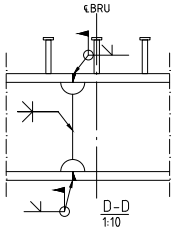

D-D
1:10

DETALJ 7

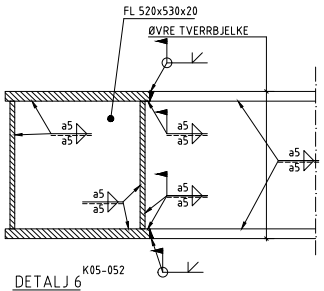

DETALJ 6
MONTASJESKJØT BUE/ØVRE TVERRBJELKE
1:10
K05-052

DETALJ 7

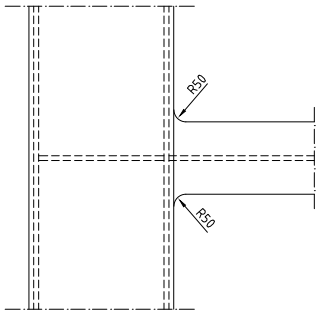

DETALJ 7
MONTASJESKJØT BUE/ØVRE TVERRBJELKE
1:10

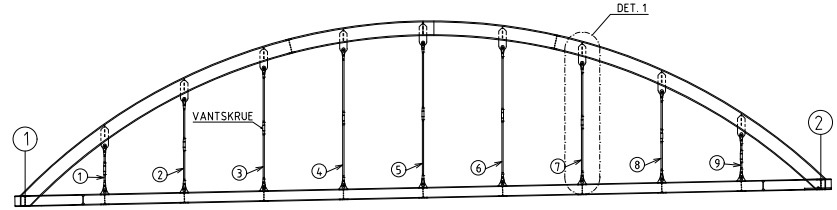

OPPRISS
1:100

MERKNADER

SE TEGNING K05-051

HENGERE: ET SYSTEM SOM «MACALLOY TENSION ROD SYSTEM» S460 M48 KVALITET 1,4462 IHT NS-EN 10088-3 ELLER TILSVARENDE SKAL BRUKES. ALLE DELER SKAL VÆRE SYREFASTE.

HENGERSYSTEMET SKAL VÆRE JUSTERBART UNDER LAST.

HENGERE SKAL UTRUSTES MED VANTSKRUE.

MACCALLOY TECHNO TENSIONER ELLER TILSVARENDE SKAL BRUKES VED SIDEN AV VANTSKRUER FOR KONTROLL AV KRAFT I HENGERE.

MONTASJE IHT LEVERANDØRENS ANVISNINGER.

SYSTEMET SKAL VÆRE ETA (EUROPEAN TECHNICAL APPROVAL) GODKJENT.

MONTASJE REKKEFØLGE - FORSLAG

1. UNDERGURT SVEISES MED OVERHØYDE IHT TEGNING K05-053

2. UNDERGURT, LANGSGÅENDE BJELKER, BUE OG TVERRBJELKER MONTERES TIL EN MONTASJEENHET VED BRUSTEDET

3. HENGERE MONTERES OG STRAMMES SLIK AT VEKT AV TVERRBJELKER OG UNDERGURT HOLDES

4. MONTASJEENHET LØFTES INN PÅ FORSKALING MED DEFINERTE OVERHØYDER SOM UNDERGURT. JEKKER MÅ VÆRE FORHÅNDSPLASSERT UNDER INNFESTNINGSPUNKTER FOR HENGERE.

5. BETONGPLATE STØPES OG HERDES

6. ETTERSTRAMMING AV HENGERE SLIK AT EGENVEKT AV BRUDEKKET BÆRES AV HENGERNE

7. FORSKALING SENKES JEVNT IHT OVERHØYDEDIAGRAM (K05-053) VED HJELP AV JEKKENE

8. JUSTERING AV HENGERE, SE BESKRIVELSE PROSESS 85.429

TABELL HENGERE:

POS.	MÅL A (mm)	ANTALL	⊗
1	1834	2	106
2	3695	2	107
3	4919	2	97
4	5608	2	93
5	5821	2	92
6	5570	2	93
7	4846	2	97
8	3605	2	107
9	1757	2	106

MÅL A= SPENNINGSFRI LENGDE SOM HENGER SKAL PRODUSERES ETTER. DE ANGITTE LASTENE ØKER MÅL A MED 1mm

⊗ HENGERKREFTER (kN), INKLUDERT BELASTNING AV ALT STÅL OG BETONGPLATE.

TIL TEKNISK GODKJENNING 07.10.2016

Revisjon	Revisjonen gjelder	Utarb	Kontr	Godkjent	Rev. dato
		.			.

Tegningsdato	
Bestiller	Statens Vegvesen
Produsent for	Region øst
Produsent av	REINERTSEN AS
E16 Hpr. 11 Bagn - Bjørgo	
05-1931 KLOSBØLE BRU	
K05, STÅL, HENGERE OG MONTASJEDETALJER	
ARBEIDSGRUNNLAG	
PROF-nummer	104164
Arkivnummer	2013037198
Byggverksnummer	05-1931
Målestokk A1	1:100, 1:10

Utarbeidet av	Kontrollert av	Godkjent av	Konsulentarkiv
AD	BG	EN	2700025

Tegningsnummer / revisjonsbokstav: K05-054

B Interaction

There are several types of interaction methods that can be used when connecting the transversal beam to the deck and therefore an investigation was made to find the most suitable. Two methods were tested, the surface-based tie constraint and connector elements, described in Section 2.3.The connector elements was placed in the positions where the dowels between the deck and the transversal beams are.

With these two constraints there are different possibilities to do the connection. In reality, the transversal beam and deck are connected with dowels in two rows. Since the transversal beam is modelled using beam element for level 1 and 2, it is only possible to do the connection in one row for those levels. In level 3, it was tested to have connector elements and the surface-based tie constraint in both one and two lines. For the surface-based tie constraint it was also investigated how the results were affected if the surface of the deck was constraint to the surface of the transversal beam and to a line in the middle of the transversal beam. The effect of the interaction method used was investigated by looking at the secondary bending moment in the first transversal beam. The results from level 3 can be seen in Figure B.1.

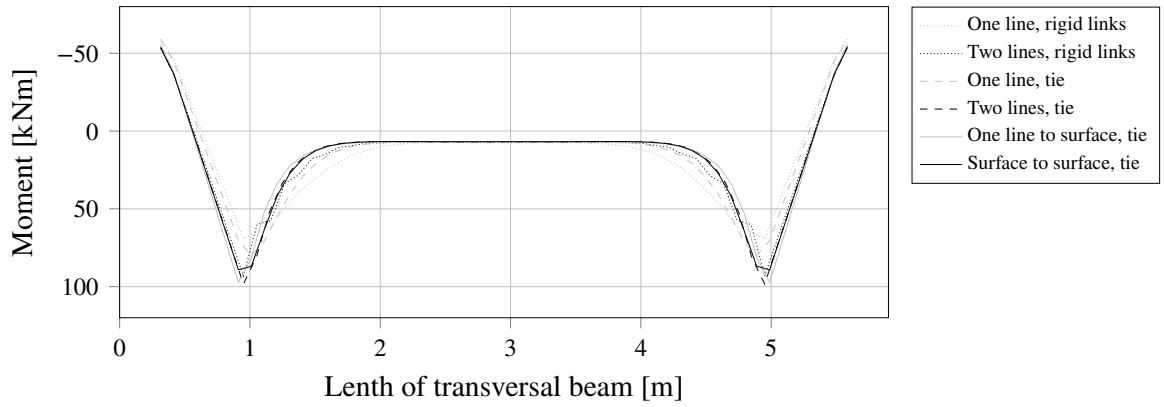

Figure B.1 Secondary bending moment in the first transversal beam for the different interaction methods.

It is possible to deduce that the two interactions made in one line creates a connection that is less stiff than the other interactions. The interaction with connector elements should represent the reality in the most suitable manner but demands higher computational capacity than the surface-based tie constraint. Since four interaction methods gave similar results and since the surface-based tie constraint is less computational heavy it was concluded that the surface-based tie constraint with two lines constraint was the most suitable method.

C Convergence study

A convergence study was made for all three levels to decide a suitable size of the mesh. Different mesh sizes, from 0.5 m to 0.05 m, were tested and values for secondary bending moment in the first transversal beam, bending moment in transversal direction in the deck and the deflection in mid span of the bridge were compared. The result from the convergence study of level 1 can be seen in Table C.1, where the percentage shows the percentage change of the results. It can be concluded that for level 1, the model has converged for the mesh size 0.25 m in the deck and the longitudinal beam. In the transversal beams however, the model did not converge satisfying, so therefore a smaller mesh size was tested. It showed that the transversal beams needed the mesh size 0.01 m to reach convergence, and the same mesh size was used in the transversal beams in the beam grillage. The results from the convergence study of level 2 can be seen in Table C.2 and it can be concluded that for the mesh size 0.1 m the model has converged. In Table C.3, the results from the convergence study of level 3 can be seen and it can be concluded that the model has converged for the mesh size 0.1 m. To sum up, in level 1, the mesh size 0.01 m was used for the transversal beams and the transversal beams in the beam grillage and the mesh size 0.25 m was used for the rest of the model. In level 2 and 3 the mesh size 0.1 m was used.

Table C.1 Convergence study for level 1.

	Secondary bending moment in transversal beam		Bending moment in transversal deck		Deflection in longitudinal beam	
Mesh size [m]	Magnitude [kNm]	Difference [%]	Magnitude [kNm]	Difference [%]	Magnitude [mm]	Difference [%]
Uniform load						
0.5	63.27	38.1	61.07	1.9	-9.47	0.1
0.25	102.17	33.8	62.24	0.3	-9.46	0.1
0.1	154.24	7.3	62.43	0.0	-9.45	0.0
0.05	166.47	0.1	62.46	-	-9.45	-
0.025	166.49		-		-	
Temperature load						
0.5	33.92	36.87	62.54	0.1	1.84	0.5
0.25	53.73	33.0	62.49	0.0	1.85	0.0
0.1	80.24	7.2	62.49	0.0	1.85	0.0
0.05	86.46	3.9	62.49	-	1.85	-
0.025	89.96		-		-	
Maximum traffic load						
0.5	129.05	15.0	83.74	1.4	1.57	8.3
0.25	151.85	16.5	84.94	0.7	1.44	4.9
0.1	181.91	3.7	85.58	0.2	1.37	1.4
0.05	188.91	2.0	85.79	-	1.35	-
0.025	192.83		-		-	
Minimum traffic load						
0.5	-25.86	34.3	0.007	53.0	-13.12	0.0
0.25	-39.34	39.8	0.0149	4.0	-13.12	0.0
0.1	-65.35	8.5	0.00155	1.2	-13.12	0.0
0.05	-71.45	4.6	0.00157	-	-13.12	-
0.025	-74.87		-		-	

Table C.2 Convergence study for level 2.

	Secondary bending moment in transversal beam		Bending moment in transversal deck		Deflection in longitudinal beam	
Mesh size [m]	Magnitude [kNm]	Difference [%]	Magnitude [kNm]	Difference [%]	Magnitude [mm]	Difference [%]
Uniform load						
0.5	66.19	19.5	93.58	1.5	-10.20	1.3
0.25	82.25	7.7	93.44	4.4	-10.33	1.0
0.1	89.18	1.8	89.34	4.0	-10.43	0.3
0.05	90.85		93.11		-10.46	
Temperature load						
0.5	37.35	19.7	111.92	0.9	1.46	4.8
0.25	46.49	7.7	110.90	3.8	1.39	3.6
0.1	50.35	1.8	106.65	2.8	1.34	1.5
0.05	51.30		109.71		1.32	
Maximum traffic load						
0.5	68.72	19.9	148.66	1.5	1.57	7.6
0.25	85.83	9.4	146.41	4.5	1.45	4.8
0.1	94.72	1.8	139.86	4.7	1.38	1.5
0.05	96.45		146.90		1.36	
Minimum traffic load						
0.5	-22.06	19.7	-5.61	53.0	-13.82	1.1
0.25	-27.46	14.2	-5.73	4.0	-13.98	0.8
0.1	-31.99	1.4	-5.78	1.2	-14.10	0.2
0.05	-32.43		-5.97		-14.13	

Table C.3 Convergence study for level 3.

	Secondary bending moment in transversal beam		Bending moment in transversal deck		Deflection in longitudinal beam	
Mesh size [m]	Magnitude [kNm]	Difference [%]	Magnitude [kNm]	Difference [%]	Magnitude [mm]	Difference [%]
Uniform load						
0.5	113.49	13.0	89.95	1.1	-8.97	5.0
0.25	100.12	2.0	91.0	2.2	-9.44	1.8
0.1	98.35	0.4	88.93	3.6	-9.61	0.5
0.05	98.71		85.71		-9.66	
Temperature load						
0.5	-68.14	14.7	112.75	3.1	1.86	11.3
0.25	-59.42	1.5	109.25	0.8	1.65	4.2
0.1	-58.55	0.4	108.42	0.8	1.58	0.6
0.05	-58.81		107.58		1.57	
Maximum traffic load						
0.5	40.72	18.9	143.76	2.7	1.41	2.8
0.25	34.26	1.7	147.72	1.7	1.37	2.2
0.1	33.69	2.8	145.14	0.7	1.34	1.5
0.05	34.64		144.03		1.32	
Minimum traffic load						
0.5	-122.27	14.3	-4.63	7.4	-12.66	3.6
0.25	-106.95	1.8	-5.0	0.5	-13.10	0.9
0.1	-105.08	0.8	-5.03	1.7	-13.22	0.0
0.05	-105.94		-5.12		-13.22	

D Verification

1 INPUT

1.1 Geometry

1.1.1 Arch

Radius arch $r_{ar} := 23.38m$

Width flange $wf_{ar} := 0.6m$

Thickness of flange $tf_{ar} := 0.04m$

Height of web $hw_{ar} := 0.53m$

Thickness of web $tw_{ar} := 0.02m$

1.1.2 Longitudinal beams

Length longitudinal beam $L_{lb} := 33m$

Length longitudinal beam made of shell $L_{lb.shell} := 9 \cdot 2 \cdot 0.822m = 14.8\,m$

Length longitudinal beam made of beam element $L_{lb.beam} := 8 \cdot (3.3m - 2 \cdot 0.822m) = 13.25\,m$

Width flange $wf_{lb} := 0.2m$

Thickness of flange $tf_{lb} := 0.03m$

Height of web $hw_{lb} := 0.382m$

Thickness of web $tw_{lb} := 0.016m$

Number of longitudinal beams $n_{lb} := 2$

1.1.3 Transversal beams

Length transversal beam, level 1 and 2 $L_{tb} := 5.9m$

Length transversal beam, level 3 $L_{tb.3} := 5.9m$

Width flange $wf_{tb} := 0.38m$

Thickness of flange $tf_{tb} := 0.036m$

Height of web $hw_{tb} := 0.37m$

Thickness of web $tw_{tb} := 0.016m$

Center to center distance $cc_{tb} := 3.3m$

Number of transversal beams $n_{tb} := 11$

1.1.4 Hangers

Diameter of hanger $d_{ha} := 0.048m$

Center to center distance $cc_{ha} := 3.3m$

Number of hangers $n_{ha} := 18$

Length of hanger type 1 $L_{ha\_1} := 2.733m$

Length of hanger type 2 $L_{ha\_2} := 4.616m$

Length of hanger type 3 $L_{ha\_3} := 5.865m$

Length of hanger type 4 $L_{ha\_4} := 6.582m$

Length of hanger type 5 $L_{ha\_5} := 6.816m$

1.1.5 Bracings

Length bracing $L_{br} := 5.9m$

Width flange $wf_{br} := 0.3m$

Thickness of flange $tf_{br} := 0.04m$

Height of web $hw_{br} := 0.53m$

Thickness of web $tw_{br} := 0.02m$

1.1.6 Deck

Length $L_{de} := 33m$

Width $w_{de} := 4m$

Height $h_{de} := 0.38m$

1.1.7 End part, level 3

Length end part in longitudinal direction $L_{l.end1} := 1.105m$

$L_{l.end2} := 1.72m$

$L_{l.end3} := 0.074m$

Width flange $wf_{end1} := 0.63m$

$wf_{end2} := 0.2m$

Thickness of flange $tf_{end} := 0.03m$

Height of web $hw_{end} := 0.382m$

Thickness of web $tw_{end} := 0.016m$

Angle of inclined stiffener $\alpha_{end} := 44.2deg$

Length of end part in transversal direction $L_{t.end} := 5.9m - wf_{end1} = 5.27\,m$

1.2 Material

E-modulus concrete $E_{conc} := 36GPa$

Poisson's ratio concrete $v_{conc} := 0.2$

Expansion coefficient concrete $\alpha_{conc} := 1 \cdot 10^{-5}$

Density concrete $\rho_{conc} := 2500 \frac{kg}{m^3}$

E-modulus steel $E_{steel} := 210GPa$

Poisson's ratio steel $v_{steel} := 0.3$

Density steel $\rho_{steel} := 7850 \frac{kg}{m^3}$

1.3 Loads

Uniform load $Q := 20 \frac{kN}{m^2}$

Point load traffic $Q_{traffic} := 150kN$

Uniform load traffic $q_{traffic} := 9 \frac{kN}{m^2}$

2 CALCULATIONS

2.1 Effective width of transverse beam in beam grillage

Calculated according to EN-1992-1-1 (5.3.2.1)

Effective width on each side of beam

$$b_{eff.1} := 0.2 \cdot cc_{tb} + 0.1 \cdot L_{tb} = 1.25\,m$$

$$b_{eff.1} := if\left(b_{eff.1} \le 0.2 \cdot L_{tb}, b_{eff.1}, 0.2 \cdot L_{tb}\right) = 1.18 \cdot m$$

$$b_{eff.2} := 0.2 \cdot cc_{tb} + 0.1 \cdot L_{tb} = 1.25\,m$$

$$b_{eff.2} := if\left(b_{eff.1} \le 0.2 \cdot L_{tb}, b_{eff.1}, 0.2 \cdot L_{tb}\right) = 1.18 \cdot m$$

Total effective witdh

$$b_{eff} := b_{eff.1} + b_{eff.2} + wf_{tb} = 2.74\,m$$

Width composite section

$$w_{tbg.m} := b_{eff} = 2.74\,m$$

Width sub section in transverse beam grillage

$$w_{tbg.s} := cc_{tb} - w_{tbg.m} = 0.56\,m$$

Length of deck

$$L_{de} := L_{de} + w_{tbg.m} = 35.74\,m$$

2.2 Length of arch

Half of midpoint angle of arch circle

$$\alpha_{ar} := \operatorname{asin}\left(\frac{\frac{L_{lb}}{2}}{r_{ar}}\right) = 0.78$$

Midpoint angle of arch circle

$$\beta_{ar} := 2 \cdot \alpha_{ar} = 1.57$$

Length of arch

$$L_{ar} := r_{ar} \cdot \beta_{ar} = 36.63\,m$$

2.3 Cross section area

Cross section area of arch

$$A_{ar} := wf_{ar} \cdot tf_{ar} \cdot 2 + hw_{ar} \cdot tw_{ar} \cdot 2 = 0.07\,m^2$$

Cross section area of hanger

$$A_{ha} := \frac{d_{ha}^{\,2} \cdot \pi}{4} = 1.81 \times 10^{-3}\,m^2$$

Cross section area of longitudinal beam

$$A_{lb} := wf_{lb} \cdot tf_{lb} \cdot 2 + hw_{lb} \cdot tw_{lb} = 0.02\,m^2$$

Cross section area of transversal beam

$$A_{tb} := wf_{tb} \cdot tf_{tb} \cdot 2 + hw_{tb} \cdot tw_{tb} = 0.03\,m^2$$

Cross section area of bracing

$$A_{br} := wf_{br} \cdot tf_{br} \cdot 2 + hw_{br} \cdot tw_{br} = 0.03\,m^2$$

Cross section area of arch

$$A_{ar} := wf_{ar} \cdot tf_{ar} \cdot 2 + hw_{ar} \cdot tw_{ar} \cdot 2 = 0.07\,m^2$$

Cross section area of deck

$$A_{de} := w_{de} \cdot h_{de} = 1.52\,m^2$$

2.4 Volume

Volume of arch

$$V_{ar} := A_{ar} \cdot L_{ar} \cdot 2 = 5.07 \cdot m^3$$

Volume of hanger

$$V_{ha} := 2 \cdot A_{ha} \cdot \begin{pmatrix} 2 \cdot L_{ha\_1} \cdots \\ + 2 \cdot L_{ha\_2} \cdots \\ + 2 \cdot L_{ha\_3} \cdots \\ + 2 \cdot L_{ha\_4} \cdots \\ + L_{ha\_5} \end{pmatrix} = 0.17 \cdot m^3$$

Volume of longitudinal beam, level 1 and 2

$$V_{lb} := A_{lb} \cdot L_{lb} \cdot n_{lb} = 1.2 \cdot m^3$$

Volume of transversal beam

$$V_{tb} := A_{tb} \cdot L_{tb} \cdot n_{tb} = 2.16 \cdot m^3$$

Volume of bracing

$$V_{br} := A_{br} \cdot L_{br} \cdot 2 = 0.41 \cdot m^3$$

Volume of deck

$$V_{de} := A_{de} \cdot L_{de} = 54.32 \cdot m^3$$

Volume of longitudinal beam made of beam element

$$V_{lb.beam} := A_{lb} \cdot L_{lb.beam} \cdot n_{lb} = 0.48 \cdot m^3$$

Volume of longitudinal beam made of shell element

$$V_{lb.shell} := A_{lb} \cdot L_{lb.shell} \cdot n_{lb} = 0.54 \cdot m^3$$

Volume of flanges in end part

$$V_{end.f} := \begin{bmatrix} wf_{end1} \cdot L_{l.end1} + \left[wf_{end2} + \frac{\left(wf_{end1} - wf_{end2} \right)}{2} \right] \cdot L_{l.end2} \cdots \\ + L_{l.end3} \cdot wf_{end2} \end{bmatrix} \cdot tf_{end} = 0.04 \cdot m^3$$

Volume of web in end part

$$V_{end.w} := \left(L_{l.end1} + L_{l.end2} + L_{l.end3} \right) \cdot \left(hw_{end} + tf_{end} \cdot 2 \right) \cdot tw_{end} = 0.02 \cdot m^3$$

Volume of first stiffener in end part

$$V_{end.stiff1} := wf_{end1} \cdot \left(hw_{end} + tf_{end} \cdot 2 \right) \cdot tf_{end} = 8.35 \times 10^{-3} \cdot m^3$$

Volume of second stiffener in end part

$$V_{end.stiff2} := wf_{end1} \cdot \left(hw_{end} + tf_{end} \cdot 2 \right) \cdot tw_{end} = 4.46 \times 10^{-3} \cdot m^3$$

Volume of third stiffener in end part

$$V_{end.stiff3} := wf_{end1} \cdot \frac{\left(hw_{end} + tf_{end} \cdot 2 \right)}{\sin\left(\alpha_{end} \right)} \cdot tf_{end} = 0.01 \cdot m^3$$

Total volume of end part

$$V_{end} := 4 \cdot \left(2 \cdot V_{end.f} + V_{end.w} + V_{end.stiff1} + V_{end.stiff2} + V_{end.stiff3} \right) = 0.52 \cdot m^3$$

2.5 Reaction force from selfweight

Selfweight of total bridge

$$g_{1.2} := \left[\left(V_{ar} + V_{ha} + V_{lb} + V_{tb} + V_{br}\right)\cdot\rho_{steel} + V_{de}\cdot\rho_{conc}\right]\cdot g = 2.02 \times 10^{3}\cdot kN$$

$$g_{3} := \left[\begin{matrix}\left(V_{ar} + V_{ha} + V_{lb.beam} + V_{lb.shell} + V_{tb} + V_{br} + V_{end}\right)\cdot\rho_{steel} \cdots \\ + V_{de}\cdot\rho_{conc}\end{matrix}\right]\cdot g = 2.05 \times 10^{3}\cdot kN$$

Reaction forces from selfweigt

$$R_{self.1.2} := \frac{g_{1.2}}{4} = 506.21\cdot kN$$

$$R_{self.3} := \frac{g_{3}}{4} = 512.82\cdot kN$$

Reaction force from Brigade/PLUS

Level 1

$$R_{brigade.1} := 506.25kN$$

$$diff := 1 - \frac{R_{brigade.1}}{R_{self.1.2}} = -0.008\cdot\%$$

Level 2

$$R_{brigade.2} := 506.26kN$$

$$diff := 1 - \frac{R_{brigade.2}}{R_{self.1.2}} = -0.01\cdot\%$$

Level 2

$$R_{brigade.3} := 511.24kN$$

$$diff := 1 - \frac{R_{brigade.3}}{R_{self.3}} = 0.308\cdot\%$$

2.6 Verification of uniform load

2.6.1 Reaction force

Load acting on deck

$$q := Q\cdot L_{de}\cdot w_{de} = 2.86 \times 10^{3}\cdot kN$$

Reaction forces from uniform load

$$R_{uniform} := \frac{q}{4} = 714.8\cdot kN$$

Reaction force from Brigade/PLUS

Level 1

$$R_{brigade.uniform.1} := 714.8kN$$

$$diff := 1 - \frac{R_{brigade.uniform.1}}{R_{uniform}} = 0 \cdot \%$$

Level 2

$$R_{brigade.uniform.2} := 714.80kN$$

$$diff := 1 - \frac{R_{brigade.uniform.2}}{R_{uniform}} = 0 \cdot \%$$

Level 3

$$R_{brigade.uniform.3} := 714.797kN$$

$$diff := 1 - \frac{R_{brigade.uniform.3}}{R_{uniform}} = 4.2 \times 10^{-4} \cdot \%$$

2.6.2 Bending moment in transverse beam

Load acting on transverse beam

$$q_{trans} := Q \cdot cc_{tb} = 6.6 \times 10^{4} \cdot \frac{N}{m}$$

Bending moment

$$M_{uniform} := q_{trans} \cdot \frac{w_{de}}{2} \cdot \left(0.95m + \frac{w_{de}}{4} \right) = 257.4 \cdot kN \cdot m$$

Center of gravity transversal beam

$$tp_{tb} := \frac{hw_{tb}}{2} + tf_{tb} + h_{de} = 0.6\,m$$

Center of gravity deck

$$tp_{de} := \frac{h_{de}}{2} = 0.19\,m$$

Center of gravity of composite cross section (transversal beam and deck)

$$tp_{co} := \frac{\left(A_{tb} \cdot \rho_{steel} \cdot tp_{tb} + b_{eff} \cdot h_{de} \cdot \rho_{conc} \cdot tp_{de} \right)}{A_{tb} \cdot \rho_{steel} + b_{eff} \cdot h_{de} \cdot \rho_{conc}} = 0.23\,m$$

Normal force in transversal beam from Brigade/PLUS

$N_{brigade.uniform.tb.1} := 339.14kN$

$N_{brigade.uniform.tb.2} := 292.85kN$

$N_{brigade.uniform.tb.3} := 306.47kN$

Normal force in transversal deck from Brigade/PLUS

$N_{brigade.uniform.td.1} := -310.23kN$

$N_{brigade.uniform.td.2} := -288.185kN$

$N_{brigade.uniform.td.3} := -303.315kN$

Moment in transversal beam from Brigade/PLUS

$M_{brigade.uniform.tb.1} := 34.60kN \cdot m$

$M_{brigade.uniform.tb.2} := 34.07kN \cdot m$

$M_{brigade.uniform.tb.3} := 33.41kN \cdot m$

Moment in transversal deck from Brigade/PLUS

$M_{brigade.uniform.td.1} := 62.21kN \cdot m$

$M_{brigade.uniform.td.2} := 94.33kN \cdot m$

$M_{brigade.uniform.td.3} := 89.25kN \cdot m$

Normal force in transversal sub deck 1 from Brigade/PLUS

$N_{brigade.uniform.tsd1.1} := -27.54kN$

Normal force in transversal sub deck 2 from Brigade/PLUS

$N_{brigade.uniform.tsd2.1} := -27.54kN$

Moment in transversal sub deck 1 from Brigade/PLUS

$M_{brigade.uniform.tsd1.1} := 12.42kN \cdot m$

Moment in transversal sub deck 2 from Brigade/PLUS

$M_{brigade.uniform.tsd2.1} := 12.42kN \cdot m$

Total section moment in compsite section

Level 1

$$M_{brigade.uniform.1} := M_{brigade.uniform.tb.1} + M_{brigade.uniform.td.1} \cdots + N_{brigade.uniform.tb.1} \cdot \left(tp_{tb} - tp_{co}\right) \cdots + N_{brigade.uniform.td.1} \cdot \left(tp_{de} - tp_{co}\right) \cdots + \frac{1}{2} \cdot \left[\begin{array}{l} M_{brigade.uniform.tsd1.1} + M_{brigade.uniform.tsd2.1} \cdots \\ + N_{brigade.uniform.tsd1.1} \cdot \left(tp_{de} - tp_{co}\right) \cdots \\ + N_{brigade.uniform.tsd2.1} \cdot \left(tp_{de} - tp_{co}\right) \end{array}\right] = 248.57 \cdot kN \cdot m$$

$$diff := 1 - \frac{M_{brigade.uniform.1}}{M_{uniform}} = 3.43 \cdot \%$$

Level 2

$$M_{brigade.uniform.2} := \begin{bmatrix} M_{brigade.uniform.tb.2} + M_{brigade.uniform.td.2} \cdots \\ + N_{brigade.uniform.tb.2} \cdot \left(tp_{tb} - tp_{co} \right) \cdots \\ + N_{brigade.uniform.td.2} \cdot \left(tp_{de} - tp_{co} \right) \end{bmatrix} = 248.59 \cdot kN \cdot m$$

$$diff := 1 - \frac{M_{brigade.uniform.2}}{M_{uniform}} = 3.42 \cdot \%$$

Level 3

$$M_{brigade.uniform.3} := \begin{bmatrix} M_{brigade.uniform.tb.3} \cdots \\ + M_{brigade.uniform.td.3} \cdots \\ + N_{brigade.uniform.tb.3} \cdot \left(tp_{tb} - tp_{co} \right) \cdots \\ + N_{brigade.uniform.td.3} \cdot \left(tp_{de} - tp_{co} \right) \end{bmatrix} = 248.5 \cdot kN \cdot m$$

$$diff := 1 - \frac{M_{brigade.uniform.3}}{M_{uniform}} = 3.46 \cdot \%$$

2.7 Verification of traffic load

2.7.1 Point traffic load

2.7.1.1 Reaction force

Assume load placed closest to one support and that it is carried by supports on one side

$$2 \cdot 2 \cdot Q_{traffic} = R_A + R_B$$

$$2Q_{traffic} \cdot 1.45m + 2 \cdot Q_{traffic} \cdot 3.45m - R_B \cdot L_{tb} = 0$$

$$R_{PointTraffic.B} := \frac{4.9m \cdot 2Q_{traffic}}{L_{tb}} = 249.15 \cdot kN$$

$$R_{PointTraffic.A} := 2 \cdot 2 \cdot Q_{traffic} - R_{PointTraffic.B} = 350.85 \cdot kN$$

Reaction force from Brigade/PLUS

Level 1

$$R_{brigade.PointTraffic.A.1} := 351.02kN \qquad diff := 1 - \frac{R_{brigade.PointTraffic.A.1}}{R_{PointTraffic.A}} = -0.05 \cdot \%$$

$$R_{brigade.PointTraffic.B.1} := 249.0kN \qquad diff := 1 - \frac{R_{brigade.PointTraffic.B.1}}{R_{PointTraffic.B}} = 0.06 \cdot \%$$

Level 2

$R_{brigade.PointTraffic.A.2} := 351.10kN$ $\quad diff := 1 - \frac{R_{brigade.PointTraffic.A.2}}{R_{PointTraffic.A}} = -0.07 \cdot \%$

$R_{brigade.PointTraffic.B.2} := 248.90kN$ $\quad diff := 1 - \frac{R_{brigade.PointTraffic.B.2}}{R_{PointTraffic.B}} = 0.1 \cdot \%$

Level 3

$R_{brigade.PointTraffic.A.3} := 350.945kN$ $\quad diff := 1 - \frac{R_{brigade.PointTraffic.A.3}}{R_{PointTraffic.A}} = -0.03 \cdot \%$

$R_{brigade.PointTraffic.B.3} := 249.055kN$ $\quad diff := 1 - \frac{R_{brigade.PointTraffic.B.3}}{R_{PointTraffic.B}} = 0.04 \cdot \%$

2.7.2 Uniform traffic load

2.7.2.1 Reaction force

$$q_{traffic} \cdot 3m \cdot \frac{L_{de}}{2} = R_A + R_B$$

$$q_{traffic} \cdot 3m \cdot \frac{L_{de}}{2} \cdot \left(\frac{3m}{2} + 0.95m \right) - R_B \cdot L_{tb} = 0$$

$$R_{UniformTraffic.B} := \frac{q_{traffic} \cdot L_{de} \cdot 3m \cdot 2.45m}{2 \cdot L_{tb}} = 200.36 \cdot kN$$

$$R_{UniformTraffic.A} := q_{traffic} \cdot 3m \cdot \frac{L_{de}}{2} - R_{UniformTraffic.B} = 282.13 \cdot kN$$

Level 1

$R_{brigade.UniformTraffic.A.1} := 281.50kN$ $\quad diff := 1 - \frac{R_{brigade.UniformTraffic.A.1}}{R_{UniformTraffic.A}} = 0.22 \cdot \%$

$R_{brigade.UniformTraffic.B.1} := 201.76kN$ $\quad diff := 1 - \frac{R_{brigade.UniformTraffic.B.1}}{R_{UniformTraffic.B}} = -0.7 \cdot \%$

Level 2

$R_{brigade.UniformTraffic.A.2} := 281.26kN$ $\quad diff := 1 - \frac{R_{brigade.UniformTraffic.A.2}}{R_{UniformTraffic.A}} = 0.31 \cdot \%$

$R_{brigade.UniformTraffic.B.2} := 202.0kN$ $\quad diff := 1 - \frac{R_{brigade.UniformTraffic.B.2}}{R_{UniformTraffic.B}} = -0.82 \cdot \%$

Level 3

$R_{brigade.UniformTraffic.A.3} := 282.553kN$ $\quad diff := 1 - \frac{R_{brigade.UniformTraffic.A.3}}{R_{UniformTraffic.A}} = -0.15 \cdot \%$

$R_{brigade.UniformTraffic.B.3} := 200.705kN$ $\quad diff := 1 - \frac{R_{brigade.UniformTraffic.B.3}}{R_{UniformTraffic.B}} = -0.17 \cdot \%$

2.7.2.2 Moment in mid span of transversal beam

$$q_{traffic} \cdot 3m \cdot cc_{tb} = R_A + R_B$$

$$q_{traffic} \cdot 3m \cdot cc_{tb} \cdot \left(\frac{3m}{2} + 0.95m \right) - R_B \cdot L_{tb} = 0$$

$$R_B := \frac{q_{traffic} \cdot cc_{tb} \cdot 3m \cdot 2.45m}{L_{tb}} = 37 \cdot kN$$

$$R_A := q_{traffic} \cdot 3m \cdot cc_{tb} - R_B = 52.1 \cdot kN$$

$$M_{UniformTraffic} := R_A \cdot \frac{L_{tb}}{2} - q_{traffic} \cdot cc_{tb} \cdot 2m \cdot \left(\frac{2m}{2} \right) = 94.3 \cdot kN \cdot m$$

Normal force in transversal beam from Brigade/PLUS

$$N_{brigade.UniformTraffic.tb.1} := 125.11kN$$

$$N_{brigade.UniformTraffic.tb.2} := 106.98kN$$

$$N_{brigade.UniformTraffic.tb.3} := 110.94kN$$

Normal force in transversal deck from Brigade/PLUS

$$N_{brigade.UniformTraffic.td.1} := -115.42kN$$

$$N_{brigade.UniformTraffic.td.2} := -52.86kN$$

$$N_{brigade.UniformTraffic.td.3} := -55.72kN$$

Moment in transversal beam from Brigade/PLUS

$$M_{brigade.UniformTraffic.tb.1} := 12.76kN \cdot m$$

$$M_{brigade.UniformTraffic.tb.2} := 12.49 \cdot kN \cdot m$$

$$M_{brigade.UniformTraffic.tb.3} := 11.92 \cdot kN \cdot m$$

Moment in transversal deck from Brigade/PLUS

$$M_{brigade.UniformTraffic.td.1} := 23.12kN \cdot m$$

$$M_{brigade.UniformTraffic.td.2} := 37.55kN \cdot m$$

$$M_{brigade.UniformTraffic.td.3} := 35.68kN \cdot m$$

Normal force in transversal sub deck 1 from Brigade/PLUS

$$N_{brigade.UniformTraffic.tsd1.1} := -10.51kN$$

Normal force in transversal sub deck 2 from Brigade/PLUS

$$N_{brigade.UniformTraffic.tsd2.1} := -10.51kN$$

Moment in transversal sub deck 1 from Brigade/PLUS

$$M_{brigade.UniformTraffic.tsd1.1} := 5.04kN \cdot m$$

Moment in transversal sub deck 2 from Brigade/PLUS

$$M_{brigade.UniformTraffic.tsd2.1} := 5.04kN \cdot m$$

Total section moment in compsite section

Level 1

$$M_{brigade.UniformTraffic.1} := M_{brigade.UniformTraffic.tb.1} + M_{brigade.UniformTraffic.td.1} \cdots + N_{brigade.UniformTraffic.tb.1} \cdot \left(tp_{tb} - tp_{co}\right) \cdots + N_{brigade.UniformTraffic.td.1} \cdot \left(tp_{de} - tp_{co}\right) \cdots + \frac{1}{2} \cdot \begin{bmatrix} M_{brigade.UniformTraffic.tsd1.1} \cdots \\ + M_{brigade.UniformTraffic.tsd2.1} \cdots \\ + N_{brigade.UniformTraffic.tsd1.1} \cdot \left(tp_{de} - tp_{co}\right) \cdots \\ + N_{brigade.UniformTraffic.tsd2.1} \cdot \left(tp_{de} - tp_{co}\right) \end{bmatrix} = 92.37$$

$$diff := 1 - \frac{M_{brigade.UniformTraffic.1}}{M_{UniformTraffic}} = 2.04 \cdot \%$$

Level 2

$$M_{brigade.UniformTraffic.2} := M_{brigade.UniformTraffic.tb.2} \cdots + M_{brigade.UniformTraffic.td.2} \cdots + N_{brigade.UniformTraffic.tb.2} \cdot \left(tp_{tb} - tp_{co}\right) \cdots + N_{brigade.UniformTraffic.td.2} \cdot \left(tp_{de} - tp_{co}\right) = 91.98 \cdot kN \cdot m$$

$$diff := 1 - \frac{M_{brigade.UniformTraffic.2}}{M_{UniformTraffic}} = 2.46 \cdot \%$$

Level 3

$$M_{brigade.UniformTraffic.3} := M_{brigade.UniformTraffic.tb.3} \cdots + M_{brigade.UniformTraffic.td.3} \cdots + N_{brigade.UniformTraffic.tb.3} \cdot \left(tp_{tb} - tp_{co}\right) \cdots + N_{brigade.UniformTraffic.td.3} \cdot \left(tp_{de} - tp_{co}\right) = 91.13 \cdot kN \cdot m$$

$$diff := 1 - \frac{M_{brigade.UniformTraffic.3}}{M_{UniformTraffic}} = 3.36 \cdot \%$$

E Results

E.1 Uniformly distributed load

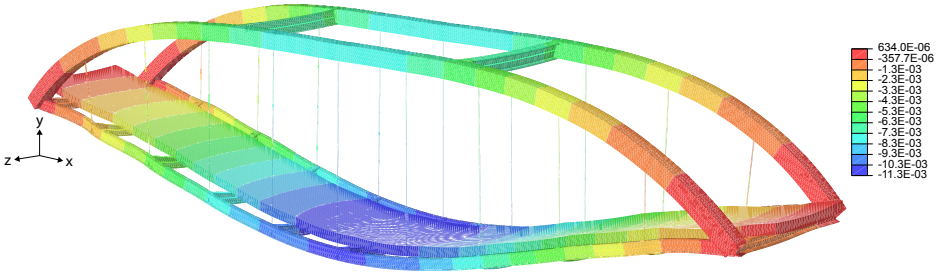

Figure E.1 *Deformation of the bridge subjected to uniformly distributed load. The contour display the deformation in y-direction [m]. The displayed model is level 2, however all levels show the same global behaviour.*

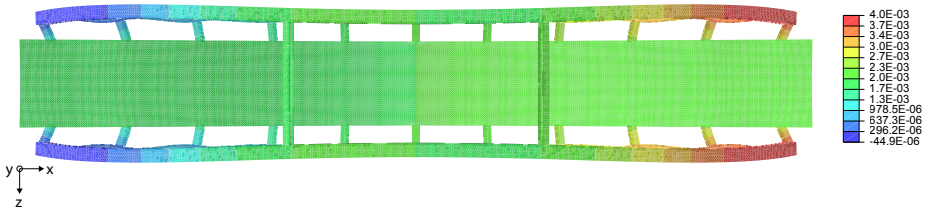

Figure E.2 *Deformation of the bridge subjected to uniformly distributed load, seen from above. The contour display the deformation in x-direction [m]. The displayed model is level 2, however all levels show the same global behaviour.*

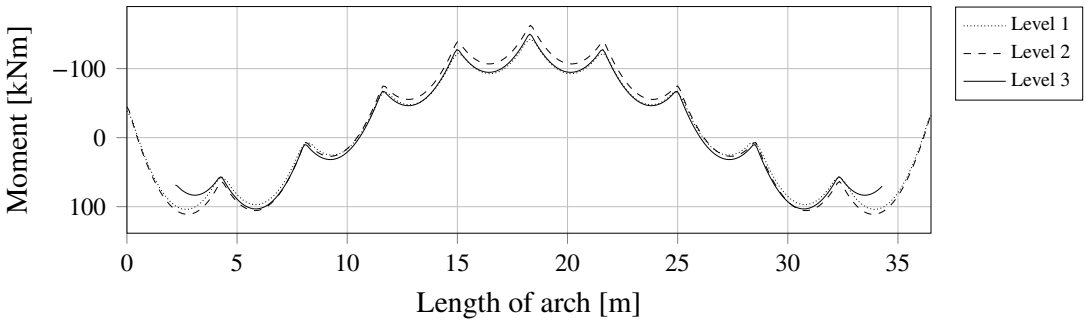

Figure E.3 *Bending moment in the arch for level 1, 2 and 3, subjected to uniformly distributed load.*

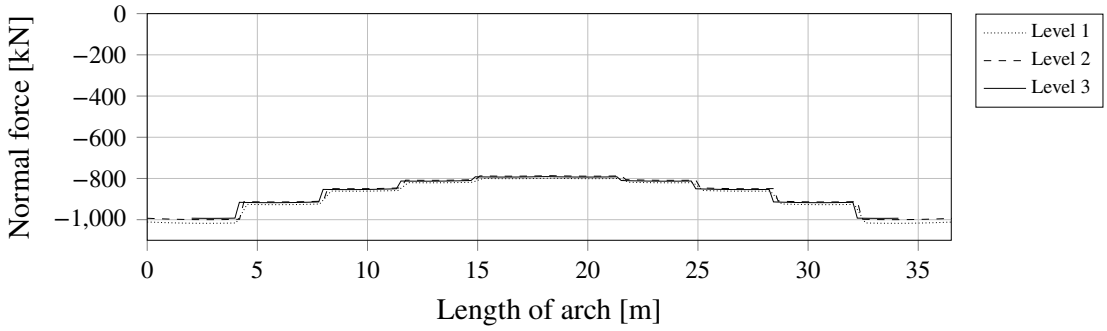

Figure E.4 Normal force in the arch for level 1, 2 and 3, subjected to uniformly distributed load.

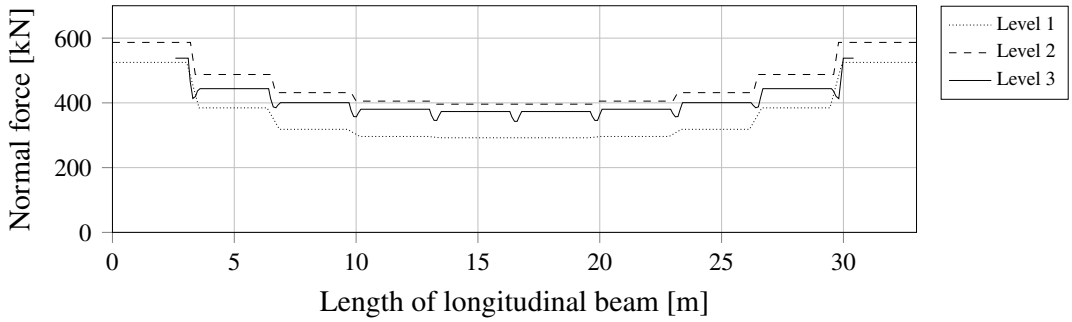

Figure E.5 Normal force in the longitudinal beam for level 1, 2 and 3, subjected to uniformly distributed load.

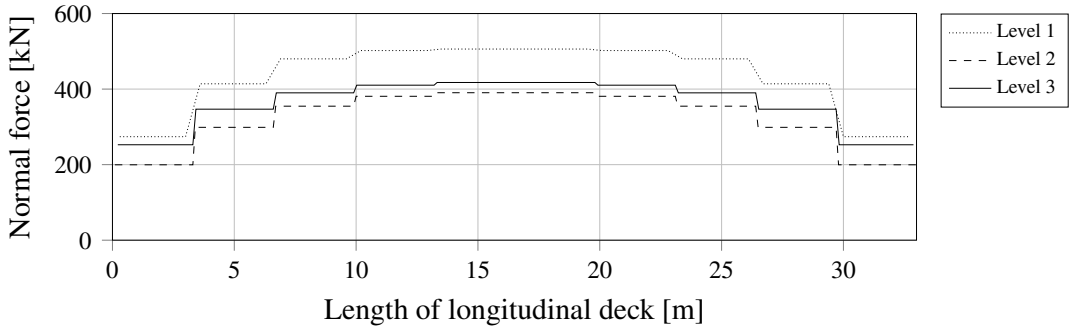

Figure E.6 The integrated normal force over half the width of the deck in the longitudinal direction for level 1, 2 and 3, subjected to uniformly distributed load.

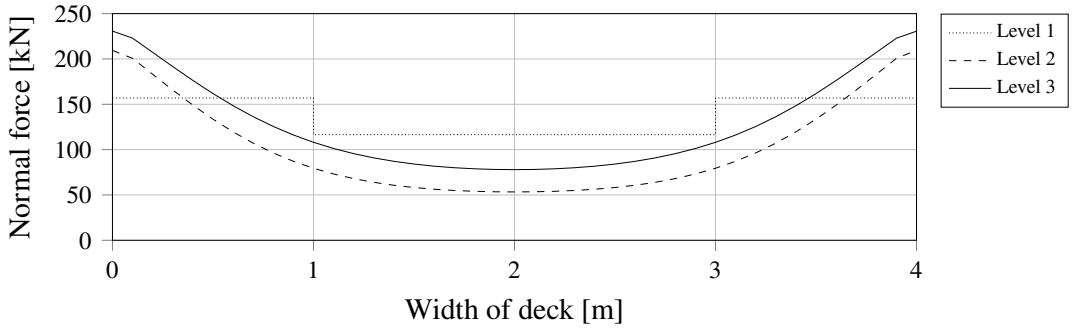

Figure E.7 Longitudinal normal force distribution along the width of the deck in the span between the first and second transversal beam for level 1, 2 and 3, subjected to the uniformly distributed load.

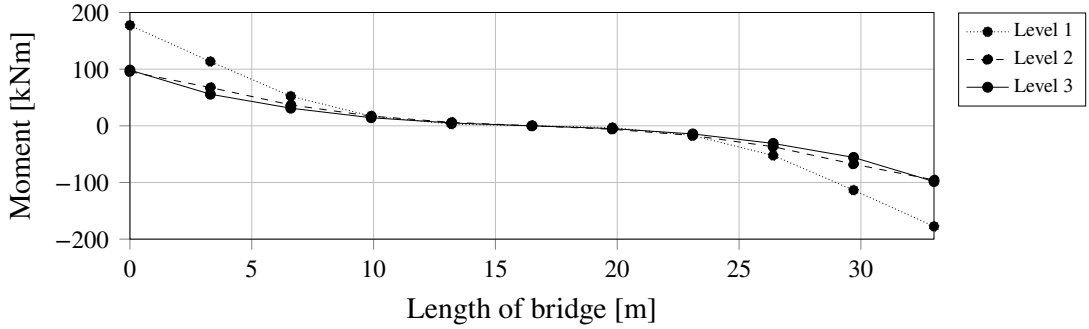

Figure E.8 Variation of maximum secondary bending moment along the bridge for level 1, 2 and 3, subjected to uniformly distributed load.

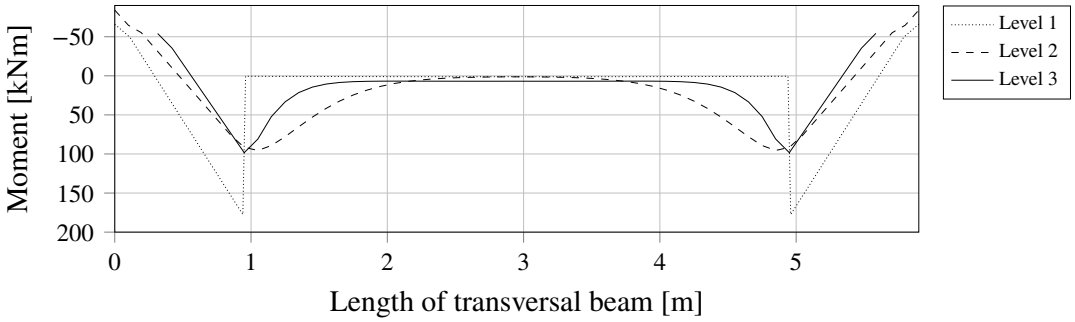

Figure E.9 Secondary bending moment in the first transversal beam for level 1, 2 and 3, subjected to uniformly distributed load.

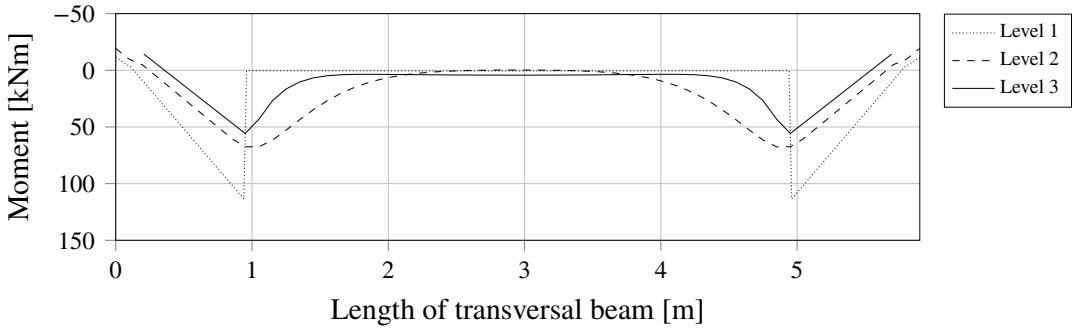

Figure E.10 Secondary bending moment in the second transversal beam for level 1, 2 and 3, subjected to uniformly distributed load.

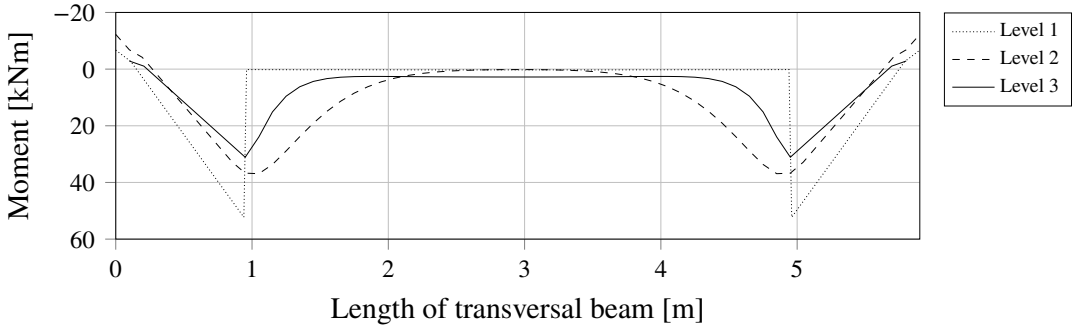

Figure E.11 Secondary bending moment in the third transversal beam for level 1, 2 and 3, subjected to uniformly distributed load.

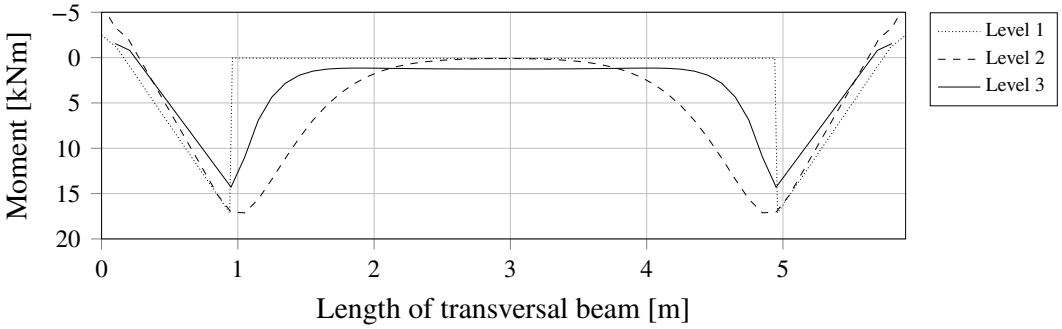

Figure E.12 Secondary bending moment in the forth transversal beam for level 1, 2 and 3, subjected to uniformly distributed load.

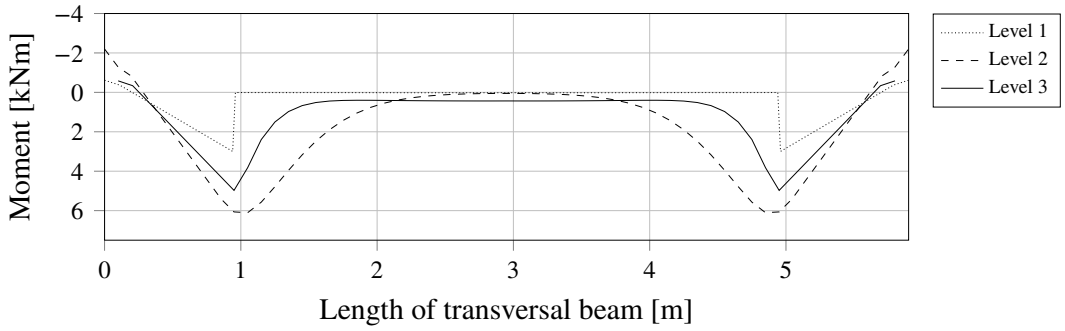

Figure E.13 Secondary bending moment in the fifth transversal beam for level 1, 2 and 3, subjected to uniformly distributed load.

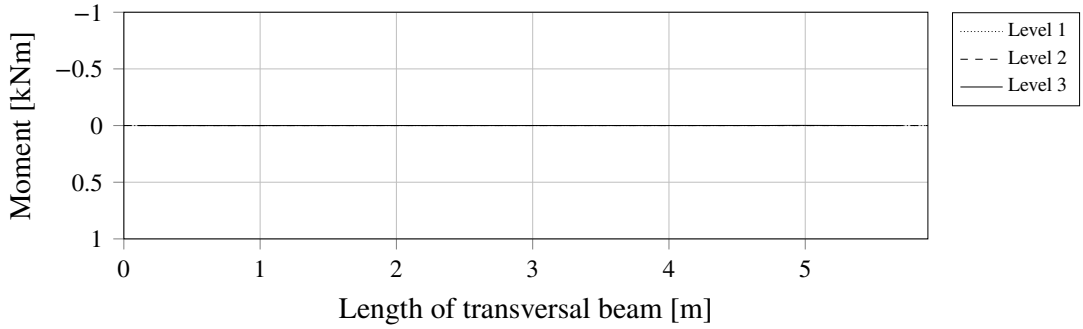

Figure E.14 Secondary bending moment in the sixth transversal beam for level 1, 2 and 3, subjected to uniformly distributed load.

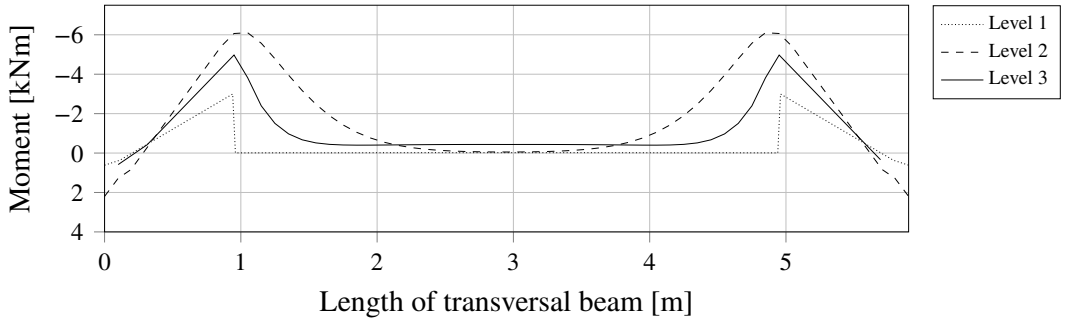

Figure E.15 Secondary bending moment in the seventh transversal beam for level 1, 2 and 3, subjected to uniformly distributed load.

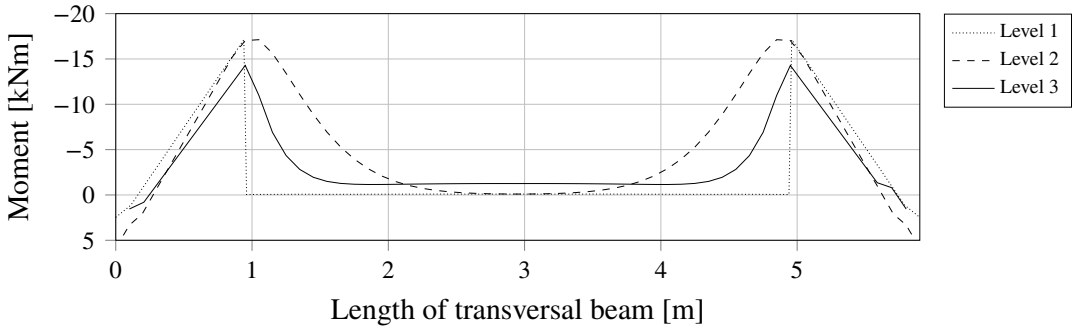

Figure E.16 Secondary bending moment in the eighth transversal beam for level 1, 2 and 3, subjected to uniformly distributed load.

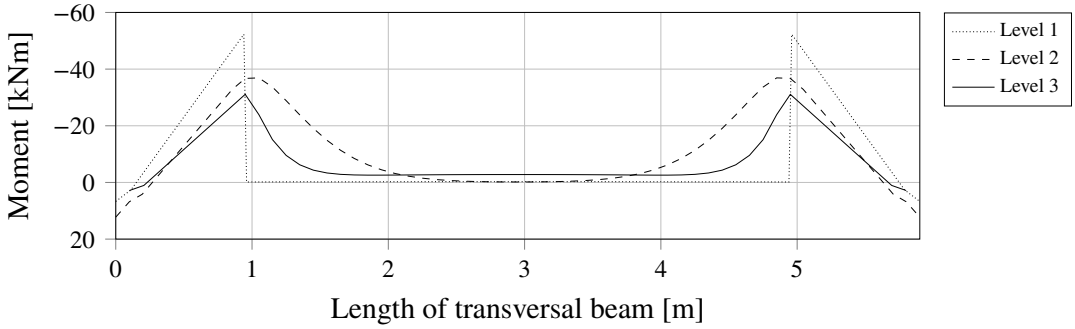

Figure E.17 Secondary bending moment in the ninth transversal beam for level 1, 2 and 3, subjected to uniformly distributed load.

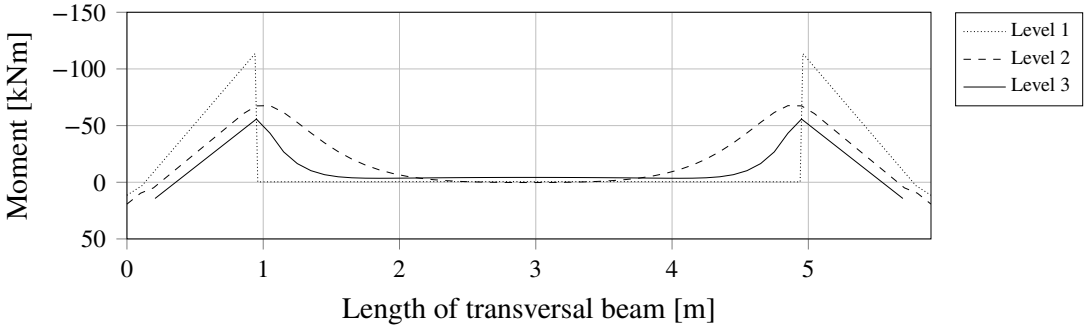

Figure E.18 Secondary bending moment in the tenth transversal beam for level 1, 2 and 3, subjected to uniformly distributed load.

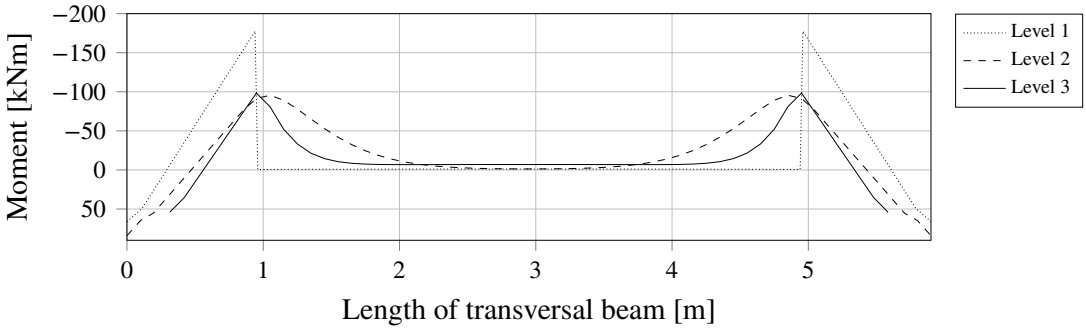

Figure E.19 Secondary bending moment in the eleventh transversal beam for level 1, 2 and 3, subjected to uniformly distributed load.

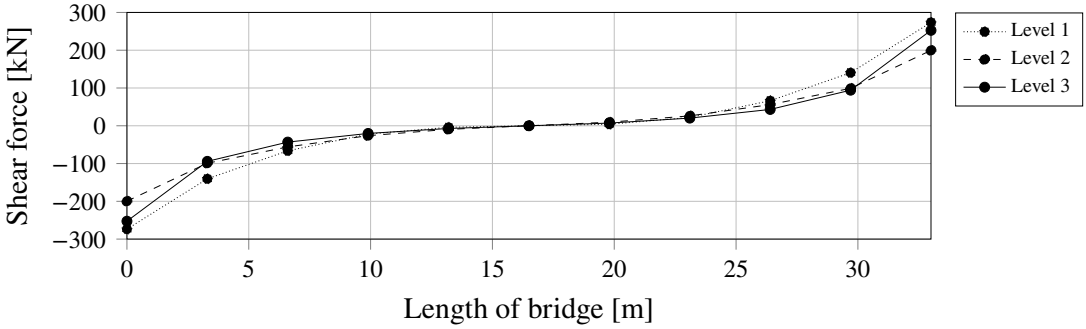

Figure E.20 Variation of maximum horizontal shear force in the transversal beam along the bridge for level 1, 2 and 3, subjected to uniformly distributed load.

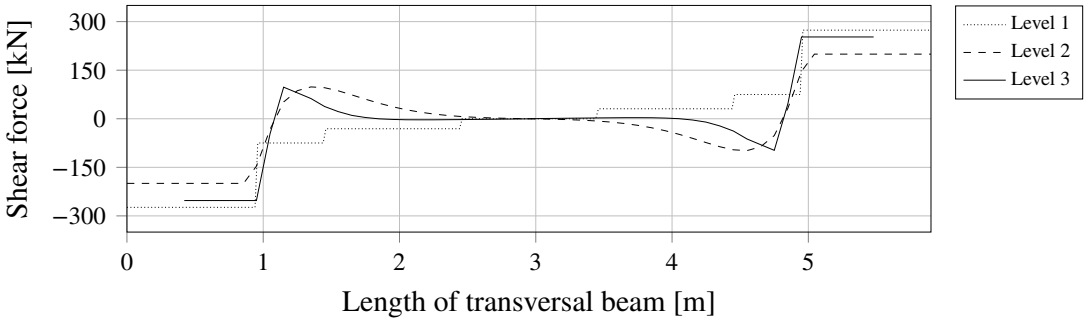

Figure E.21 Horizontal shear force in the first transversal beam for level 1, 2 and 3, subjected to uniformly distributed load.

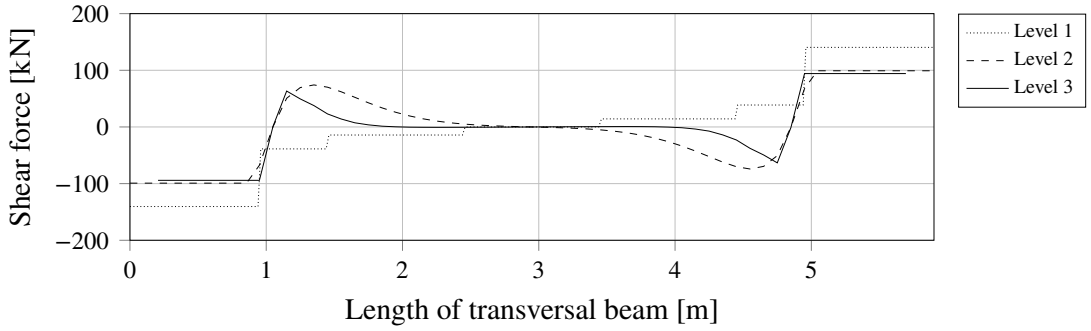

Figure E.22 Horizontal shear force in the second transversal beam for level 1, 2 and 3, subjected to uniformly distributed load.

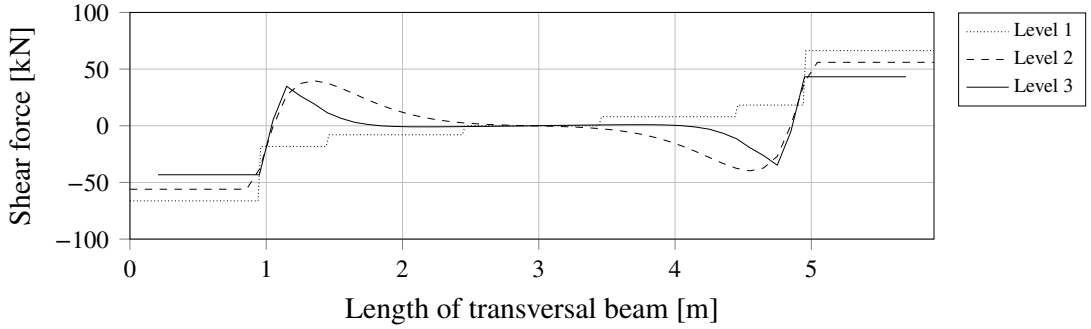

Figure E.23 Horizontal shear force in the third transversal beam for level 1, 2 and 3, subjected to uniformly distributed load.

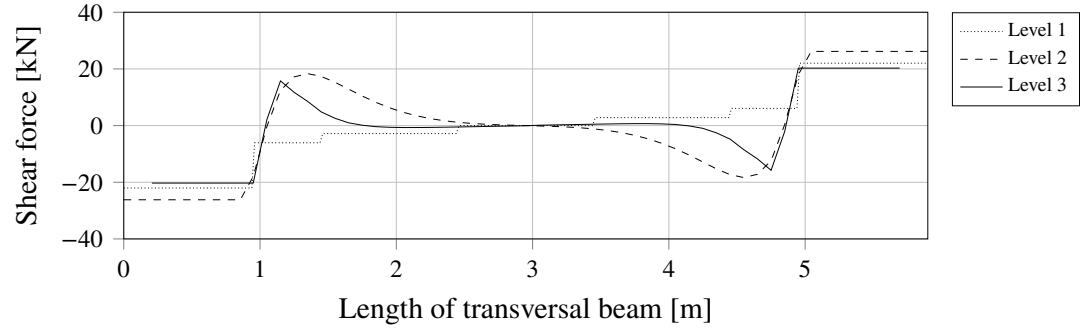

Figure E.24 Horizontal shear force in the forth transversal beam for level 1, 2 and 3, subjected to uniformly distributed load.

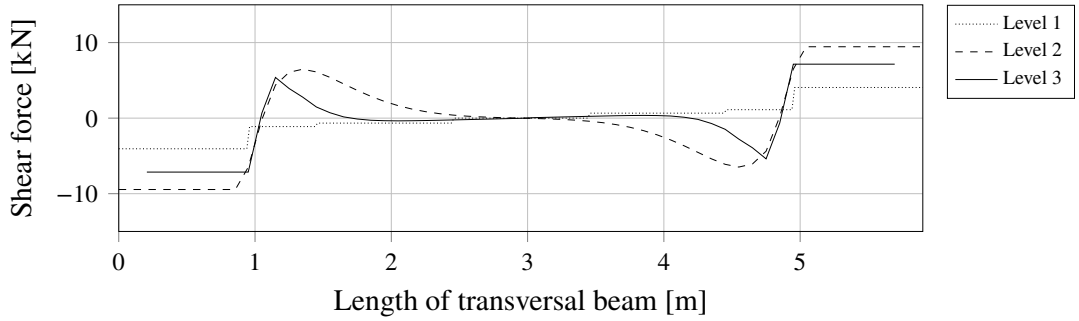

Figure E.25 Horizontal shear force in the fifth transversal beam for level 1, 2 and 3, subjected to uniformly distributed load.

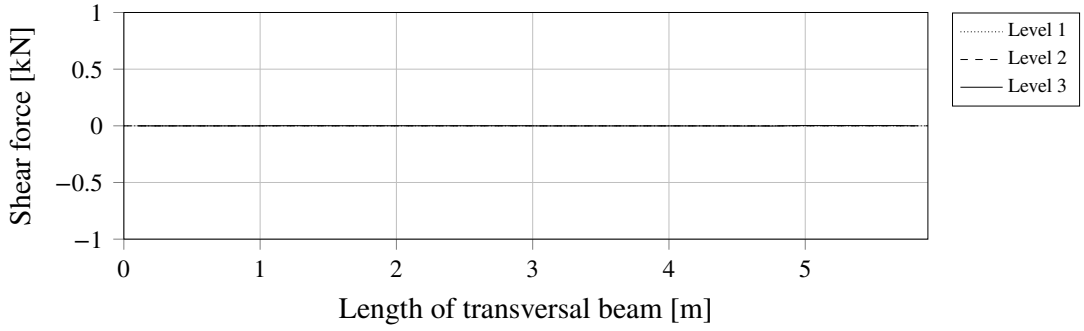

Figure E.26 Horizontal shear force in the sixth transversal beam for level 1, 2 and 3, subjected to uniformly distributed load.

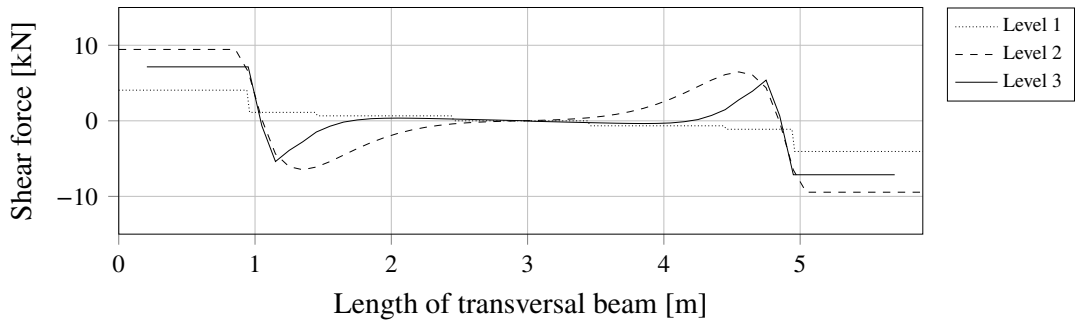

Figure E.27 Horizontal shear force in the seventh transversal beam for level 1, 2 and 3, subjected to uniformly distributed load.

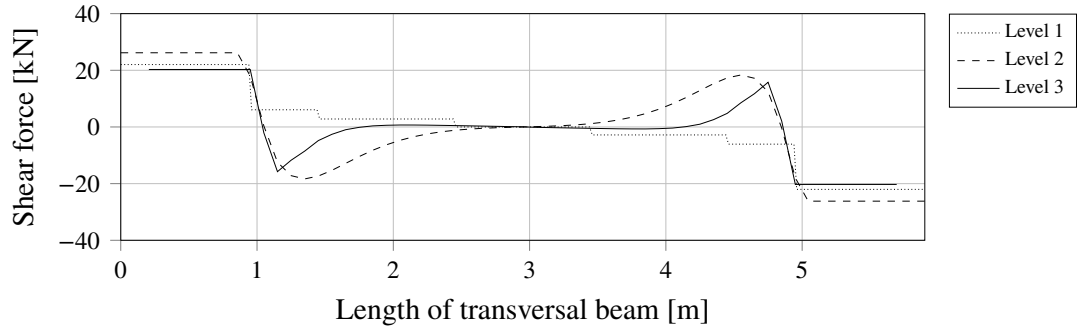

Figure E.28 Horizontal shear force in the eight transversal beam for level 1, 2 and 3, subjected to uniformly distributed load.

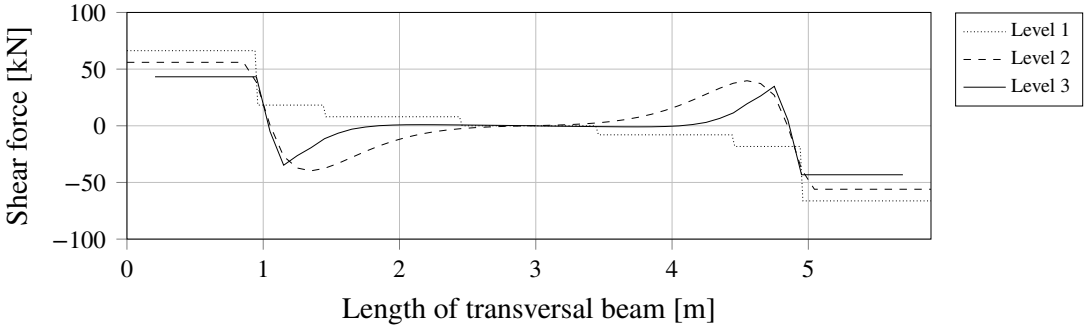

Figure E.29 Horizontal shear force in the ninth transversal beam for level 1, 2 and 3, subjected to uniformly distributed load.

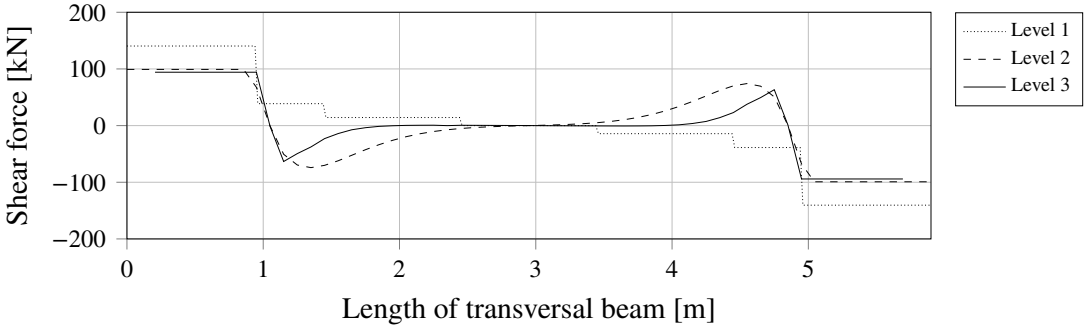

Figure E.30 Horizontal shear force in the tenth transversal beam for level 1, 2 and 3, subjected to uniformly distributed load.

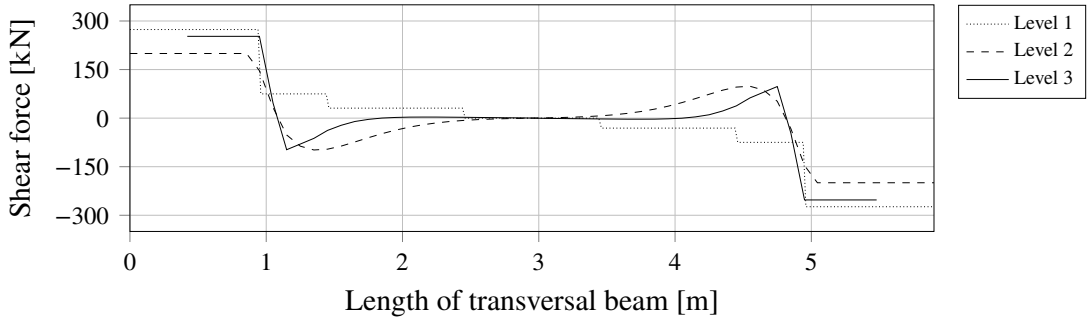

Figure E.31 *Horizontal shear force in the eleventh transversal beam for level 1, 2 and 3, subjected to uniformly distributed load.*

E.2 Temperature load

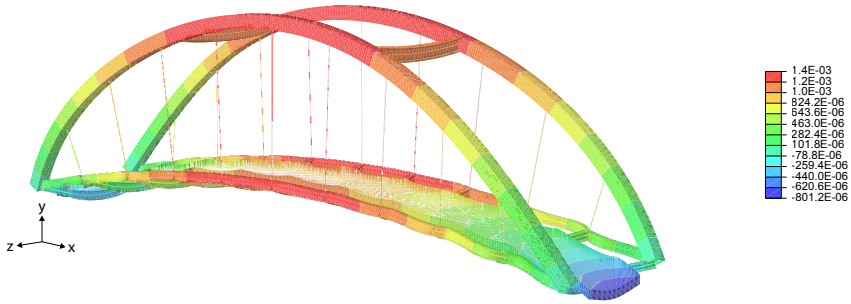

Figure E.32 *Deformation of the bridge subjected to temperature load. The contour display the deformation in y-direction [m]. The displayed model is level 2, however all levels show the same global behaviour.*

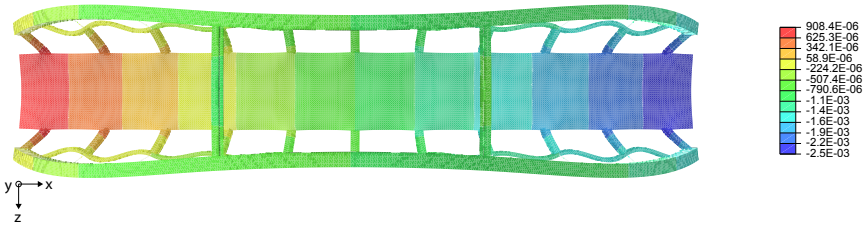

Figure E.33 *Deformation of the bridge subjected to temperature load, seen from above. The contour display the deformation in x-direction [m]. The displayed model is level 2, however all levels show the same global behaviour.*

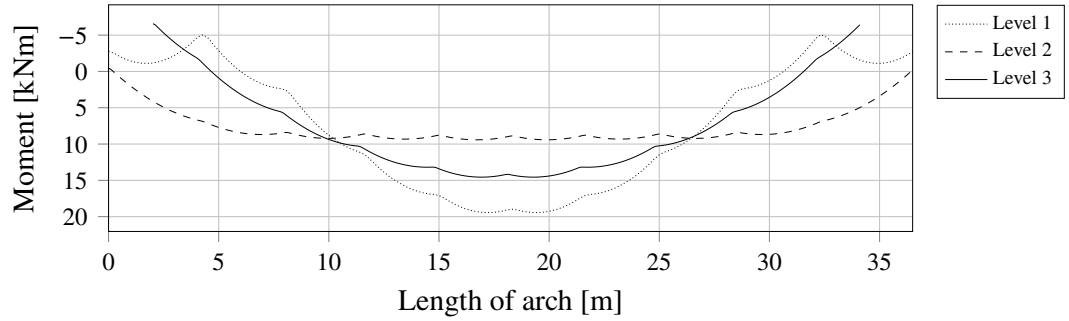

Figure E.34 Bending moment in the arch for level 1, 2 and 3, subjected to temperature load.

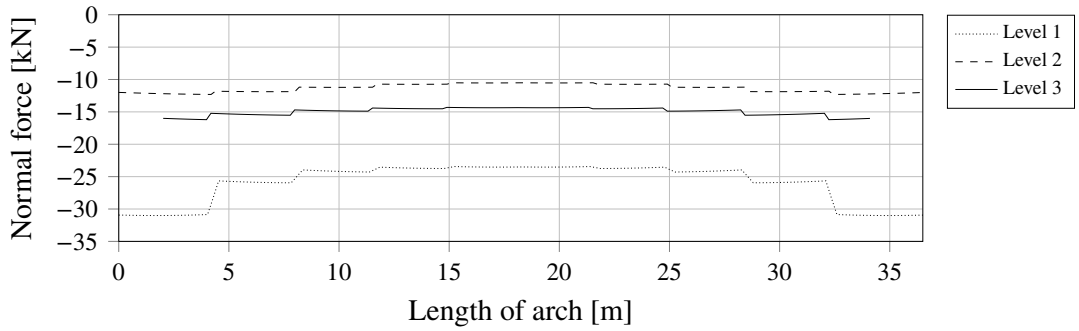

Figure E.35 Normal force in the arch for level 1, 2 and 3, subjected to temperature load.

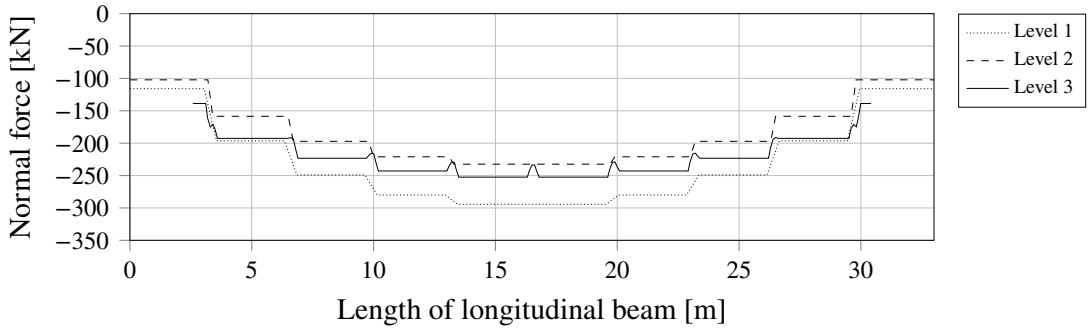

Figure E.36 Normal force in the longitudinal beam for level 1, 2 and 3, subjected to temperature load.

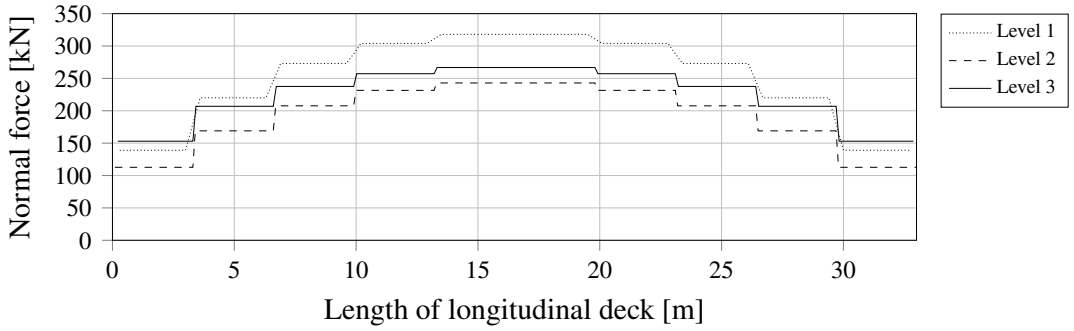

Figure E.37 The integrated normal force over half the width of the deck in the longitudinal direction for level 1, 2 and 3, subjected to temperature load.

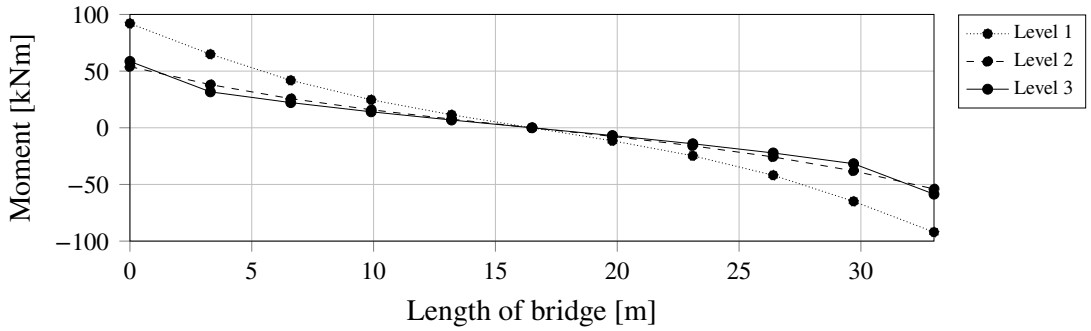

Figure E.38 Variation of maximum secondary bending moment along the bridge for level 1, 2 and 3, subjected to temperature load.

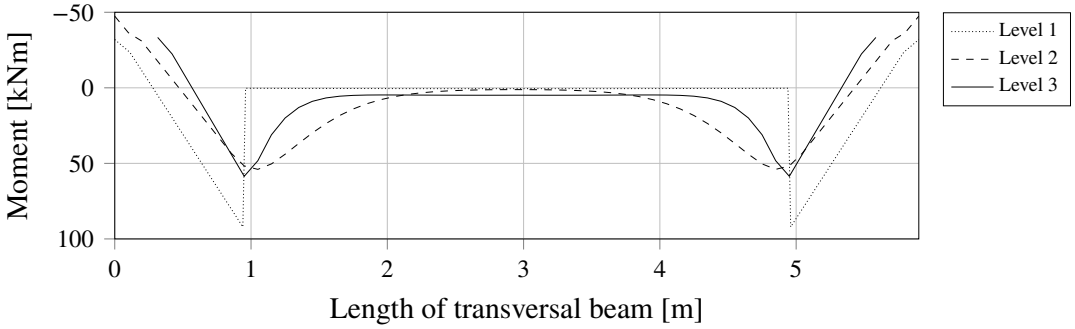

Figure E.39 Secondary bending moment in the first transversal beam for level 1, 2 and 3, subjected to temperature load.

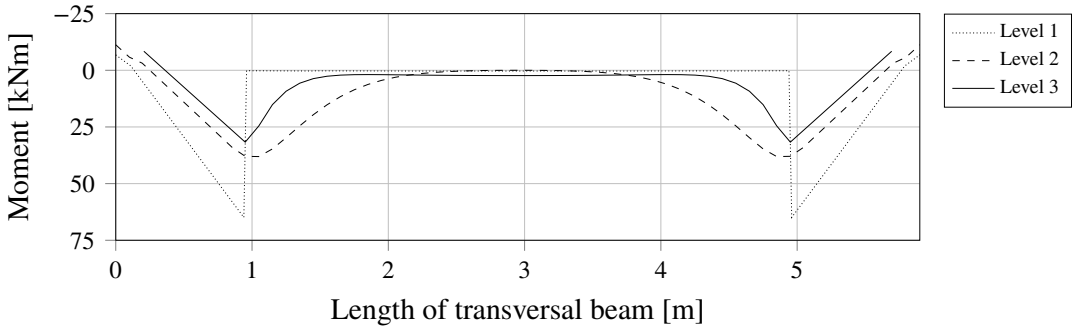

Figure E.40 Secondary bending moment in the second transversal beam for level 1, 2 and 3, subjected to temperature load.

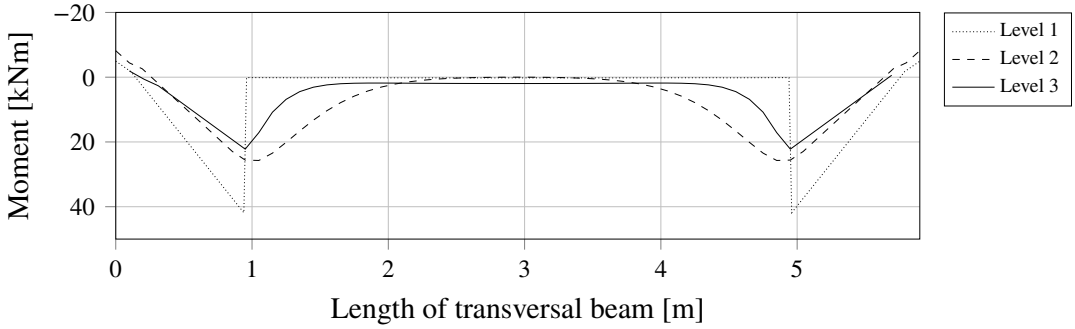

Figure E.41 Secondary bending moment in the third transversal beam for level 1, 2 and 3, subjected to temperature load.

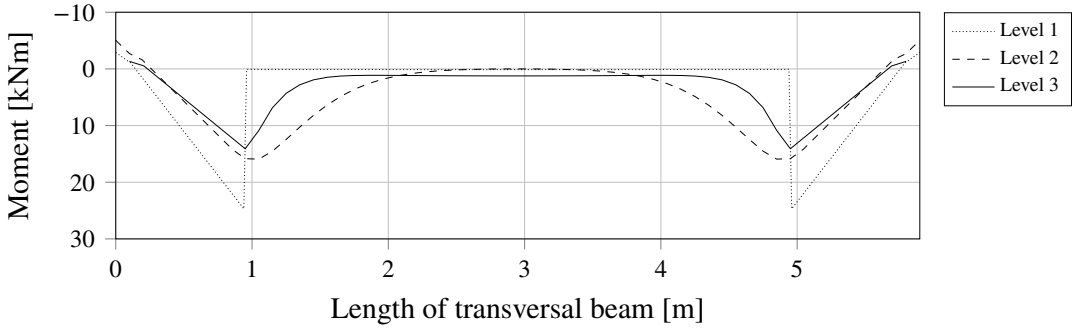

Figure E.42 Secondary bending moment in the forth transversal beam for level 1, 2 and 3, subjected to temperature load.

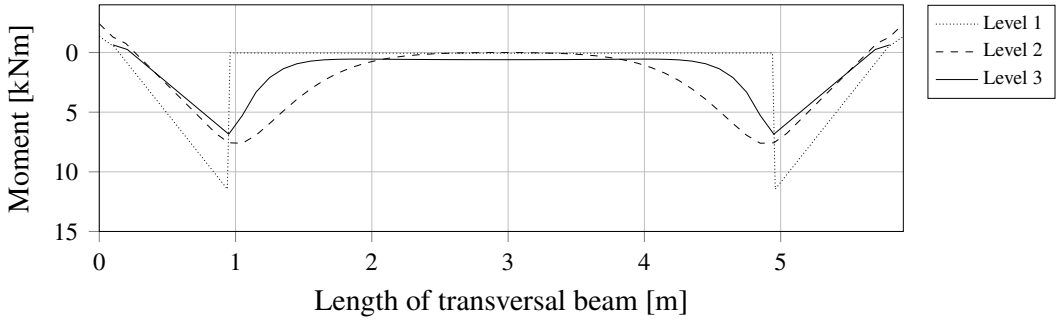

Figure E.43 Secondary bending moment in the fifth transversal beam for level 1, 2 and 3, subjected to temperature load.

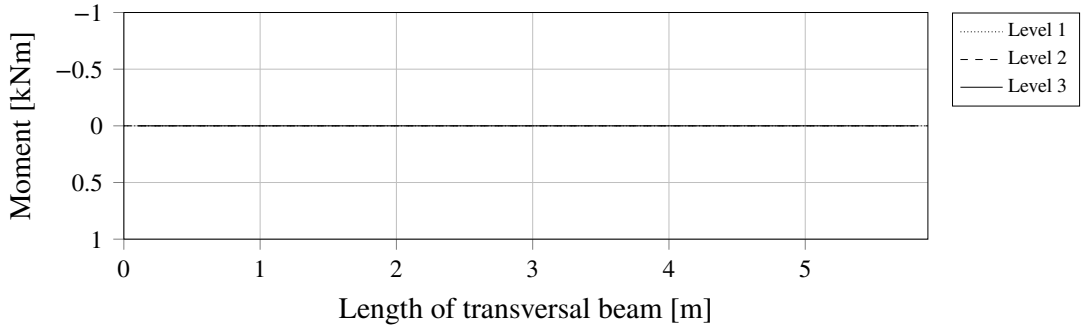

Figure E.44 Secondary bending moment in the sixth transversal beam for level 1, 2 and 3, subjected to temperature load.

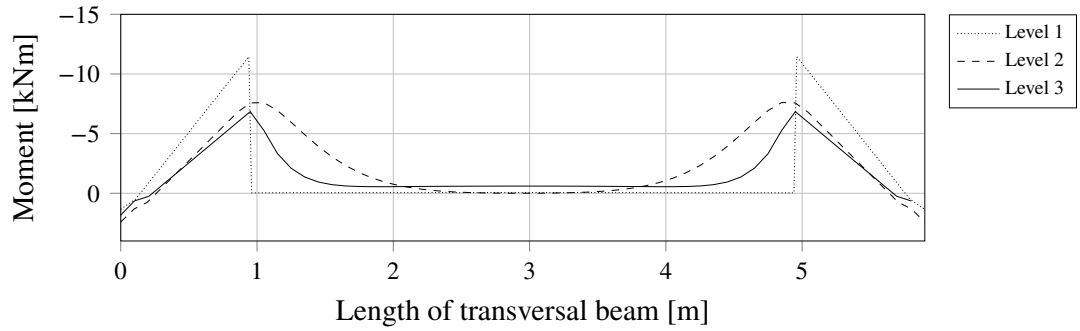

Figure E.45 Secondary bending moment in the seventh transversal beam for level 1, 2 and 3, subjected to temperature load.

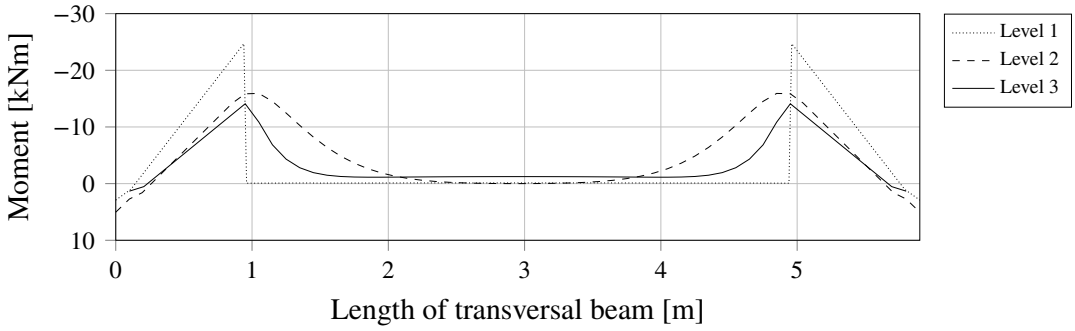

Figure E.46 Secondary bending moment in the eighth transversal beam for level 1, 2 and 3, subjected to temperature load.

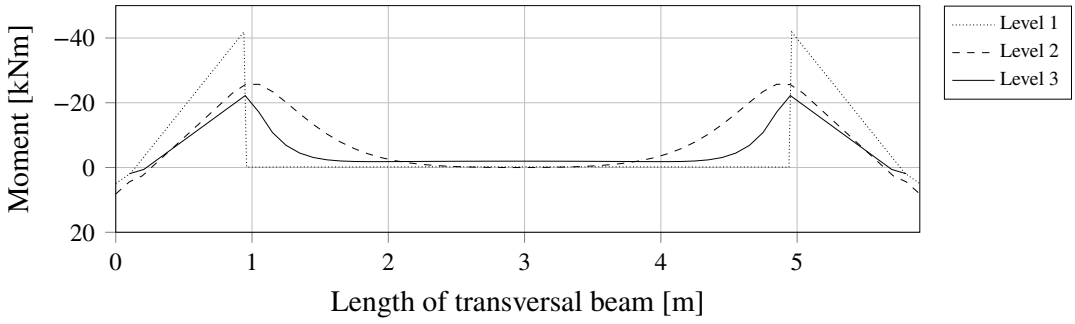

Figure E.47 Secondary bending moment in the ninth transversal beam for level 1, 2 and 3, subjected to temperature load.

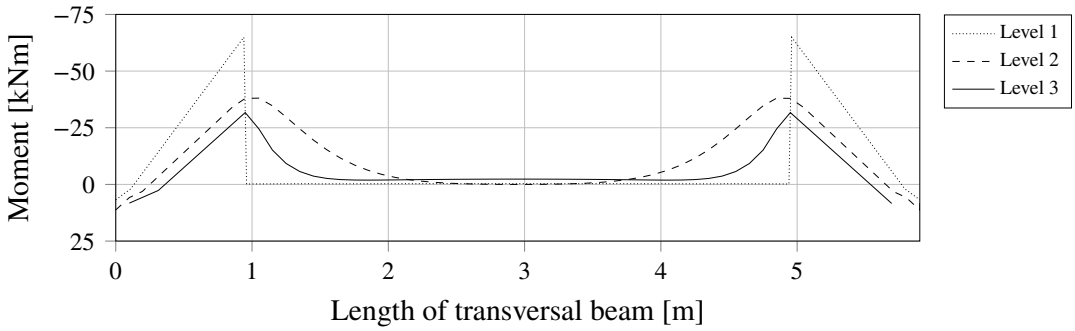

Figure E.48 Secondary bending moment in the tenth transversal beam for level 1, 2 and 3, subjected to temperature load.

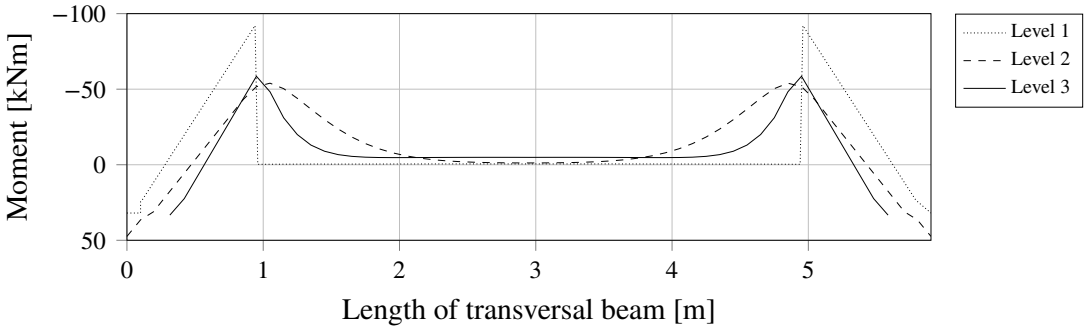

Figure E.49 Secondary bending moment in the eleventh transversal beam for level 1, 2 and 3, subjected to temperature load.

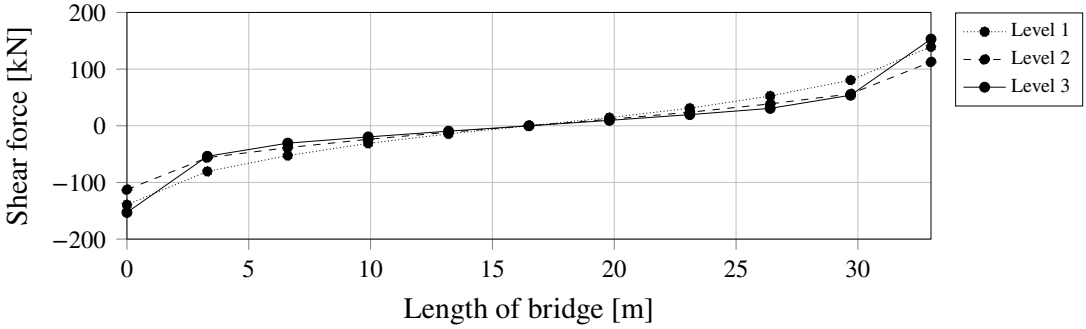

Figure E.50 Variation of maximum horizontal shear force in the transversal beam along the bridge for level 1, 2 and 3, subjected to temperature load.

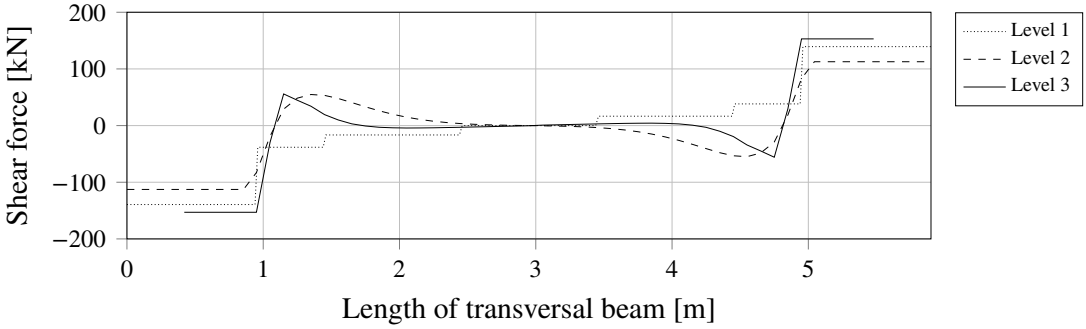

Figure E.51 Horizontal shear force in the first transversal beam for level 1, 2 and 3, subjected to temperature load.

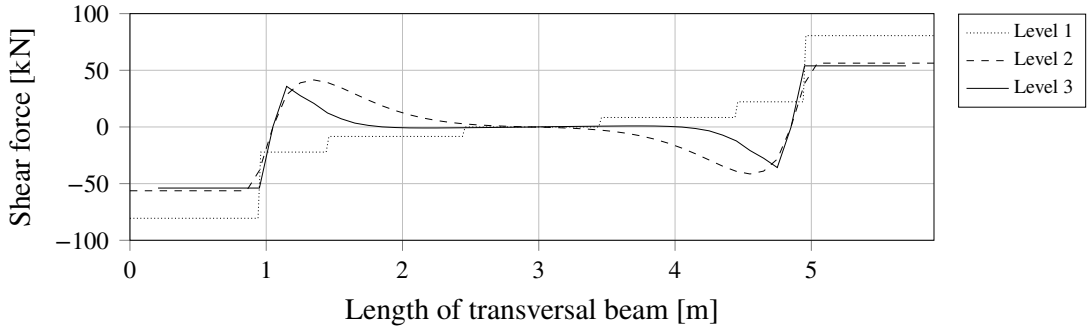

Figure E.52 Horizontal shear force in the second transversal beam for level 1, 2 and 3, subjected to uniformly distributed load.

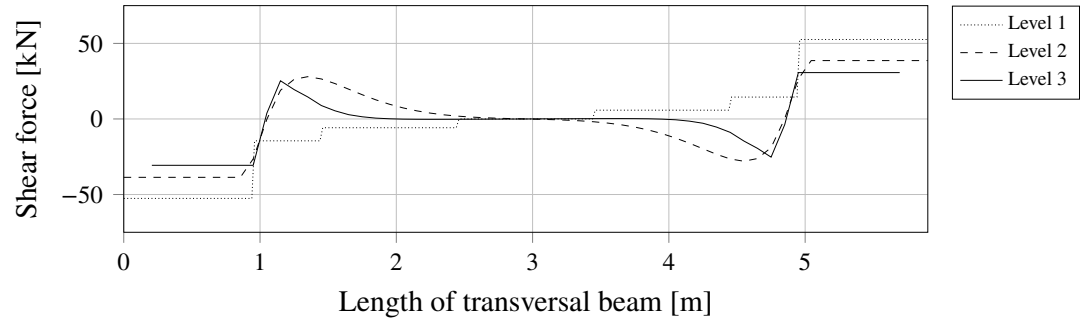

Figure E.53 Horizontal shear force in the third transversal beam for level 1, 2 and 3, subjected to temperature load.

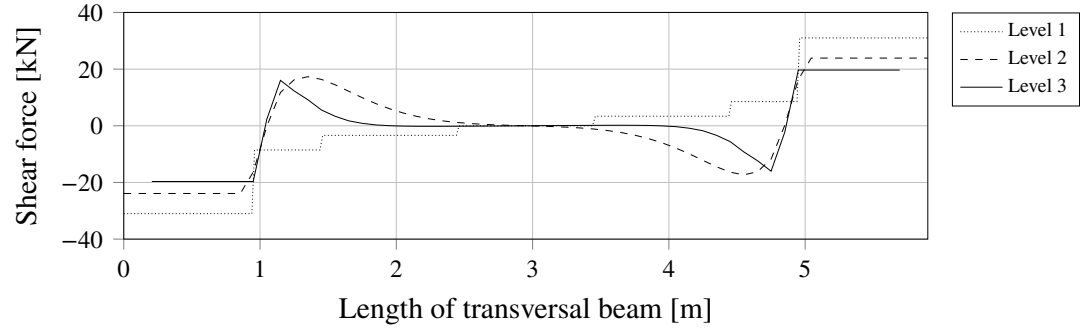

Figure E.54 Horizontal shear force in the forth transversal beam for level 1, 2 and 3, subjected to temperature load.

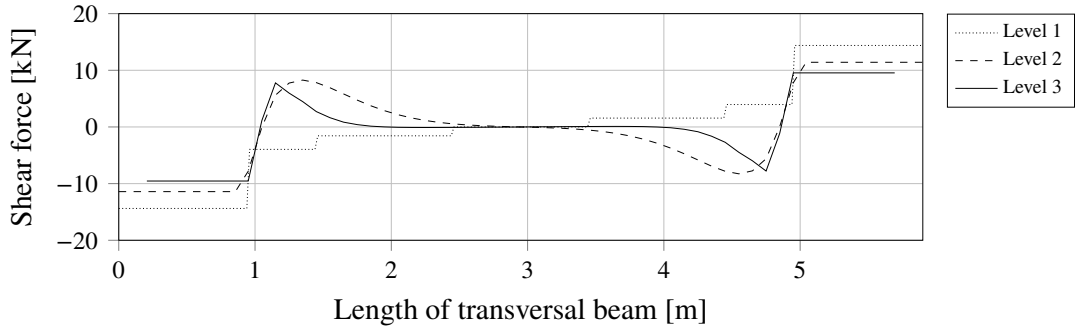

Figure E.55 Horizontal shear force in the fifth transversal beam for level 1, 2 and 3, subjected to temperature load.

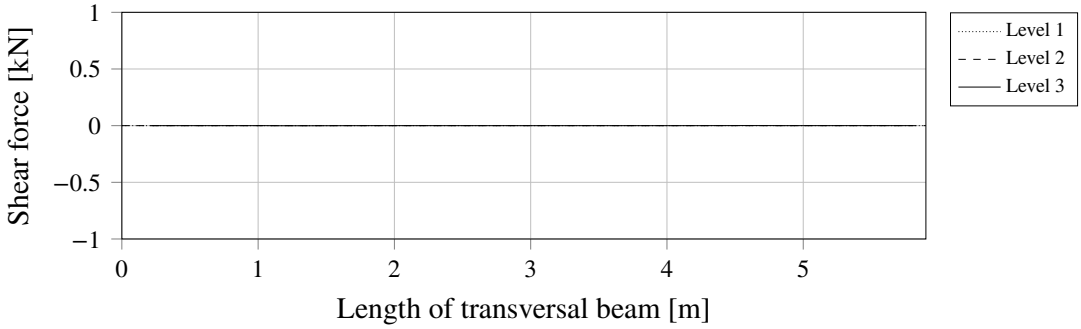

Figure E.56 Horizontal shear force in the sixth transversal beam for level 1, 2 and 3, subjected to temperature load.

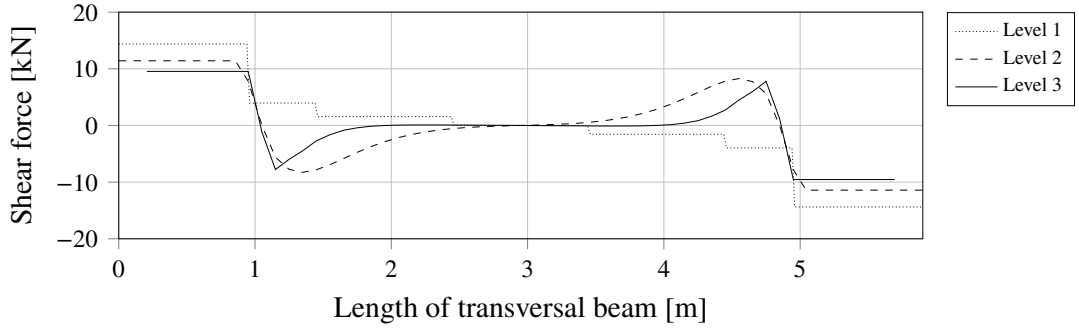

Figure E.57 Horizontal shear force in the seventh transversal beam for level 1, 2 and 3, subjected to temperature load.

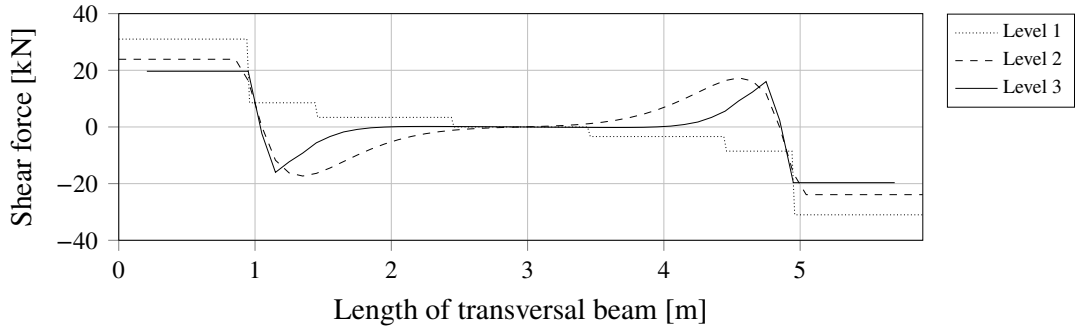

Figure E.58 Horizontal shear force in the eight transversal beam for level 1, 2 and 3, subjected to temperature load.

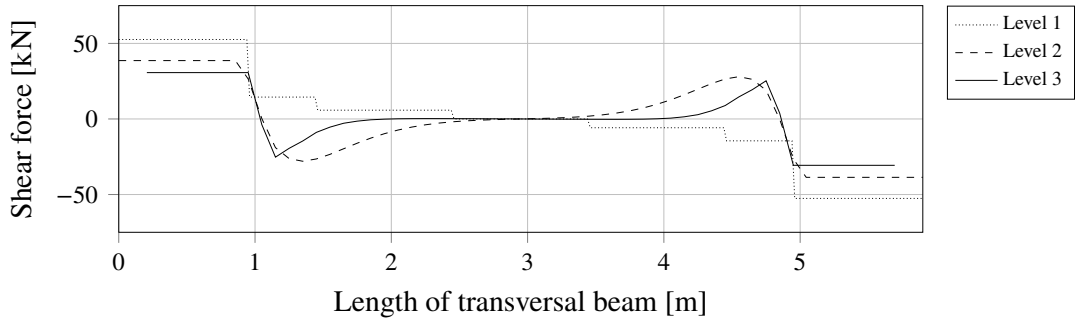

Figure E.59 Horizontal shear force in the ninth transversal beam for level 1, 2 and 3, subjected to temperature load.

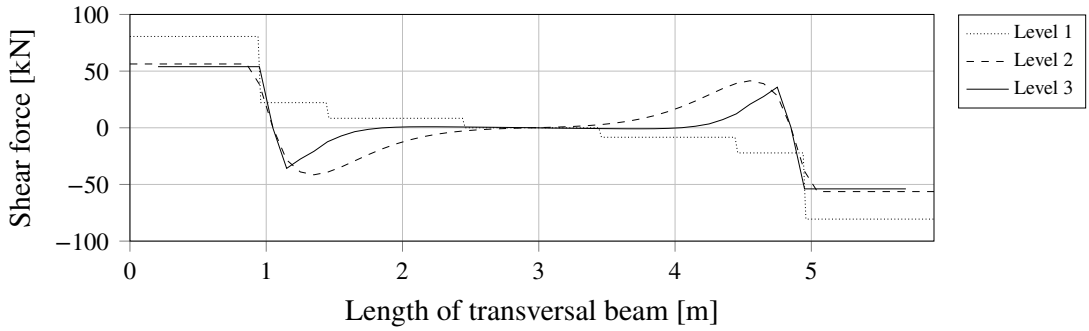

Figure E.60 Horizontal shear force in the tenth transversal beam for level 1, 2 and 3, subjected to temperature load.

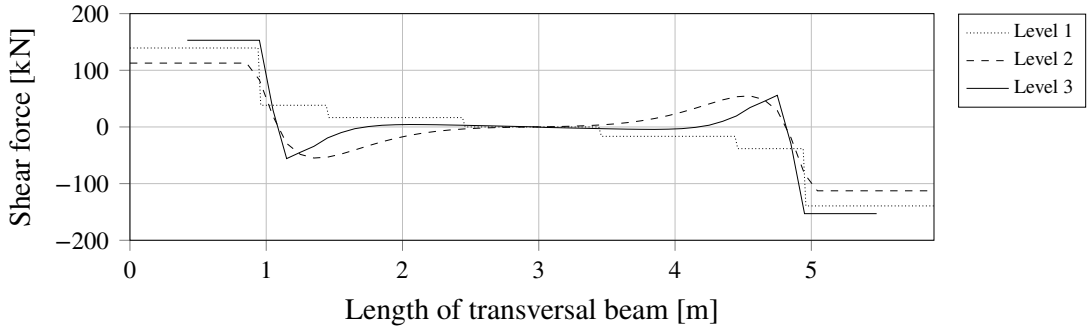

Figure E.61 *Horizontal shear force in the eleventh transversal beam for level 1, 2 and 3, subjected to temperature load.*

E.3 Concentrated traffic load

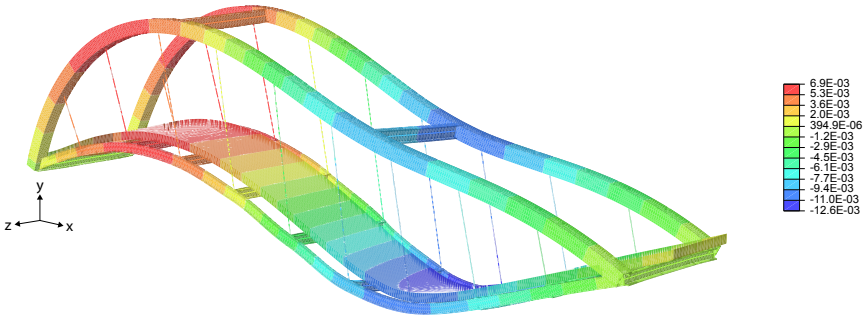

Figure E.62 *Deformation of the bridge subjected to one concentrated traffic load placed between the seventh and eight transversal beam. The contour display the deformation in y-direction [m]. The displayed model is level 2, however all levels show the same global behaviour.*

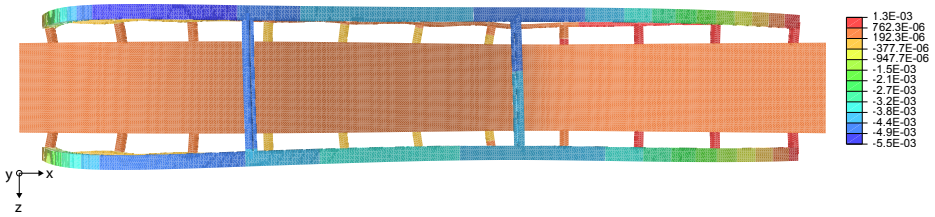

Figure E.63 *Deformation of the bridge subjected to one concentrated traffic load placed between the seventh and eight transversal beam, seen from above. The contour display the deformation in x-direction [m]. The displayed model is level 2, however all levels show the same global behaviour.*

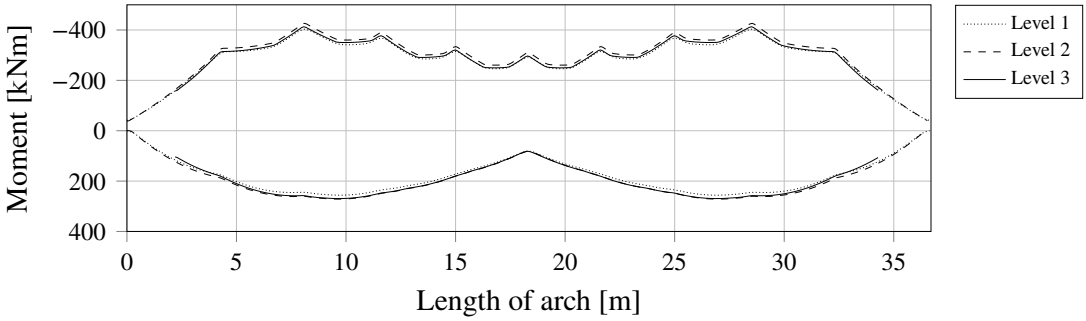

Figure E.64 Maximum and minimum bending moment in the arch for level 1, 2 and 3, subjected to the concentrated traffic load.

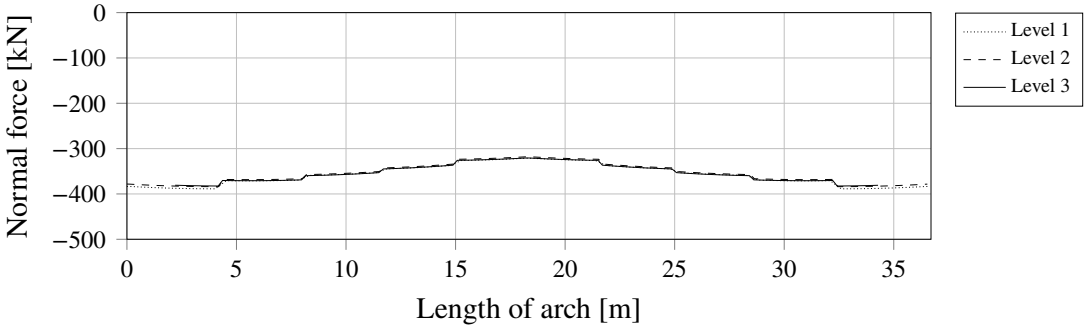

Figure E.65 Maximum and minimum normal force in the arch for level 1, 2 and 3, subjected to the concentrated traffic load.

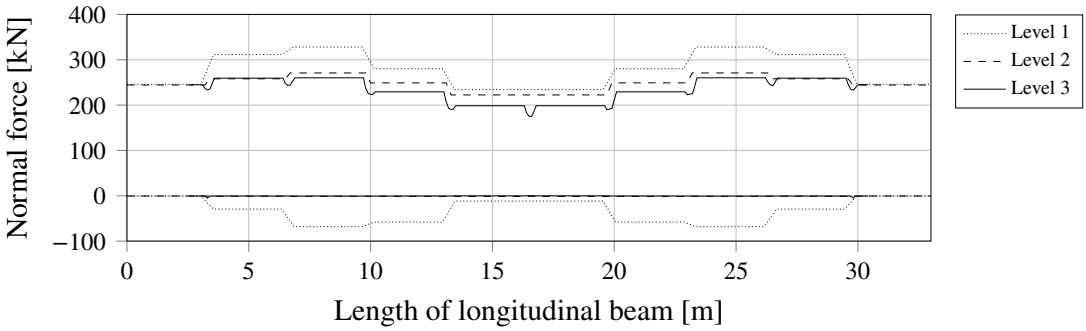

Figure E.66 Maximum and minimum normal force in the longitudinal beam for level 1, 2 and 3, subjected to the concentrated traffic load.

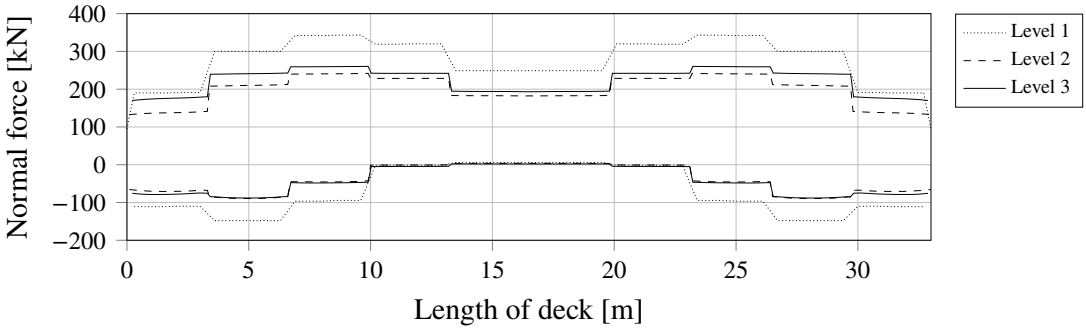

Figure E.67 The integrated maximum and minimum normal force over half of the width of the deck in the longitudinal direction for level 1, 2 and 3, subjected to the concentrated traffic load.

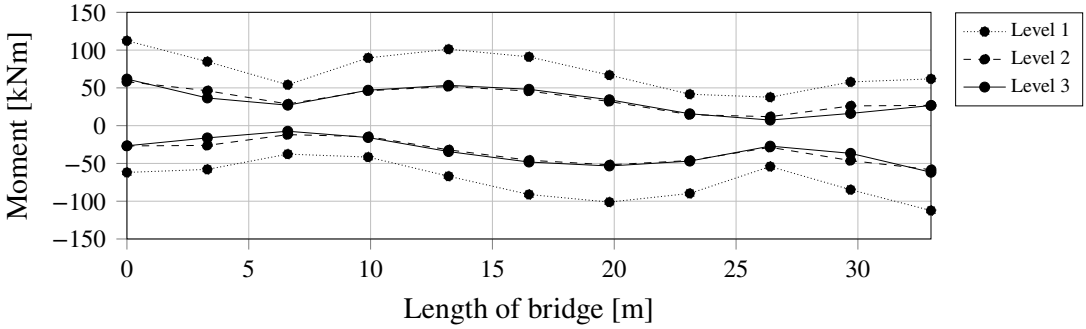

Figure E.68 Variation of maximum and minimum secondary bending moment in the transversal beams along the bridge for level 1, 2 and 3, subjected to the concentrated traffic load.

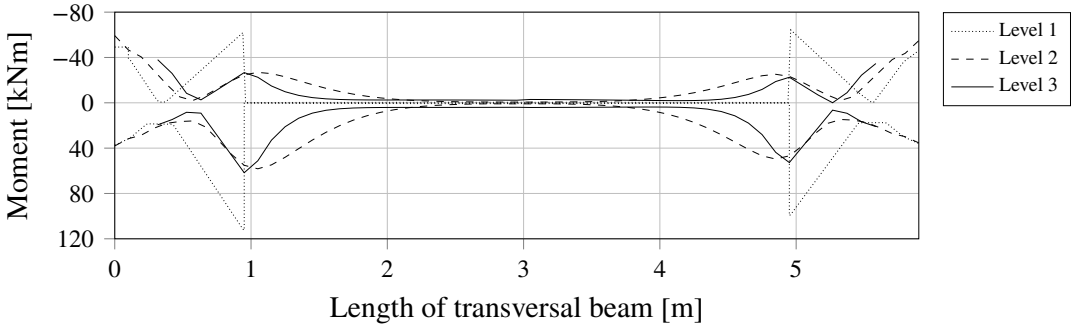

Figure E.69 Maximum and minimum secondary bending moment distribution in the first transversal beam for level 1, 2 and 3, subjected to the concentrated traffic load.

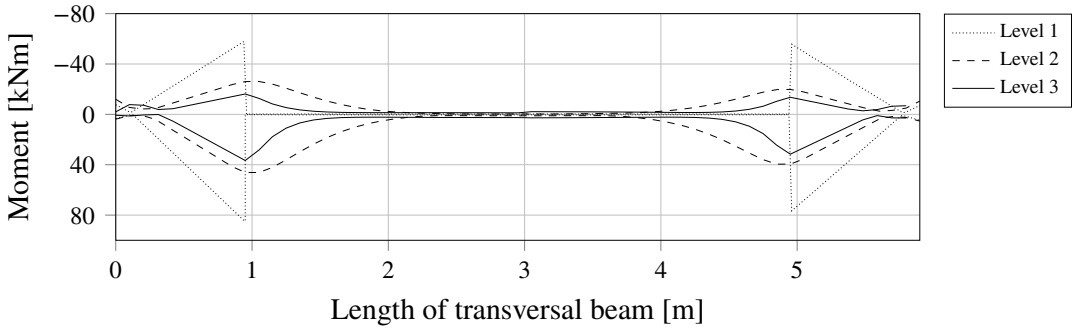

Figure E.70 Maximum and minimum secondary bending moment distribution in the second transversal beam for level 1, 2 and 3, subjected to the concentrated traffic load.

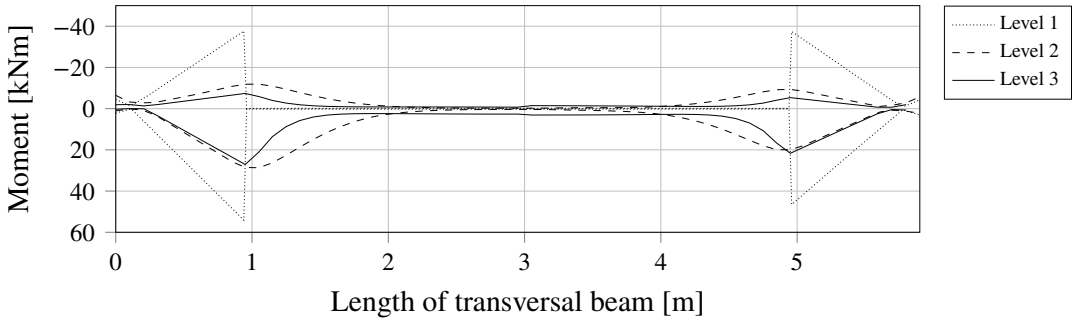

Figure E.71 Maximum and minimum secondary bending moment distribution in the third transversal beam for level 1, 2 and 3, subjected to the concentrated traffic load.

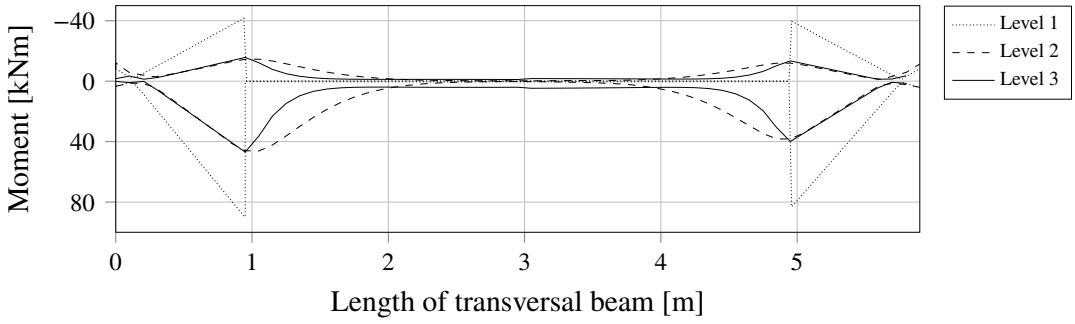

Figure E.72 Maximum and minimum secondary bending moment distribution in the forth transversal beam for level 1, 2 and 3, subjected to the concentrated traffic load.

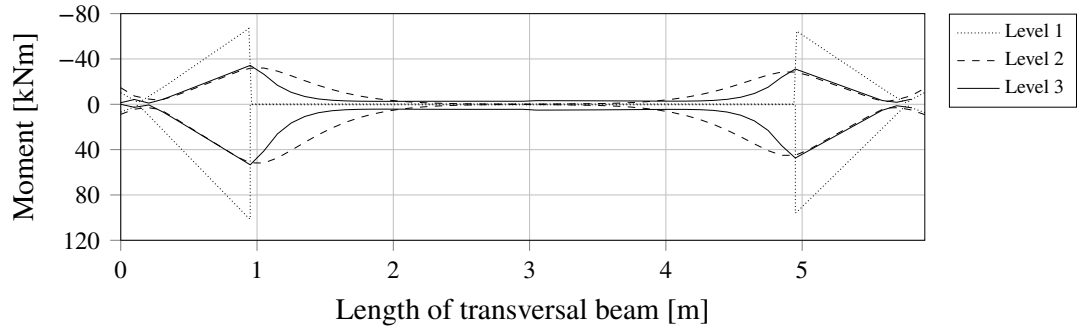

Figure E.73 Maximum and minimum secondary bending moment distribution in the fifth transversal beam for level 1, 2 and 3, subjected to the concentrated traffic load.

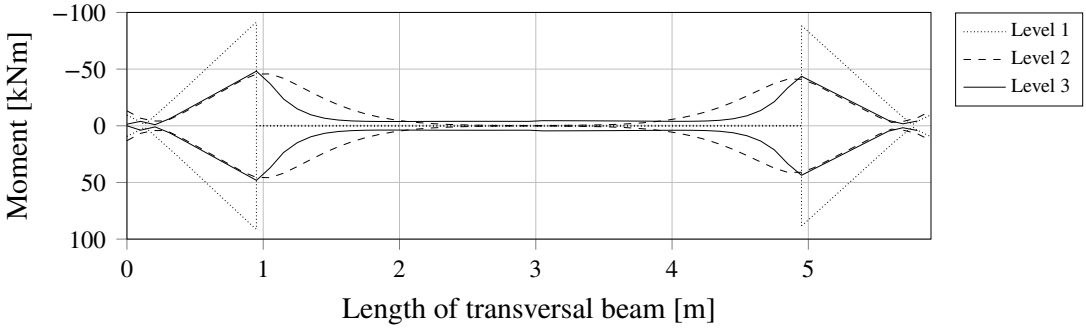

Figure E.74 Maximum and minimum secondary bending moment distribution in the sixth transversal beam for level 1, 2 and 3, subjected to the concentrated traffic load.

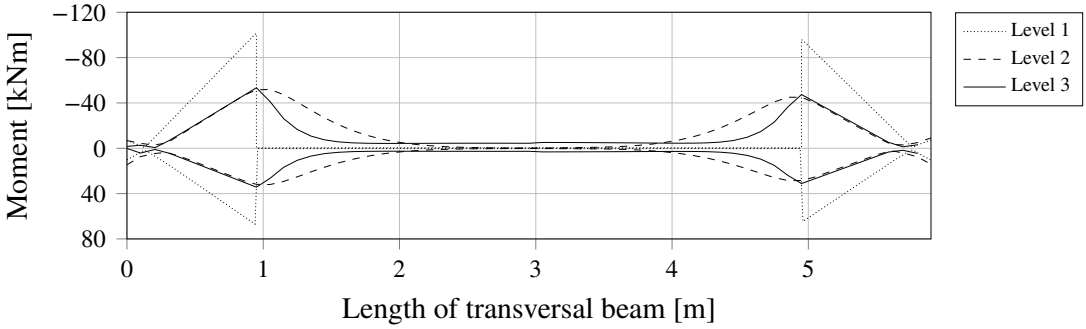

Figure E.75 Maximum and minimum secondary bending moment distribution in the seventh transversal beam for level 1, 2 and 3, subjected to the concentrated traffic load.

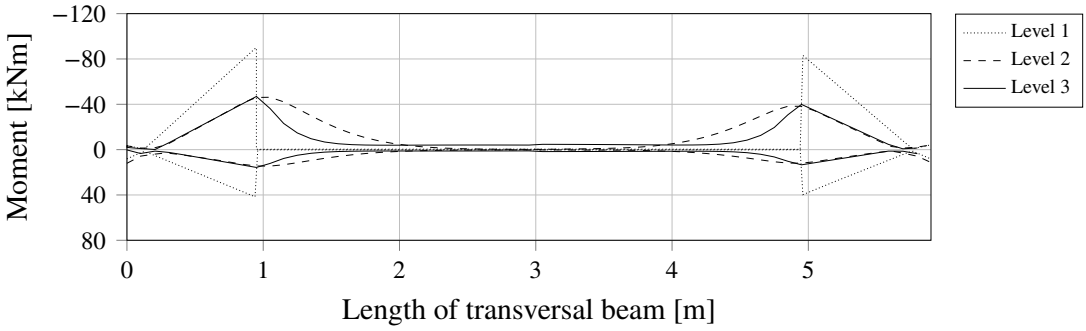

Figure E.76 Maximum and minimum secondary bending moment distribution in the eight transversal beam for level 1, 2 and 3, subjected to the concentrated traffic load.

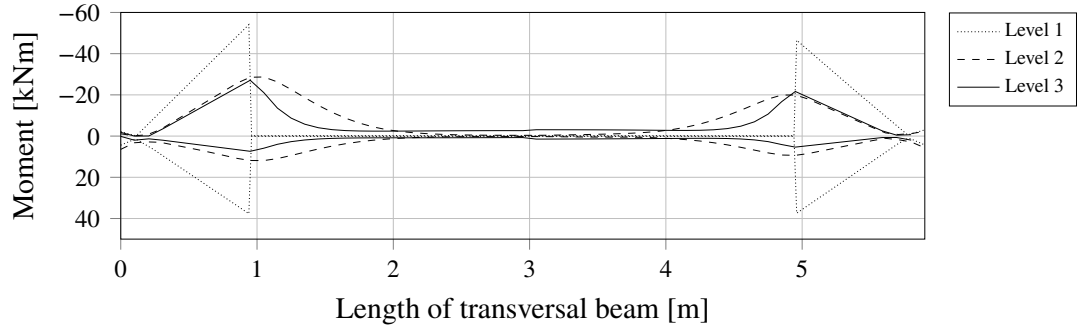

Figure E.77 Maximum and minimum secondary bending moment distribution in the ninth transversal beam for level 1, 2 and 3, subjected to the concentrated traffic load.

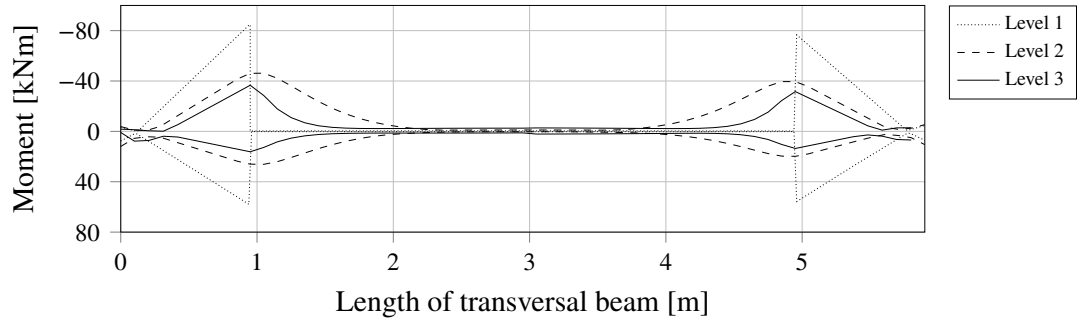

Figure E.78 Maximum and minimum secondary bending moment distribution in the tenth transversal beam for level 1, 2 and 3, subjected to the concentrated traffic load.

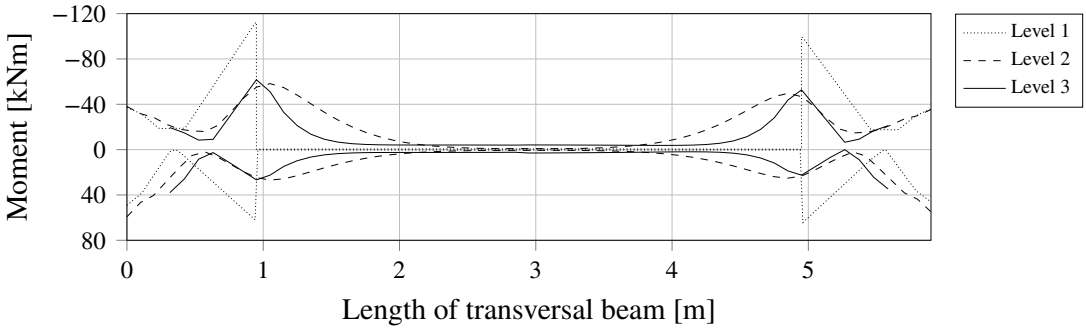

Figure E.79 Maximum and minimum secondary bending moment distribution in the eleventh transversal beam for level 1, 2 and 3, subjected to the concentrated traffic load.

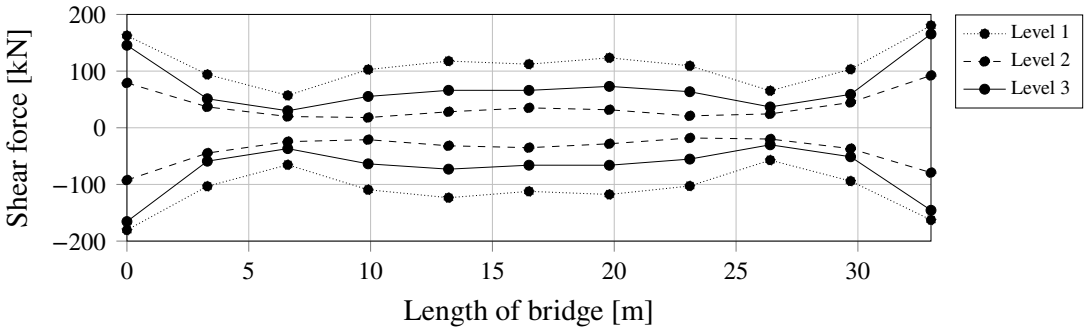

Figure E.80 Variation of maximum and minimum horizontal shear force in the transversal beam along the bridge for level 1, 2 and 3, subjected to concentrated traffic load.

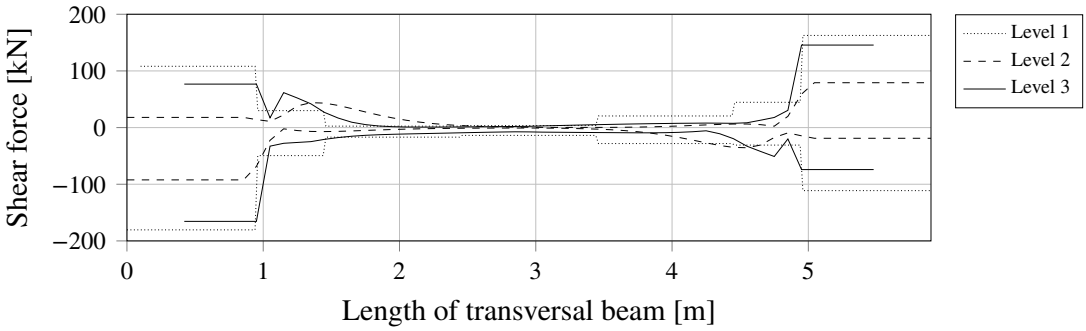

Figure E.81 Maximum and minimum horizontal shear force in the first transversal beam for level 1, 2 and 3, subjected to concentrated traffic load.

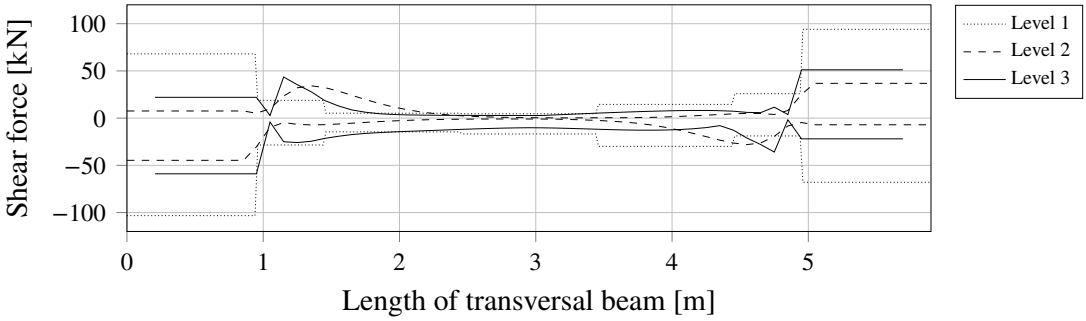

Figure E.82 Maximum and minimum horizontal shear force in the second transversal beam for level 1, 2 and 3, subjected to concentrated traffic load.

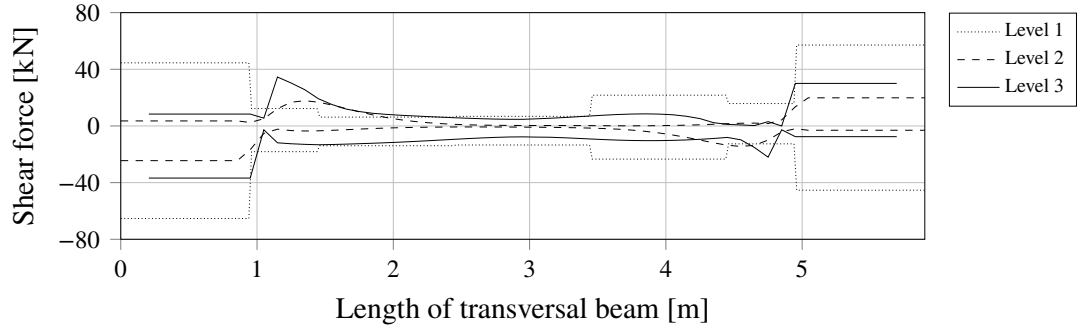

Figure E.83 Maximum and minimum horizontal shear force in the third transversal beam for level 1, 2 and 3, subjected to concentrated traffic load.

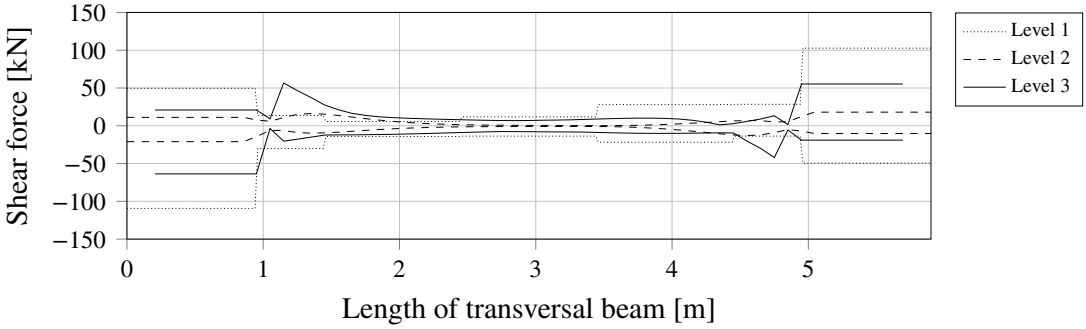

Figure E.84 Maximum and minimum horizontal shear force in the forth transversal beam for level 1, 2 and 3, subjected to concentrated traffic load.

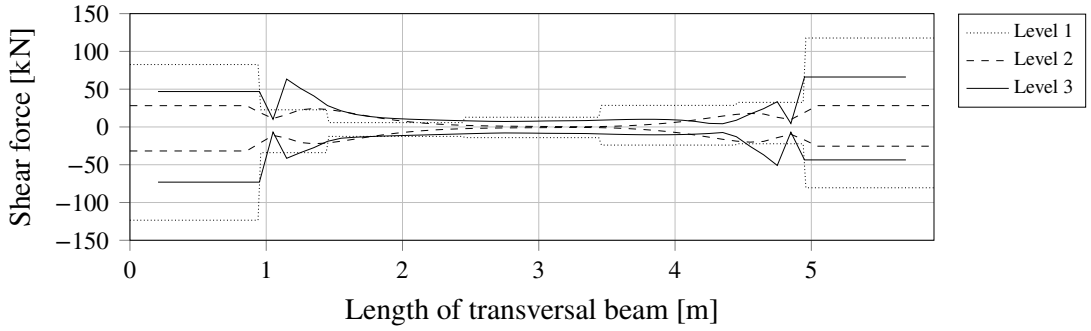

Figure E.85 Maximum and minimum horizontal shear force in the fifth transversal beam for level 1, 2 and 3, subjected to concentrated traffic load.

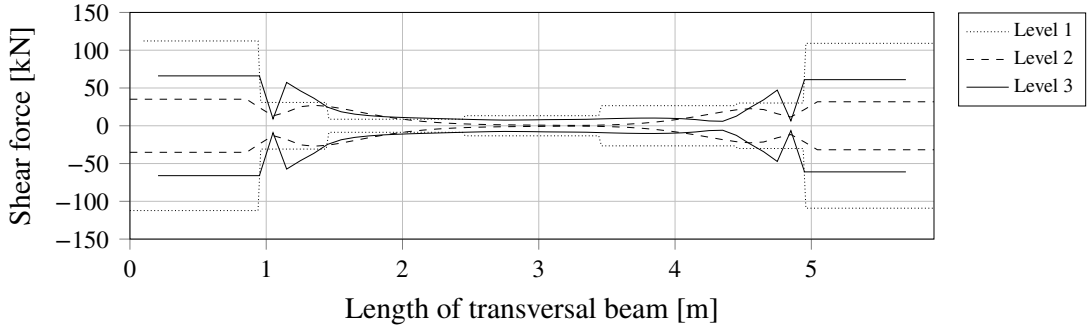

Figure E.86 Maximum and minimum horizontal shear force in the sixth transversal beam for level 1, 2 and 3, subjected to concentrated traffic load.

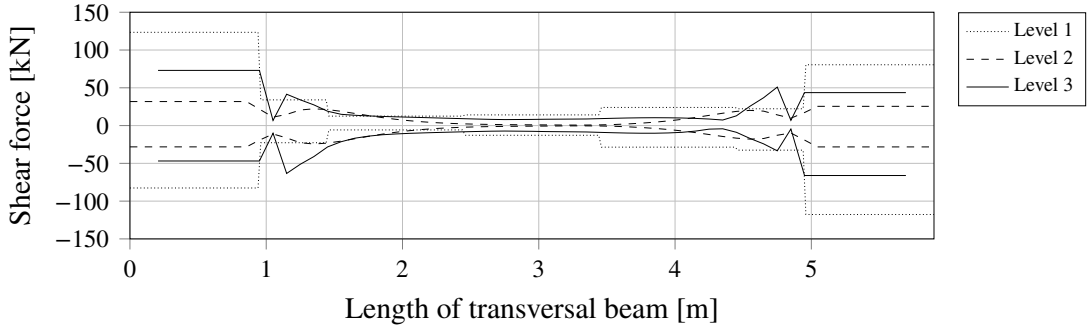

Figure E.87 Maximum and minimum horizontal shear force in the seventh transversal beam for level 1, 2 and 3, subjected to concentrated traffic load.

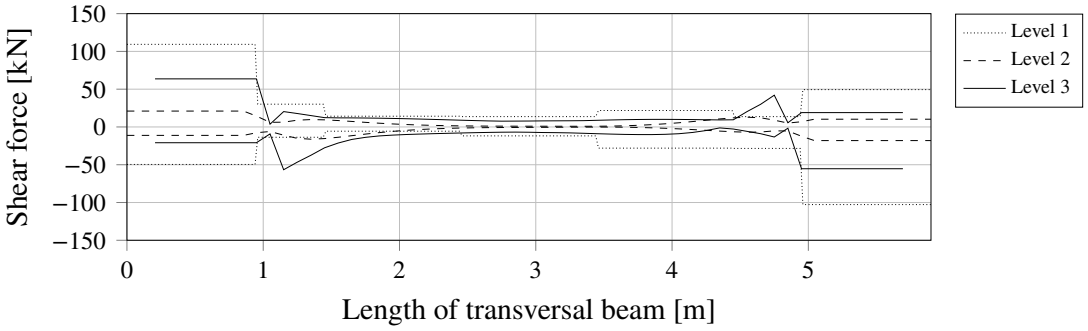

Figure E.88 Maximum and minimum horizontal shear force in the eight transversal beam for level 1, 2 and 3, subjected to concentrated traffic load.

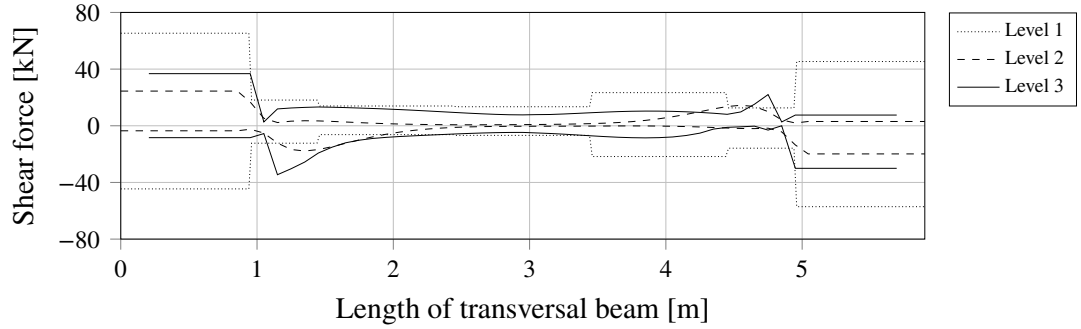

Figure E.89 Maximum and minimum horizontal shear force in the ninth transversal beam for level 1, 2 and 3, subjected to concentrated traffic load.

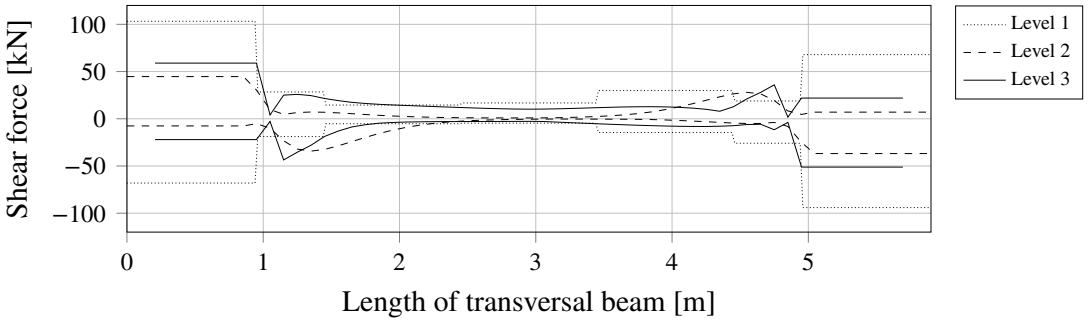

Figure E.90 Maximum and minimum horizontal shear force in the tenth transversal beam for level 1, 2 and 3, subjected to concentrated traffic load.

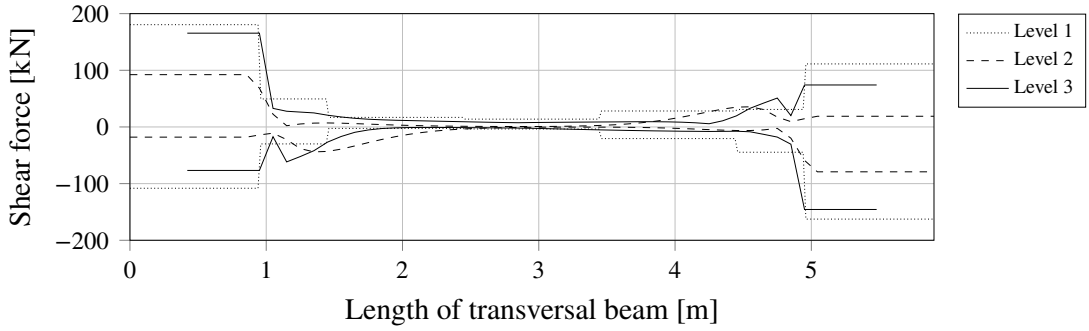

Figure E.91 Maximum and minimum horizontal shear force in the eleventh transversal beam for level 1, 2 and 3, subjected to concentrated traffic load.

E.4 Distributed traffic load

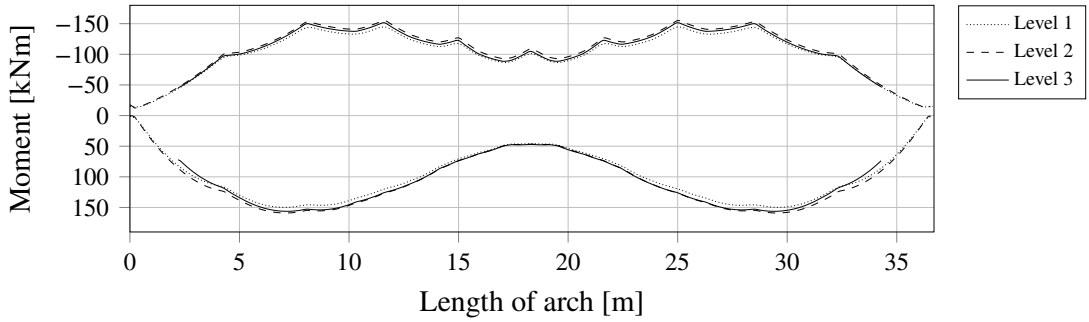

Figure E.92 Maximum and minimum bending moment in the arch for level 1, 2 and 3, subjected to the distributed traffic load.

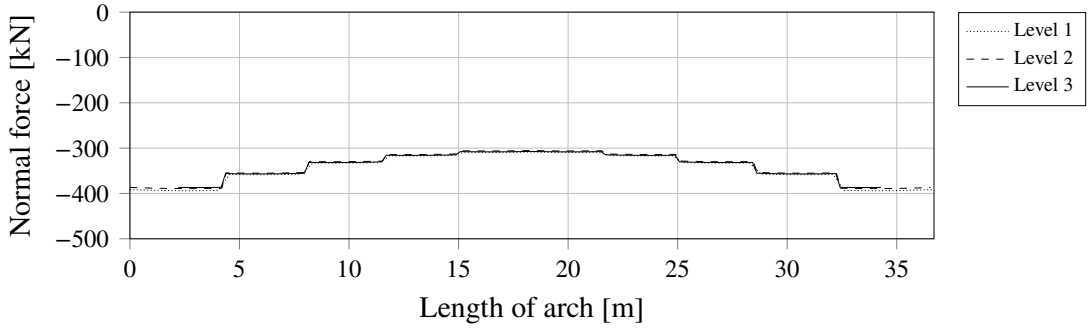

Figure E.93 Maximum and minimum normal force in the arch for level 1, 2 and 3, subjected to the distributed traffic load.

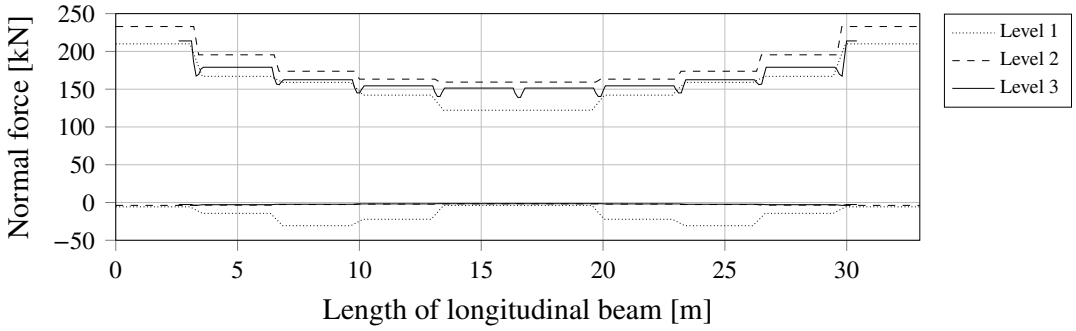

Figure E.94 Maximum and minimum normal force in the longitudinal beam for level 1, 2 and 3, subjected to the distributed traffic load.

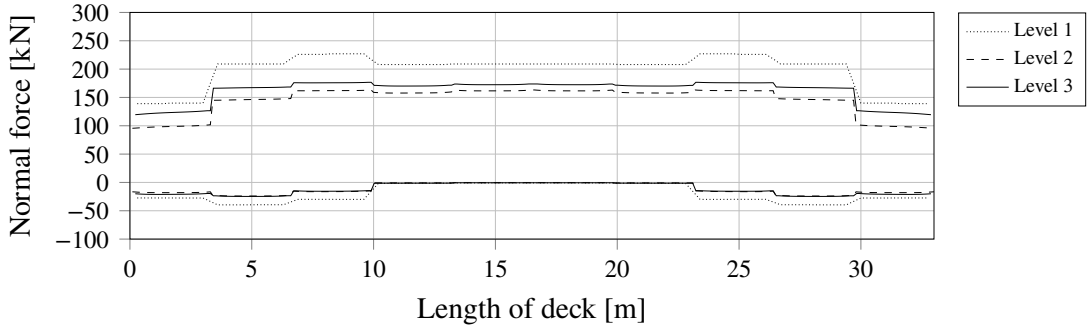

Figure E.95 The integrated maximum and minimum normal force over half of the width of the deck in the longitudinal direction for level 1, 2 and 3, subjected to the distributed traffic load.

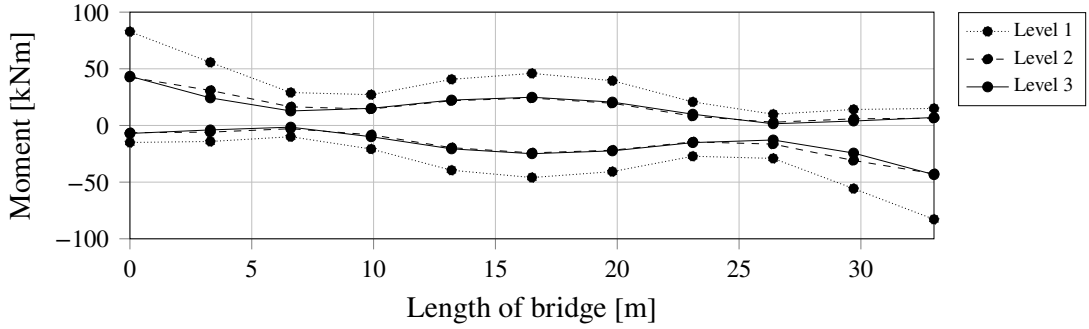

Figure E.96 Variation of maximum and minimum secondary bending moment in the transversal beams along the bridge for level 1, 2 and 3, subjected to the distributed traffic load.

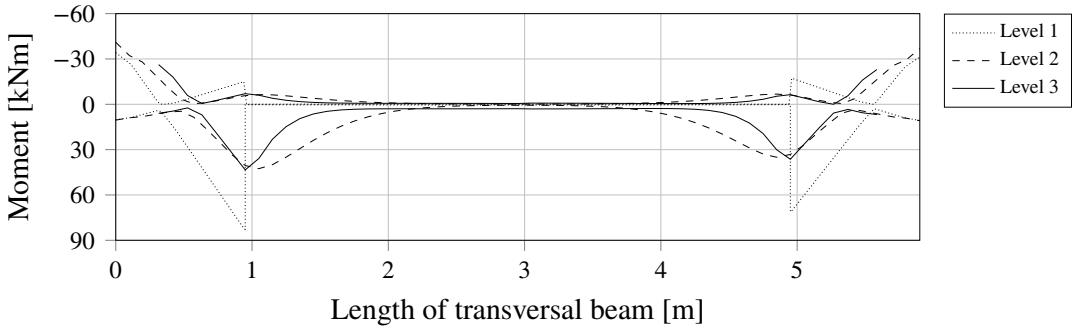

Figure E.97 Maximum and minimum secondary bending moment distribution in the first transversal beam for level 1, 2 and 3, subjected to the distributed traffic load.

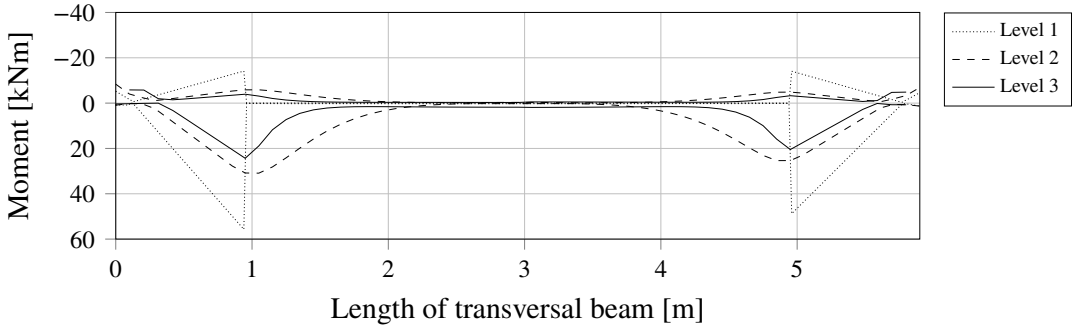

Figure E.98 Maximum and minimum secondary bending moment distribution in the second transversal beam for level 1, 2 and 3, subjected to the distributed traffic load.

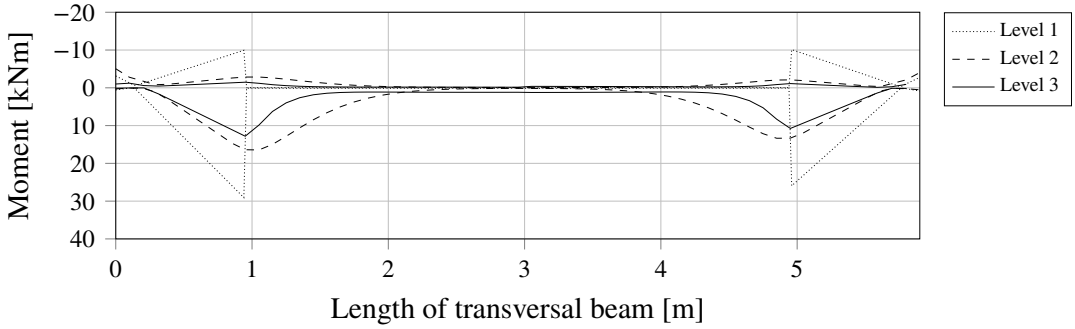

Figure E.99 Maximum and minimum secondary bending moment distribution in the third transversal beam for level 1, 2 and 3, subjected to the distributed traffic load.

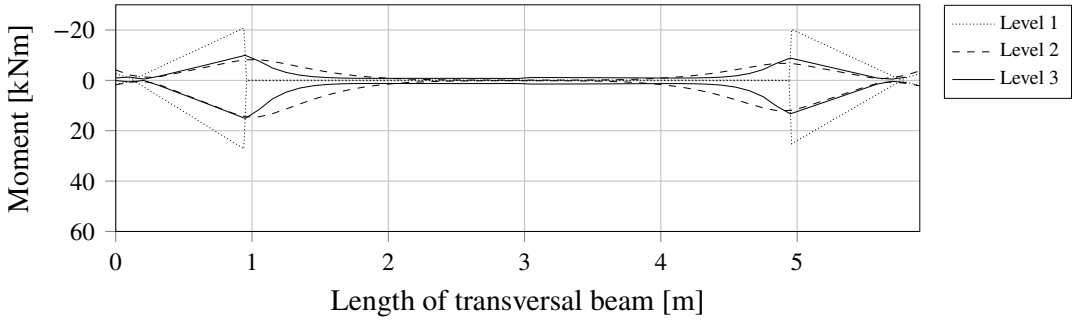

Figure E.100 Maximum and minimum secondary bending moment distribution in the forth transversal beam for level 1, 2 and 3, subjected to the distributed traffic load.

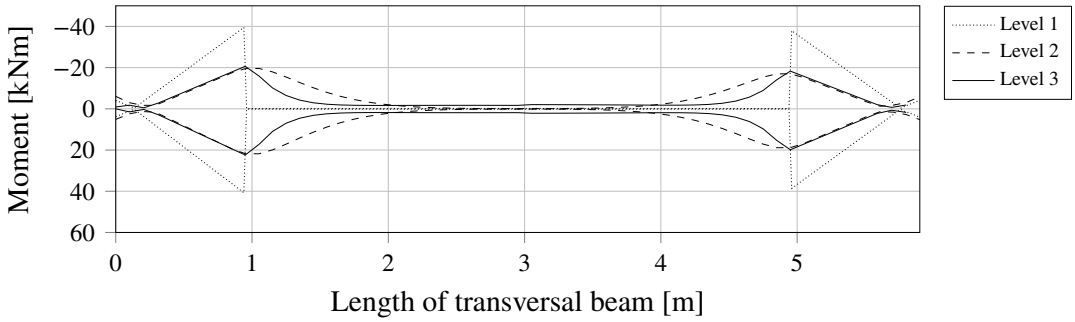

Figure E.101 Maximum and minimum secondary bending moment distribution in the fifth transversal beam for level 1, 2 and 3, subjected to the distributed traffic load.

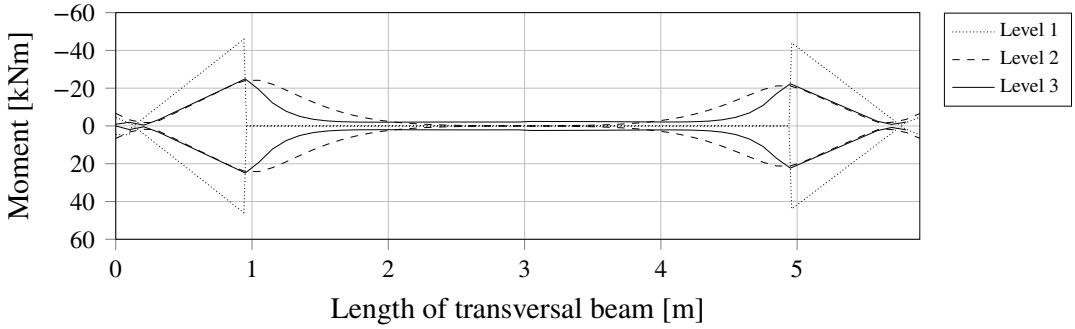

Figure E.102 Maximum and minimum secondary bending moment distribution in the sixth transversal beam for level 1, 2 and 3, subjected to the distributed traffic load.

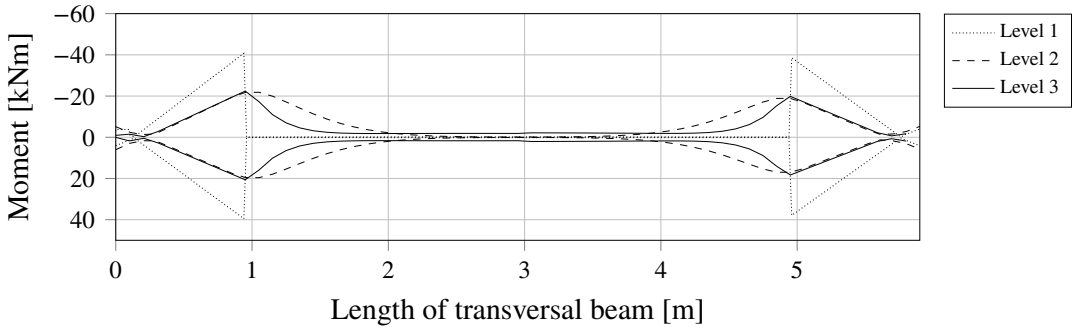

Figure E.103 Maximum and minimum secondary bending moment distribution in the seventh transversal beam for level 1, 2 and 3, subjected to the distributed traffic load.

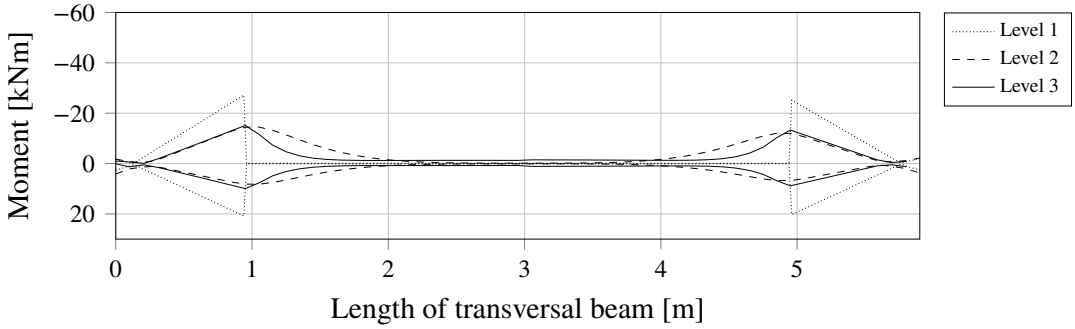

Figure E.104 Maximum and minimum secondary bending moment distribution in the eight transversal beam for level 1, 2 and 3, subjected to the distributed traffic load.

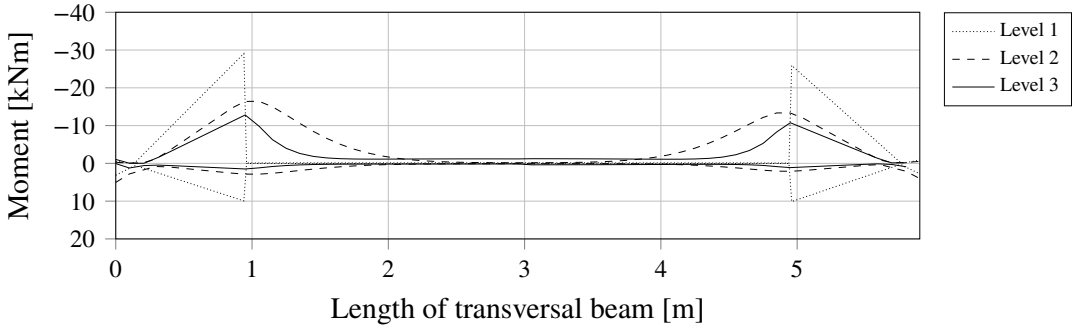

Figure E.105 Maximum and minimum secondary bending moment distribution in the ninth transversal beam for level 1, 2 and 3, subjected to the distributed traffic load.

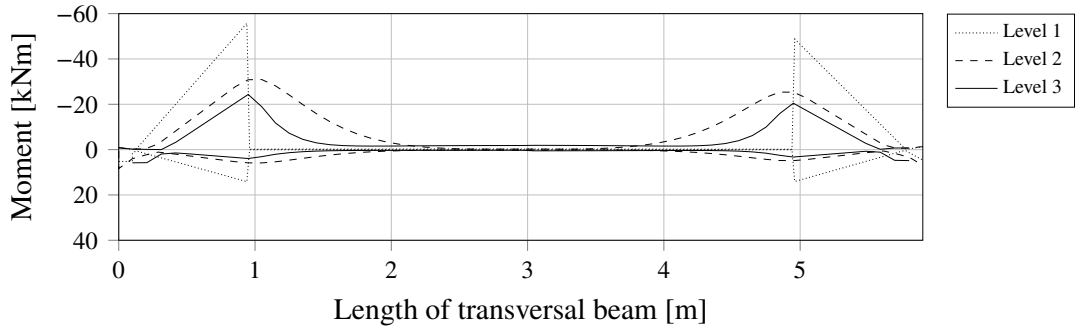

Figure E.106 Maximum and minimum secondary bending moment distribution in the tenth transversal beam for level 1, 2 and 3, subjected to the distributed traffic load.

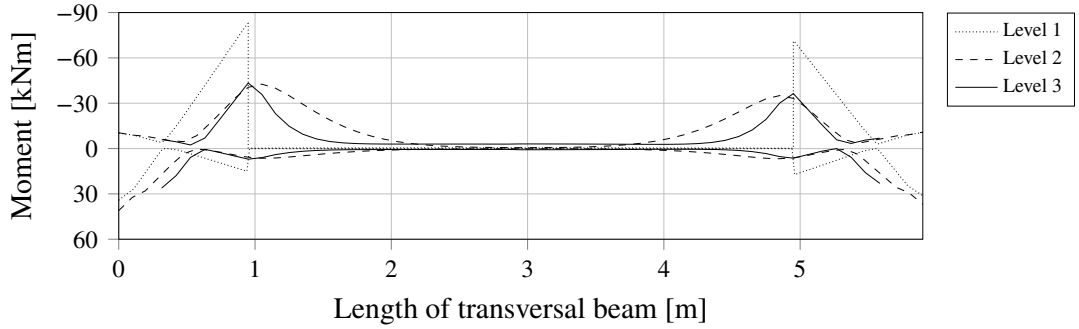

Figure E.107 Maximum and minimum secondary bending moment distribution in the eleventh transversal beam for level 1, 2 and 3, subjected to the distributed traffic load.

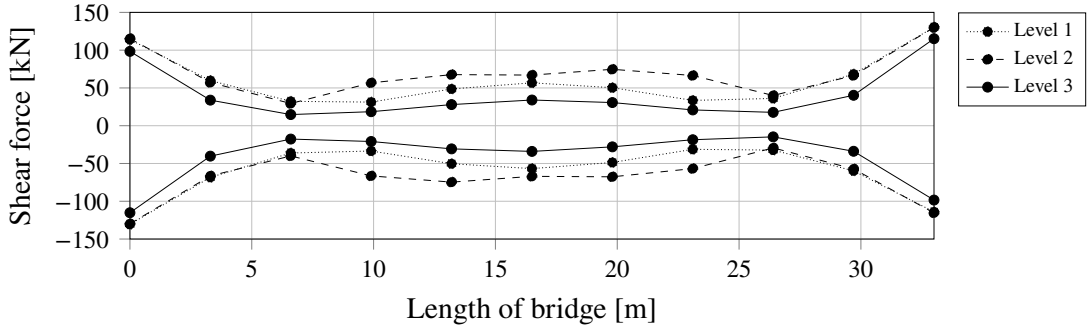

Figure E.108 Variation of maximum and minimum horizontal shear force in the transversal beam along the bridge for level 1, 2 and 3, subjected to distributed traffic load.

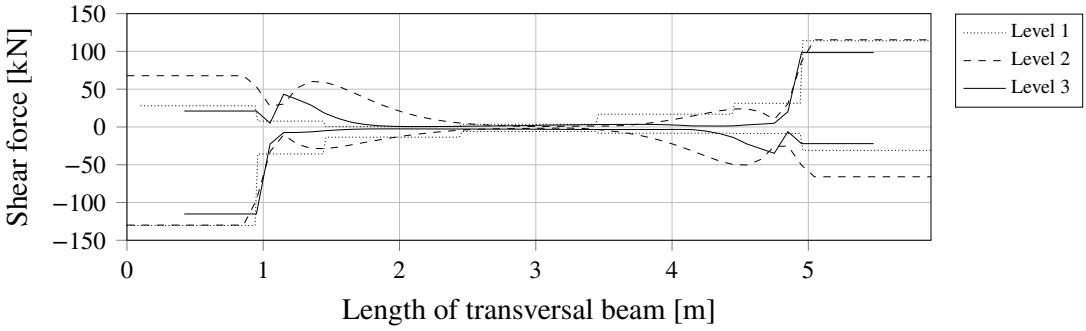

Figure E.109 Maximum and minimum horizontal shear force in the first transversal beam for level 1, 2 and 3, subjected to distributed traffic load.

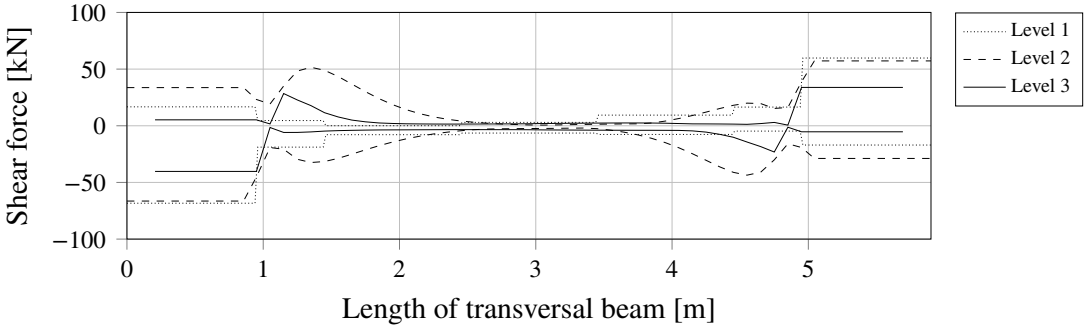

Figure E.110 Maximum and minimum horizontal shear force in the second transversal beam for level 1, 2 and 3, subjected to distributed traffic load.

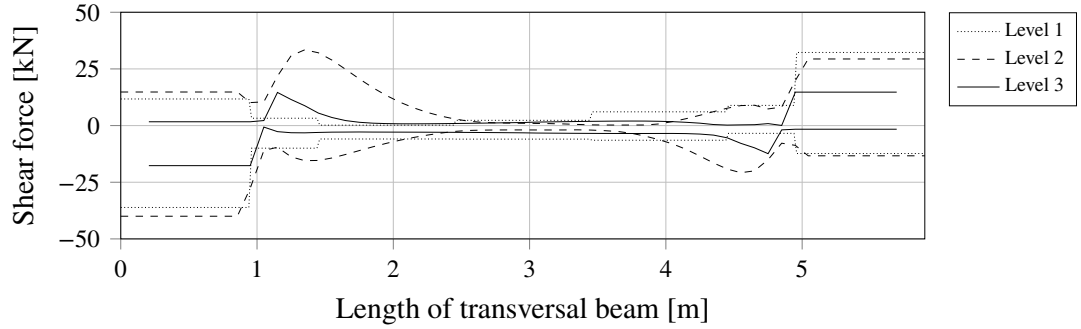

Figure E.111 Maximum and minimum horizontal shear force in the third transversal beam for level 1, 2 and 3, subjected to distributed traffic load.

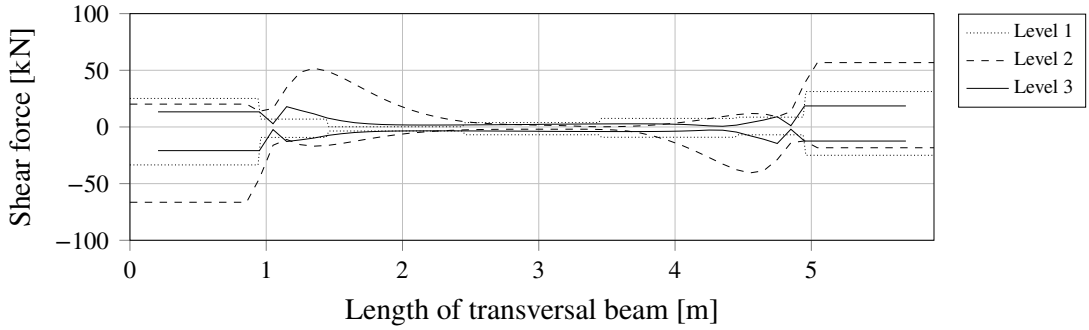

Figure E.112 Maximum and minimum horizontal shear force in the forth transversal beam for level 1, 2 and 3, subjected to distributed traffic load.

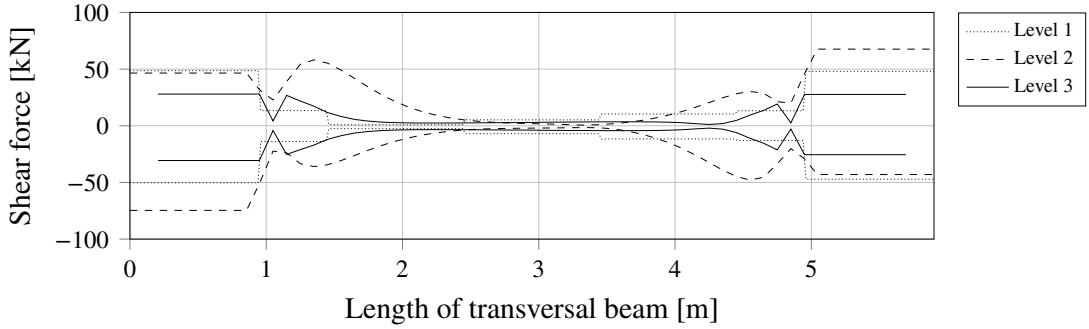

Figure E.113 Maximum and minimum horizontal shear force in the fifth transversal beam for level 1, 2 and 3, subjected to distributed traffic load.

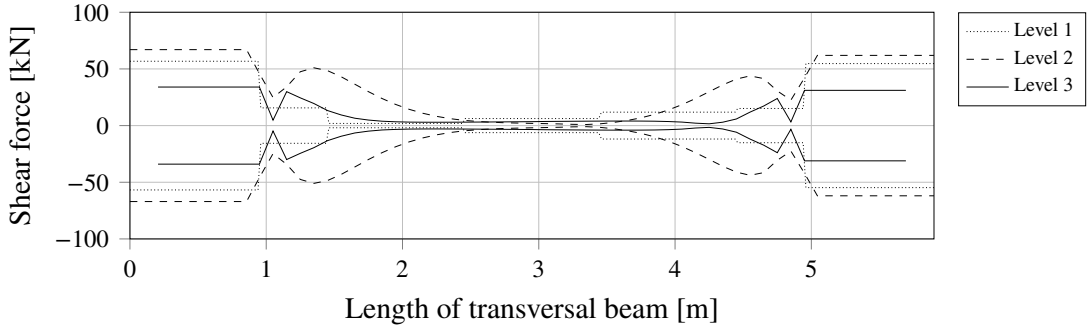

Figure E.114 Maximum and minimum horizontal shear force in the sixth transversal beam for level 1, 2 and 3, subjected to distributed traffic load.

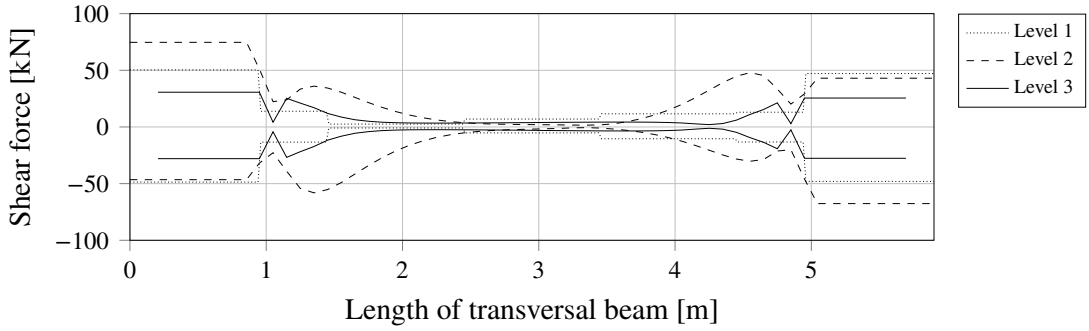

Figure E.115 Maximum and minimum horizontal shear force in the seventh transversal beam for level 1, 2 and 3, subjected to distributed traffic load.

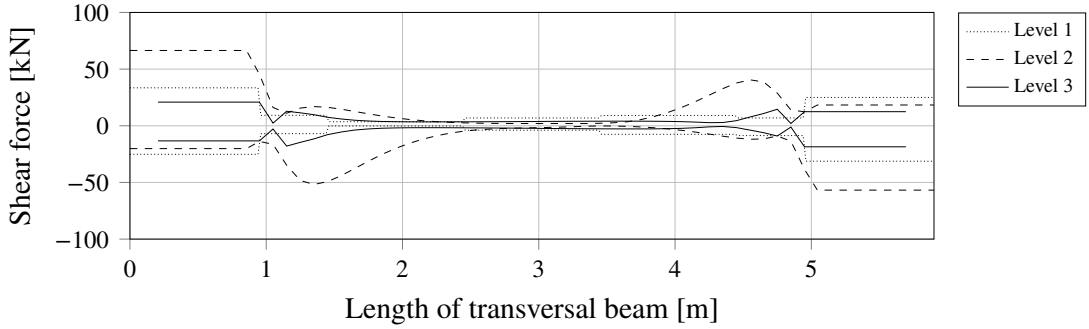

Figure E.116 Maximum and minimum horizontal shear force in the eight transversal beam for level 1, 2 and 3, subjected to distributed traffic load.

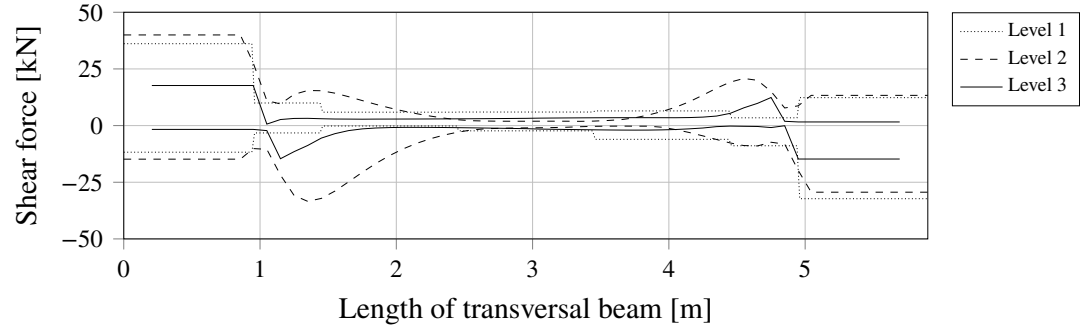

Figure E.117 Maximum and minimum horizontal shear force in the ninth transversal beam for level 1, 2 and 3, subjected to distributed traffic load.

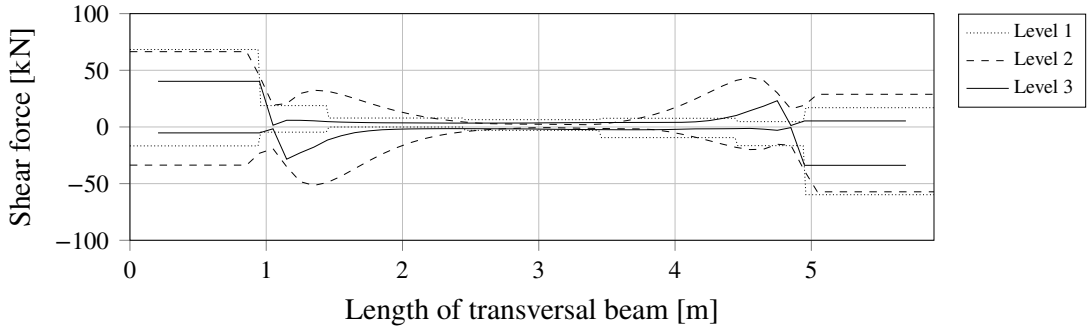

Figure E.118 Maximum and minimum horizontal shear force in the tenth transversal beam for level 1, 2 and 3, subjected to distributed traffic load.

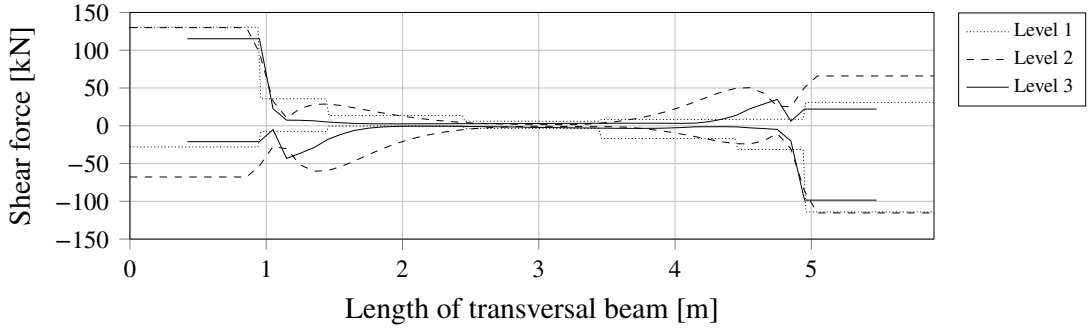

Figure E.119 Maximum and minimum horizontal shear force in the eleventh transversal beam for level 1, 2 and 3, subjected to distributed traffic load.

E.5 Parametrization

E.5.1 Uniformly distributed load

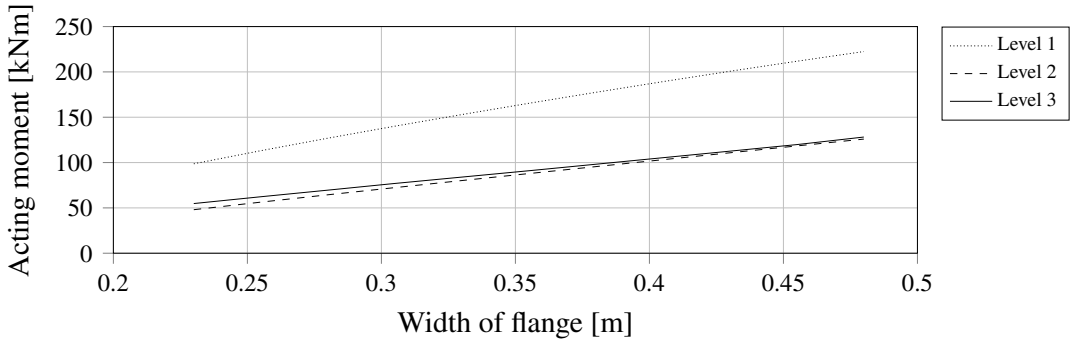

Figure E.120 Variation of maximum acting secondary bending moment for the first transversal beam, subjected to the uniformly distributed load.

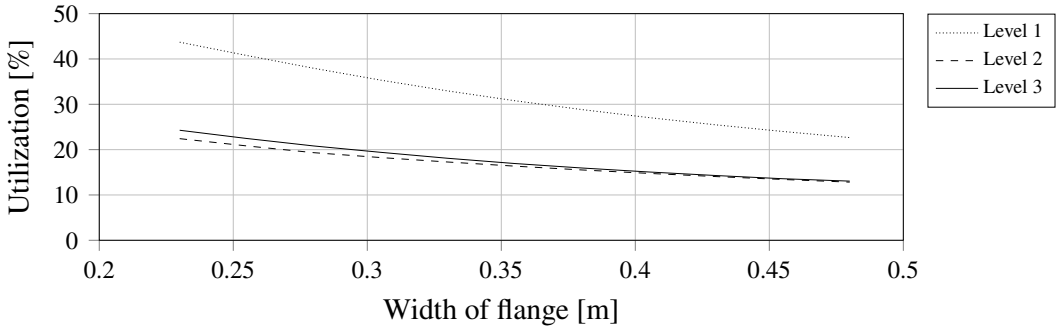

Figure E.121 The utilization ratio, regarding SLS, of the first transversal beam for different widths of the flanges for the uniformly distributed load.

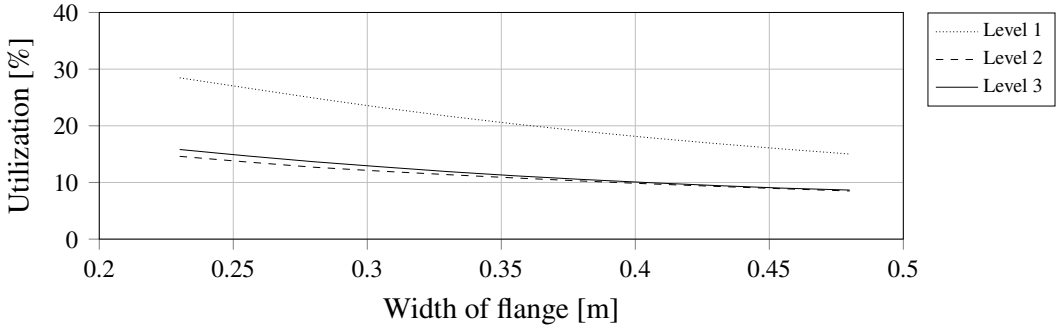

Figure E.122 The utilization ratio, regarding ULS, of the first transversal beam for different widths of the flanges for the uniformly distributed load.

E.5.2 Temperature load

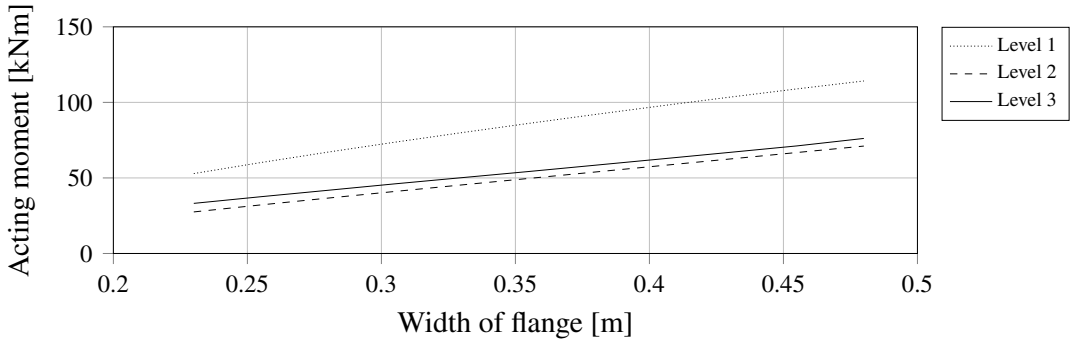

Figure E.123 Variation of maximum acting secondary bending moment for the first transversal beam, subjected to the temperature load.

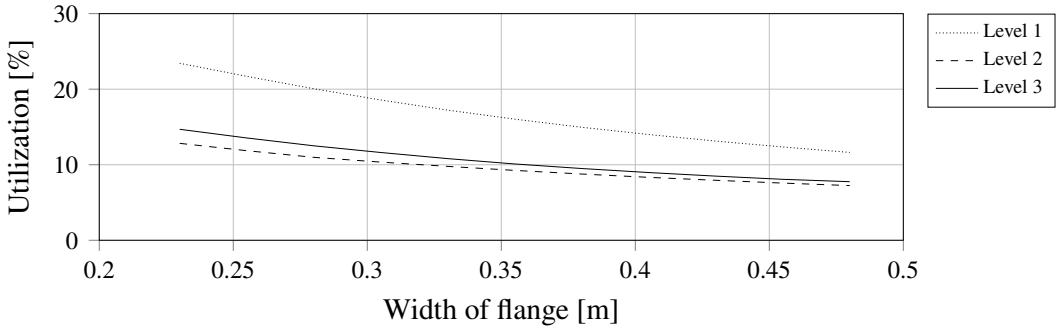

Figure E.124 The utilization ratio, regarding SLS, of the first transversal beam for different widths of the flanges for the temperature load.

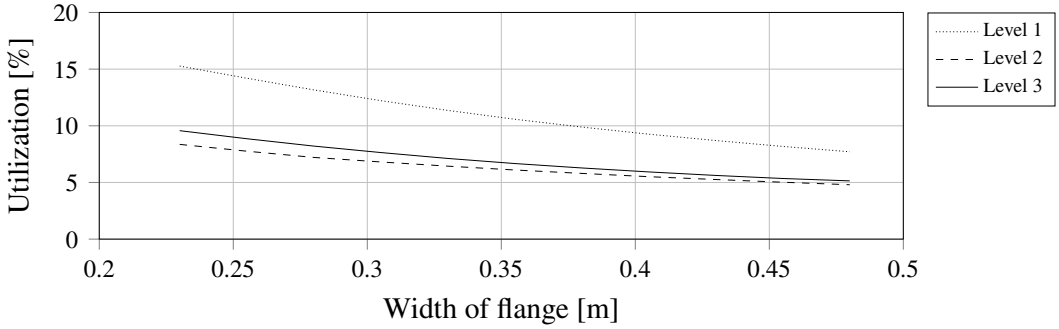

Figure E.125 The utilization ratio, regarding ULS, of the first transversal beam for different widths of the flanges for the temperature load.

E.5.3 Concentrated traffic load

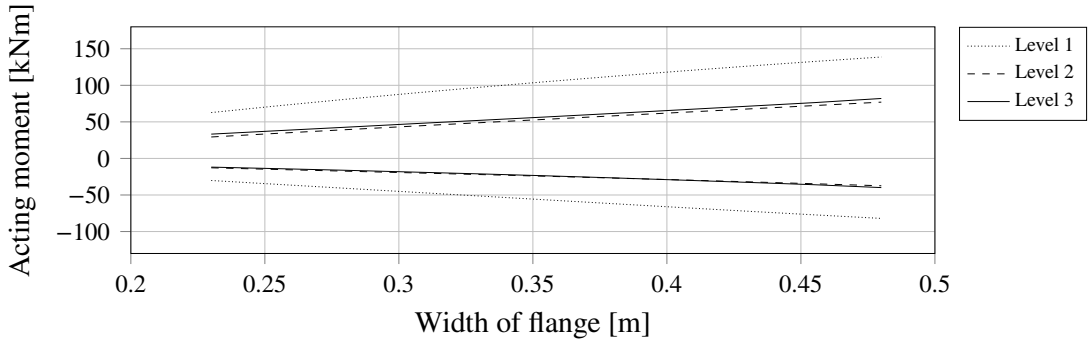

Figure E.126 Variation of maximum acting secondary bending moment for the first transversal beam, subjected to the concentrated traffic load.

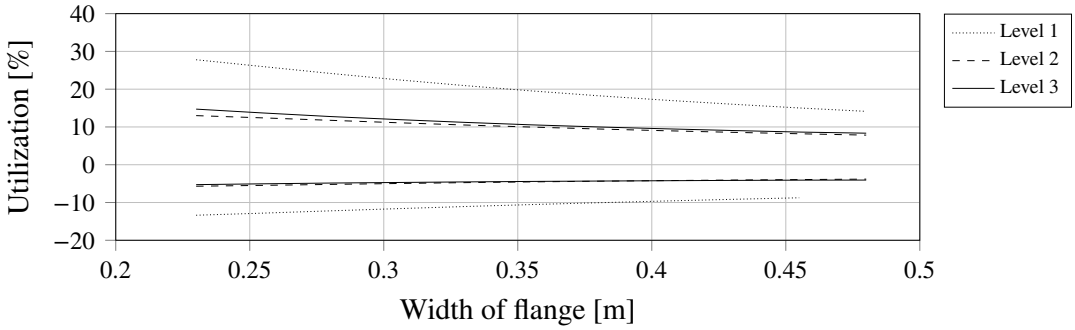

Figure E.127 The utilization ratio, regarding SLS, of the first transversal beam for different widths of the flanges for the concentrated traffic load.

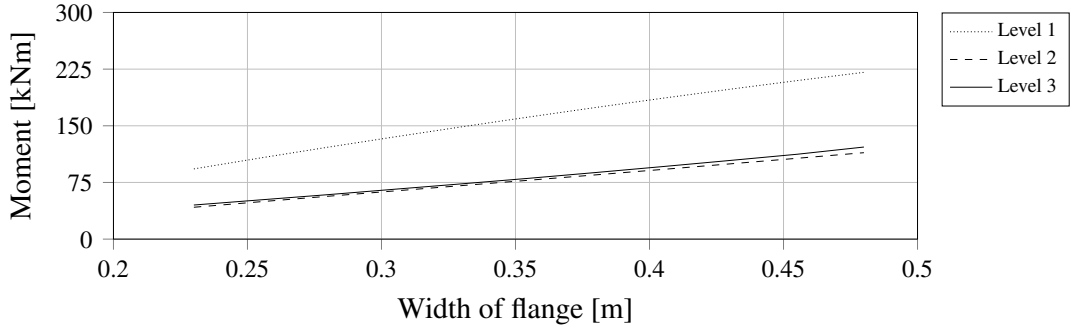

Figure E.128 The difference in maximum and minimum secondary bending moment in the first transversal beam for different widths of the flanges for the concentrated traffic load case.

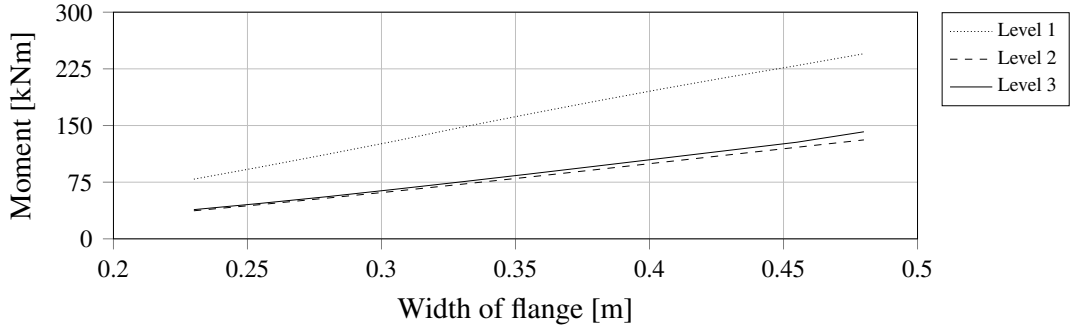

Figure E.129 The difference in maximum and minimum secondary bending moment in the sixth transversal beam for different widths of the flanges for the concentrated traffic load case.

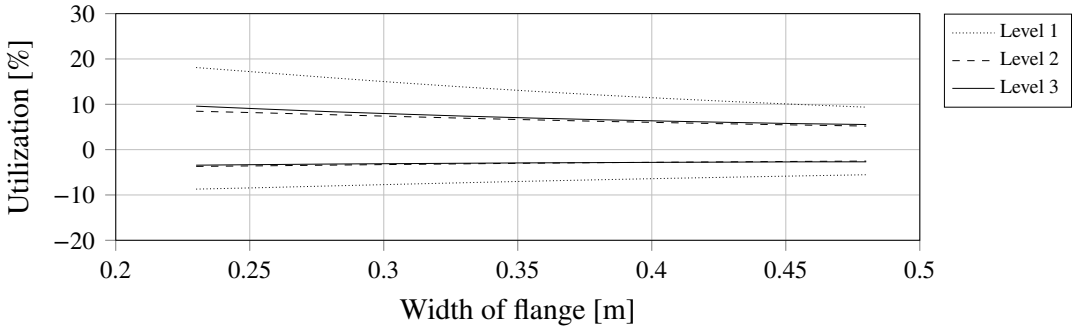

Figure E.130 The utilization ratio, regarding ULS, of the first transversal beam for different widths of the flanges for the concentrated traffic load.

E.5.4 Distributed traffic load

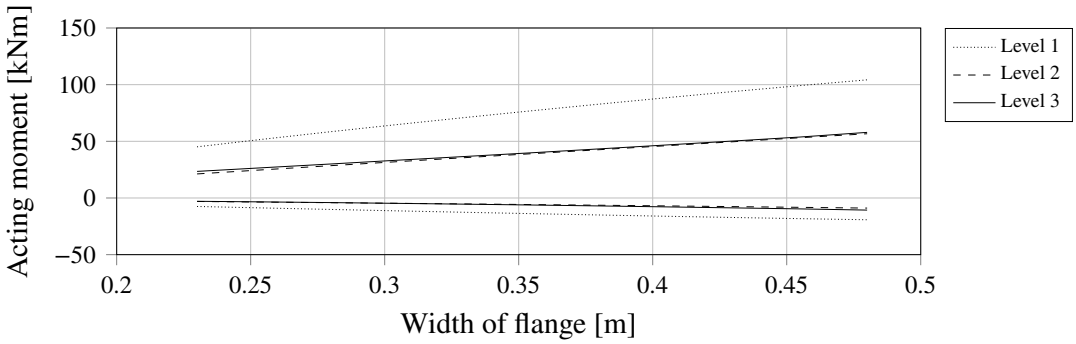

Figure E.131 Variation of maximum acting secondary bending moment for the first transversal beam, subjected to the distributed traffic load.

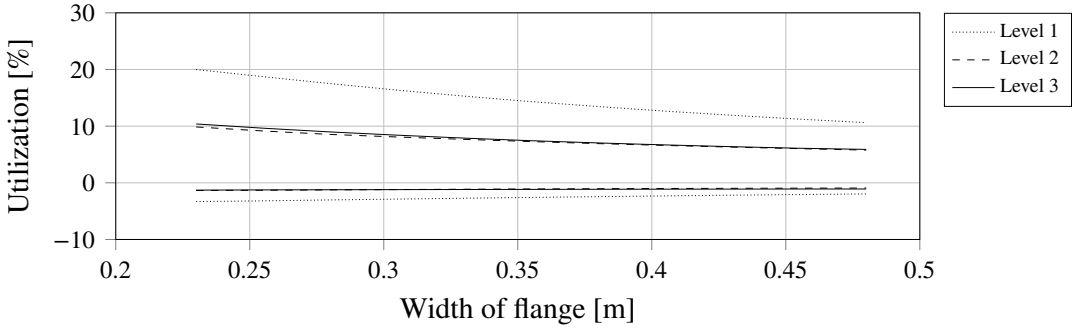

Figure E.132 The utilization ratio, regarding SLS, of the first transversal beam for different widths of the flanges for the distributed traffic load.

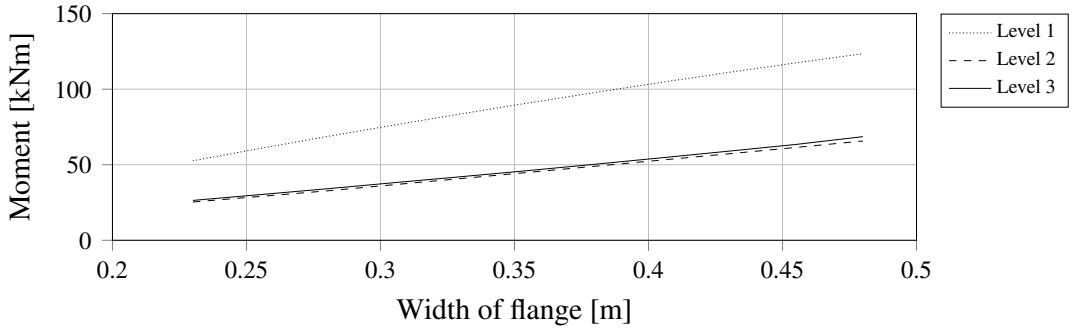

Figure E.133 The difference in maximum and minimum secondary bending moment in the first transversal beam for different widths of the flanges for the distributed traffic load case.

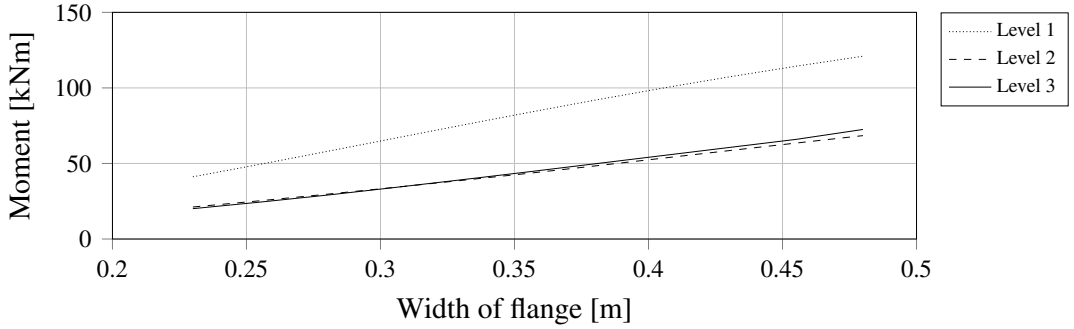

Figure E.134 The difference in maximum and minimum secondary bending moment in the sixth transversal beam for different widths of the flanges for the distributed traffic load case.

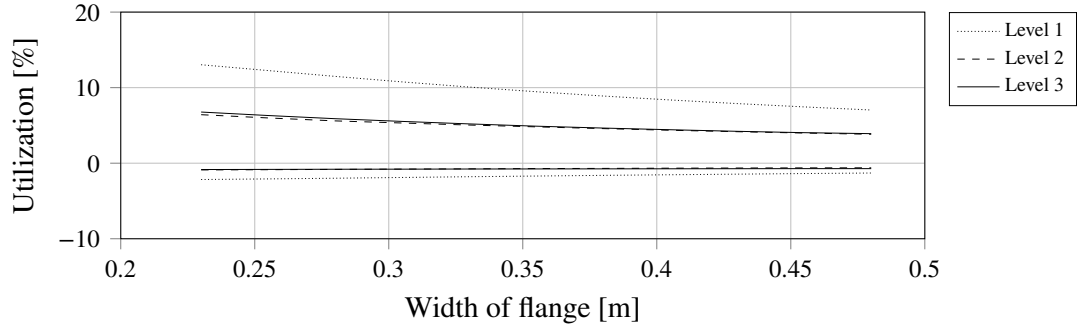

Figure E.135 The utilization ratio, regarding ULS, of the first transversal beam for different widths of the flanges for the distributed traffic load.